Noves metodologies per al tractament de bacteris creixent en forma de biofilm

Núria Blanco Cabra

NOVES METODOLOGIES PER AL TRACTAMENT DE BACTERIS CREIXENT EN FORMA DE BIOFILM

NÚRIA BLANCO CABRA

Tesi Doctoral

Barcelona, 2020

UNIVERSITAT DE BARCELONA

FACULTAT DE MEDICINA I CIÈNCIES DE LA SALUT

Programa de Doctorat en Biomedicina

NOVES METODOLOGIES PER AL TRACTAMENT DE BACTERIS CREIXENT EN FORMA DE BIOFILM

Memòria presentada per Núria Blanco Cabra per a optar al grau de doctora per la Universitat de Barcelona.

Doctoranda:

Núria Blanco Cabra

Director i tutor de la tesi:

Dr. Eduard Torrents Serra

Barcelona, 2020

ÍNDEX

LLISTAT DE FIGURES

ABREVIATURES

- **AHL**: *N-acyl homoserine lactones*
- **AMP**: *Antimicrobial peptides,* pèptids antimicrobians
- **c-di-GMP**: *Cyclic diguanylate,* diguanilat cíclic
- **CFTR**: *Cystic fibrosis transmembrane conductance regulator*, regulador de la conductància transmembrana de la fibrosi quística
- **CFU**: *Colony-forming units*, unitats formadores de colònies
- **CV**: Cristall violeta
- **CC**: *Citotoxic concentration*
- **DNasa**: Desoxiribonucleasa
- **eDNA**: *Extracellular deoxyribonucleic acid*, àcid desoxiribonucleic extracel·lular
- **EPS**: *Extracellular polymeric substances*
- **GFP:** *Green fluorescent protein*, proteïna fluorescent verda
- **MA**: *Maslinic acid,* àcid maslínic
- **MIC**: *Minimum Inhibitory Concentration*, concentració mínima inhibitòria
- **MPOC**: Malaltia pulmonar obstructiva crònica
- **MRSA**: *Methicillin-resistant Staphylococcus aureus*, *Staphylococcus aureus* resistent a la meticil·lina
- **MSCRAMMs**: *Microbial surface components recognizing adhesive matrix molecules*
- **NET***: Neutrophil extracellular traps*, trampes extracel·lulars de neutròfils
- **NO**: Òxid nítric
- **NP**: Nanopartícules
- **OA**: *Oleanolic acid*, àcid oleanòlic
- **PCR**: *Polymerase chain reaction*, reacció en cadena de la polimerasa
- **PIA**: *Polysaccharide intercellular adhesin*
- **PLGA**: *Poly(lactic-co-glycolic acid)*, àcid poli(làctic-co-glicòlic))
- **QS**: *Quorum sensing*
- **SAM**: S-Adenosil metionina
- **SCPN:** *Single-chain polymer nanoparticles*, nanopartícules de cadena única de dextrà
- **SEM**: *Scanning electron microscopy*, microscòpia electrònica de rastreig
- **SI:** *selectivity index*, índex de selectivitat
- **TCC**: *Triclocarban*

RESUM

Les infeccions bacterianes han esdevingut un greu problema a escala mundial per culpa del mal ús que hom ha fet dels antibiòtics. L'adquisició de resistències als antimicrobians s'ha accelerat i cada cop hi ha més bacteris resistents a tots els antibiòtics coneguts. Aquest problema es veu agreujat quan els bacteris formen un biofilm i les infeccions es tornen cròniques. Els bacteris creixents en forma de biofilm produeixen una matriu extracel·lular protectora i adquireixen així un mecanisme extra de protecció vers els antibiòtics. A més, en l'actualitat no hi ha cap antibiòtic desenvolupat que sigui capaç d'actuar específicament contra els biofilms bacterians madurs i, per tant, es necessiten nous procediments i fàrmacs per a poder tractar-los. En aquest treball s'estudien noves metodologies per al tractament de bacteris creixent en forma de biofilm des de tres punts de vista diferents.

En primer lloc, s'intenta buscar noves teràpies i, per això, s'analitza l'acció antimicrobiana i antibiofilm de noves molècules, que han sigut modificades químicament per a millorar el seu potencial contra els biofilms de *Staphylococcus aureus*. Una part d'aquestes molècules són derivades del triclocarban i unes altres són derivades de l'àcid oleanòlic i l'àcid maslínic. En ambdós casos s'han aconseguit molècules menys tòxiques i més actives que els compostos dels quals deriven, fins i tot contra la soca de *S. aureus* resistent a meticil·lina (MRSA).

En segon lloc, es pretén desenvolupar una tecnologia que permeti determinar, de mantera senzilla i amb precisió, la sensibilitat antibiòtica dels biofilms, ja que els mètodes que es fan servir actualment es basen en el creixement microbià en forma planctònica i no són fiables en bacteris creixent en forma de biofilm. Seguint aquest fil, s'ha desenvolupat el dispositiu "BiofilmChip", una estructura microfluídica que permet el creixement de biofilms de manera senzilla i l'anàlisi de la seva sensibilitat sense la necessitat d'usar un microscopi confocal.

En tercer i últim lloc, es volen desenvolupar noves tecnologies per al tractament de biofilms utilitzant enzims disgregadors del biofilm i fent servir mètodes alternatius d'alliberament de fàrmacs (*drug delivery*), com són les nanopartícules. Així, s'ha treballat amb els enzims alginat liasa i desoxiribonucleasa I (DNasa I), que degraden components de la matriu extracel·lular dels biofilms i en trenquen l'estructura, fent possible que els antibiòtics travessin aquesta barrera i puguin actuar. Per una banda, s'ha analitzat l'especificitat, l'activitat disgregadora i la sinergia amb antibiòtics de cinc alginat liases contra els biofilms de *Pseudomonas aeruginosa.* Per altra banda, s'ha treballat amb unes nanopartícules que milloren l'activitat de l'antibiòtic tobramicina, ja que contenen l'enzim DNasa I que permet la penetració d'aquest antibiòtic en els biofilms de *S. aureus* i *P. aeruginosa*. Aquestes nanopartícules, a més, estan marcades amb un fluoròfor, la qual cosa ha permès visualitzar la seva interacció amb la matriu extracel·lular del biofilm.

INTRODUCCIÓ

1. ELS BIOFILMS BACTERIANS

Un **biofilm o biopel·lícula** és un conjunt de bacteris adherits a una superfície (viva o inerta) amb una matriu extracel·lular protectora que és produïda per la mateixa comunitat de bacteris [1]. Les primeres evidències d'observació microscòpica de biofilms daten del s. XVII, juntament amb les primeres descripcions de bacteris per part d'Antonie van Leeuwenhoek (1632–1723) [2]. La teoria general d'aquestes comunitats microbianes, però, no es va promulgar fins al 1978 [3] i el terme "*biofilm*" va ser introduït en medicina el 1985 [2], en ambdós casos per part del Dr. John William Costerton (1934–2012), microbiòleg pioner en recerca de biopel·lícules i conegut com el "pare dels biofilms" [4].

Els bacteris que creixen formant un biofilm difereixen dels que creixen de forma planctònica (lliure), ja que **s'adapten** a aquesta forma de creixement amb diferents **patrons fenotípics** i una **expressió de gens diferencial**. A nivell morfològic poden tenir canvis en l'alteració de la paret cel·lular o la modificació d'apèndix com flagels i fímbries [5]. A més, la **matriu extracel·lular** que uneix els bacteris que formen un biofilm fa que aquests creixin en una alta densitat cel·lular no permetent la difusió de les molècules lliurement. Per tant, es crea en el biofilm un **gradient de concentració** de nutrients, oxigen i productes metabòlics que provoca que els bacteris també s'hi adaptin, com per exemple disminuint la seva taxa metabòlica o canviant la seva forma de respiració [1]. Aquests canvis que experimenten els bacteris en el biofilm també poden suposar una **tolerància als antibiòtics**, fent que siguin necessàries concentracions d'aquests fàrmacs fins a 1000 vegades superiors que en els bacteris planctònics per a poder erradicar-los [6].

Els biofilms poden ser comunitats d'una sola espècie bacteriana o de diferents espècies bacterianes (que anomenem polimicrobians o mixtes). Són **omnipresents**, ja que el 80 % del total de la biomassa bacteriana es troba en forma de biofilm [7] i tenen un impacte en molts àmbits. En el medi aquàtic marí, per exemple, els biofilms acceleren el procés de corrosió que danya les estructures de vaixells, oleoductes i ports [8]. En l'agricultura tenen conseqüències en la nutrició, protecció i també infecció de les plantes [9]. També són molt importants les biopel·lícules en la indústria, per la formació d'aquestes estructures en intercanviadors de calor i canonades. En concret, en la indústria alimentària, la contaminació per biofilms causa grans pèrdues econòmiques [8, 10].

També són un tema preocupant per a la salut pública, ja que la formació de biofilm és la responsable d'aproximadament el **75 % de totes les infeccions microbianes** humanes. Els biofilms estan implicats en les infeccions pulmonars cròniques i en altres infeccions com l'osteomielitis, l'otitis o la placa bacteriana a les dents. A més, són una causa important d'**infeccions nosocomials** per la formació d'aquestes biopel·lícules en implants i catèters. Els microorganismes més freqüentment associats a infeccions nosocomials són *Escherichia coli*, *Staphylococcus aureus* (en molts casos resistent a meticil·lina, MRSA), *Pseudomonas aeruginosa* i *Klebsiella pneumoniae*, tots ells productors de biofilms [7].

1.1. LA MATRIU EXTRACEL·LULAR

Només un 10 % del que es considera la biomassa total del biofilm correspon als bacteris. La resta, el 90 %, a la matriu [11]. La matriu extracel·lular dels biofilms és un conglomerat de diferents **biopolímers** que són els responsables de l'**adhesió** a la superfície, així com de l'**agregació** i la **cohesió** dels bacteris entre ells [1]. A més de conferir una **barrera protectora** que dóna resistència al sistema immune de l'hoste i procura la tolerància a certs agents antimicrobians [11, 12], aquesta matriu també proporciona una **font de nutrients** als bacteris i manté una **retenció d'aigua** que impedeix la dessecació del biofilm [13]. El conjunt de biopolímers components de la matriu, conegut en anglès amb les sigles EPS (*extracellular polymeric substances*), comprèn exopolisacàrids, proteïnes, DNA extracel·lular, lípids i aigua. La composició de l'EPS, la qual ja varia entre les diverses famílies i espècies microbianes, pot arribar fins i tot a ser diferent entre soques de la mateixa espècie. Les figures 1 i 2 mostren un esquema de la distribució dels components de la matriu extracel·lular de *P. aeruginosa* PAO1 i de *S. aureus*, respectivament.

1.1.1. Exopolisacàrids

Són polímers de carbohidrats formats per cadenes de monosacàrids que constitueixen una gran part de la matriu. Alguns dels polisacàrids que poden formar part de la matriu extracel·lular són homopolisacàrids (formats per monosacàrids iguals), com en el cas dels **glucans** i **fructans** dels biofilms orals que formen diverses espècies de *Streptococcus*, o la **cel·lulosa** que forma part dels biofilms de diferents espècies de les famílies Enterobacteriaceae [14] i Pseudomonadaceae [15]. En canvi, la majoria dels polisacàrids de la matriu són heteropolisacàrids (constituïts per diferents tipus

de monosacàrids) i, a més, poden contenir en l'estructura substituents orgànics o inorgànics que els provoquen una càrrega aniònica o catiònica. [11].

En molts bacteris, els **polisacàrids són essencials** per a la formació de biofilm, i la falta de producció d'aquests, a causa de mutacions, impedeix el desenvolupament de biofilms madurs [16, 17]. Tanmateix, en els biofilms polimicrobians pot haver-hi espècies bacterianes que no produeixin polisacàrids, servint-se dels biopolímers dels bacteris que sí que en produeixen [18].

En els biofilms de *Staphylococcus epidermidis i S. aureus*, una substància característica és la **PIA** (*polysaccharide intercellular adhesin*), un polisacàrid policatiònic compost de poli-β-1,6-N-acetilglucosamines (**PNAG**) amb alguns residus desacetilats. Aquest carbohidrat és important en la producció del biofilm, així com en la protecció contra el sistema immune de l'hoste i el tractament antibiòtic [19]. El PNAG, a més, interacciona amb el DNA de la matriu, reforçant la seva estructura [20].

En els biofilms de *P. aeruginosa* hi ha tres tipus de polisacàrids amb importants funcions estructurals: l'**alginat**, el **Psl** i el **Pel**. L'alginat és un heteropolisacàrid carregat negativament que està compost per dos polímers (β-D-manuronat i α-L-guluronat) disposats en diferents blocs d'un dels polímers o de seqüències dels dos polímers. Aquest polisacàrid, que està O-acetilat en alguns residus del manuronat, és molt abundant en les algues marines brunes i també forma part de la matriu d'altres bacteris com *Azotobacter vinelandii* [13]. Tot i que l'alginat està involucrat en l'establiment de microcolònies al principi de la formació del biofilm, la seva principal funció és en l'arquitectura d'aquest, donant estabilitat en els biofilms madurs en crear una capa amb un aspecte mucós. D'aquesta manera, l'alginat també **defensa el biofilm** del sistema immune protegint-lo contra la fagocitosi [21], els antibiòtics com la tobramicina [12] i la dessecació [22]. La producció d'alginat en *P. aeruginosa* està regulada, entre d'altres, pel gen *mucA*. S'ha vist que la degradació de la proteïna MucA per causes d'estrès cel·lular o la mutació del gen *mucA* indueixen una sobreproducció d'alginat i converteixen la soca en mucoide [23]. El Psl és un polisacàrid no carregat, format per unitats de D-manosa, D-glucosa i L-ramnosa [24]; i el Pel és un polisacàrid catiònic, format per N-acetilglucosamina i N-acetilgalactosamina [25]. Tant el Psl com el Pel tenen un paper important en **iniciar i mantenir l'estructura del biofilm** de *P. aeruginosa*, així com en l'adherència entre cèl·lules i amb la superfície, tot i que difereixen en la importància estructural entre soques. Específicament, la soca PAO1, depèn principalment del Psl en la formació de la matriu i, en canvi, la soca PA14 és Pel-dependent [24].

1.1.2. Proteïnes

La majoria de proteïnes de la matriu extracel·lular són **enzims** que estan involucrats en la degradació dels diferents biopolímers; són, per tant, glucosidases, proteases, desoxiribonucleases i lipases. Aquest procés de degradació és necessari, tant per a obtenir una font d'energia i carboni com per a la propagació del biofilm i la formació de noves microcolònies. Exemples d'enzims necessaris per a la dispersió són l'**alginat liasa** que produeix *P. aeruginosa* o la proteasa **Spl** i la **termonucleasa** produïdes per *S. aureus* [26].

També hi ha altres proteïnes, però, que tenen una important **funció estructural**. Per exemple en *Bacillus subtilis,* la proteïna **BslA** contribueix a la hidrofobicitat del biofilm, a més de ser molt important en la seva arquitectura [27].

La proteïna **CdrA** és molt important en els biofilms de *P. aeruginosa*, ja que promou l'agregació unint-se al polisacàrid Psl [28]. Aquest bacteri també produeix dues proteïnes d'unió a polisacàrid (lectines), **LecA** i **LecB**, que ajuden a la unió entre cèl·lules bacterianes [5].

En el gènere *Staphylococcus* existeixen les proteïnes anomenades amb les sigles **MSCRAMMs** (*microbial surface components recognizing adhesive matrix molecules*), unes adhesines que intervenen en l'adhesió inicial del bacteri al teixit de l'hoste, com són la **proteïna A** i les proteïnes d'unió a fibronectina (**FnBPs**)[29]. Altres proteïnes importants en la matriu extracel·lular d'aquest gènere són les proteïnes de superfície **SasC** i **SasG** [30].

A més, també tenen una funció estructural en el biofilm alguns apèndixs proteínics dels bacteris com els **pilis**, les **fímbries** o els **flagels**. El pili de tipus IV de *P. aeruginosa* per exemple, s'uneix al DNA extracel·lular, podent actuar com a reforç de l'estructura del biofilm [31].

1.1.3. Àcid desoxiribonucleic extracel·lular (eDNA)

El DNA present en l'estructura de la matriu extracel·lular es coneix com a **DNA extracel·lular** (eDNA). Es creia que aquest només era material residual de lisis cel·lular bacteriana fins que alguns estudis van fer veure la importància de la seva presència en la formació del biofilm, tot demostrant l'efecte que tenen els enzims disgregadors de DNA en l'eliminació de biofilms [32]. L'ús de l'eDNA com a material adhesiu és emprat generalment per a tots els bacteris que formen biofilms, tot i que la funció específica i la proporció d'aquest dins el biofilm són molt variables [33]. El paper més

important de l'eDNA en la formació del biofilm és en la **fase d'adhesió** dels bacteris a la superfície, ja que sembla contribuir en les interaccions àcid-base que es donen en aquesta fase [34]. A més de l'adhesió, l'eDNA també es considera en el manteniment de la **integritat estructural** del biofilm de moltes espècies i en la patogenicitat, ja que actua com a **quelant d'alguns agents antimicrobians** catiònics i d'altres molècules afavorint la resistència antibiòtica [33].

Tot i ser un component essencial en la formació dels biofilms del gènere *Staphylococcus*, l'eDNA és un component majoritari en els biofilms de *S. aureus*, mentre que en els que forma *S. epidermidis*, és molt poc abundant [20]. En la matriu de *P. aeruginosa*, en canvi, l'eDNA és sis vegades més abundant que les proteïnes, i divuit vegades més abundant que els carbohidrats [35].

En els biofilms formats ***in vitro***, l'origen d'aquest compost sembla ser la **lisi d'una subpoblació** de bacteris del biofilm, tant en *P. aeruginosa* [36] com en *Staphylococcus*. En el segon cas la lisi es produeix mitjançant l'**autolisina AtlE**, tot i que no es pot descartar que existeixi una secreció activa de DNA en ambdós casos [11]. En els biofilms formats en teixits humans (***in vivo***), però, com en el cas de les infeccions pulmonars, la majoria de l'eDNA és **derivat dels leucòcits polimorfonuclears**, formant el que s'anomena **trampes extracel·lulars de neutròfils** (*neutrophil extracellular traps*, NET) [37], i aquest eDNA sembla que s'acumula **només a les zones externes** del biofilm, contribuint en les funcions de **protecció** [38].

1.1.4. Lípids

Els lípids de la matriu extracel·lular actuen generalment com a **surfactants**, dispersant les substàncies hidrofòbiques i fent que puguin ser aprofitables pels bacteris, com per exemple els **rhamnolípids** que es troben a la matriu de *P. aeruginosa* [39]. Altres lípids també presents en aquest bacteri, com els **lipopolisacàrids** de la membrana cel·lular externa dels bacteris Gram-negatius, poden intervenir en l'**adhesió cel·lular** i les **propietats viscoelàstiques** del biofilm [40].

1.1.5. Aigua

L'aigua és el **component més abundant** de la matriu del biofilm, representant fins a un 97 % de l'espai d'aquest. Per tant, és essencial per al biofilm mantenir la hidratació i evitar la pèrdua d'aigua. Per això, la majoria dels EPS són altament **higroscòpics** i retenen l'aigua sense cap mecanisme d'unió específic. A més, es creu que en els processos d'assecament ambiental en el biofilm es produeix un

desacoblament hidràulic, eliminant l'intercanvi d'aigua amb l'exterior i impedint així la deshidratació del biofilm [11].

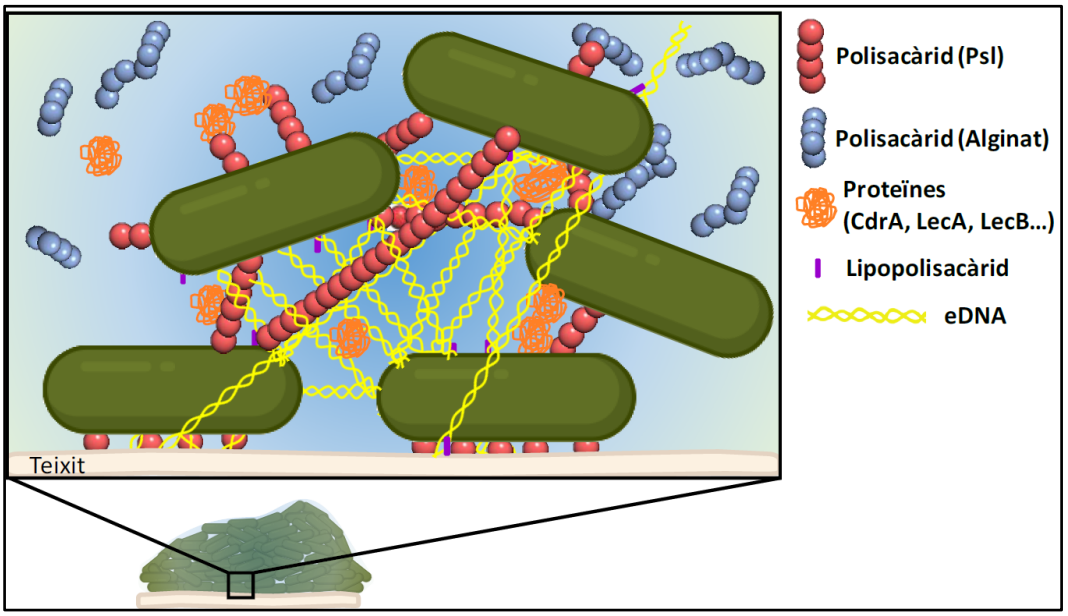

***Figura 1**: Esquema representatiu de la matriu extracel·lular del biofilm de P. aeruginosa PAO1.*

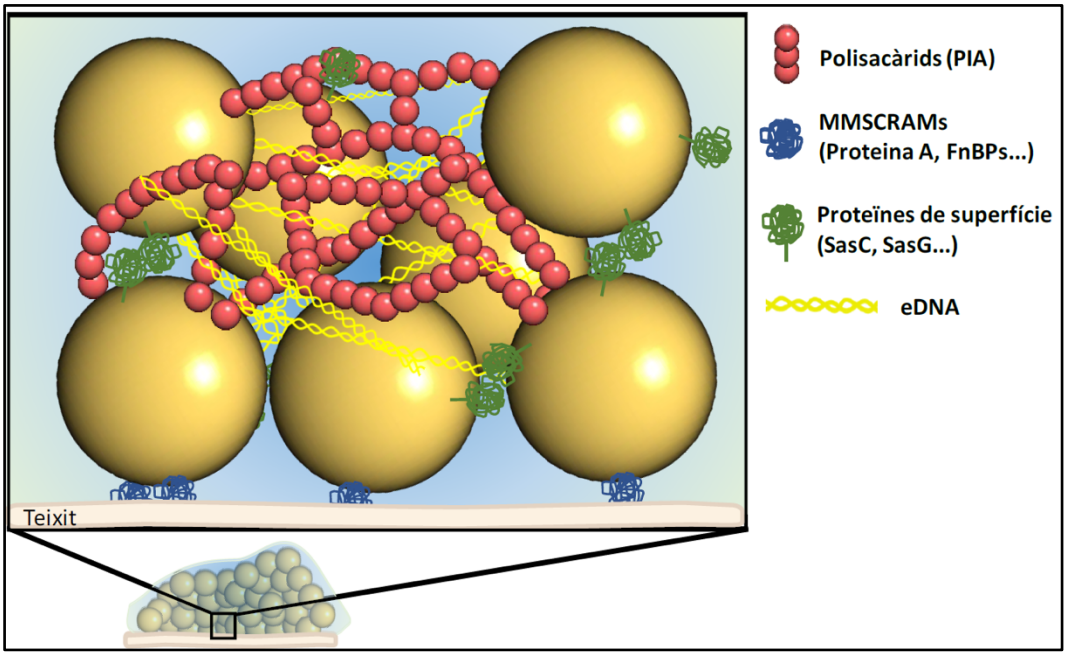

***Figura 2**: Esquema representatiu de la matriu extracel·lular del biofilm de S. aureus.*

1.2.EL PROCÉS DE FORMACIÓ DELS BIOFILMS

La formació de biofilm es dóna en resposta a **estímuls ambientals** que varien segons els organismes. Aquests estímuls poden ser des de canvis en el contingut nutricional del medi on estiguin creixent, fins a canvis de temperatura, osmolaritat, pH o oxigen [41]. També se sap que l'estrès ambiental que provoca una **concentració subinhibitòria d'antibiòtic** (més baixa que la concentració mínima inhibitòria) pot estimular la formació de biofilm [42].

Els primers estudis de desenvolupament dels biofilms es van fer en el bacteri *P. aeruginosa*. Així, es va determinar que aquest bacteri presenta cinc estadis de desenvolupament del biofilm: 1) adhesió inicial a la superfície, 2) adhesió irreversible a través de la producció de la matriu extracel·lular, 3) desenvolupament del biofilm, 4) maduració i 5) alliberació o dispersió [43]. Posteriors estudis han demostrat que altres bacteris, que també tenen flagels com *E. coli* o *Vibrio cholerae* i inclús bacteris no mòbils com *S. aureus*, segueixen una seqüència de desenvolupament molt semblant [44]. S'han establert, per tant, **tres fases generals** en el desenvolupament dels biofilms (Figura 3).

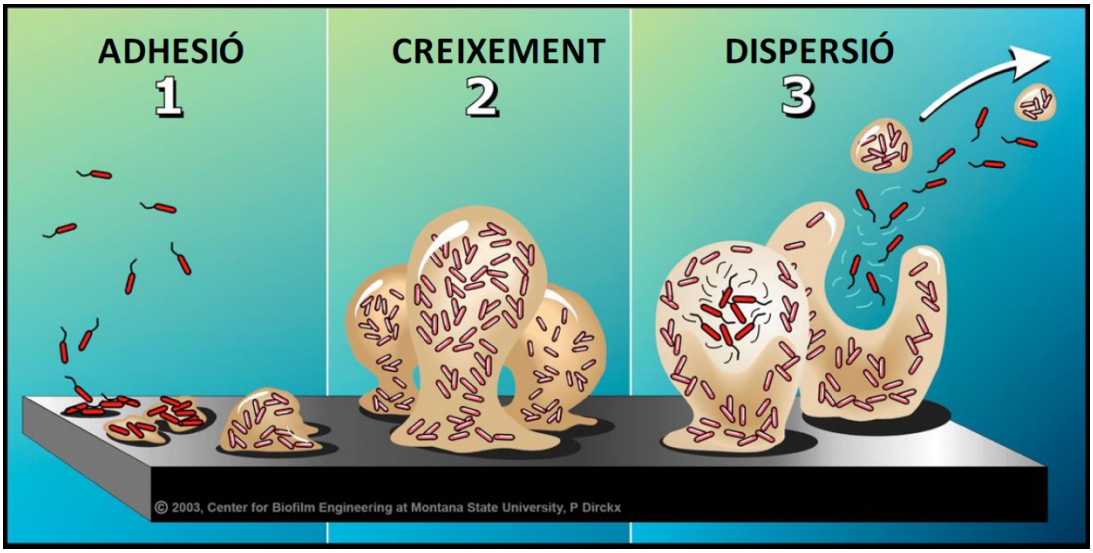

***Figura 3**: Fases del desenvolupament dels biofilms. (Figura modificada de [45]).*

1.2.1. Fase d'adhesió a la superfície

L'adhesió inicial dels bacteris en monocapa a la superfície es dóna gràcies a diferents factors segons l'espècie bacteriana. En *S. aureus* i *S. epidermidis*, per exemple, els **àcids teicoics** de la paret cel·lular i la proteïna de superfície **autolisina** estan involucrats en l'adhesió a **superfícies abiòtiques** [46]. En canvi, en la colonització de **teixits vius** són les **MSCRAMMs** les responsables de l'adhesió en aquests bacteris, unint-se a proteïnes humanes com el **fibrinogen** o la **fibronectina** [29]. En l'adhesió inicial dels biofilms de *P. aeruginosa* estan implicats els **flagels**, els **pilis**, les **fímbries**, l'**eDNA** i l'exopolisacàrid **Pel** [30]. Al final d'aquesta fase, l'adhesió dels bacteris a la superfície es fa molt més forta, considerant-se irreversible. A més, en el cas de les espècies mòbils s'inhibeix la transcripció dels gens necessaris per a formar el **flagel** i, per tant, aquest es **perd** [47, 48].

1.2.2. Fase de creixement i maduració

Després de l'adhesió a la superfície, els bacteris comencen a produir la **matriu extracel·lular**, que permet la unió de bacteris entre ells i la superposició de capes de bacteris formant clústers (**microcolònies**). Posteriorment, el biofilm comença a madurar creant una arquitectura tridimensional. Se sap que la forma d'aquesta estructura depèn de moltes variables, una de les quals és la força mecànica que exerceix el fluid on està embegut el biofilm (anomenat ***shear stress*** en anglès)[44, 47]. Un altre factor determinant de l'arquitectura poden ser els **nutrients del medi** on creix el biofilm; en el cas de *P. aeruginosa*, per exemple, aquests factors determinen que es formin unes estructures tridimensionals en forma de bolet (*mushroom-like*) [49].

Els sistemes de ***Quorum sensing*** (QS) dels bacteris són uns sistemes de senyalització que regulen els gens a través de molècules alliberades al medi (autoinductors) en resposta a **fluctuacions en la densitat de la població**. Aquestes molècules s'uneixen a un receptor i activen diferents sistemes de senyalització segons el bacteri. En el gènere *Staphylococcus*, el QS es dóna a través del sistema de senyalització Agr i en *P. aeruginosa*, el QS comprèn tres sistemes interconnectats: Las, Rhl i Pqs. Aquests sistemes s'activen quan la densitat de la població supera un llindar determinat, com és en el cas dels biofilms. Alguns autors creuen que el QS està directament implicat en la **fase de maduració** del biofilm, estimulant processos com l'adhesió cel·lular o la producció de components de la matriu extracel·lular [11, 50, 51]. Tanmateix, hi ha altres estudis que demostren que el sistema de QS no s'activa fins a la **fase de dispersió** del biofilm [52].

1.2.3. Fase d'alliberació o dispersió

En aquesta fase hi ha una **destrucció** d'una part de l'estructura del biofilm per part d'**enzims** i **surfactants**, normalment en les capes superiors, per a alliberar alguns bacteris i que aquests **colonitzin un nou nínxol** i tornin a començar el procés de formació de biofilm [41]. Els surfactants no només influeixen en la dispersió cel·lular, sinó que també causen la **necrosis de leucòcits**, evitant així la immunitat humana [53].

Diversos estudis demostren que els sistemes de **QS** regulen la **inhibició de la síntesi de compostos** de la matriu, així com la **producció de surfactants**, d'**enzims** que destrueixen la matriu i altres molècules [52]. D'aquesta manera, el sistema Las, en *P. aeruginosa*, inhibeix la producció del polisacàrid Pel i el sistema Pqs estimula la producció de surfactants [54, 55]. En *S. aureus* s'inhibeixen les proteïnes d'unió a fibronectina (FnBPs) i la proteïna A a través del sistema de QS Agr [56], que també controla la producció de surfactants (PSMs) i proteases [57].

1.3. ELS BIOFILMS EN LES INFECCIONS BACTERIANES

Els biofilms són els causants d'aproximadament el **75 % de totes les infeccions microbianes** humanes [7]. Un dels factors que diferencia aquestes infeccions és que els bacteris que creixen en forma de biofilm són molt més resistents als antimicrobians que els mateixos bacteris quan creixen de forma planctònica. En general, els mecanismes de tolerància i persistència són els causants d'aquesta capacitat de sobreviure als antimicrobians, més que no pas els mecanismes de resistència genètica (Figura 4) [58].

Un bacteri **resistent** és aquell que pot créixer en presència d'una concentració de l'agent antimicrobià (bactericida o bacteriostàtic) que normalment inhibiria el creixement. En cultius planctònics, la resistència a un agent antimicrobià se sol mesurar usant la **concentració mínima inhibitòria** (MIC, *Minimum Inhibitory Concentration*), que és la mínima concentració en la qual aquest agent inhibirà el creixement del cultiu. Per tant, un bacteri resistent necessitarà una concentració superior a la MIC per a ser inhibit. La resistència genètica explica una petita part de la capacitat dels biofilms a sobreviure a antimicrobians, i aquesta pot ser deguda a **mutacions** o a **adquisició de material genètic** que codifiqui per gens de resistència; tot i que també hi ha bacteris que són **intrínsecament resistents** a alguns antimicrobians (tal com ho són els Gram-negatius a la vancomicina) (Figura 4) [59].

La **tolerància**, en canvi, és la **causa fonamental** que els antimicrobians no siguin efectius contra el biofilm. Aquesta es defineix com la capacitat que té el bacteri de sobreviure (sense créixer ni morir) en presència d'un agent antimicrobià bactericida. Una mesura de la tolerància és la **concentració mínima bactericida** (MBC, *minimum bactericidal concentration*), que és la mínima concentració que destrueix el 99,9 % de les cèl·lules bacterianes d'un cultiu [60]. El principal mecanisme que proveeix tolerància al biofilm és la **matriu extracel·lular**, ja que és molt impermeable a certs antimicrobians i en redueix la difusió a l'interior, com passa per exemple amb l'antibiòtic tobramicina en els biofilms de *P. aeruginosa* [12]. Un altre mecanisme que pot donar tolerància als bacteris és la **reducció de la taxa de creixement** o la **reducció del metabolisme**. Aquestes reduccions fenotípiques les trobem sobretot en els bacteris de les regions profundes dels biofilms, ja que l'**heterogeneïtat** en l'estructura fa que hi hagi menys disponibilitat d'oxigen i nutrients en aquestes regions (Figura 4) [60].

Així com la resistència i la tolerància són característiques del conjunt d'una població bacteriana, la **persistència** és l'habilitat d'una part de la població (normalment menys d'un 1 %) de sobreviure a altes concentracions d'un antimicrobià. En un biofilm, per tant, pot haver-hi una subpoblació tolerant a un antimicrobià (per causes genètiques o fenotípiques) que persisteix "**dorment**" davant l'actuació d'aquest i repobla el biofilm quan l'acció de l'antimicrobià ha acabat (Figura 4) [60].

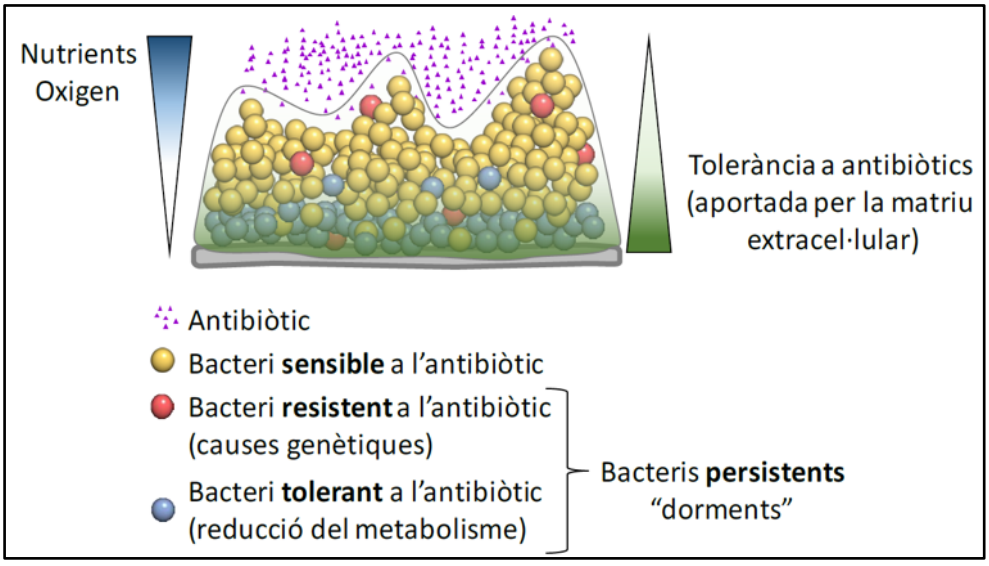

***Figura 4**: Resistència, tolerància i persistència en un biofilm bacterià.*

Les infeccions causades per biofilms en el cos humà es poden donar en dispositius externs o en els mateixos teixits del cos. A la figura 5 es representen les infeccions més comunament associades a biofilm en el cos humà, i en aquest apartat es fa una breu explicació d'algunes d'elles.

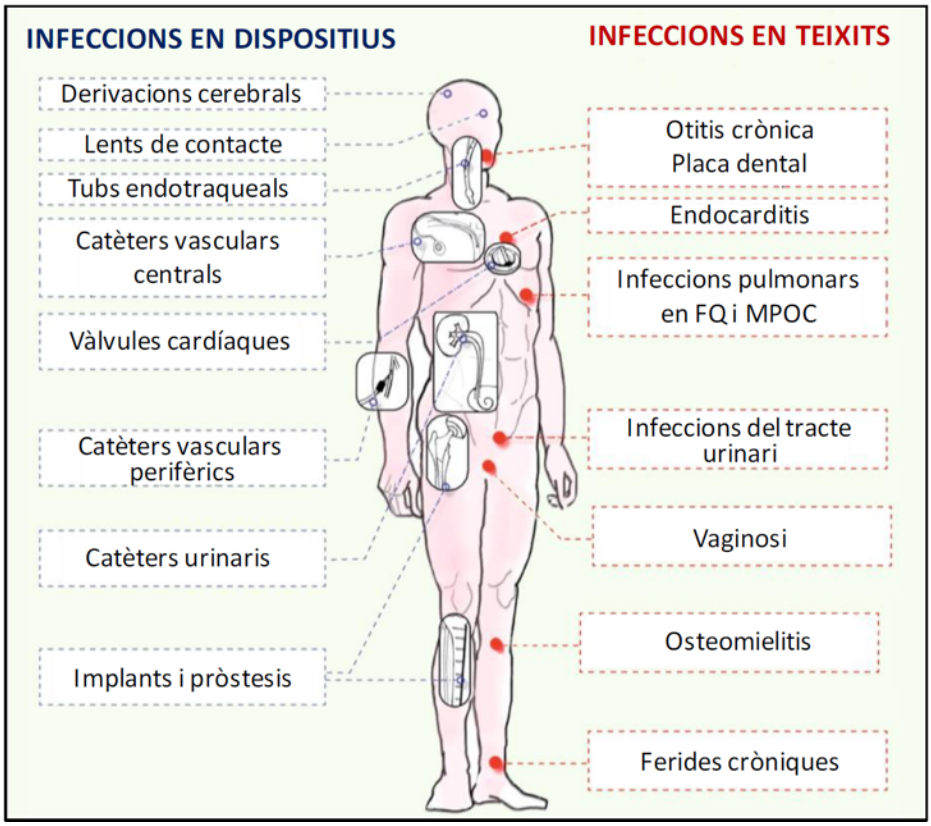

***Figura 5**: Infeccions associades a biofilms en el cos humà. (Figura adaptada de [61]).*

1.3.1. Biofilms en malalties respiratòries cròniques

La **fibrosi quística** (FQ) o mucoviscidosi és una malaltia genètica autosòmica recessiva que pot ser causada per més de 1500 possibles mutacions en el gen regulador de la conductància transmembrana de la fibrosi quística (CFTR, *cystic fibrosis transmembrane conductance regulator*). Aquest gen tradueix per una proteïna que forma un canal de clor implicat en moltes secrecions de les mucoses del cos com les intestinals, les pancreàtiques o les hepàtiques. Les mutacions en el gen CFTR provoquen una disfunció del canal i fan que les secrecions siguin molt espesses, creant diverses patologies. La patologia que té la principal causa de mortalitat en els malalts de FQ és el **bloqueig de les vies aèries dels pulmons**. En els malalts de FQ hi ha una **falta de líquid periciliar**, que és necessari per al moviment dels cilis de les vies respiratòries que transporten el moc on s'acumulen

els possibles patògens. En aquests malalts el moc no es pot eliminar normalment, s'acumula en les vies respiratòries i permet que els bacteris puguin créixer formant un biofilm. Aquestes infeccions es tornen cròniques i provoquen la pèrdua de capacitat pulmonar i en molts casos la mort [62, 63]. Patògens importants en aquestes infeccions són ***S. aureus*** i ***Haemophilus influenzae*** en infants i ***Burkholderia cenocepacia, Achromobacter xylosoxidans, Stenotrophomonas maltophilia, Mycobacterium abscessus*** i ***P. aeruginosa*** en adults [64]. Les infeccions per *P. aeruginosa* són les més abundants i les que més mortalitat causen. Quan hi ha la primera colonització de *P. aeruginosa* al pulmó, aquest bacteri sol canviar el seu fenotip a mucoide i formar un biofilm, convertint la infecció en **crònica i recurrent al llarg de tota la vida** del pacient. És per això que com més tardana és la primera colonització de *P. aeruginosa*, millor pronòstic de la malaltia hi ha [65].

La **malaltia pulmonar obstructiva crònica** (MPOC) es caracteritza per una obstrucció irreversible de les vies respiratòries que provoca una disminució de la funció pulmonar. Tot i que és per causes diferents de la FQ, en la MPOC també hi ha una **acumulació del moc** a les vies respiratòries que no s'elimina, i això també provoca la formació de biofilms. En aquest cas, les colonitzacions solen ser de ***H. influenzae*** i ***P. aeruginosa*** [66].

1.3.2. Biofilms en dispositius mèdics

L'ús de dispositius mèdics com els **implants artificials**, els **catèters** i les **pròtesis** tenen un petit però clínicament important risc d'infecció, que normalment acaba generant la formació d'un biofilm. Els principals formadors de biofilms en els dispositius mèdics són els *Staphylococcus.* Un dels bacteris d'aquest gènere, que freqüentment forma biofilms en aquests dispositius, és ***Staphylococcus epidermidis***, però el més preocupant clínicament és ***S. aureus,*** ja que les seves infeccions són més agressives que els altres bacteris d'aquest gènere. Les infeccions de catèters i pròstesis per *S. aureus* poden acabar generant **endocarditis**, **artritis bacteriana** i, fins i tot, **sèpsia**. En aquests casos, l'únic tractament possible, a més de la teràpia antibiòtica, és la **substitució del dispositiu** [67].

1.3.3. Biofilms en ferides cròniques

Una ferida crònica és una ferida encallada en la **fase inflamatòria** que no pot avançar en la curació, a causa de la presència de **teixit necròtic**, **cossos estranys** o **bacteris**. Les ferides cròniques més comunes són les úlceres per pressió, les úlceres venoses i arterials, i les úlceres del peu diabètic. En aproximadament un 90 % dels casos, els bacteris en aquestes ferides formen un biofilm [68]. No està clar de quina manera concreta els biofilms contribueixen a la cronicitat de les ferides, però és segur que la matriu extracel·lular obstaculitza l'**actuació dels agents antimicrobians** externs i interns, impedint així la reepitelització. A més, els bacteris contribueixen a una **activació contínua de la resposta immune**, sobreestimulant les citocines proinflamatòries i provocant d'aquesta manera dany en el teixit de l'hoste (Figura 6) [69]. Els bacteris que més freqüentment formen biofilm en ferides cròniques són ***P. aeruginosa, S. aureus***, i ***Enterococcus faecalis*** [58].

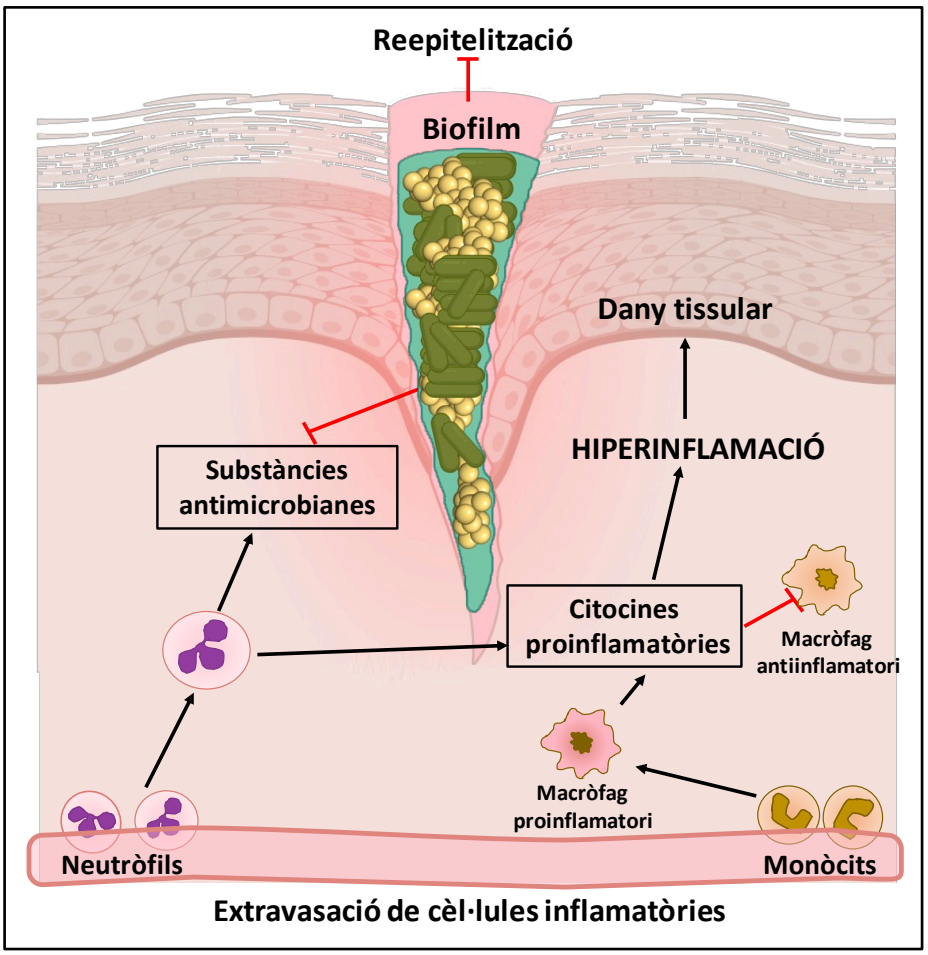

Figura 6: *Biofilm en una ferida crònica. Les fletxes negres indiquen activació i les vermelles inhibició. (Il·lustració realitzada amb Biorender.com)*

1.3.4. Biofilms orals

La microbiota oral té diferents localitzacions. En les localitzacions mucoses com la llengua, el paladar o els llavis hi ha una descamació contínua i per tant només es pot formar una monocapa de bacteris i no arriba a originar-se un biofilm. En altres localitzacions, però, els bacteris s'acumulen i formen la **placa dental**, que té les característiques típiques d'un biofilm. Aquestes localitzacions poden ser fissures en les peces dentals, implants, o zones per sobre o sota la vora gingival de les peces dentals (biofilm supragingival o subgingival). En la formació del biofilm oral es dóna una **"successió" d'espècies bacterianes**: la colonització inicial de la superfície la fan espècies del gènere ***Streptococcus***, que s'uneixen a receptors salivals. Posteriorment s'hi afegeixen microorganismes **anaeròbics** com ***Fusobacterium nucleatum*** i, cap a l'estadi final del biofilm, sol haver-hi un **complex de bacteris anaeròbics** format per ***Porphyromonas gingivalis***, ***Tannerella forsythia*** i ***Treponema denticola***, majoritàriament [70, 71]. A la figura 7 estan representades les espècies que poden formar part en els diferents estadis de formació del biofilm i les unions entre elles.

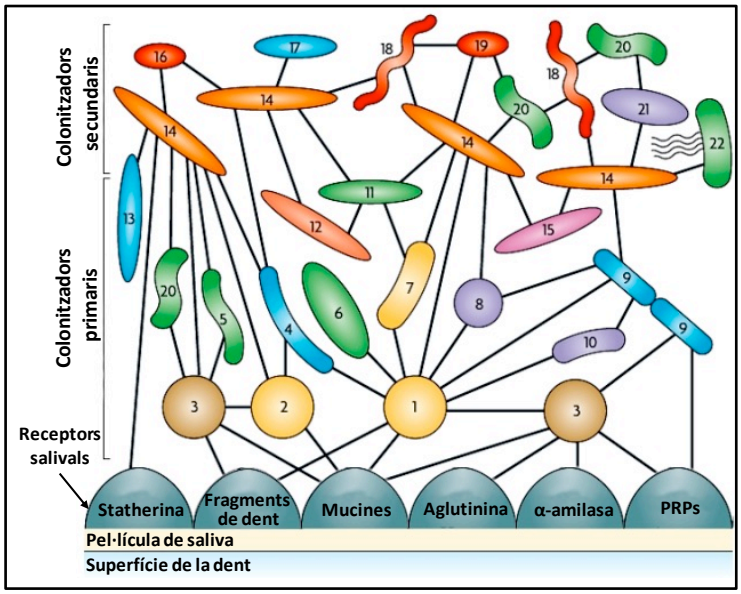

***Figura 7**: Bacteris implicats en la formació del biofilm oral. (Figura modificada de[71])*
(1. Streptococcus oralis i Streptococcus sanguinis; 2. Streptococcus mitis; 3. Streptococcus gordonii; 4. Capnocytophaga ochracea; 5. Propionibacterium acnes; 6. Haemophilus parainfluenzae; 7. Prevotella loescheii; 8. Veillonella spp.; 9. Actinomyces oris i Actinomyces naeslundii; 10. Eikenella corrodens; 11. Actinomyces israelii; 12. Capnocytophaga gingivalis; 13. Capnocytophaga sputigena; 14. F. nucleatum; 15. Prevotella denticola; 16. Aggregatibacter actinomycetemcomitans; 17. Eubacterium spp.; 18. T. denticola; 19. T. forsythia; 20. P. gingivalis; 21. Prevotella intermedia; 22. Selenomonas flueggei).

2. MÈTODES DE QUANTIFICACIÓ I SISTEMES DE DIAGNÒSTIC DE BIOFILMS

És essencial, per a poder erradicar els biofilms de les infeccions cròniques, poder-los estudiar a fora del cos humà, al laboratori, mitjançant **tècniques *in vitro***. Per tal d'aconseguir-ho, es necessiten sistemes de formació de biofilms que s'assimilin el més possible a les infeccions reals i d'aquesta manera poder saber amb certesa la sensibilitat antibiòtica, així com per a investigar nous compostos i estratègies antibiofilm. Així i tot, els mètodes *in vitro* sempre manquen de molts factors presents en el cos humà, com la resposta immune, per això també són molt importants els sistemes de formació de biofilms amb **procediments *in vivo***. Tanmateix, també són fonamentals uns bons mètodes de **quantificació de la biomassa o de l'activitat metabòlica del biofilm**, no només per a provar l'eficàcia de compostos antibiofilm, sinó també per a realitzar estudis bàsics dels biofilms; saber-ne els detalls de l'estructura i la formació, i així trobar noves tècniques que permetin que el tractament sigui més eficaç.

Actualment, però, en la majoria de laboratoris de microbiologia dels hospitals es fan servir paràmetres que determinen l'eficàcia antibiòtica usant bacteris en creixement planctònic (MIC), ja que els mètodes provats fins ara per a veure l'eficàcia antibiòtica en biofilms de mostres clíniques no han demostrat fer una predicció del tractament més acurada que les MIC [72]. Són necessaris, per tant, nous mètodes que puguin servir per a determinar la sensibilitat antibiòtica de manera eficaç en mostres clíniques i així millorar el tractament antibiòtic de pacients amb infeccions cròniques. A més, els mètodes haurien de ser simples, sense el requeriment d'equipament sofisticat ni personal altament qualificat.

2.1. DISPOSITIUS I MÈTODES DE FORMACIÓ DE BIOFILMS *IN VITRO*

El 1998 es va establir el mètode de **microplaques** (Figura 8A) per al creixement de biofilms *in vitro* [73]. Aquest mètode és el més comunament usat i es basa en plaques de poliestirè amb múltiples pous (6, 12, 24, 48, 96...), on es posa el cultiu bacterià i aquest s'adhereix a les parets dels pous formant el biofilm. Aquest mètode és útil per a comprovar la capacitat que tenen les diferents soques bacterianes o els mutants de produir biofilm, i també per a confirmar l'eficàcia antibiofilm de múltiples compostos, ja que el fet que en una sola placa pugui haver-hi molts pous independents permet fer un cribratge d'alt rendiment (*high-throughput screening*). A més, és un mètode amb un

cost econòmic molt baix i que no necessita gaire material ni expertesa per ser usat. Tanmateix, aquest mètode té moltes limitacions; no permet estudiar el biofilm en estadis de desenvolupament primaris, sinó que es necessita una mínima densitat en el biofilm per a poder veure diferències. A més, cal realitzar rentats per eliminar el creixement planctònic, i aquests rentats poden desadherir part del biofilm. Així mateix, també hi ha problemes en la mesura de la biomassa, ja que el biofilm es forma bàsicament en la interfase entre l'aire i el líquid, però una part del cultiu també sedimenta per gravetat i s'enganxa a la base del pou, i això pot donar una sobreestimació en la mesura de la biomassa [74].

Per tal de millorar el mètode de microplaques, es va idear el **dispositiu de Calgary** [75] (Figura 8A), que consisteix a afegir a la tapa de la placa unes puntes (PEGS) que encaixen dins dels pous. En aquestes puntes és on es formarà el biofilm, evitant així el problema de la sedimentació i els rentats. No obstant això, aquest mètode té molts dels problemes del mètode anterior, ja que en cap dels dos casos permet una visualització del biofilm amb el microscopi. A més, en el dispositiu de Calgary es requereix desenganxar el biofilm format en les puntes per a poder-lo quantificar, i això dóna molta variabilitat en els experiments, ja que hi ha molta agregació i no sempre es pot arribar a desenganxar la totalitat del biofilm [58, 74].

Un altre mètode de formació de biofilms *in vitro*, dissenyat especialment per l'estudi de biofilms en estadis de desenvolupament primaris és el "**Biofilm Ring Test"** (Figura 8B). Es basa en la capacitat que té el bacteri d'immobilitzar perles magnètiques en formar el biofilm. Es barreja la suspensió de bacteris amb les perles en els pous de la microplaca i es mesura la mobilitat de les perles magnètiques amb un imant. Per tant, com menys es mouen les perles, més biofilm s'ha format. Els avantatges d'aquest mètode són que no requereix rentats ni tincions per mesurar i que es poden fer diverses mesures en el temps i no només al final, però igual que els altres dos mètodes mencionats anteriorment, no dóna informació de l'estructura ni mesura del gruix del biofilm [76].

Un altre sistema que permet reproduir millor que els altres l'heterogeneïtat existent en el biofilm per la difusió limitada d'oxigen és el model "**Alginate beads**", que consisteix a fer créixer els bacteris en unes boles d'alginat d'aproximadament 20 µm de diàmetre que mimetitzen la matriu extracel·lular del biofilm. Els clústers de bacteris que es formen són similars als agregats presents en els biofilms de malalts de FQ o en les ferides cròniques. Aquest model, a més, permet la visualització directament al microscopi i és un bon sistema per a estudiar la diversitat fenotípica existent en un biofilm a causa de l'heterogeneïtat i veure com això influencia en la resistència antibiòtica, però té

limitacions, ja que no permet estudiar la formació dels components de la matriu extracel·lular del biofilm [77]. També hi ha d'altres sistemes que mimetitzen els **biofilms en ferides cròniques**, amb un medi ric en el qual s'afegeix plasma boví i sang de cavall, anomenat "*wound-like media, WLM*" [58, 78].

Els dispositius fins ara explicats es consideren "**dispositius estàtics**", ja que es basen en models tancats, amb uns nutrients limitats. Els "**dispositius dinàmics**", en canvi, són dispositius on contínuament hi ha un subministrament de medi al biofilm, i això fa que el creixement es pugui considerar més semblant a la infecció que es dóna al cos humà, ja que proporcionen un *shear stress* (força mecànica que exerceix el medi) que mimetitza les condicions *in vivo*, com per exemple les que es donen en les vies respiratòries [58, 79].

El **dispositiu de Robbins** [80] (Figura 8C), el "**drip-flow reactor**" [81] i altres **reactors** com el de **Rotary** [82, 83] són exemples de dispositius dinàmics, en els que una bomba peristàltica fa passar medi contínuament per un sistema de tubs o un reactor, que contenen unes peces de vidre, plàstic o altres materials on els bacteris s'enganxaran i formaran el biofilm. El gran avantatge d'aquests dispositius és que els biofilms estan formats en un continu *shear stress* i que permeten visualitzar el biofilm al microscopi quan ja ha crescut. El problema, però, és que no es pot visualitzar directament, sinó que es necessita treure les peces del sistema, la qual cosa pot afectar el biofilm a causa de la manipulació [74].

Un mètode dinàmic i que també permet la visualització directament del biofilm al microscopi són les "**flow-cells**" [84] (Figura 8E). En aquest sistema, la bomba peristàltica fa passar medi per unes cambres segellades amb un cobreobjectes on es forma el biofilm. Aquestes cambres estan separades, la qual cosa permet fer créixer biofilms de diferents espècies bacterianes al mateix moment. El sistema també conté un mecanisme per a atrapar bombolles que puguin entrar dins del sistema i causar pertorbacions en el biofilm. A més de permetre la visualització del biofilm en diferents temps del creixement sense haver de desmuntar el sistema, aquest mètode permet el reciclatge de les cambres únicament canviant el cobreobjectes i, per aquest motiu, el fa més econòmic. El principal inconvenient són les grans dimensions que suposen tots els tubs i dispositius que conté el sistema, que permet només fer créixer un nombre limitat de biofilms alhora i que requereix una gran despesa de medi de cultiu.

Els **sistemes de microfluídica** per al creixement de biofilms comprenen sistemes a microescala, amb canals on el volum és molt petit. Aquests sistemes, com per exemple el **BioFlux** [85] (Figura 8D), permeten el creixement alhora de molts biofilms i per tant es consideren un sistema d'alt rendiment (*high-throughput*), on els biofilms poden estar exposats a moltes condicions diferents. En concret, el sistema BioFlux consta d'una microplaca on els pous estan connectats per microcanals on creixen els biofilms. Els sistemes de microfluídica són els més prometedors per a poder analitzar l'activitat antibiòtica en laboratoris d'hospitals, ja que són molt versàtils i, gràcies a les seves petites dimensions, no requereixen una despesa de medi gaire elevada. El principal problema d'aquests sistemes és la maquinària necessària i el cost del material, que normalment és molt elevat i no és reciclable. A més en el dispositiu BioFlux la mida dels canals és massa petita per a fer estudis de biofilms madurs [74, 79].

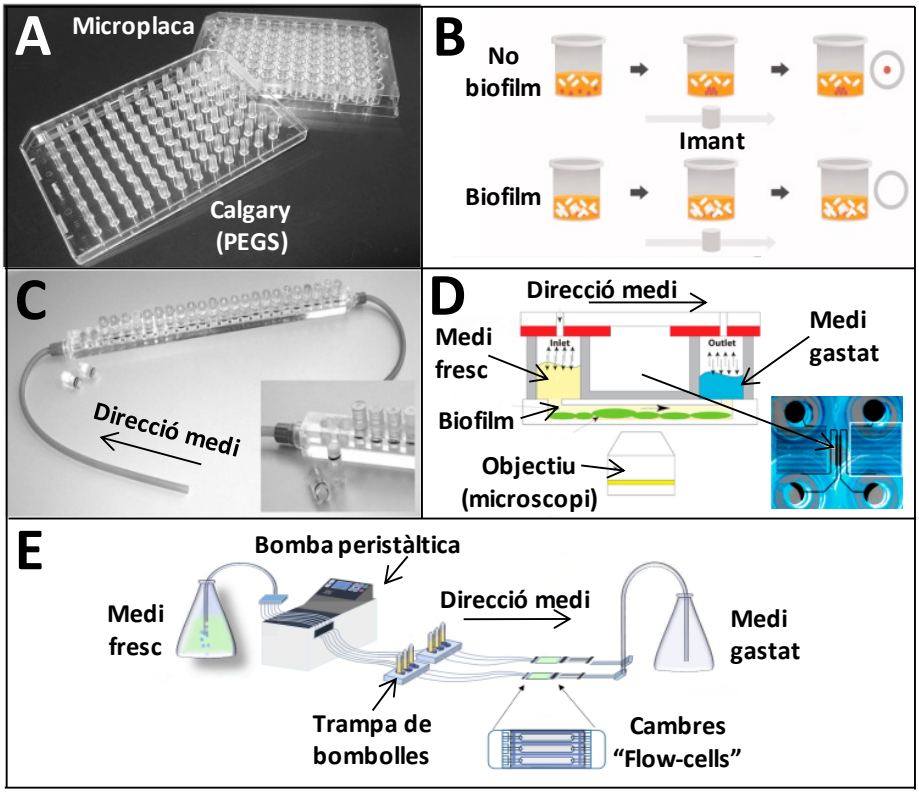

***Figura 8**: Dispositius de formació de biofilm in vitro: A) Microplaques i dispositiu de Calgary, B) Biofilm Ring Test, C) Dispositiu de Robbins, D) Bioflux, E) Sistema de Flow-cells. (Figura modificada de [74, 85, 86]).*

2.2. MÈTODES DE FORMACIÓ DE BIOFILMS *IN VIVO*

Per a estudiar les infeccions *in vivo*, se solen fer servir models animals que mimetitzen les infeccions agudes. En aquestes infeccions, però, l'animal no sol durar més d'un dia viu i per tant no serveixen per a mimetitzar una infecció crònica com és un biofilm [87].

Alguns dels mètodes més utilitzats, que inicialment es van desenvolupar per permetre una infecció crònica, posen els **bacteris embeguts en alguna matriu d'alginat o agarosa** [88] per a aconseguir un creixement del bacteri més lent i prevenir que el sistema immune de l'animal erradiqui la infecció fàcilment. Altres models implanten un **biofilm preformat** en un catèter, un implant [89] o un tub endotraqueal [90]. Aquests sistemes, que s'han provat en diversos animals com rates o ratolins, però, requereixen una cirurgia per implantar les boles o el catèter inoculats amb bacteri que causa una alta mortalitat [91]. Un altre model es basa a **injectar subcutàniament el bacteri** per a aconseguir un abscés que produeix una infecció crònica. Aquest model no necessita procediments d'infecció invasius ni encapsular els bacteris i, en tenir la infecció a la part externa del cos, permet veure l'evolució de la infecció amb tècniques com la bioluminescència [87].

També hi ha models que utilitzen animals amb la mutació del gen CFTR [92], però s'ha vist que, en general, no mimetitzen la malaltia pulmonar que es dóna en els humans malalts de FQ i, per tant, no serveixen per estudiar les infeccions cròniques pulmonars que es donen en aquests malalts [93].

2.3. MÈTODES DE QUANTIFICACIÓ DE LA BIOMASSA I L'ACTIVITAT METABÒLICA DEL BIOFILM

Un mètode de quantificació molt usat en bacteris en creixement planctònic són les **CFU** (*colony-forming units*, unitats formadores de colònies). Aquest mètode consisteix a sembrar una dilució del cultiu que es vulgui quantificar en una placa d'agar i calcular la concentració de bacteris viables en funció de les colònies crescudes a la placa. Aquest mètode és senzill, però no és òptim per a quantificar bacteris creixent en forma de biofilm, ja que requereix desenganxar el biofilm de la superfície on estigui format per a sembrar-lo, procediment que és complicat i que dóna lloc a molta variabilitat, perquè es produeix un grau d'agregació bacteriana molt diferent entre mostres. A més, aquest mètode només detecta la part cultivable del biofilm i no té en compte els bacteris que no formen colònies en l'agar [94].

La tècnica de la **qPCR** (*quantitative polymerase chain reaction*, reacció en cadena de la polimerasa quantitativa) també s'ha fet servir per a quantificar biofilms, però és una tècnica molt costosa pel material que necessita i a més, pot sobreestimar el nombre de cèl·lules presents al biofilm a causa de l'eDNA que forma part de la matriu extracel·lular [95].

Una de les primeres tècniques que es va desenvolupar per quantificar biofilms formats en microplaques és el **cristall violeta** (**CV**), un colorant bàsic que s'uneix a molècules carregades negativament com són la majoria dels EPS i les cèl·lules. Tot i que actualment segueix sent la tècnica més usada per la seva senzillesa, no permet diferenciar entre components dins del biofilm ni entre cèl·lules mortes i vives, a més de ser una tècnica que té molt poca reproductibilitat [96].

Les **sals de tetrazole** (com el **TTC** i l'**XTT**) són uns compostos que es redueixen a formazan quan són metabolitzats per les cèl·lules. Aquesta reacció és colorimètrica i, per tant, permet mesurar l'activitat metabòlica dels bacteris segons la intensitat del color. Aquestes sals es poden fer servir per quantificar l'activitat metabòlica de biofilms, però no permeten comparar entre espècies bacterianes i, a més, són tòxiques pels bacteris, per la qual cosa no permet fer diverses quantificacions en el temps [97]. La **resazurina** és un altre mètode, similar a les sals de tetrazole, per quantificar l'activitat metabòlica del biofilm però amb més sensibilitat. Tot i això, els desavantatges són els mateixos que en les sals de tetrazole [74].

La **impedància elèctrica** és la mesura de la resistència d'un sistema electroquímic a un determinat voltatge. Els sistemes biològics com els biofilms són un sistema electroquímic, i s'ha demostrat que durant la formació d'un biofilm hi ha un canvi en la mesura de la impedància d'aquest biofilm [98]. Per això, hi ha alguns dispositius que permeten quantificar la formació del biofilm a temps real, mesurant la impedància, com per exemple el dispositiu "**xCELLigence**" [99]. Aquest dispositiu, però, a més de ser molt costós econòmicament, només mesura el creixement dels biofilms a la base dels pous de les microplaques, i no a la interfase aire-líquid que és on es forma realment [100].

Els mètodes explicats fins ara, no permeten quantificar components de la matriu extracel·lular del biofilm individualment. Una manera de poder fer-ho és realitzar una anàlisi *ex situ* del biofilm, fent una **extracció dels components**. Aquesta extracció es pot fer amb mètodes físics (ultrasons, ultracentrifugació, liofilització...) o també amb reactius químics (etanol, formaldehid, formamida, hidròxid de sodi, EDTA, glutaraldehid...) [101]. Un cop extrets, els components es poden caracteritzar utilitzant diverses tècniques, com per exemple la microscòpia [102].

L'**AFM** (*atomic force microscopy,* microscopi de forces atòmiques) se sol fer servir per visualitzar components concrets de la matriu extracel·lular, però també permet fer mapes topogràfics a escala nanomètrica, així com mesurar la interacció del biofilm amb la superfície [103]. El **microscopi electrònic de rastreig** (SEM, *scanning electron microscopy*) també permet estudiar la composició del biofilm a alta resolució i veure l'efecte dels antimicrobians en l'estructura. Aquesta tècnica s'acostuma a fer servir per a confirmar els resultats trobats amb altres mètodes de quantificació [74], ja que requereix una deshidratació de la mostra i això fa que es perdi part de l'estructura real. El **CryoSEM** (*scanning electron cryomicroscopy*) i l'**ESEM** (*environmental scanning electron microscopy*) són variants del SEM que no necessiten deshidratació i per tant permeten veure millor l'estructura real, tot i que tenen menys resolució que el SEM [58].

Malgrat no tenir tanta resolució com els microscopis electrònics, els microscopis de fluorescència i sobretot el microscopi confocal són els més usats per visualitzar biofilms. El **microscopi de rastreig làser confocal** (CLSM, *confocal laser scanning microscopy*) dirigeix la il·luminació a un punt concret de la mostra i elimina la llum que prové d'altres plans, permetent fer una reconstrucció tridimensional de la mostra. El microscopi confocal, per tant, permet reconstruir l'estructura del biofilm i visualitzar-lo a temps real, sense processament [104]. Les **tincions específiques** de components de la matriu extracel·lular són una altra tècnica per quantificar els components de la matriu *in situ*. Aquestes tincions es poden fer servir amb els microscopis de fluorescència o confocal i també amb espectrofotòmetres o citometria de flux.

Així, se solen fer servir **lectines** (proteïnes que s'uneixen específicament a polisacàrids) per visualitzar i quantificar els exopolisacàrids de la matriu extracel·lular, com per exemple la **Concavalina A** provinent de la planta *Canavalia ensiformis,* que s'uneix a l'alginat o el **WGA** *(wheat germ aglutinin*) que prové de *Triticum vulgaris* i el **CW** (*calcofluor white*) que s'uneixen al polisacàrid Pel [104, 105]. Pels lípids, s'acostumen a fer servir els tints ***Nile red*** i **DID** [104], i per les proteïnes, una tinció específica és el **SYPRO Ruby** [106]. El **TOTO-1** és un colorant que s'uneix a àcids nucleics i és molt impermeable a l'entrada de les cèl·lules, per això és útil per a la tinció específica de l'eDNA [107].

Per a les cèl·lules bacterianes del biofilm, una bona tècnica de visualització és fer servir bacteris genèticament modificats perquè expressin **proteïnes fluorescents**, com per exemple la **GFP** (*green fluorescent protein*, proteïna de fluorescència verda). Amb les proteïnes fluorescents es pot distingir entre bacteris diferents dins del biofilm i també es pot mirar la mostra a temps real, sense haver de

tenyir-la [84]. Una altra tècnica molt usada per a la tinció de bacteris és el "**Live/dead**", una barreja de dos colorants: el SYTO9 (tenyeix de color verd i travessa les membranes cel·lulars) i el *propidium iòdide* (tenyeix de color vermell i no travessa les membranes cel·lulars), per tant les cèl·lules vives queden tenyides de color verd i les que tenen la membrana danyada queden tenyides de vermell. Aquesta tinció és molt utilitzada, ja que permet fer una distribució espacial dels bacteris viables dins del biofilm, però és important fer servir controls de viabilitat dels bacteris en cada biofilm i no comparar biofilms de diferents espècies entre ells per a no mal interpretar les dades de viu i mort, ja que els tints tenen diferent afinitat segons l'espècie bacteriana i la penetració del làser del microscopi pot ser diferent en cada biofilm [108]. Una altra tècnica de visualització de cèl·lules bacterianes és el **FISH** (*fluorescent in situ hybridization*, hibridació in situ per fluorescència), que permet la identificació de diferents espècies bacterianes dins del biofilm [109].

És necessari, un cop s'han realitzat les imatges al microscopi, fer una anàlisi computacional per a obtenir la quantificació. El software més utilitzat en biofilms és el **COMSTAT** [110], que està dissenyat específicament per a quantificar paràmetres dels biofilms com la biomassa, la rugositat o el gruix a partir d'imatges de microscòpia confocal. Aquestes quantificacions, però, s'han d'acompanyar sempre d'una anàlisi estadística per tal de tenir en compte la variabilitat natural que es produeix en els diferents biofilms [110].

3. NOVES ESTRATÈGIES PER A COMBATRE BIOFILMS

Els antibiòtics són la principal teràpia contra les infeccions bacterianes agudes, però quan les infeccions es tornen cròniques i formen biofilms, aquests mateixos antibiòtics ja no són tan efectius per culpa dels mecanismes de tolerància, persistència i resistència que els bacteris adquireixen en aquestes condicions de creixement. Aquests mecanismes, com la baixa penetrabilitat dels antibiòtics a causa de la matriu extracel·lular produïda pels microorganismes, requeririen dosis d'antibiòtics fins a 1000 vegades superiors a la MIC per a ser efectius, dosis impossibles d'administrar *in vivo* per la toxicitat i pels efectes secundaris que produirien [6]. Tot i que la resistència genètica no és el principal mecanisme de supervivència dels biofilms, diversos estudis han conclòs que l'exposició duradora a antibiòtics que es necessita en el tractament de biofilms estimula el desenvolupament de resistències en els bacteris [111]. Els bacteris multiresistents són una causa emergent de mortalitat i constitueixen un dels problemes sanitaris més greus, a causa de la manca de nous antibiòtics contra els quals no hi hagi resistències conegudes [112, 113].

A més, no hi ha cap antibiòtic desenvolupat específicament per a l'erradicació dels biofilms madurs. Els antimicrobians que podrien ser efectius contra els biofilms haurien de tenir múltiples mètodes d'acció i també múltiples dianes, ja que així seria més difícil que els bacteris adquirissin resistència [114]. Els biofilms polimicrobians tenen una dificultat afegida, ja que necessiten antimicrobians que siguin efectius contra totes les espècies presents. Altrament, també s'haurien d'eliminar els substrats de la matriu extracel·lular i no només els bacteris, ja que els components de la matriu podrien ser reutilitzats per tornar a formar més fàcilment el biofilm un cop l'efecte antimicrobià hagués acabat. Per erradicar els biofilms es requereix, doncs, l'eliminació de la matriu extracel·lular protectora i destruir tant els bacteris residents en ella com els dispersats [115].

Són necessàries, per tant, noves teràpies per a actuar contra els biofilms. Les molècules amb mecanismes d'acció diferents del dels antibiòtics, els enzims que disgreguin la matriu extracel·lular o els nanosistemes poden ser algunes d'aquestes noves teràpies.

3.1.MOLÈCULES ANTI-QUORUM SENSING

Com s'ha descrit en el primer capítol, els sistemes de *Quorum sensing* (QS) dels bacteris són uns sistemes de senyalització que regulen els gens a través de molècules alliberades al medi (autoinductors) en resposta a fluctuacions en la densitat de la població. En els sistemes de QS, les molècules alliberades al medi s'uneixen a un receptor i activen diferents sistemes de senyalització. En els bacteris Gram-negatius, els autoinductors són AHL (*N-acyl homoserine lactones*) i en els Gram-positius són oligopèptids AIP (*autoinducing peptide*). També hi ha les molècules AI-2 (*autoinducer-2*) que estan presents en els dos tipus de bacteris.

Tot i que hi ha molta controvèrsia en la funció específica del QS en la formació, manteniment i dispersió dels biofilms, la prevenció d'aquest sistema de senyalització ha demostrat tenir certs efectes inhibitoris en el biofilm. Per això, les **molècules anti-QS** poden ser un bon tractament per les infeccions cròniques. La inhibició del QS es pot fer a diferents nivells: bloqueig o degradació de l'autoinductor, impediment de la unió de l'autoinductor al receptor o inhibició de la cascada de transducció del senyal [116].

Els bacteris que no poden sintetitzar correctament els autoinductors, com els mutants *lasI* de *P. aeruginosa* i els mutants *cepI* de *B. cepacia,* són defectius en la formació de biofilm [117, 118]. Es va veure, per tant, que **bloquejar o degradar els autoinductors** podien ser bones estratègies antibiofilm. Aquest bloqueig es pot realitzar en el moment de la **síntesi de l'autoinductor**, com en el cas de la molècula cicloleucina, que inhibeix la formació d'AHL actuant contra un dels seus precursors en la formació, la molècula SAM (S-Adenosil metionina) [119]. També es pot donar un **bloqueig directe de l'autoinductor**, com fa el compost baicalina, que bloqueja l'AHL afectant la formació dels biofilms de *B. cenocepacia, Burkholderia multivorans* i *P. aeruginosa*, a més d'incrementar la susceptibilitat d'aquests biofilms a l'antibiòtic tobramicina [120].

Per altra banda, també es pot inhibir el QS pel que fa a l'autoinductor degradant-lo enzimàticament, és el que s'anomena **Quorum quenching (QQ)**. L'estratègia de QQ més utilitzada és la degradació de la molècula AHL i es pot catalitzar amb diferents enzims: les AHL lactonases i les AHL acilases són enzims que hidrolitzen parts de la molècula d'AHL; en canvi, les AHL oxidases i les AHL reductases només modifiquen la seva estructura (Figura 9). Aquests enzims són produïts per moltes espècies diferents de bacteris i també d'organismes eucariotes. Un exemple d'aquests enzims és l'AiiA, una

lactonasa produïda per bacteris del gènere *Bacillus* que actua contra els biofilms de *P. aeruginosa* i *Vibrio cholerae* [114, 121].

Alguns anàlegs de la molècula AHL, en els que l'anell de lactona està canviat per una altra estructura, **inhibeixen el receptor de QS**, ja que competeixen amb l'AHL per unir-s'hi, però no activen posteriorment la cascada de senyalització [122]. També la molècula hamamelitannin, provinent de la planta *Hamamelis virginiana*, sembla que bloqueja el receptor de l'autoinductor i inhibeix la formació de biofilm en *S. aureus*, a més d'incrementar la sensibilitat a l'antibiòtic vancomicina i afectar l'alliberament d'eDNA. El seu mecanisme d'acció específic, però, encara no s'ha validat [123].

El sistema de QS també es pot bloquejar a nivell de la **cascada de transducció del senyal** que es dóna quan l'autoinductor s'uneix al receptor. Per exemple el compost cinamaldehid, que dóna l'aroma típica de la canyella, inhibeix la formació de biofilms de *S. epidermidis* i del gènere *Vibrio* bloquejant la cascada de senyal que produeix l'autoinductor AI-2 en unir-se al receptor [124, 125].

Només amb la inhibició del QS no és possible d'erradicar els biofilms. En combinació amb altres agents antimicrobians, però, les molècules anti-QS poden ser un tractament prometedor. Tot i això, encara no tenim prou coneixements dels mecanismes moleculars d'inhibició d'aquests compostos [116, 126].

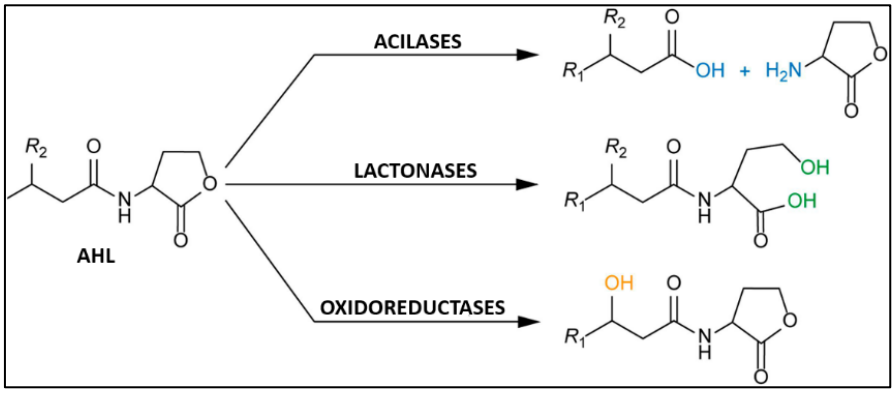

***Figura 9**: Degradació de l'autoinductor AHL amb enzims. (Figura modificada de [127]).*

3.2. PÈPTIDS ANTIMICROBIANS

Els **pèptids antimicrobians (AMP, *antimicrobial peptides*)** són oligopèptids d'entre 5 i 100 aminoàcids que produeixen tots els éssers vius com a part de la resposta immune innata contra virus, bacteris i paràsits [128]. Aquestes proteïnes s'han postulat com a bones alternatives als antibiòtics convencionals, ja que tenen múltiples dianes i actuen principalment destruint les membranes cel·lulars, la qual cosa redueix les probabilitats que els bacteris desenvolupin resistència contra ells [129]. A més, poden actuar contra cèl·lules metabòlicament inactives i s'ha demostrat que tenen sinergia amb alguns antibiòtics [130]. Els AMP són eficaços principalment contra els bacteris en creixement planctònic, però una petita part ha demostrat tenir acció antibiofilm deguda a diferents mecanismes (Figura 10) [130].

El LL-37 és un pèptid antimicrobià produït pels humans que es troba sobretot a les mucoses del cos i que, tot i no tenir gaire activitat contra bacteris en creixement planctònic, és capaç d'inhibir la formació dels biofilms de *P. aeruginosa* i sembla que també d'algunes soques de *S. aureus, S. epidermidis i Burkholderia*, estimulant la **motilitat de les cèl·lules** i repercutint en el **sistema de QS** [131, 132]. D'aquest pèptid se n'han produït sintèticament fragments i modificacions (GF-17, LL-31, LL7-31 i LL7-37, entre d'altres) que milloren la seva activitat i amplien l'espectre d'acció [133].

D'altres AMP han demostrat **interaccionar amb els missatgers secundaris** que controlen la formació del biofilm, com per exemple els pèptids sintètics 1018, DJK-5 i DJK-6, que promouen la degradació del missatger secundari guanosina tetrafosfat (ppGpp) prevenint la formació de biofilm *en P. aeruginosa* [134, 135].

Un altre mètode d'acció dels AMP és la **degradació d'alguns components de la matriu extracel·lular**. Aquest mètode d'acció permet que els mateixos pèptids antimicrobians puguin actuar contra les cèl·lules planctòniques un cop alliberades. El pèptid PI, per exemple, que prové del gènere de paparres *Ixodes*, degrada l'EPS en *Streptococcus mutans* [136]; i l'AMP humà l'hepcidin 20 sembla que destrueix el polisacàrid PIA i a més, s'uneix a l'eDNA impedint la seva acció en *S. epidermidis* [137]. Un altre pèptid que actua contra l'eDNA és la piscidin-3, produïda pel gènere de peixos *Morone*, que s'ha demostrat que destrueix aquest component en la matriu dels biofilms de *P. aeruginosa* [138].

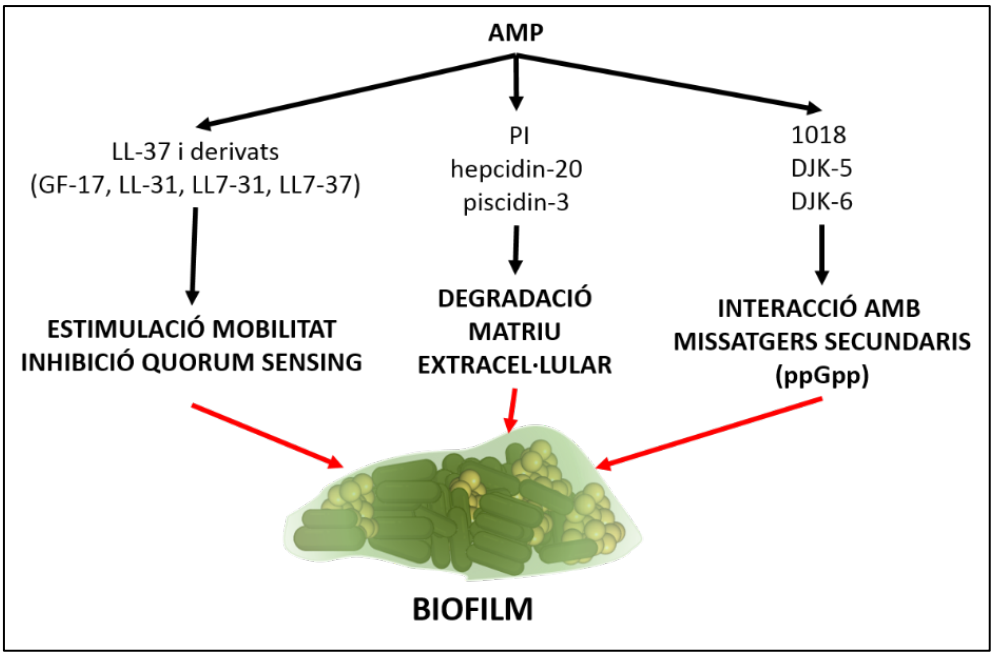

***Figura 10**: Mecanismes antibiofilm dels pèptids antimicrobians.*

Tot i les seves característiques atractives, els AMP tenen alguns desavantatges. El seu **índex terapèutic és baix**, perquè la seva activitat en condicions fisiològiques és més reduïda que *in vitro*. A la concentració terapèutica necessària, doncs, solen tenir un cert nivell de toxicitat. Aquestes proteïnes, a més, tenen tendència a patir **agregació** entre elles i són molt sensibles a **la degradació de les proteases**, la qual cosa disminueix la seva vida mitjana *in vivo* [132]. Totes aquestes limitacions expliquen el fet que molts AMP que semblen prometedors no passin els assajos clínics i la seva aplicació quedi restringida a l'ús tòpic [139]. És per això que es duen a terme estratègies per tal d'incrementar l'estabilitat dels AMP i augmentar la seva vida mitjana, reduint així la dosi necessària i, per tant, els efectes tòxics per a les cèl·lules humanes [132].

3.3. ENZIMS PER A LA DISGREGACIÓ DE LA MATRIU EXTRACEL·LULAR

Com que la principal causa que els antibiòtics no siguin efectius contra el biofilm és la barrera física que proporciona la matriu extracel·lular, una de les possibles estratègies per erradicar els biofilms és atacar aquesta matriu i disgregar-la [133]. Aquesta disgregació incrementa la susceptibilitat al sistema immune de l'hoste i als antimicrobians. Això es deu al fet que la teràpia no ataca directament els bacteris i per tant és més difícil que aquests adquireixin resistències. La disgregació de la matriu, però, sempre ha d'anar acompanyada d'un tractament antimicrobià, ja que s'ha demostrat en experiments *in vivo* amb ratolins que l'alliberació de bacteris que suposa la disgregació de la matriu provoca una dispersió generalitzada que sol acabar amb septicèmia [140]. Un dels mecanismes de disgregació de la matriu extracel·lular és fer servir **enzims que degradin els components principals** que mantenen aquesta matriu unida (eDNA, proteïnes i polisacàrids) (Figura 12)

L'eDNA és un element estructural clau en molts biofilms, i per això l'enzim **desoxiribonucleasa (DNasa)**, que disgrega el DNA, ha resultat ser molt eficaç en dispersar biofilms sense afectar a la viabilitat dels bacteris [32, 141]. La **DNasa I**, que es troba principalment en el pàncrees és la que més s'ha estudiat, i la més utilitzada és la forma bovina, amb estudis que demostren la dispersió d'un gran nombre de biofilms diferents [133]. A més, la DNasa I humana obtinguda de manera recombinant, anomenada "**Dornase alpha**", es fa servir com a teràpia en malalts de FQ, ja que redueix la viscositat de l'esput i ajuda a l'eliminació del moc [142, 143]. Altres formes d'aquesta endonucleasa, que també tenen acció per a dispersar biofilms, són la **streptodornase** provinent dels bacteris del gènere *Steptococcus* [144] o la **NucB**, produïda per *Bacillus licheniformis* [145]. La figura 11 mostra com l'antibiòtic pot penetrar i erradicar un biofilm de *P. aeruginosa* tractat amb DNasa.

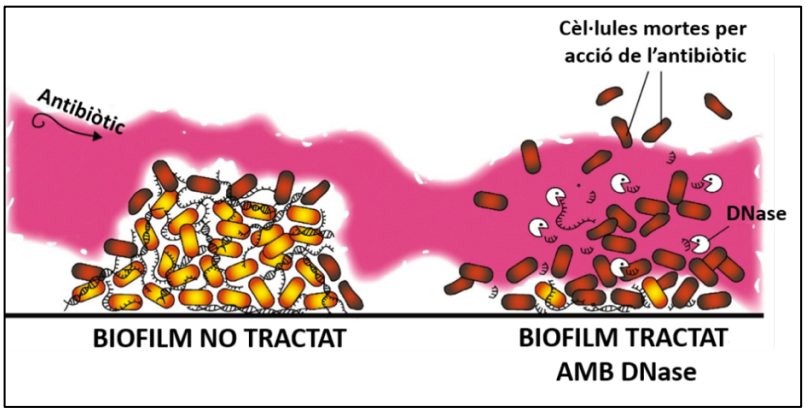

***Figura 11**: Acció d'un antibiòtic en un biofilm de P. aeruginosa no tractat i tractat amb DNasa. (Figura modificada de [146]).*

Les **glucosidases**, els enzims que degraden polisacàrids, també poden tenir un gran efecte en dispersar biofilms, ja que per molts bacteris són un component essencial en la formació de la matriu extracel·lular. En els biofilms de *P. aeruginosa*, per exemple, els enzims que degraden específicament els polisacàrids que constitueixen la seva matriu, com **l'alginat liasa** (que degrada específicament l'alginat) i les hidrolases específiques contra Psl i Pel (**PslGh** i **PelAh** respectivament), són molt efectives en la disrupció d'aquest biofilm [147]. En canvi, altres glucosidases que no són específiques de cap dels components de la matriu extracel·lular que forma *P. aeruginosa*, com la **cel·lulasa** (que hidrolitza l'enllaç β(1,4)) i **l'alfa-amilasa** (que hidrolitza l'enllaç α(1,4)) també disgreguen aquests biofilms, tot i que no són tan efectives [69, 147]. Aquests dos últims enzims, l'alfa amilasa i la cel·lulasa, també poden degradar la matriu extracel·lular dels biofilms de *S. aureus* [69], així com l'enzim **DspB (*Dispersin B*)**, que degrada el PNAG que forma la PIA en la matriu dels biofilms d'aquest gènere de bacteris [148].

Els altres enzims estudiats en la degradació de la matriu extracel·lular dels biofilms són les **proteases**, que degraden les proteïnes presents en aquesta estructura. Algunes de les proteases que resulten ser eficaces en degradar biofilms de *S. aureus*, com són **l'aureolisina** i les cisteïna-proteases **ScpA** i **SscpB,** són produïdes per aquest mateix bacteri [149]. Una altra proteasa molt activa és la **proteïnasa K**, una serina-proteasa que degrada els biofilms produïts per *S. aureus* i *Listeria monocytogenes*, entre altres bacteris [150, 151].

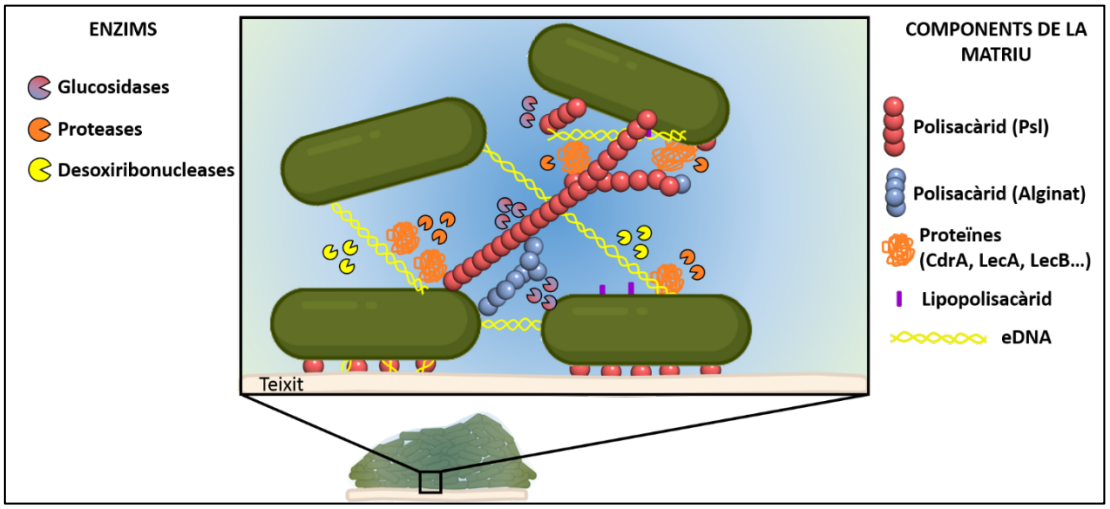

***Figura 12**: Esquema representatiu de la degradació de la matriu extracel·lular del biofilm de P. aeruginosa PAO1 per l'acció d'enzims.*

3.4. NANOSISTEMES

En els últims anys, la nanotecnologia ha proveït de nous materials a escala nanomètrica per a moltes aplicacions en la medicina i la recerca. És el cas dels nanosistemes d'alliberament de fàrmacs com són els liposomes i les nanopartícules. En el tractament de les infeccions microbianes, aquests nanosistemes poden proporcionar molts avantatges envers els antibiòtics convencionals, ja que permeten encapsular diferents molècules antimicrobianes en la mateixa partícula, minimitzant així l'aparició de resistències, a més de vèncer-ne algunes com són les bombes d'expulsió de fàrmacs. En el tractament de biofilms, els nanosistemes poden actuar en diferents estadis del biofilm: poden impedir l'adhesió que inicia el procés de formació del biofilm, poden interaccionar amb la matriu extracel·lular i entrar a l'interior del biofilm o també poden evitar la dispersió i colonització d'altres nínxols. La mida, solubilitat, càrrega i altres factors fisicoquímics permeten dirigir els nanosistemes que contenen el fàrmac al lloc de la infecció, reduint així els efectes secundaris d'aquest. A més, també permeten prolongar l'alliberació del fàrmac en el temps, necessitant una dosi menor d'aquest per a erradicar la infecció [152, 153]. Existeixen una gran quantitat de nanosistemes amb diverses formulacions, en aquest apartat se'n fa una breu descripció dels més utilitzats.

3.4.1. Liposomes

Els **liposomes** són estructures esfèriques formades per una bicapa de fosfolípids que rodeja un espai interior aquós (Figura 13). Són biocompatibles, biodegradables i relativament no tòxics. Aquesta estructura en bicapa els permet transportar tant agents antimicrobians hidròfils (a l'interior aquós) com hidròfobs (en la membrana de fosfolípids) i aquesta encapsulació redueix la toxicitat dels agents a la vegada que millora la seva efectivitat, incrementant així l'índex terapèutic. A més, els liposomes incrementen la concentració intracel·lular dels fàrmacs gràcies a la fusió que es pot donar entre la membrana del bacteri i el liposoma. Els liposomes es poden classificar segons la composició de la bicapa que forma la membrana, la rigidesa o elasticitat d'aquesta, les modificacions en la superfície i la capacitat de desencadenar l'alliberament de l'antimicrobià encapsulat. En el tractament de biofilms, els liposomes que tenen càrrega exterior positiva són més actius perquè interaccionen amb la superfície del biofilm, que normalment té càrrega negativa. També hi ha liposomes equipats amb lectines o anticossos que tenen afinitat amb molècules que es troben a la matriu extracel·lular del biofilm i permeten així dirigir l'agent antimicrobià cap al lloc de la infecció. La mida dels liposomes també és important, ja que s'ha demostrat que la majoria de liposomes estables i efectius en

alliberar l'antimicrobià al lloc de la infecció tenen una mida menor a 500 nm. Els lípids de la bicapa són normalment rígids, amb fosfolípids saturats i més concentració de colesterol [112, 154].

Els **liposomes convencionals** són els que no tenen cap modificació en la superfície i la seva membrana està formada bàsicament per fosfolípids amb colesterol o sense. Existeixen dues formulacions d'aquests liposomes dissenyats per a tractar pacients afectats de FQ, l'**Arikayce®** i el **Lipoquin®**, que carreguen amikacina i ciprofloxacina respectivament [155, 156]. En el cas dels biofilms que es formen en els malalts de FQ, l'encapsulació dels antibiòtics permet obtenir una major concentració en el lloc de la infecció gràcies al fet que l'antibiòtic no s'allibera fins a arribar a les vies respiratòries en forma d'aerosols [154]. S'han dissenyat molts altres liposomes convencionals, amb modificacions en la composició i mida que permeten millorar l'encapsulació, l'alliberació prolongada i l'estabilitat, entre altres beneficis [112].

Uns altres liposomes vàlids per al tractament de la FQ són els **Fluidosomes™**, dissenyats per facilitar la fusió amb les membranes bacterianes. Aquests liposomes encapsulen l'antibiòtic tobramicina i són més fluids gràcies al fet que contenen el lípid fosfatidiletanolamina a la membrana. Tot i que són més inestables, els Fluidosomes™ milloren l'alliberació del fàrmac versus els liposomes convencionals, i han demostrat augmentar l'eficàcia de la tobramicina *in vivo* contra els biofilms de *B. cepacia, Stenotrophomonas maltophilia, P. aeruginosa* i *S. aureus* [157].

Altres variants de liposomes **encapsulen enzims i metalls antimicrobians**. L'encapsulació d'enzims millora la seva acció contra els biofilms, com per exemple els liposomes que encapsulen els enzims cloroperoxidasa, lactoperoxidasa i glucosa oxidasa junts i que inhibeixen el creixement dels biofilms orals de *Streptococcus gordonii* en presència de saliva més efectivament que si s'administren separadament [158]. L'encapsulació conjunta d'antibiòtic amb metalls antimicrobians també s'ha provat com a estratègia antibiofilm. Els liposomes que contenen l'antibiòtic gentamicina i el metall gal·li han demostrat ser més efectius contra els biofilms de *P. aeruginosa* que la gentamicina sola, reduint, a més, la toxicitat del gal·li [159].

Les noves estratègies d'aquests nanosistemes són prometedores. Inclouen liposomes **embeguts en hidrogel** per facilitar la retenció i tractar ferides cròniques, liposomes **adherits a la superfície de partícules sòlides** per a aconseguir un efecte sinèrgic dels dos nanosistemes, o liposomes **adherits a la superfície d'implants ortopèdics** per a impedir la formació de biofilms en aquests dispositius mèdics [154].

Les limitacions que poden tenir els liposomes són la **poca solubilitat**, la **inestabilitat**, les **fugues del fàrmac** i la **baixa capacitat de càrrega**, aspectes que ja s'han millorat canviant i afegint compostos a la formulació. Tanmateix, són necessàries tècniques d'esterilització que no incloguin calor, irradiació ni productes químics, ja que els liposomes són sensibles a les altes temperatures i es poden oxidar i hidrolitzar fàcilment. Per això, se solen esterilitzar per filtració si la seva mida ho permet, amb el risc que puguin quedar partícules virals. Un altre problema és que la fabricació i producció a gran escala són costoses tècnicament i econòmica. Per últim, un altre inconvenient que necessita ser millorat és la **toxicitat a llarg termini**, produïda per l'administració repetida de liposomes catiònics al cos humà [112, 154].

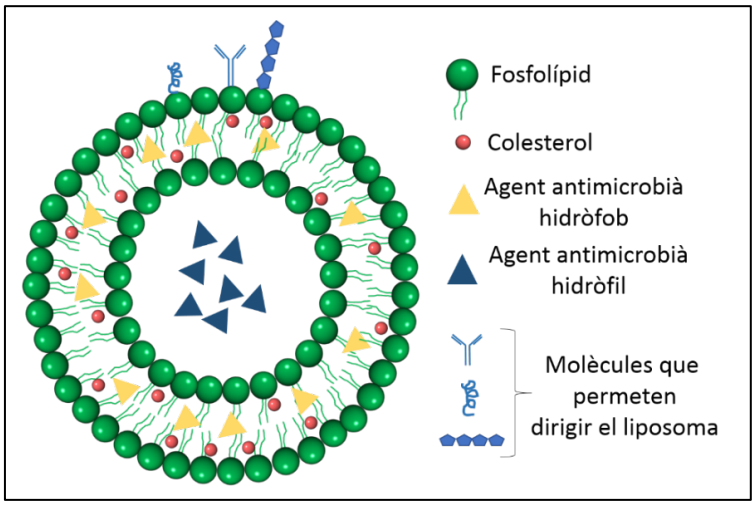

***Figura 13**: Estructura d'un liposoma.*

3.4.2. Nanopartícules orgàniques

Les principals nanopartícules (NP) orgàniques estan formades per polímers. Les **NP polimèriques** són biodegradables, biocompatibles i estables tant en l'ambient fisiològic com en conservació. A més, són fàcils de fabricar a gran escala i la seva degradació es pot controlar amb la modificació de la ràtio dels components, permetent així una alliberació prolongada del fàrmac quan és necessari [160]. Els polímers que formen aquestes NP poden ser naturals o sintètics i poden tenir poder antimicrobià *per se*, com és el cas del **quitosan**, un polímer natural que s'obté a través de la desacetilació de la quitina present en molts artròpodes. També es poden usar polímers artificials per fer NP, els més usats dels quals són el **PLGA** (*poly(lactic-co-glycolic acid)*, àcid poli(làctic-co-glicòlic)) i el **PCL** (*poly(ε-caprolactone),* poli(ε-caprolactona)) [112]. Aquestes NP polimèriques es

poden fabricar amb diferents mètodes i permeten encapsular compostos amb moltes propietats químiques i físiques diferents. A més, han demostrat millorar l'acció dels antibiòtics encapsulats i la majoria dels polímers fan que les NP no siguin gens tòxiques. Un exemple és el fàrmac **Quinsair™**, una formulació de NP de PLGA que encapsulen levofloxacina dissenyada per al tractament d'infeccions en FQ [161]. Per tal de millorar la seva acció antibiofilm, s'han fet algunes modificacions en la superfície de les NP polimèriques amb el procés de **funcionalització** (Figura 14). Un exemple d'això són les funcionalitzacions amb enzims que degraden la matriu extracel·lular. D'aquesta manera, primerament es degrada la matriu, per a després poder alliberar l'antibiòtic a l'interior del biofilm. Les NP de quitosan amb ciprofloxacina i alginat liasa [162] i les NP de PLGA també amb ciprofloxacina i funcionalitzades amb DNasa I [141], han demostrat, per exemple, ser molt eficients en la degradació de biofilms de *P. aeruginosa*, més que no pas amb el tractament de l'enzim i l'antibiòtic per separat.

També hi ha NP orgàniques formades per **lípids**. Aquests poden ser col·loides, compostos per lípids amb alta temperatura de fusió (**SLN*, sòlid lípid-nanoparticles***) (Figura 14) o **micel·les polimèriques** (Figura 14), formades per un copolímer amb una part hidròfila i una hidròfoba com per exemple l'òxid de polipropilè o el polietilenglicol (PEG). Un exemple són les micel·les polimèriques de PEG que encapsulen l'agent antibacterià triclosan. Aquestes són efectives contra els biofilms de *S. aureus,* ja que el fàrmac s'allibera amb la hidròlisi que provoquen les lipases dels mateixos bacteris. A més, aquestes micel·les tenen una part de l'estructura que es protona amb el pH àcid com el que envolta els biofilms, facilitant així l'adherència al lloc de la infecció [163].

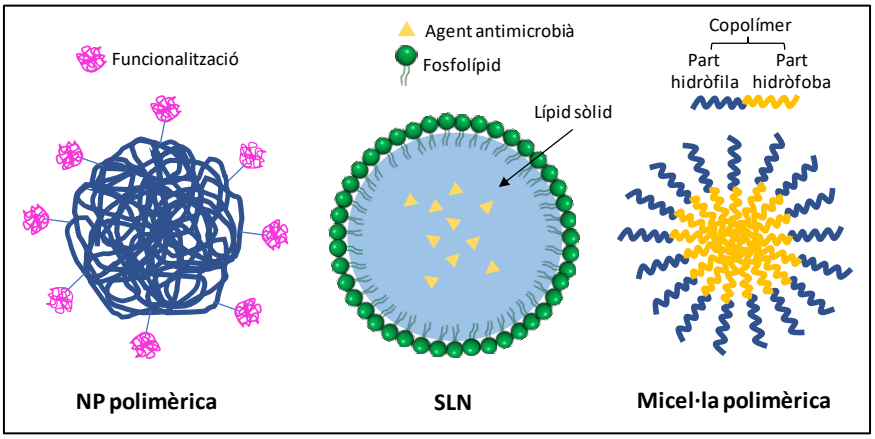

***Figura 14**: Estructura d'una NP polimèrica funcionalitzada, una SLN (solid lípid-nanoparticle) i una micel·la polimèrica.*

3.4.3. Nanopartícules inorgàniques

Les principals NP inorgàniques que s'han provat en la teràpia contra els biofilms estan formades per òxid de zinc (ZnO), plata (Ag) i sílice (SiO_2). Aquestes NP solen ser més petites que les NP orgàniques i els liposomes, amb l'avantatge de tenir una alta ràtio superfície/volum que els permet interaccionar millor amb el biofilm. En alguns casos, les mateixes NP tenen activitat **antimicrobiana *per se***, i no necessiten encapsular fàrmacs per a poder ser utilitzades en la teràpia contra els biofilms. La seva **inestabilitat**, que provoca agregacions de NP, i la seva **possible toxicitat** són els principals problemes d'aquestes nanoestructures [164].

L'**òxid de zinc** té activitat antimicrobiana, ja que danya la membrana dels bacteris, i les NP de ZnO han demostrat inhibir l'establiment del biofilm, tot i que la seva activitat per a erradicar biofilms ja formats no és tan eficaç [165]. La **plata** també és un material molt utilitzat en medicina gràcies a la seva activitat bactericida. En biofilms, les AgNP podrien ser un bon adjuvant als antibiòtics coneguts, ja que el tractament conjunt ha resultat eficaç en l'erradicació d'alguns biofilms en bacteris Gram-positius i Gram-negatius [166]. Les NP de plata també poden ser efectives combinades amb altres NP. És el cas d'unes NP de **sílice mesoporosa** que incorporen AgNP a dins dels porus. Aquestes estructures permeten evitar l'agregació de les AgNP, les quals a més de tenir funció bactericida permeten enllaçar i unir l'enzim DNasa I a la seva superfície i penetrar millor a l'interior dels biofilms (Figura 15) [167].

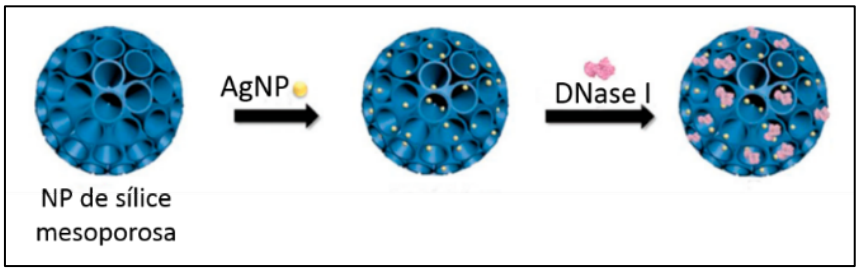

***Figura 15**: NP de sílice mesoporosa amb AgNP i DNasa I. (Figura modificada de[167]).*

3.5.ALTRES ESTRATÈGIES ANTIBIOFILM

A part dels enzims, hi ha d'altres molècules que es poden fer servir com a teràpia per a disgregar la matriu extracel·lular. L'**òxid nítric (NO)** és produït en petites concentracions durant la fase de dispersió en moltes espècies bacterianes, estimulant l'alliberació d'una part dels bacteris per tal de colonitzar un nou nínxol i començar el procés de formació de biofilm. El mecanisme d'acció del NO sembla que involucra, en alguns microorganismes, una disminució dels nivells del missatger secundari diguanilat cíclic (c-di-GMP, *cyclic diguanylate*) i estimula l'activitat de les fosfodiesterases que degraden aquest missatger, tot i que en altres microorganismes com *S. aureus*, el NO actua amb una cascada de senyals independent de c-di-GMP [168, 169]. En concentracions més elevades que les que es produeixen a la fase de dispersió, el NO ha demostrat ser efectiu erradicant biofilms de moltes espècies bacterianes com *P. aeruginosa*, *V. cholerae, B. licheniformis, B. subtilis* i *S. aureus* [168], però si les concentracions són massa altes, poden ser tòxiques pels teixits, ja que aquest gas pot actuar com a immunosupressor i inhibidor de l'angiogènesi, a més de poder anul·lar l'acció dels antibiòtics [170, 171].

Els **bacteriòfags**, virus que infecten específicament bacteris, també s'han postulat com a possible teràpia contra el biofilm. Aquests podrien destruir-lo gràcies al fet que alguns dels enzims que produeixen poden degradar la matriu extracel·lular. Aquests virus també han demostrat tenir sinergia amb alguns antibiòtics i reduir la biomassa de biofilms creats per bacteris multiresistents. Tanmateix, s'ha de tenir en compte que el sistema immune atacarà aquests virus, ja que seran reconeguts com a agents patògens pel cos. A més, el tractament amb aquests virus podria augmentar la transmissió de gens de virulència i resistència antibiòtica entre els bacteris del biofilm [172, 173].

Una altra estratègia que s'ha estudiat és el tractament amb **anticossos** contra elements específics de la matriu extracel·lular del biofilm. N'és un exemple l'anticòs contra la proteïna DNABII, que es troba en molts biofilms i que té la funció de donar integritat estructural a l'eDNA. Aquests anticossos, doncs, desestabilitzen els biofilms i, en combinació amb antibiòtics, han demostrat eficàcia *in vivo* contra biofilms de diferents espècies de bacteris, incloent-hi una *E. coli* uropatògena i un model d'infecció crònica de *P. aeruginosa* en pulmó [115, 174].

Molts **compostos derivats de plantes** tenen propietats antimicrobianes. Els anomenats "**olis essencials**" són bàsicament una mescla de compostos terpenoides i fenòlics que difereixen segons

l'espècie de planta d'on provenen [175]. Aquests compostos solen tenir mecanismes d'acció no específics i que dificulten l'adquisició de resistències. S'ha demostrat que alguns d'aquests olis essencials tenen activitat contra el biofilm, com per exemple l'oli essencial de canyella que inhibeix el sistema de QS gràcies al fet que conté el compost cinamaldehid i els compostos carvacrol i timol, dos terpens purificats dels olis essencials de l'orenga i el timó respectivament que són actius contra els biofilms de *S. aureus* i *L. monocytogenes* [10, 176].

La **mel** és un altre compost natural amb conegudes propietats antimicrobianes, gràcies a la seva baixa activitat hídrica, la seva capacitat de formar radicals hidroxil i el seu baix pH. Molts tipus de mel també han demostrat tenir mecanismes moleculars antibiofilm, reprimint certs gens de virulència i de QS, però no s'han esbrinat completament [172]. És el cas de la mel produïda a partir del nèctar de l'arbust de Manuka (*Leptospermum scoparium*), que es troba sobretot a Nova Zelanda. Aquesta mel conté el reactiu MGO (*methylglyoxal*), un component antibacterià que sembla ser la clau de la seva activitat antibiofilm. La mel de Manuka pot inhibir la formació de biofilm en diferents soques de *S. aureus*, i aquesta mel en combinació amb l'antibiòtic rifampicina ha demostrat eliminar biofilms preformats de la soca MRSA [177].

Una de les estratègies per a erradicar la formació de biofilms en els dispositius mèdics i altres superfícies consisteix a recobrir-los amb un agent antimicrobià. Aquest procediment, però, sol necessitar una quantitat de biocida molt elevada i l'activitat antibiofilm del dispositiu és limitada en el temps. Una alternativa que evita aquests inconvenients, ja que no necessita cap agent antimicrobià, són les **modificacions de superfícies** [115]. La topografia Sharklet™, inspirada en la pell dels taurons, inhibeix la colonització de superfícies i per tant la formació de biofilm en dispositius mèdics per part de *S. aureus* i *S. epidermidis* [178].

Altres tècniques es basen en la degradació del biofilm de manera física, usant magnetisme, fototeràpia i ultrasons. En el primer cas es fan servir **NP metàl·liques** que penetren i disgreguen el biofilm gràcies a l'aplicació d'un camp magnètic. La **fototeràpia** és una tècnica no invasiva, de baix cost i mínim risc de generar resistències que es basa en unes molècules (fotosensibilitzants) que en presència de llum visible i oxigen produeixen espècies reactives d'oxigen (ROS), que generen estrès oxidatiu i degraden la matriu extracel·lular. Per altra banda, els **ultrasons** també indueixen la disgregació del biofilm, facilitant així la penetració dels antibiòtics [179].

OBJECTIUS

Aquest treball es centra en buscar solucions a les infeccions cròniques de bacteris que creixen en forma de biofilm, des de trobar nous fàrmacs i tecnologies antibiofilm fins a desenvolupar nous mètodes d'estudi d'aquests biofilms. Els objectius concrets es llisten a continuació:

1. Determinar l'activitat antimicrobiana i antibiofilm de noves molècules.

2. Desenvolupar una tecnologia que permeti determinar la sensibilitat antibiòtica dels biofilms amb precisió i sense la necessitat d'aparells ni dispositius complexes.

3. Desenvolupar nous sistemes de tractament de biofilms utilitzant enzims disgregadors de la matriu extracel·lular del biofilm i estudiar la seva efectivitat en sistemes d'alliberació de fàrmacs (*drug delivery)* basats en nanopartícules.

4. Optimitzar la formació i anàlisi de biofilms *in vitro* de diferents espècies i soques bacterianes.

ARTICLES

INFORME SOBRE EL FACTOR D'IMPACTE DELS ARTICLES PRESENTATS

Jo, Dr. Eduard Torrents, com a director de la tesi de la Núria Blanco Cabra, declaro que l'estat i el factor d'impacte dels articles publicats en aquesta tesi a data de submissió és el següent:

- L'article 1, titulat "***Pentafluorosulfanyl-containing Triclocarban Analogs with Potent Antimicrobial Activity***" es va publicar a la revista "*Molecules"* al novembre del 2018. El factor d'impacte d'aquesta revista al 2018 era de **3.06** (2n quartil).

- L'article 2, titulat "***Novel Oleanolic and Maslinic Acid Derivatives as a Promising Treatment against Bacterial Biofilm in Nosocomial Infections: An in Vitro and in Vivo Study"*** es va publicar a la revista "*ACS Infectous Diseases*" al juliol del 2019. El factor d'impacte d'aquesta revista al 2019 era de **4.614** (1r quartil i 1r decil).

- L'article 3, titulat "***A new BiofilmChip device as a personalized solution for testing biofilm antibiotic resistance.***" es presenta com a manuscrit.

- L'article 4, titulat "***Characterization of different alginate lyases for dissolving Pseudomonas aeruginosa biofilms***" es va publicar a la revista "*Scientific Reports*" al juny del 2020. L'últim índex d'impacte disponible d'aquesta revista, al 2019, era de **3.998** (1r quartil).

- L'article 5, titulat "***Tobramycin and DNase I dextran-based single-chain nanoparticles interaction with Pseudomonas aeruginosa extracellular biofilm matrix***." es presenta com a manuscrit.

- L'article 6, presentat a l'annex 1, titulat "***Aerobic Vitamin B12 Biosynthesis Is Essential for Pseudomonas aeruginosa Class II Ribonucleotide Reductase Activity During Planktonic and Biofilm Growth***" es va publicar a la revista "*Frontiers in Microbiology*" al maig del 2018. El factor d'impacte d'aquesta revista al 2018 era de **4.259** (1r quartil).

- L'article 7, presentat a l'annex 2, titulat "***Optimal environmental and culture conditions allow the in vitro coexistence of Pseudomonas aeruginosa and Staphylococcus aureus in stable biofilms***" es va publicar a la revista "*Scientific Reports*" al novembre del 2019. El factor d'impacte d'aquesta revista al 2019 era de **3.998** (1r quartil).

Dr. Eduard Torrents Serra

Director de la Tesi

INFORME SOBRE LA PARTICIPACIÓ DE LA DOCTORANDA EN ELS ARTICLES PRESENTATS

Jo, Dr. Eduard Torrents, com a director de la tesi declaro que la participació de la doctoranda Núria Blanco Cabra en els articles presentats en aquesta tesi és la següent:

- Article 1: La Núria comparteix el primer lloc en l'article amb l'Eugènia Pujol. La Núria ha participat activament en tots els experiments d'anàlisi de l'activitat antimicrobiana i antibiofilm dels compostos (Taules 1 i 2, i figures 3 i 4), mentre que l'Eugènia Pujol és la responsable de la síntesi d'aquests compostos (Figures 1 i 2) i ha participat en l'escriptura del manuscrit. Aquest article probablement formarà part de la tesi de l'Eugènia Pujol, parlant únicament de la síntesi química dels compostos.

- Article 2: La Núria és la primera autora de l'article i la responsable de l'escriptura del manuscrit. La Núria ha participat activament en tots els experiments d'anàlisi de l'activitat antimicrobiana i antibiofilm dels compostos (Taules 1, S1 i S2, i figures 1, 2, 3 i 4). La Dra. Marija Vukomanovic ha ajudat en l'anàlisi del SEM i la Laura Moya-Andérico en l'optimització dels experiments de *Galleria mellonella*. Els altres autors són els responsables de la síntesi química dels compostos de l'article. Aquest article també es presenta a la tesi de la Laura Moya-Andérico, on parla única i exclusivament de l'ús de *G. mellonella* com a model *in vivo* d'infeccions.

- Article 3: La Núria comparteix el primer lloc en l'article amb la Dra. Maria José López. La Núria ha participat activament en tots els experiments de l'article i en l'escriptura del manuscrit juntament amb la Dra. Maria José López, que és la responsable del disseny del dispositiu de microfluídica.

- Article 4: La Núria comparteix el primer lloc en l'article amb el Dr. Bernhard Paetzold. La Núria ha participat activament en els experiments de les Figures 4, S3, S4 i Taula S9.

- Article 5: La Núria és la primera autora de l'article i la responsable de l'escriptura del manuscrit. La Núria ha participat activament en tots els experiments de l'article. Els altres autors són els responsables de la síntesi i caracterització de les nanopartícules.

- Article 6: Aquest article es presenta a l'annex, ja que el rol de la Núria en aquest no és tant significatiu com en els altres articles. La Núria ha participat en els experiments de biofilm en continu (Figura 5). Aquest article va formar part de la tesi presentada per la Dra. Anna Crespo al 2017.

- Article 7: Aquest article es presenta a l'annex, ja que el rol de la Núria en aquest no és tant significatiu com en els altres articles. La Núria ha participat en els experiments de biofilm en continu (figures 6 i 7).

A banda dels mencionats, aquests articles no han format part d'altres tesis doctorals.

Dr. Eduard Torrents Serra

Director de la Tesi

ARTICLE 1

Pentafluorosulfanyl-containing Triclocarban Analogs with Potent Antimicrobial Activity

Publicat a la revista *Molecules* (Q2, IF_{2018} = 3.06)

DOI: 10.3390/molecules23112853

Novembre 2018

Autors: Eugènia Pujol [1,#], **Núria Blanco-Cabra** [2,#], Esther Julián [3], Rosana Leiva [1], Eduard Torrents [2,*] i Santiago Vázquez [1,*]

1: Laboratori de Química Farmacèutica (Unitat Associada al CSIC), Facultat de Farmàcia i Ciències de l'Alimentació, and Institute of Biomedicine (IBUB), Universitat de Barcelona

2: Bacterial Infections and Antimicrobial Therapies, Institute for Bioengineering of Catalonia (IBEC)

3: Departament de Genètica i de Microbiologia, Facultat de Biociències, Universitat Autònoma de Barcelona

#: Aquestes coautores han contribuït de manera igualitària en aquest article.

*: Correspondència: Dr. Eduard Torrents (etorrents@ibecbarcelona.eu);
Dr. Santiago Vázquez (svazquez@ub.edu)

El material suplementari (procediment, esquemes de la síntesi i espectroscòpia RMN dels compostos) es pot trobar a la següent pàgina:

https://www.mdpi.com/1420-3049/23/11/2853/s1

molecules

MDPI

Article

Pentafluorosulfanyl-containing Triclocarban Analogs with Potent Antimicrobial Activity

Eugènia Pujol [1,†], Núria Blanco-Cabra [2,†], Esther Julián [3], Rosana Leiva [1], Eduard Torrents [2,*] and Santiago Vázquez [1,*]

1 Laboratori de Química Farmacèutica (Unitat Associada al CSIC), Facultat de Farmàcia i Ciències de l'Alimentació, and Institute of Biomedicine (IBUB), Universitat de Barcelona, Av. Joan XXIII, 27-31, 08028 Barcelona, Spain; epujol@ub.edu (E.P.); rosana.leiva58@gmail.com (R.L.)

2 Bacterial Infections and Antimicrobial Therapies, Institute for Bioengineering of Catalonia (IBEC), The Barcelona Institute of Science and Technology, Baldiri Reixac 15-21, 08028 Barcelona, Spain; nblanco@ibecbarcelona.eu

3 Departament de Genètica i de Microbiologia, Facultat de Biociències, Universitat Autònoma de Barcelona, 08193 Bellaterra, Spain; esther.julian@uab.cat

* Correspondence: etorrents@ibecbarcelona.eu (E.T.); svazquez@ub.edu (S.V.); Tel.: +34-934-034-756 (E.T.); +34-934-024-533 (S.V.)

† These authors contributed equally to this paper.

Academic Editor: Marta Barniol-Xicota
Received: 16 October 2018; Accepted: 26 October 2018; Published: 2 November 2018

Abstract: Concerns have been raised about the long-term accumulating effects of triclocarban, a polychlorinated diarylurea widely used as an antibacterial soap additive, in the environment and in human beings. Indeed, the Food and Drug Administration has recently banned it from personal care products. Herein, we report the synthesis, antibacterial activity and cytotoxicity of novel *N*,*N*′-diarylureas as triclocarban analogs, designed by reducing one or more chlorine atoms of the former and/or replacing them by the novel pentafluorosulfanyl group, a new bioisostere of the trifluoromethyl group, with growing importance in drug discovery. Interestingly, some of these pentafluorosulfanyl-bearing ureas exhibited high potency, broad spectrum of antimicrobial activity against Gram-positive bacterial pathogens, and high selectivity index, while displaying a lower spontaneous mutation frequency than triclocarban. Some lines of evidence suggest a bactericidal mode of action for this family of compounds.

Keywords: antibacterial; Gram-positive; *N*,*N*′-diarylureas; pentafluorosulfanyl; *Staphylococcus aureus*; triclocarban

1. Introduction

The presence of *N*,*N*′-diarylureas in medicinal chemistry is of great importance due to their broad spectrum of biological activities. They have been widely studied in the field of insecticides [1] and infectious diseases such as malaria [2], schistosomiasis and tuberculosis [3,4], immunology [5,6] and oncology [7], among others. Triclocarban (TCC) is a *N*,*N*′-diarylurea commonly used as an antimicrobial agent in personal care products such as bar soaps, deodorants, detergents, and other disinfectants [8]. In recent years, public concerns have been raised regarding its potential toxicological effects in mammals and its environmental accumulation [9–11]. Studies show that, when applied in the skin, this antibacterial is absorbed through it and can even be detected in human plasma, urine, and milk [10–13]. Furthermore, TCC has been recognized as an endocrine disruptor at high concentrations [9,10], resulting in hormonal effects, and more recently, the mechanisms through which it can alter cardiac function have been elucidated [14]. Moreover, it has been reported that

Molecules **2018**, *23*, 2853

TCC is a potent inhibitor of soluble epoxide hydrolase, which may lead to alterations in human physiology [15]. Due to its three chlorine atoms, the biodegradation of TCC is so slow that it can persist in the environment for years [11,14]. Indeed, studies have demonstrated that it accumulates in aquatic habitats [9,13,16–19]. On the basis of the above, the safety of this antimicrobial agent in long-term daily use has not yet been demonstrated. Since 2017, the Food and Drug Administration (FDA) has banned the use of TCC and triclosan, a related antimicrobial agent, in consumer products. Therefore, the development of alternative agents to TCC and triclosan for the use in consumer products is an appealing topic to researchers [20].

The trifluoromethyl group is commonly used in medicinal chemistry as a bioisosteric replacement of chlorine atoms. Therefore, it is not surprising that a few *N*,*N*′-diarylureas containing a trifluoromethyl unit also displayed promising antibacterial activities [1]; this is the case for cloflucarban (TFC, 3-trifluoromethyl-4,4′-dichlorocarbanilide), a trifluoromethyl-substituted diarylurea that shares not only the same spectrum of activity with TCC, but also a similar pattern of absorption, distribution, excretion and toxicity [21–23].

Very recently, a new bioisoster of the trifluoromethyl unit has been introduced in medicinal chemistry: the pentafluorosulfanyl group (SF_5), a relatively new polyfluorinated substituent that has been applied in agro and material chemistry [24,25]. When compared to its isostere trifluoromethyl group, the SF_5-group is considered a "super-trifluoro-methyl group", since it bears advantageous properties, including tetragonal bipyramidal shape, high electronegativity (3.65 vs. 3.36 for the trifluoromethyl group), high lipophilicity, large steric volume (slightly less than that of *tert*-butyl but greater than trifluoromethyl), and confirmed hydrolytic and chemical stability [24,26–31]. Due to its unique properties, the presence of SF_5 in medicinal chemistry has been increasing in the last decade, to the extent that it is nowadays considered to be an extremely attractive substituent in medicinal applications [24–27]. Indeed, a new antimalarial SF_5-containing drug, DSM-265, has recently entered clinical trials [32].

Despite the increasing research around the pentafluorosulfanyl group, little is known about the environmental impact of SF_5-containing molecules [33]. Among the performed studies, it has been shown that the degradation of SF_5-substituted aryl compounds results in environmentally-mild products [34].

Bearing in mind that the presence of SF_5 in this field is increasing in the last few years [24], and that it has a more environmentally-benign profile compared to the chlorine atom, the aim of the present work was to introduce this novel group on the *N*,*N*′-diarylurea scaffold in order to obtain new antimicrobial agents (Figure 1). Herein, we report the design, synthesis, and biological evaluation of novel SF_5-analogs of TCC, which could be a good starting point for a new generation of antibacterial ingredients.

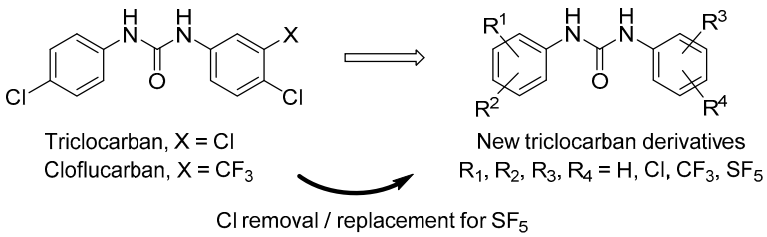

Figure 1. Chemical structures of triclocarban, cloflucarban, and general structure of the new *N*,*N*′-diarylureas presented in this work.

Molecules **2018**, *23*, 2853

2. Results and Discussion

2.1. Chemistry

All the *N*,*N*′-diarylureas were prepared following a quite simple and straightforward procedure, which consisted of the coupling of phenyl isocyanates with the corresponding anilines under three slightly different reaction conditions. In turn, aryl isocyanates were commercially available or formed in situ from their corresponding anilines by reaction with triphosgene in the presence of triethylamine as a base, in an organic solvent such as toluene. Compounds were synthesized in low to moderate yields, since it was observed that dimerization products from the starting aromatic amines were often predominant (Scheme 1 and Figure 2). The structure of these diarylureas was confirmed by IR, ^{1}H, ^{13}C, and ^{19}F NMR, elemental analysis, and/or HRMS (see material and methods section and supplementary materials for further details).

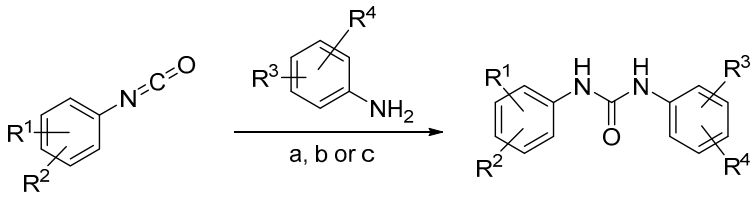

Scheme 1. Synthesis of novel diarylureas. (a) CH_2Cl_2, rt, overnight; (b) pyridine, rt, 1 h; (c) *n*-BuLi, anhydrous THF, −78 °C to rt, overnight. See Figure 2, material and methods section and supplementary materials for details.

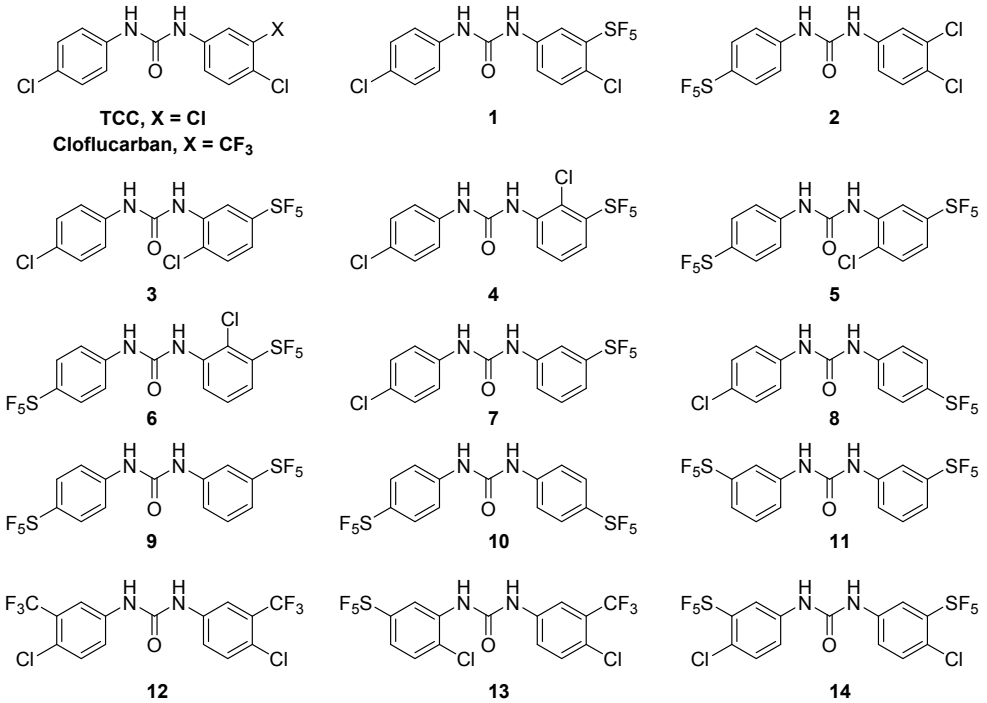

Figure 2. Pentafluorosulfanyl ureas **1**–**14**. Compounds **1** to **6** and **8** are new. Compounds **9**, **11**, **13** and **14** have been recently disclosed by us in a patent application [35]. Compounds **7** [36], **10** [37] and **12** [1] were previously known.

Molecules **2018**, *23*, 2853

2.2. Antibacterial Activity, Selectivity Index and Structure-Activity Relationships

The antibacterial activity of the final compounds against several Gram-positive and Gram-negative bacterial pathogens was evaluated by determination of the minimum inhibitory concentration values (MIC_{50}) (Table 1). To check if these molecules had a safer profile than TCC, and to demonstrate their possible use as topic antibacterial compounds, we next evaluated their toxicity (CC_{50}, cytotoxic concentration 50%) on eukaryotic cells using a macrophages viability measure. In agreement with previous reports, TCC and cloflucarban displayed antibacterial activity in Gram-positive bacteria (Table 1), whereas no activity was detected against Gram-negative pathogens (data not shown) [38]. Similarly, the new analogs synthesized in this work did not show antibacterial activity against the Gram-negative pathogens *P. aeruginosa* and *E. coli* (data not shown). It is worthy of note that while the activity of TCC and cloflucarban in Gram-positive bacteria was restricted to the *Staphylococcus* genera included in this work (*S. aureus*, *S. epidermidis*, and a *S. aureus* methicillin resistant clinical isolate), most of the newly-designed pentafluorosulfanyl derivatives had a broader antimicrobial activity spectrum than TCC and cloflucarban, being active against *Streptococcus mutants* and *Enterococcus faecalis* bacterial strains. Remarkably, although clinical isolates are usually more resistant to antibiotics, the clinical isolate *S. aureus* methicillin resistant (MRSA) showed almost the same antimicrobial sensitivity as the other laboratory strain, indicating no mechanisms of resistance to these compounds in this clinical isolate (Table 1).

Table 1. MIC_{50}, cytotoxicity and selectivity index (SI) of compounds **1–14**.[a]

Compound	MIC_{50} (μg/mL) [b,c]					CC_{50} (μg/mL) [d]
	S. aureus	*S. aureus MRSA*	*S. epidermis*	*S. mutants*	*E. faecalis*	
TCC	0.5 (29)	0.5 (29)	0.5 (29)	NA [e]	NA	14.5
TFC	0.5 (27.4)	0.5 (27.4)	0.5 (27.4)	NA	>20	13.7
1	1 (4.8)	1 (4.8)	1 (4.8)	5	1 (4.8)	4.8
2	1 (4.8)	1 (4.8)	1 (4.8)	5	1 (4.8)	4.8
3	0.5 (110)	0.5 (110)	1 (55)	NA	NA	55
4	0.5 (56)	0.5 (56)	0.5 (56)	NA	5	28
5	0.5 (10.2)	0.5 (10.2)	0.5 (10.2)	0.5 (10.2)	0.5 (10.2)	5.6
6	0.5 (8.4)	0.5 (8.4)	0.5 (8.4)	0.5 (8.4)	0.5 (8.4)	4.2
7	0.5 (26.2)	0.5 (26.2)	0.5 (26.2)	>20	5	13.1
8	0.5 (26)	0.5 (26)	0.5 (26)	NA	0.5 (26)	13
9	0.5 (25)	0.5 (25)	0.5 (25)	0.5 (25)	0.5 (25)	12.5
10	0.05 (412)	0.05 (412)	0.5 (41.2)	0.5 (41.2)	0.5 (41.2)	20.6
11	0.5 (67)	0.5 (67)	0.5 (67)	0.5 (67)	>10	33.5
12	0.5 (67.6)	0.3 (112.7)	0.5 (67.6)	2 (16.9)	2 (16.9)	33.8
13	0.5 (49.2)	0.5 (49.2)	0.5 (49.2)	0.5 (49.2)	0.5 (49.2)	24.6
14	0.5 (20)	0.5 (20)	0.5 (20)	0.5 (20)	0.5 (20)	10

[a] For each tested compound, MIC_{50} values are represented in the first row, whereas SI values are indicated in brackets. [b] MIC_{50} values were determined against the following Gram-positive bacterial strains: *Staphylococcus aureus* (ATCC 12600); *Staphylococcus aureus methyciline resistant*; *Staphylococcus epidermis* (ATCC 1798); *Streptococcus mutants* (ATCC 25175); *Enterococcus faecalis* (ATCC 19433). [c] All the compounds were inactive against two Gram-negative bacterial strains: *Escherichia coli* (ATCC 700926) and *Pseudomonas aeruginosa* (ATCC 15692). [d] CC_{50} values were determined against murine macrophages cells (J-774A.1). [e] NA, no antibacterial activity detected (MIC_{50} > 100 μg/mL).

Taking into account the very similar activities and cytotoxicities of TCC and cloflucarban, we first synthesized pentafluorosulfanyl analog **1**, that maintained the potency of the parent compounds against the *Staphylococcus* genera, and was additionally active against *S. mutants* and *E. faecalis* bacterial strains. However, **1** was more cytotoxic than TCC and cloflucarban, resulting in lower selectivity indexes. A similar trend was observed with compound **2**. Notwithstanding, the cytotoxicity does not seem to be directly related with the introduction of the SF_5 group, since two isomers of **1**, ureas **3** and **4**, were less cytotoxic, although they were not active against *S. mutants* and *E. faecalis*. Further replacement of the Cl of the left-hand ring in **3** and **4** for SF_5, as in **5** and **6**, respectively, restored the activity against *S. mutants* and *E. faecalis* but, again, in line with an increase in cytotoxicity.

Molecules **2018**, *23*, 2853

While these initial results showed that the replacement of a chlorine atom for the pentafluorosulfanyl group was indeed a promising approach, the higher cytotoxicity of several of these novel derivatives remained as a worrying issue. Hence, we next evaluated the removal of a chlorine atom of the aforementioned compounds. Ureas **7** and **8**, conceptually generated by the removal of a chlorine atom in **1** and **2**, respectively, were endowed with very similar antimicrobial activities and cytotoxicities than TCC. Finally, replacement of the remaining chlorine atom in **7** by a second pentafluorosulfanyl group led to **9**, a compound with similar cytotoxicity than TCC but with broader spectrum of action. Similarly, moving from **8** to **10** gave rise to a very promising compound, active against the five Gram-positive bacterial strains studied and with selectivity indexes of up to 412. Isomer **11**, although being also an interesting compound, was less potent than **10**.

Finally, starting from cloflucarban, we briefly evaluated the introduction of a fourth electron withdrawing group. The three evaluated compounds, **12**–**14**, were active against the five Gram-positive bacterial strains with cytotoxicities similar or slightly better than those of TCC and cloflucarban. Overall, it seems that the introduction of a fourth electron withdrawing group is not worthwhile.

2.3. Diarylureas Show a Bacteriolytic Mode of Action

To better understand how the different compounds affect the viability of *S. aureus*, bacterial cells were stained using the Live/Dead viability test and visualized under the fluorescent microscope. This experiment allows us to observe the membrane integrity, since Syto9 green only labels bacterial DNA if the cells are viable and propidium iodide can only enter bacteria cells with a damaged membrane, staining the whole cell red.

Treatment of bacterial cells during 4 h with TCC and novel compounds **3**, **5**, **6** and **9**–**13**, increased the proportion of non-viable cells and diminished the total cells, particularly with compounds **3**, **5**, **6** and **12**, suggesting a bacteriolytic mode of action for this chemical family of compounds (Figure 3A).

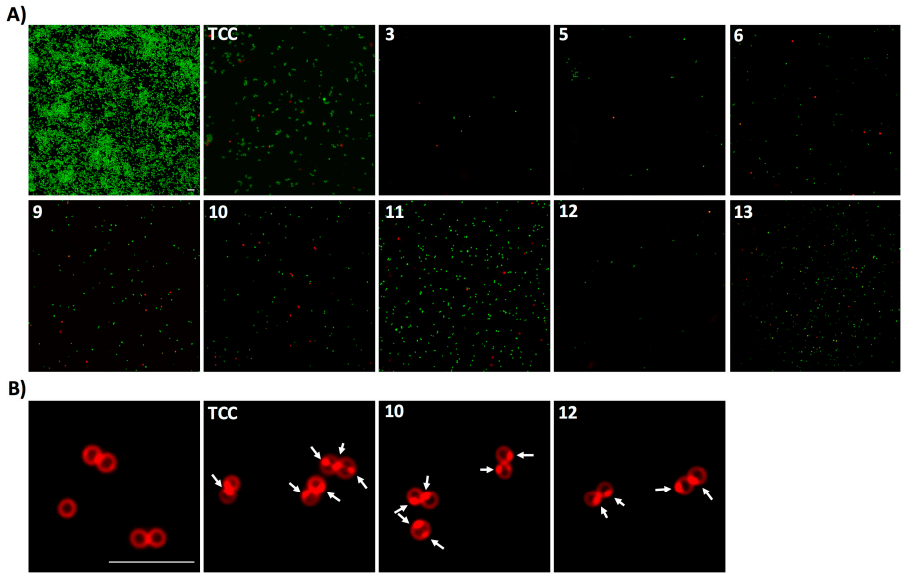

Figure 3. (**A**) Live/Dead analysis of *S. aureus*. Green fluorescence indicates live cells, and red fluorescence suggests dead cells. (**B**) Membrane damage analysis by FM 4-46 staining. Scale bar correspond to 5 μm.

Additionally, we microscopically visualized the changes in bacterial cell integrity by label plasma membrane of living cells using the vital stain FM 4-64 (Figure 3B). Staining the untreated cells resulted

Molecules **2018**, *23*, 2853

in uniform membrane accumulations. On the other hand, cells treated with TCC and compounds **10** and **12** resulted in stained membrane blebs, possibly originating from severe membrane deformations, which is an indication that the primary antibacterial mode of action of these compounds may involve membrane damage.

2.4. Antimicrobial Activity of the New Diarylureas on Removal of Biofilms in Catheters and on Disinfection on Contaminated Surfaces

Given that TCC is widely used as an antimicrobial agent in personal care products (soaps, deodorants, detergents, and others), we tested the capacity of TCC derivatives in disinfecting a contaminated surface area. As shown in Figure 4A, compounds **9**, **10**, **12** and **13** have substantial capacity to remove a contaminated glass area at the same level as TCC, indicating the same capacity of these new compounds to be used as a disinfectant.

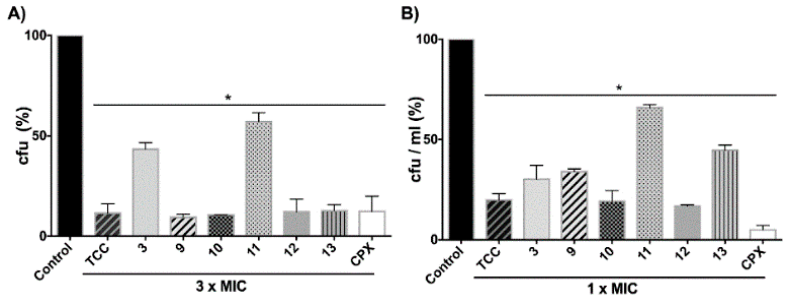

Figure 4. (**A**) Antibacterial effect of compounds on disinfection of contaminated surfaces by *S. aureus* and (**B**) on biofilms growing on catheters. * indicates statistically significant difference to the control (untreated) experiment (p-value < 0.05 in pairwise t-test calculated with GraphPad 6.0). CPX was used as a control in all antimicrobial experiments, with a MIC_{50} of 0.5 μg/mL against all the bacteria pathogens tested. cfu, colony-forming unit.

Furthermore, *S. aureus* is one of the leading causes of catheter-related bacteremia due to the colonization of surgical devices in hospitals by a biofilm form of growth. For that reason, it is highly important to develop protocols and new methodologies to treat and remove pre-existing biofilms in medical devices, especially in catheters. Hence, we studied whether the selected compounds were active in terms of removing biofilms formed in a catheter mode of infection by this bacteria, and we compared the results with TCC and the antibiotic ciprofloxacin (CPX), which is endowed with potent anti-biofilm activity. It is worth noting that compounds **10** and **12** showed the same percentage of biofilm removing capacity in catheters than TCC, whereas the reduction produced by these compounds is similar to the reduction of biofilm due to the treatment with ciprofloxacin (Figure 4B).

2.5. New Compounds Show Less Spontaneous Mutation Rates Compared to TCC

Increasing resistance to antimicrobials is an enormous problem for our society. For this reason, during the development of new antimicrobials, it is common to assess the frequency of spontaneous, resistant mutants within a bacterial population to warrant that this is not a serious issue that compromises further development [39]. We therefore studied the spontaneous mutation rates of *S. aureus* induced by TCC and selected diarylureas as described in the materials and methods section. As indicated in Table 2, TCC had a mutation rate of 4×10^{-9}, similar to that of **12** (5×10^{-10}). Interestingly, compounds **3**, **9**, **10** and **13**, at the same concentration as TCC, showed no induced mutation rates, which indicated the difficulty that such compounds have in inducing any spontaneous resistance in *S. aureus*.

Table 2. Spontaneous mutation rates in *S. aureus* to different diarylureas.

Compound (10 μg/ mL)	Frequency of Mutation
TCC	4×10^{-9}
3	0
9	0
10	0
11	5×10^{-1}
12	5×10^{-10}
13	0

3. Materials and Methods

3.1. Chemical Synthesis

3.1.1. General Methods

Commercially-available reagents and solvents were used without further purification unless stated otherwise. 2-chloro-3-(pentafluoro-λ^6-sulfanyl)aniline, 2-chloro-5-(pentafluoro-λ^6-sulfanyl)aniline and 4-chloro-3-(pentafluoro-λ^6-sulfanyl)aniline were synthesized according to a reported procedure [40]. Preparative normal phase chromatography was performed on a CombiFlash Rf 150 (Teledyne Isco, Lincoln, NE, USA) with pre-packed RediSep Rf silica gel cartridges. Thin-layer chromatography was performed with aluminum-backed sheets with silica gel 60 F_{254} (Merck, Darmstadt, Germany, ref 1.05554), and spots were visualized with UV light and 1% aqueous solution of $KMnO_4$. Melting points were determined in open capillary tubes with a MFB 595010M Gallenkamp. 400 MHz ^{1}H, 100.6 MHz ^{13}C and 376.5 MHz ^{19}F NMR spectra were recorded on a Varian Mercury 400 or on a Bruker 400 Avance III spectrometers. Then, 500 MHz ^{1}H NMR spectra were recorded on a Varian Inova 500 spectrometer. The chemical shifts are reported in ppm (δ scale) relative to internal tetramethylsilane, and coupling constants are reported in Hertz (Hz). Assignments given for the NMR spectra of the compounds have been carried out on the basis of DEPT, COSY ^{1}H/^{1}H (standard procedures), and COSY ^{1}H/^{13}C (gHSQC and gHMBC sequences) experiments. IR spectra were run on Perkin-Elmer Spectrum RX I (Waltham, MA, USA) or Nicolet Avatar 320 FT-IR spectrophotometers. Absorption values are expressed as wave-numbers (cm^{-1}); only significant absorption bands are given. High-resolution mass spectrometry (HRMS) analyses were performed with an LC/MSD TOF Agilent Technologies spectrometer. The elemental analyses were carried out in a Flash 1112 series Thermofinnigan elemental microanalyzator (A5) to determine C, H, N and S. HPLC/MS were determined with a HPLC Thermo Ultimate 3000SD (Thermo Scientific Dionex, Waltham, MA, USA) coupled to a photodiode array detector DAD-3000 (Thermo Scientific Dionex, Waltham, MA, USA) and mass spectrometer LTQ XL ESI-ion trap (Thermo Scientific, Waltham, MA, USA) with Xcalibur v2.2 acquisition software (Thermo Scientific, Waltham, MA, USA) (HPLC-PDA-MS). 5 μL of sample 0.5 mg/mL in methanol were injected, using a ZORBAX Extend-C18 3.5 μm 2.1 × 50 mm column (Agilent, Santa Clara, CA, USA) at 30 °C. The mobile phase was a mixture of A = formic acid 0.05% in water and B = formic acid 0.05% in acetonitrile with the method described as follows: flow 0.6 mL/min, 5% B-95% A 3 min, 100% B 4 min, 95% B-5% A 8 min. Purity is given as % of absorbance at 254 nm; UV-Vis spectra were collected every 0.2 s between 650 and 275 nm; data from mass spectra were analyzed by electrospray ionization in positive mode every 0.3 s between 50 and 1000 Da. The analytical samples of all of the new compounds, which were subjected to pharmacological evaluation, possessed a purity of ≥95%, as evidenced by either their elemental analyses or their HPLC-MS.

3.1.2. General Procedures for the Synthesis of Aryl Isocyanates

A solution of aniline (1 Eq) in toluene (5 or 10 mL) was treated with triphosgene (0.5 Eq). Triethylamine (1 Eq) was immediately added, and the reaction mixture was stirred at 70 °C for 2 h. Afterwards pentane (1 mL) was added, and a white precipitate was formed. The mixture was

filtered and pentane was evaporated under vacuum at room temperature to give the corresponding isocyanate in toluene solution that was used in the next step without further purification.

3.1.3. General Procedure A for the Synthesis of Ureas **2**–**6**

To a solution of the previously-obtained aryl isocyanate was added the substituted aniline in dichloromethane (5 mL). The suspension was stirred at room temperature overnight. Crude ureas were purified by column chromatography or were crystallized in the appropriate solvent.

3.1.4. General Procedure B for the Synthesis of Ureas **1**, **7** and **8**

The commercially-available 4-chlorophenylisocyanate (1 Eq) was added with stirring to a solution of the required pentafluorosulfanylaniline (1 Eq) in pyridine (1.5 or 2 mL). The mixture was allowed to stand at room temperature for 1 h. Afterwards it was poured into water and the precipitate formed was removed by filtration. The final compounds were purified by crystallization from methanol or by column chromatography (hexane/ethyl acetate mixtures).

3.1.5. General Procedure C for the Synthesis of Ureas **9**–**14**

The aniline was dissolved in anhydrous THF (5 or 12 mL) under argon and cooled to −78 °C on a dry ice in acetone bath. Afterwards 2.5 M *n*-butyllithium in hexanes (1.1, 1.2 or 1.3 Eq) was added dropwise. The reaction mixture was then removed from the dry ice in acetone bath and tempered to 0 °C with an ice bath. The appropriate isocyanate, prepared in the previous step or commercially available, was then stirred under argon and continuously added to the reaction mixture. The mixture was stirred at room temperature overnight. Methanol (4 or 5 mL) was added to quench any unreacted *n*-butyllithium. Purification by column chromatography provided the desired diarylureas.

1-(4-Chloro-3-(pentafluoro-λ^6-sulfanyl)phenyl)-3-(4-chlorophenyl) urea **1**. From 4-chlorophenylisocyanate (151 mg, 0.98 mmol) and 4-chloro-3-(pentafluoro-λ^6-sulfanyl)aniline (250 mg, 0.98 mmol) in pyridine (1.5 mL) and following general procedure B, a white solid (280 mg) was obtained. Column chromatography (hexane/ ethyl acetate) furnished urea **1** (66 mg, 17%) as a white solid, mp 222–223 °C. IR (KBr) ν: 412, 503, 569, 599, 654, 678, 752, 789, 811, 824, 854, 864, 891, 926, 1012, 1039, 1093, 1127, 1241, 1284, 1300, 1385, 1401, 1479, 1493, 1546, 1576, 1595, 1650, 3084, 3129, 3182, 3298 cm^{-1}. ^{1}H NMR (400 MHz, DMSO-d_6) δ: 7.34 [m, 2 H, 3′(5′)-H], 7.49 [m, 2 H, 2′(6′)-H], 7.60 (dd, J = 8.8 Hz, J' = 2.0 Hz, 1 H, 6-H), 7.64 (d, J = 8.8 Hz, 1 H, 5-H), 8.38 (d, J = 2.0 Hz, 1 H, 2-H), 9.04 (broad s, 1 H) and 9.30 (broad s, 1 H) (2 NH). ^{13}C NMR (100.6 MHz, CD_3OD) δ: 120.7 (m, CH, C2), 121.9 [CH, C2′(6′)], 122.9 (C, C4), 124.1 (CH, C6), 129.0 (C, C4′), 129.8 [CH, C3′(5′)], 133.9 (CH, C5), 139.0 (C, C1 or C1′), 140.1 (C, C1′ or C1), 154.5 (C, CO). The signal for C3 was not observed. ^{19}F NMR (376.5 MHz, DMSO-d_6) δ: 66.8 (d, J = 152.3 Hz, 4 F, SF_4F), 85.9 (quint, J = 152.3 Hz, 1 F, SF_4F). Anal. calcd for $C_{13}H_9Cl_2F_5N_2OS{\cdot}0.1C_5H_{12}$: C 39.13, H 2.48, N 6.76, S 7.74. Found: C 38.92, H 2.65, N 6.67, S 7.47.

1-(3,4-Dichlorophenyl)-3-(4-pentafluoro-λ^6-sulfanyl)phenyl) urea **2**. From 3,4-dichlorophenylisocyanate (222 mg, 1.18 mmol) in dichloromethane (3 mL) and 4-(pentafluoro-λ^6-sulfanyl)aniline (259 mg, 1.18 mmol) in toluene (3 mL) and following general procedure A, urea **2** (130 mg, 30% yield) was obtained as a white solid. The analytical sample was obtained by crystallization from dichloromethane (119 mg), mp (dichloromethane) 226–227 °C. IR (KBr) ν: 614, 667, 694, 825, 849, 859, 1030, 1104, 1133, 1194, 1234, 1265, 1302, 1325, 1378, 1390, 1412, 1477, 1504, 1545, 1595, 1665, 3116, 3205, 3356 cm^{-1}. ^{1}H NMR (400 MHz, DMSO-d_6) δ: 7.36 (dd, J = 12.0 Hz, J' = 4.0 Hz, 1 H, 6-H), 7.53 (d, J = 12.0 Hz, 1 H, 5-H), 7.65 [m, 2 H, 2′(6′)-H], 7.81 [m, 2 H, 3′(5′)-H], 7.87 (d, J = 4.0 Hz, 1 H, 2-H), 9.13 (broad s, 1 H) and 9.33 (broad s, 1 H) (2 NH). ^{13}C NMR (100.6 MHz, DMSO-d_6) δ: 117.8 [CH, C2′(6′)], 118.7 (CH, C6), 119.6 (CH, C2), 123.6 (C, C4), 126.8 [m, CH, C3′(5′)], 130.6 (CH, C5), 131.1 (C, C3), 139.5 (C, C1), 142.8 (C, C1′), 146.2 (m, C, C4′), 152.0 (C, CO). ^{19}F NMR (376.5 MHz, DMSO-d_6) δ: 65.1 (d, J = 150.8 Hz, 4 F, $S\underline{F}_4F$), 89.2 (quint, J = 150.8 Hz, 1 F, $SF_4\underline{F}$). Anal. calcd for $C_{13}H_9Cl_2F_5N_2OS$: C 38.35, H 2.23, N 6.88, S 7.87. Found: C 38.63, H 2.30, N 6.61, S 7.54.

1-(2-Chloro-5-(pentafluoro-λ^6-sulfanyl)phenyl)-3-(4-chlorophenyl) urea **3**. By following general procedure for the synthesis of aryl isocyanates, 2-chloro-5-(pentafluoro-λ^6-sulfanyl)aniline (300 mg, 1.18 mmol) in toluene (5 mL) was reacted with triphosgene (175 mg, 0.59 mmol) in the presence of triethylamine (0.16 mL, 1.18 mmol) to afford 2-chloro-5-(pentafluoro-λ^6-sulfanyl)phenylisocyanate in toluene solution. From this previously-obtained isocyanate and 4-chloroaniline (151 mg, 1.18 mmol) in dichloromethane (5 mL) and following general procedure A, a white gum (443 mg) was obtained. Column chromatography (hexane/ ethyl acetate) furnished urea **3** (226 mg, 47% overall yield) as a white solid, mp 195–196 °C. IR (KBr) ν: 503, 578, 602, 621, 664, 731, 807, 831, 844, 863, 951, 1015, 1065, 1090, 1234, 1285, 1420, 1461, 1492, 1547, 1591, 1645, 1702, 2848, 2925, 3285, 3325 cm^{-1}. ^{1}H NMR (400 MHz, DMSO-d_6) δ: 7.35 [m, 2 H, 3′(5′)-H], 7.51 [m, 2 H, 2′(6′)-H], 7.54 (dd, *J* = 8.8 Hz, *J*′ = 2.8 Hz, 1 H, 4-H), 7.72 (d, *J* = 8.8 Hz, 1 H, 3-H), 8.84 (d, *J* = 2.8 Hz, 1 H, 6-H), 8.66 (broad s, 1H) and 9.69 (broad s, 1 H) (2 NH). ^{13}C NMR (100.6 MHz, DMSO-d_6) δ: 117.5 (m, CH, C6), 120.0 [CH, C2′(6′)], 120.0 (m, CH, C4), 125.2 (C, C2), 126.1 (C, C4′), 128.8 [CH, C3′(5′)], 129.9 (CH, C3), 136.6 (C, C1), 137.9 (C, C1′), 151.4 (quint, $^2J_{CF}$ = 17.2 Hz, C, C5), 151.9 (C, CO). ^{19}F NMR (376.5 MHz, DMSO-d_6) δ: 63.8 (d, *J* = 151.5 Hz, 4 F, S<u>F</u>$_4$F), 86.7 (quint, *J* = 151.5 Hz, 1 F, SF$_4$<u>F</u>). HRMS-ESI$^+$ *m/z* [M + H]$^+$ calcd for [$C_{13}H_9Cl_2F_5N_2OS$ + H$^+$]: 406.9806, found: 406.9803. HPLC (254 nm): t_R = 4.45 min (100%).

1-(2-Chloro-3-(pentafluoro-λ^6-sulfanyl)phenyl)-3-(4-chlorophenyl) urea **4**. By following general procedure for the synthesis of aryl isocyanates, 2-chloro-3-(pentafluoro-λ^6-sulfanyl)aniline (300 mg, 1.18 mmol) in toluene (5 mL) was reacted with triphosgene (175 mg, 0.59 mmol) in the presence of triethylamine (0.16 mL, 1.18 mmol) to afford 2-chloro-3-(pentafluoro-λ^6-sulfanyl)phenylisocyanate in toluene solution. From this previously-obtained isocyanate and 4-chloroaniline (151 mg, 1.18 mmol) in dichloromethane (5 mL) and following general procedure A, a white solid (194 mg) was obtained. Column chromatography (hexane/ ethyl acetate) gave urea **4** (40 mg, 8% overall yield) as a white solid, mp 218–219 °C. IR (KBr) ν: 605, 652, 711, 729, 779, 799, 810, 840, 849, 875, 931, 1014, 1054, 1089, 1155, 1224, 1250, 1284, 1302, 1398, 1417, 1463, 1493, 1546, 1594, 1663, 1713, 3217, 3305, 3340 cm^{-1}. ^{1}H NMR (400 MHz, DMSO-d_6) δ: 7.36 [m, 2 H, 3′(5′)-H], 7.50 [m, 2 H, 2′(6′)-H], 7.56 (t, *J* = 8.4 Hz, 1 H, 5-H), 7.78 (dd, *J* = 8.4 Hz, *J*′ = 1.2 Hz, 1 H, 4-H), 8.35 (dd, *J* = 8.4 Hz, *J*′ = 1.2 Hz, 1 H, 6-H), 8.65 (broad s, 1 H) and 9.63 (broad s, 1 H) (2 NH). ^{13}C NMR (100.6 MHz, CD_3OD) δ: 121.5 [CH, C2′(6′)], 125.1 (m, CH, C4), 126.5 (CH, C6), 128.0 (CH, C5), 129.0 (C, C2), 129.9 [CH, C3′(5′)], 139.1 (C, C1), 139.5 (C, C1′), 152.7 (m, C, C3), 154.3 (C, CO). ^{19}F NMR (376.5 MHz, DMSO-d_6) δ: 67.7 (d, *J* = 152.3 Hz, 4 F, S<u>F</u>$_4$F), 86.2 (quint, *J* = 152.3 Hz, 1 F, SF$_4$<u>F</u>). Anal. calcd for $C_{13}H_9Cl_2F_5N_2OS$: C 38.35, H 2.23, N 6.88, S 7.87. Found: C 38.71, H 2.36, N 6.63, S 7.60.

1-(2-Chloro-5-(pentafluoro-λ^6-sulfanyl)phenyl)-3-(4-(pentafluoro-λ^6-sulfanyl)phenyl) urea **5**. By following general procedure for the synthesis of aryl isocyanates, 2-chloro-5-(pentafluoro-λ^6-sulfanyl)aniline (500 mg, 1.96 mmol) in toluene (10 mL) was reacted with triphosgene (290 mg, 0.98 mmol) in the presence of triethylamine (0.27 mL, 1.96 mmol) to afford 2-chloro-5-(pentafluoro-λ^6-sulfanyl)phenylisocyanate in toluene solution. From this previously-obtained isocyanate and 4-(pentafluoro-λ^6-sulfanyl)aniline (272 mg, 1.07 mmol) in dichloromethane (5 mL) and following general procedure A, a yellowish gum (443 mg) was obtained. Column chromatography (hexane/ ethyl acetate) gave urea **5** (55 mg, 10% overall yield) as a white solid, mp 224–225 °C. IR (KBr) ν: 582, 598, 647, 665, 723, 805, 828, 848, 860, 949, 1043, 1063, 1105, 1196, 1239, 1272, 1288, 1327, 1419, 1466, 1506, 1522, 1560, 1597, 1618, 1670, 1685, 3094, 3141, 3209, 3383 cm^{-1}. ^{1}H NMR (400 MHz, DMSO-d_6) δ: 7.59 (dd, *J* = 8.8 Hz, *J*′ = 2.8 Hz, 1 H, 4-H), 7.67 [m, 2 H, 2′(6′)-H], 7.75 (d, *J* = 8.8 Hz, 1 H, 3-H), 7.84 [m, 2 H, 3′(5′)-H], 8.82 (d, *J* = 2.8 Hz, 1 H, 6-H), 8.78 (broad s, 1 H) and 10.06 (broad s, 1 H) (2 NH). ^{13}C NMR (100.6 MHz, CD_3OD) δ: 119.0 [CH, C2′(6′)], 119.6 (quint, $^3J_{CF}$ = 5.2 Hz, CH, C6), 121.8 (quint, $^3J_{CF}$ = 4.4 Hz, CH, C4), 126.9 (C, C2), 128.1 [quint, $^3J_{CF}$ = 4.7 Hz, CH, C3′(5′)], 130.6 (CH, C3), 137.6 (C, C1), 143.6 (C, C1′), 149.1 (m, C, C4′ or C5), 153.65 (m, C, C5 or C4′), 153.70 (C, CO). ^{19}F NMR (376.5 MHz, CD_3OD) δ: 63.8 (d, *J* = 150.6 Hz, 4 F, S<u>F</u>$_4$F), 65.1 (d, *J* = 150.6 Hz, 4 F, S<u>F</u>$_4$F),

86.6 (quint, J = 150.6 Hz, 1 F, $SF_4\underline{F}$), 89.0 (quint, J = 150.6 Hz, 1 F, $SF_4\underline{F}$). HRMS-ESI$^-$ m/z $[M - H]^-$ calcd for $[C_{13}H_8ClF_{10}N_2OS_2\text{-}H]^-$: 496.9612, found: 496.9624. HPLC (254 nm): t_R = 4.22 min (100%).

1-(2-Chloro-3-(pentafluoro-λ^6-sulfanyl)phenyl)-3-(4-(pentafluoro-λ^6-sulfanyl)phenyl) urea **6**. By following general procedure for the synthesis of aryl isocyanates, 4-(pentafluoro-λ^6-sulfanyl)aniline (453 mg, 2.06 mmol) in toluene (10 mL) was reacted with triphosgene (306 mg, 1.03 mmol) in the presence of triethylamine (0.29 mL, 2.06 mmol) to afford 4-(pentafluoro-λ^6-sulfanyl)phenylisocyanate in toluene solution. From this previously-obtained isocyanate and 2-chloro-3-(pentafluoro-λ^6-sulfanyl)aniline (285 mg, 1.12 mmol) in dichloromethane (5 mL) and following general procedure A, a white solid (920 mg) was obtained. Column chromatography (hexane/ethyl acetate) gave urea **6** (89.6 mg, 16% overall yield) as a white solid, mp 245–246 °C. IR (KBr) ν: 541, 580, 598, 655, 708, 728, 779, 826, 854, 1054, 1102, 1158, 1195, 1225, 1262, 1301, 1412, 1464, 1506, 1546, 1596, 1668, 3134, 3209, 3341 cm^{-1}. ^{1}H NMR (400 MHz, DMSO-d_6) δ: 7.58 (t, J = 8.4 Hz, 1 H, 5-H), 7.66 [m, 2 H, 2′(6′)-H], 7.78–7.87 [complex signal, 3 H, 4-H, 3′(5′)-H], 8.34 (dd, J = 8.4 Hz, J' = 1.2 Hz, 1 H, 6-H), 8.80 (broad s, 1 H) and 9.99 (broad s, 1 H) (2 NH). ^{13}C NMR (100.6 MHz, CD_3OD) δ: 119.0 [CH, C2′(6′)], 125.3 (quint, $^3J_{CF}$ = 5.2 Hz, CH, C4), 126.7 (CH, C6), 128.0–128.1 [complex signal, 1 C and 3 CH, C2, C5 and C3′(5′)], 139.2 (C, C1), 143.7 (C, C1′), 149.1 (m, C, C4′ or C3), 153.0 (m, C, C3 or C4′), 153.9 (C, CO). ^{19}F NMR (376.5 MHz, DMSO-d_6) δ: 65.1 (d, J = 150.6 Hz, 4 F, $S\underline{F}_4F$), 67.7 (d, J = 152.7 Hz, 4 F, $S\underline{F}_4F$), 86.1 (quint, J = 152.7 Hz, 1 F, $SF_4\underline{F}$), 89.1 (quint, J = 150.6 Hz, 1 F, $SF_4\underline{F}$). Anal. calcd for $C_{13}H_9ClF_{10}N_2OS$: C 31.30, H 1.82, N 5.62, S 12.86. Found: C 31.30, H 1.82, N 5.31, S 12.61.

1-(4-Chlorophenyl)-3-(3-(pentafluoro-λ^6-sulfanyl)phenyl) urea **7**. From 4-chlorophenylisocyanate (300 mg, 1.95 mmol) and 3-(pentafluoro-λ^6-sulfanyl)aniline (427 mg, 1.95 mmol) in pyridine (2 mL) and following general procedure B, urea **7** (448 mg, 62% yield) was obtained as a pale white solid by crystallization from methanol, mp (methanol) 204–205 °C (reported 203.5-205 °C [36]). IR (KBr) ν: 644, 686, 698, 752, 781, 794, 804, 842, 872, 926, 940, 1013, 1063, 1091, 1115, 1177, 1237, 1288, 1306, 1401, 1422, 1443, 1485, 1558, 1597, 1660, 3069, 3097, 3195, 3318 cm^{-1}. ^{1}H NMR (400 MHz, DMSO-d_6) δ: 7.33 [m, 2 H, 3(5)-H], 7.45–7.59 [complex signal, 5 H, 2(6)-H, 4′-H, 5′-H, 6′-H], 8.23 (t, J = 4.0 Hz, 1 H, 2′-H), 8.95 (broad s, 1 H) and 9.16 (broad s, 1 H) (2 NH). ^{13}C NMR (100.6 MHz, DMSO-d_6) δ: 114.9 (m, CH, C2′), 118.8 (m, CH, C4′), 120.1 [CH, C2(6)], 121.8 (m, CH, C6′), 125.7 (C, C4), 128.5 [CH, C3(5)], 129.6 (CH, C5′), 138.2 (C, C1 or C1′), 140.3 (C, C1′ or C1), 152.3 (C, CO), 153.2 (dquint, $^2J_{CF}$ = 16.1 Hz, C, C3′). ^{19}F NMR (376.5 MHz, DMSO-d_6) δ: 63.6 (d, J = 151.0 Hz, 4 F, $S\underline{F}_4F$), 87.7 (quint, J = 151.0 Hz, 1 F, $SF_4\underline{F}$). Anal. calcd for $C_{13}H_{10}ClF_5N_2OS$: C 41.89, H 2.70, N 7.52, S 8.60. Found: C 42.00, H 2.74, N 7.39, S 8.47.

1-(4-Chlorophenyl)-3-(4-(pentafluoro-λ^6-sulfanyl)phenyl) urea **8**. From 4-chlorophenylisocyanate (300 mg, 1.95 mmol) and 4-(pentafluoro-λ^6-sulfanyl)aniline (427 mg, 1.95 mmol) in pyridine (2 mL) and following general procedure B, urea **8** (580 mg, 80% yield) was obtained as a pale white solid by crystallization from methanol, mp (methanol) 231–232 °C. IR (KBr) ν: 666, 699, 754, 782, 802, 829, 868, 1016, 1090, 1102, 1193, 1216, 1239, 1269, 1300, 1411, 1492, 1504, 1547, 1594, 1610, 1664, 1711, 3086, 3140, 3202, 3324 cm^{-1}. ^{1}H NMR (400 MHz, DMSO-d_6) δ: 7.34 [m, 2 H, 3(5)-H], 7.50 [m, 2 H, 2(6)-H], 7.64 [d, J = 8.0 Hz, 2 H, 2′(6′)-H], 7.80 [m, 2 H, 3′(5′)-H], 8.96 (broad s, 1 H) and 9.22 (broad s, 1 H) (2 NH). ^{13}C NMR (100.6 MHz, DMSO-d_6) δ: 117.6 [CH, C2′(6′)], 120.1 [CH, C2(6)], 125.9 (C, C4), 126.8 [quint, $^3J_{CF}$ = 4.02 Hz, CH, C3′(5′)], 128.7 [CH, C3(5)], 138.2 (C, C1), 143.0 (C, C1′), 146.1 (dquint, $^2J_{CF}$ = 16.1 Hz, C, C4′), 152.1 (C, CO). ^{19}F NMR (376.5 MHz, DMSO-d_6) δ: 65.2 (d, J = 150.8 Hz, 4 F, $S\underline{F}_4F$), 89.3 (quint, J = 150.8 Hz, 1 F, $SF_4\underline{F}$). Anal. calcd for $C_{13}H_{10}ClF_5N_2OS$: C 41.89, H 2.70, N 7.52, S 8.60. Found: C 42.03, H 2.89, N 7.41, S 8.55.

1-(3-(Pentafluoro-λ^6-sulfanyl)phenyl)-3-(4-(pentafluoro-λ^6-sulfanyl)phenyl) urea **9**. By following general procedure for the synthesis of aryl isocyanates, 3-(pentafluoro-λ^6-sulfanyl)aniline (350 mg, 1.60 mmol) in toluene (5 mL) was reacted with triphosgene (237 mg, 0.80 mmol) in the presence of triethylamine (0.22 mL, 1.60 mmol) to afford 3-(pentafluoro-λ^6-sulfanyl)phenylisocyanate in toluene solution. From this previously-obtained isocyanate, 4-(pentafluoro-λ^6-sulfanyl)aniline (246 mg, 1.12 mmol) in

anhydrous THF (5 mL) and 2.5 M *n*-butyllithium in hexanes (0.6 mL, 1.46 mmol) and following general procedure C, a brown gum (742 mg) was obtained after quenching any unreacted *n*-butyllithium with methanol (5 mL). Column chromatography (hexane/ ethyl acetate) gave urea **9** (102 mg, 52% overall yield) as a pale white solid, mp 216–217 °C [35]. IR (KBr) ν: 1103, 1196, 1229, 1304, 1410, 1487, 1549, 1597, 1665, 3088, 3134, 3204, 3321 cm^{-1}. ^1H NMR (400 MHz, DMSO-d_6) δ: 7.48–7.57 (complex signal, 2 H, 4-H, 5-H), 7.58 (dt, J = 8.0 Hz, J' = 2.0 Hz, 1 H, 6-H), 7.67 [m, 2 H, 2′(6′)-H], 7.81 [m, 2 H, 3′(5′)-H], 8.24 (m, 1 H, 2-H), 9.27 (broad s, 1 H) and 9.34 (broad s, 1 H) (2 NH). ^{13}C NMR (100.6 MHz, DMSO-d_6) δ: 115.3 (m, CH, C2), 117.9 [CH, C2′(6′)], 119.2 (m, CH, C4), 122.1 (CH, C6), 126.8 [m, CH, C3′(5′)], 129.7 (CH, C5), 140.1 (C, C1), 142.8 (C, C1′), 146.3 (dquint, $^2J_{CF}$ = 16.1 Hz, C, C4′), 152.2 (C, CO), 153.2 (dquint, $^2J_{CF}$ = 16.1 Hz, C, C3). ^{19}F NMR (376.5 MHz, DMSO-d_6) δ: 63.6 (d, J = 150.4 Hz, 4 F, S$\underline{F}_4$F), 65.1 (d, J = 151.0 Hz, 4 F, S$\underline{F}_4$F), 87.6 (quint, J = 150.4 Hz, 1 F, $SF_4\underline{F}$), 89.2 (quint, J = 151.0, 1 F, $SF_4\underline{F}$). HRMS-ESI$^-$ m/z [M − H]$^-$ calcd for $[C_{13}H_{10}F_{10}N_2OS_2\text{-}H]^-$: 463.0002, found: 463.0017. HPLC (254 nm): t_R = 4.04 min (100%).

1,3-bis(4-(Pentafluoro-λ^6-sulfanyl)phenyl) urea **10**. By following general procedure for the synthesis of aryl isocyanates, 4-(pentafluoro-λ^6-sulfanyl)aniline (259 mg, 1.18 mmol) in toluene (5 mL) was reacted with triphosgene (175 mg, 0.59 mmol) in the presence of triethylamine (0.16 mL, 1.18 mmol) to afford 4-(pentafluoro-λ^6-sulfanyl)phenylisocyanate in toluene solution. From this previously-obtained isocyanate, 4-(pentafluoro-λ^6-sulfanyl)aniline (235 mg, 1.07 mmol) in anhydrous THF (5 mL) and 2.5 M *n*-butyllithium in hexanes (0.53 mL, 1.28 mmol) and following general procedure C, an orange gum (618 mg) was obtained after quenching any unreacted *n*-butyllithium with methanol (4 mL). Column chromatography (hexane/ethyl acetate) gave urea **10** (120 mg, 24% overall yield) as a white solid, mp 235 °C (dec) (reported 285.9–287.6 °C, followed by immediate decomposition [37]). IR (ATR) ν: 668, 685, 752, 780, 798, 818, 1013, 1100, 1192, 1212, 1245, 1307, 1317, 1358, 1401, 1411, 1504, 1544, 1593, 1659, 1713, 1974, 2010, 2035, 2066, 2846, 2017, 2958, 3205, 3297, 3323 cm^{-1}. ^1H NMR (400 MHz, DMSO-d_6) δ: 7.66 [d, J = 8.8 Hz, 4 H, 2(6)-H], 7.82 [m, 4 H, 3(5)-H], 9.37 (broad s, 2 H, NH). ^{13}C NMR (100.6 MHz, DMSO-d_6) δ: 117.8 [CH, C2(6)], 126.8 [m, CH, C3(5)], 142.7 (C, C1), 146.4 (quint, $^2J_{CF}$ = 16.1 Hz, C, C4), 152.0 (C, CO). ^{19}F NMR (376.5 MHz, DMSO-d_6) δ: 65.1 (d, J = 150.4 Hz, 4 F, S$\underline{F}_4$F), 89.1 (quint, J = 150.4 Hz, 1 F, $SF_4\underline{F}$). Anal. calcd for $C_{13}H_{10}F_{10}N_2OS_2 \cdot 0.65C_5H_{12}$: C 38.18, H 3.51, N 5.48, S 12.54. Found: C 38.56, H 3.19, N 5.48, S 12.17.

1,3-bis(3-(Pentafluoro-λ^6-sulfanyl)phenyl) urea **11**. By following general procedure for the synthesis of aryl isocyanates, 3-(pentafluoro-λ^6-sulfanyl)aniline (350 mg, 1.60 mmol) in toluene (5 mL) was reacted with triphosgene (237 mg, 0.80 mmol) in the presence of triethylamine (0.22 mL, 1.60 mmol) to afford 3-(pentafluoro-λ^6-sulfanyl)phenylisocyanate in toluene solution. From this previously-obtained isocyanate, 3-(pentafluoro-λ^6-sulfanyl)aniline (351 mg, 1.60 mmol) in anhydrous THF (5 mL) and 2.5 M *n*-butyllithium in hexanes (0.86 mL, 2.08 mmol) and following general procedure C, a beige solid (710 mg) was obtained after quenching any unreacted *n*-butyllithium with methanol (4 mL). Column chromatography (hexane/ ethyl acetate) gave urea **11** (183 mg, 49% overall yield) as a pale white solid. The analytical sample was obtained by crystallization from ethyl acetate, mp (ethyl acetate) 267–268 °C [35]. IR (KBr) ν: 1117, 1242, 1314, 1418, 1485, 1599, 1663, 3102, 3202, 3310 cm^{-1}. ^1H NMR (400 MHz, DMSO-d_6) δ: 7.48–7.57 (complex signal, 4 H, 4-H, 5-H), 7.61 (m, 2 H, 6-H), 8.21 (m, 2 H, 2-H), 9.27 (broad s, 2 H, NH). ^{13}C NMR (100.6 MHz, DMSO-d_6) δ: 115.3 (m, CH, C2), 119.2 (m, CH, C4), 122.2 (CH, C6), 129.7 (CH, C5), 140.2 (C, C1), 152.5 (C, CO), 153.2 (quint, $^2J_{CF}$ = 16.1 Hz, C, C3). ^{19}F NMR (376.5 MHz, DMSO-d_6) δ: 63.6 (d, J = 151.0 Hz, 4 F, S$\underline{F}_4$F), 87.6 (quint, J = 151.0 Hz, 1 F, $SF_4\underline{F}$). HRMS-ESI$^-$ m/z [M − H]$^-$ calcd for $[C_{13}H_{10}F_{10}N_2OS_2\text{-}H]^-$: 463.0002, found: 463.0022. HPLC (254 nm): t_R = 4.01 min (100%).

1,3-bis(4-Chloro-3-(trifluoromethyl)phenyl) urea **12**. From the commercially available 4-chloro-3-(trifluoromethyl)phenylisocyanate (261 mg, 1.18 mmol) in anhydrous THF (12 mL), 4-chloro-3-(trifluoromethyl)aniline (209 mg, 1.07 mmol) in anhydrous THF (12 mL) and 2.5 M *n*-butyllithium in hexanes (0.49 mL, 1.18 mmol) and following general procedure C, an orange gum

(468 mg) was obtained after quenching any unreacted *n*-butyllithium with methanol (4 mL). Column chromatography (hexane/ethyl acetate) gave urea **12** (156 mg, 35% overall yield) as a beige solid, mp 231–232 °C (reported 231–232 °C [1]). IR (ATR) ν: 654, 664, 677, 742, 749, 773, 804, 829, 886, 897, 940, 964, 1031, 1057, 1111, 1129, 1168, 1214, 1227, 1263, 1294, 1318, 1405, 1421, 1478, 1529, 1545, 1594, 1659, 1695, 1713, 1842, 1943, 2144, 2211, 2351, 1852, 2919, 3312, 3328, 3607, 3643, 3669, 3695 cm^{-1}. ^1H NMR (400 MHz, DMSO-d_6) δ: 7.61 (d, J = 8.4 Hz, 2 H, 5-H), 7.67 (dd, J = 8.4 Hz, J' = 2.0 Hz, 2 H, 6-H), 8.08 (d, J = 2.0 Hz, 2 H, 2-H), 9.33 (broad s, 2 H, NH). ^{13}C NMR (100.6 MHz, DMSO-d_6) δ: 117.2 (q, $^3J_{CF}$ = 5.9 Hz, CH, C2), 122.79 (q, $^1J_{CF}$ = 273.0 Hz, C, CF_3), 122.80 (q, $^3J_{CF}$ = 1.9 Hz, C, C4), 123.5 (CH, C6), 126.7 (q, $^2J_{CF}$ = 30.6 Hz, C, C3), 132.0 (CH, C5), 138.9 (C, C1), 152.3 (C, CO). ^{19}F NMR (376.5 MHz, DMSO-d_6) δ: −61.5 (S, 3 F, CF_3). HRMS-ESI$^-$ m/z $[M - H]^-$ calcd for $[C_{15}H_8Cl_2F_6N_2O\text{-}H]^-$: 414.9845, found: 414.9839. HPLC (254 nm): t_R = 3.52 min (100%).

1-(4-Chloro-3-(trifluoromethyl)phenyl)-3-(2-chloro-5-(pentafluoro-λ^6-sulfanyl)phenyl) urea **13**. By following general procedure for the synthesis of aryl isocyanates, 2-chloro-5-(pentafluoro-λ^6-sulfanyl)aniline (350 mg, 1.38 mmol) in toluene (5 mL) was reacted with triphosgene (204 mg, 0.69 mmol) in the presence of triethylamine (0.19 mL, 1.38 mmol) to afford 2-chloro-5-(pentafluoro-λ^6-sulfanyl)phenylisocyanate in toluene solution. From this previously-obtained isocyanate, 4-chloro-3-(trifluoromethyl)aniline (296 mg, 1.51 mmol) in anhydrous THF (12 mL) and 2.5 M *n*-butyllithium in hexanes (0.73 mL, 1.78 mmol) and following general procedure C, a brown oil (767 mg) was obtained after quenching any unreacted *n*-butyllithium with methanol (5 mL). Column chromatography (hexane/ethyl acetate) gave urea **13** (138 mg, 22% overall yield) as a white solid, mp 156–157 °C [35]. IR (ATR) ν: 632, 666, 684, 701, 727, 742, 760, 801, 812, 840, 855, 863, 906, 950, 963, 1034, 1065, 1111, 1126, 1175, 1216, 1229, 1260, 1283, 1301, 1329, 1372, 1408, 1459, 1485, 1513, 1546, 1582, 1592, 1608, 1654, 1695, 1715, 1769, 1905, 1925, 2025, 2179, 2323, 2369, 2851, 2917, 2953, 3276, 3328, 3671, 3733, 3795, 3815 cm^{-1}. ^1H NMR (400 MHz, DMSO-d_6) δ: 7.58 (dd, J = 8.8 Hz, J' = 2.4 Hz, 1 H, 4′-H), 7.62–7.71 (complex signal, 2 H, 5-H, 6-H), 7.73 (d, J = 8.8 Hz, 1 H, 3′-H), 8.05 (d, J = 1.2 Hz, 1 H, 2-H), 8.79 (d, J = 2.4 Hz, 1 H, 6′-H), 8.73 (broad s, 1 H) and 10.04 (broad s, 1 H) (2 NH). ^{13}C NMR (100.6 MHz, DMSO-d_6) δ: 116.9 (q, $^3J_{CF}$ = 5.7 Hz, CH, C2), 117.8 (m, CH, C6′), 120.5 (m, CH, C4′), 122.7 (q, $^1J_{CF}$ = 273.0 Hz, C, CF_3), 123.1 (m, C, C4), 123.3 (CH, C6), 125.7 (C, C2′), 126.8 (q, $^2J_{CF}$ = 30.8 Hz, C, C3), 130.0 (CH, C3′), 132.2 (CH, C5), 136.3 (C, C1′), 138.5 (C, C1), 151.4 (m, C, C5′), 152.0 (C, CO). ^{19}F NMR (376.5 MHz, DMSO-d_6) δ: –61.5 (S, 3 F, CF_3), 63.9 (d, J = 151.4 Hz, 4 F, S$\underline{F}_4$F), 86.5 (quint, J = 151.4 Hz, 1 F, $SF_4\underline{F}$). HRMS-ESI$^-$ m/z $[M - H]^-$ calcd for $[C_{14}H_8Cl_2F_8N_2OS\text{-}H]^-$: 472.9534, found: 472.9534. HPLC (254 nm): t_R = 3.63 min (100%).

1,3-bis(4-Chloro-3-(pentafluoro-λ^6-sulfanyl)phenyl) urea **14**. By following general procedure for the synthesis of aryl isocyanates, 4-chloro-3-(pentafluoro-λ^6-sulfanyl)aniline (350 mg, 1.37 mmol) in toluene (5 mL) was reacted with triphosgene (204 mg, 0.69 mmol) in the presence of triethylamine (0.20 mL, 1.37 mmol) to afford 4-chloro-3-(pentafluoro-λ^6-sulfanyl)phenylisocyanate in toluene solution. From this previously-obtained isocyanate, 4-chloro-3-(pentafluoro-λ^6-sulfanyl)aniline (278 mg, 1.09 mmol) in anhydrous THF (5 mL) and 2.5 M *n*-butyllithium in hexanes (0.60 mL, 1.42 mmol) and following general procedure C, an orange gum (675 mg) was obtained after quenching any unreacted *n*-butyllithium with methanol (4 mL). Column chromatography (hexane/ethyl acetate) gave urea **14** (136 mg, 23% overall yield) as a white solid, mp 237–238 °C [35]. IR (ATR) ν: 1042, 1130, 1227, 1290, 1396, 1477, 1545, 1587, 1645, 1699, 3030, 3138, 3306 cm^{-1}. ^1H NMR (400 MHz, DMSO-d_6) δ: 7.64 (d, J = 8.8 Hz, 2 H, 5-H), 7.68 (dd, J = 8.8 Hz, J' = 2.0 Hz, 2 H, 6-H), 8.34 (d, J = 2.0 Hz, 2 H, 2-H), 9.47 (broad s, 2 H, NH). ^{13}C NMR (100.6 MHz, DMSO-d_6) δ: 119.0 (m, CH, C2), 120.4 (C, C4), 123.7 (CH, C6), 133.0 (CH, C5), 138.9 (C, C1), 150.0 (m, C, C3), 152.4 (C, CO). ^{19}F NMR (376.5 MHz, DMSO-d_6) δ: 66.9 (d, J = 152.5 Hz, 4 F, S$\underline{F}_4$F), 85.8 (quint, J = 152.5 Hz, 1 F, $SF_4\underline{F}$). HRMS-ESI$^-$ m/z $[M - H]^-$ calcd for $[C_{13}H_8Cl_2F_{10}N_2OS_2\text{-}H]^-$: 530.9223, found: 530.9236. HPLC (254 nm): t_R = 4.35 min (98%).

3.2. Bacterial Strains and Growth Conditions

Wild-type *Staphylococcus aureus* CECT 86 (ATCC 12600), *Staphylococcus epidermidis* CECT 231 (ATCC 1798), *Streptococcus mutans* CECT 479 (ATCC 25175), *Enterococcus faecalis* CECT 481 (ATCC 19433), *Escherichia coli* K12 MG1655 CECT 433 (ATCC 700926) and *Pseudomonas aeruginosa* PAO1 CECT 4122 (ATCC 15692) were obtained from the Spanish Type Culture Collection (CECT). *Staphylococcus aureus* MRSA was kindly obtained from Dr Joan Gavaldà laboratory. All strains were routinely cultivated in TSB (tryptic soy broth) or LB (Luria-Bertani) medium (Scharlab) at 37 °C.

3.3. Antibacterial Susceptibility Testing

Bacterial strains were tested in the presence of different compounds; each strain was grown in TSB medium to $OD_{550} \approx 0.1$ and plated in a microtiter plate (Corning 3596 Polystyrene Flat Bottom 96 Well, Corning, NY, USA) with different compound concentrations according to the Clinical Laboratory Standards Institute (CLSI) guidelines, as previously described [41]. The plate was incubated at 37 °C and 150 rpm and growth curves were monitored for 8 h taking the absorbance (OD_{550} nm) every 15 min in an SPARK Multimode microplate reader (Tecan, Männedorf, Switzerland). The minimal inhibitory concentration 50% (MIC_{50}) was defined as the compound concentration that reduces bacterial growth, determined as the OD_{550}, by 50%.

3.4. Antibacterial Effect of Compounds on Cleaning a Surface

Sterile cover glasses (2.4 cm × 5 cm) (Duran) were placed into a petri dish with a solution of peptone water (Sigma-Aldrich, St. Louis, MO, USA) inoculated with *S. aureus* at an $OD_{550} \approx 0.1$ and incubated at 20 °C without shaking. After 16 h, the cover glasses were washed with phosphate buffered saline (PBS), and the different compounds were added at a concentration of 3 × MIC. After 1 h of incubation, the covers were placed directly on agar plates to quantify viable cells (cfu/mL). The viable counts at control experiment were 550 ± 114 cfu.

3.5. Antibacterial Effect of Compounds on Biofilms Growing on Catheters

Sterile pieces of catheter (1 cm width and 2 mm diameter) were incubated in 10 ml tubes with 1 mL TSB with 0.2% glucose inoculated with *S. aureus* at $OD_{550} \approx 0.1$. After three days without shaking at 37 °C, all tubes were washed three times with PBS to remove non-adhered bacteria (planktonic) and, after, the different compounds were added at a 1 × MIC concentration. After overnight incubation, tubes were washed three times with PBS and 1 mL PBS + 0.05% TWEEN solution was added to each tube. All tubes were placed in an ultrasonic bath (VWR) for 5 min and then vortexed for 30 s to remove adhered bacteria (growing in biofilm). The control group contained media only. Biofilm viable cells (cfu) were determined by plating serial dilutions on agar plates. The viable counts at control experiment were $3.8 \times 10^6 \pm 1.2 \times 10^6$ cfu/mL.

3.6. Fluorescent Microscopy Viability Test Analysis

S. aureus was grown in TSB medium at 37 °C and 150 rpm to reach an OD_{550} of 0.2, where different compounds were added at 1 × MIC. After 4 h in shaking conditions, cells (1 mL) were centrifuged and stained using the LIVE/DEAD BacLight Bacterial Viability kit (Thermo Fisher Scientific). After 30 min at room temperature under dark conditions, cells were washed with PBS to remove nonspecific stain. Fluorescent bacteria were visualized by a Nikon inverted fluorescent microscope ECLISPSE Ti-S/L100 (Nikon) coupled with a DS-Qi2 Nikon camera (Nikon). To access membrane integrity, cells were also stained with 10 µg/mL of *N*-(3-triethylammoniumpropyl)-4-(6-(4-(diethylamino)phenyl)hexatrienyl)pyridinium dibromide (FM® 4-64, Thermo Fisher Scientific). The dye was added after a 10 min treatment with the compounds at 1 × MIC on *S. aureus* grown in TSB medium at 37 °C and 150 rpm until an $OD_{550} \approx 1$.

3.7. Spontaneous Mutation Frequency to Resistance

A culture of *S. aureus* (10^{10} cfu/mL) was plated in TSA agar plates containing different compounds at 10 μg/mL. The inoculum viable cells were determined by cfu counting. The spontaneous compound-resistant mutation frequency was calculated by dividing the number of resistant colonies by the total viable cells.

3.8. Mammalian Cytotoxicity Determination

J-774A.1 murine macrophages cells (DSMZ ACC 170) were seeded in a microtiter plate (2×10^4 cells per well) (Corning 3596 Polystyrene Flat Bottom 96 Well, Corning), infected with the different compounds at different concentrations, and diluted in complete medium (Gibco) without antibiotics. After 24 h at 37 °C, the supernatants were removed and a 10% of MTT solution (3-[4,5-dimethylthiazol-2-yl]-2,5-diphenyltetrazolium bromide, Sigma-Aldrich) was added to determine cell viability. The formazan produced after 3 h was dissolved with acidic isopropanol, and absorbance was measured at 550 nm with a SPARK Multimode microplate reader (Tecan). CC_{50} was calculated with GraphPad Prism 6.00 (GraphPad Software) as the concentration of compound that reduces the cell viability by 50%.

4. Patents

A PCT patent application has been filed. See PCT WO2018/010856A1 (priority data 13 July 2016).

5. Conclusions

Thirteen new diarylureas featuring the scarcely-explored pentafluorosulfanyl group have been synthesized as analogs of TCC, a widely-used antimicrobial agent that has recently been banned by the FDA. Overall, the novel derivatives showed similar potency and comparable or broader spectrum of activity than TCC. Compound **10**, with higher potency, a broader spectrum of activity, and higher selectivity index emerged as the most promising compound. A bactericidal mode of action for this family of ureas was suggested by preliminary experiments. It is worthy of note that some of these new molecules removed preexisting *S. aureus* biofilms, which is important in food industry as well as in hospital settings, and displayed a lower spontaneous mutation frequency in *S. aureus* than TCC.

Supplementary Materials: The following are available online. copies of the ^{1}H, ^{13}C and ^{19}F NMR spectra of the new compounds.

Author Contributions: E.P., N.B.-C., E.J. and R.L. performed the experiments; all the authors analyzed the data; E.P. wrote the first draft of the article; E.P., E.T. and S.V. reviewed and edited the manuscript; E.T. and S.V. designed and supervised the experiments and secured funding.

Funding: This research was funded by the *Ministerio de Economía Industria y Competitividad* (Agencia Estatal de Investigación, AEI) and *Fondo Europeo de Desarrollo Regional* (MINECO-FEDER) (Projects SAF2017-82771 and BIO2015-63557-R) and Generalitat de Catalunya (2017 SGR 106, 2017 SGR1079 and CERCA programme). E.P. thanks the Institute of Biomedicine of the Universitat de Barcelona (IBUB) for a PhD grant.

Acknowledgments: The authors wish to thank Josep Astola, Zoe Downer and Johanna Binding for technical assistance.

Conflicts of Interest: E.P., R.L. and S.V. are inventors of the Universitat de Barcelona patent application on the compounds reported here. The other authors declare no conflict of interest. The founding sponsors had no role in the design of the study; in the collection, analyses, or interpretation of data; in the writing of the manuscript, and in the decision to publish the results.

References

1. Schetty, G.; Stammbach, W.; Zinkernagel, R. Insecticidal Derivatives of Diphenyl Urea. U.S. Patent 2745874, 15 May 1956.

2. Zhang, Y.; Anderson, M.; Weisman, J.L.; Lu, M.; Choy, C.J.; Boyd, V.A.; Price, J.; Siga, M.; Clark, J.; Connelly, M.; et al. Evaluation of diarylureas for activity against *Plasmodium falciparum*. *ACS Med. Chem. Lett.* **2010**, *1*, 460–465. [CrossRef] [PubMed]
3. Cowan, N.; Dätwyler, P.; Ernst, B.; Wang, C.; Vennerstro, J.L.; Spangenberg, T.; Keiser, J. Activities of *N*,*N*′-diarylurea MMV665852 analogs against *Schistosoma mansoni*. *Antimicrob. Agents Chemother.* **2015**, *59*, 1935–1941. [CrossRef] [PubMed]
4. Brown, J.R.; North, E.J.; Hurdle, J.G.; Morisseau, C.; Scarborough, J.S.; Sun, D.; Korduláková, J.; Scherman, M.S.; Jones, V.; Grzegorzewicz, A.; et al. The structure-activity relationship of urea derivatives as anti-tuberculosis agents. *Bioorg. Med. Chem.* **2011**, *19*, 5585–5595. [CrossRef] [PubMed]
5. Sviripa, V.; Zhang, W.; Conroy, M.D.; Schmidt, E.S.; Liu, A.X.; Truong, J.; Chunming, L.; Watt, D.S. Fluorinated *N*,*N*′-diarylureas as AMPK activators. *Bioorg. Med. Chem. Lett.* **2013**, *23*, 1600–1603. [CrossRef] [PubMed]
6. Jin, Q.; Nie, H.; McCleland, B.W.; Widdowson, K.L.; Palovich, M.R.; Elliott, J.D.; Goodman, R.M.; Burman, M.; Sarau, H.M.; Ward, K.W.; et al. Discovery of potent and orally bioavailable *N*,*N*′-diarylurea antagonists for the CXCR2 chemokine receptor. *Bioorg. Med. Chem. Lett.* **2004**, *14*, 4375–4378. [CrossRef] [PubMed]
7. Denoyelle, S.; Chen, T.; Chen, L.; Wang, Y.; Klosi, E.; Halperin, J.A.; Aktas, B.H.; Chorev, M. In vitro inhibition of translation initiation by *N*,*N*′-diarylureas–potential anti-cancer agents. *Bioorg. Med. Chem. Lett.* **2012**, *22*, 402–409. [CrossRef] [PubMed]
8. Roman, D.P.; Barnett, E.H.; Balske, R.J. Cutaneous antiseptic activity of 3,4,4′-trichlorocarbanilide. *Proc. Sci. Sect. Toilet. Goods Assoc.* **1957**, *28*, 1213–1214.
9. Ahn, C.K.; Zhao, B.; Chen, J.; Cherednichenko, G.; Sanmarti, E.; Denison, M.S.; Lasley, B.; Pessah, I.N.; Kültz, D.; Chang, D.P.Y.; et al. In vitro biologic activities of the antimicrobials triclocarban, its analogs, and triclosan in bioassay screens: Receptor-based bioassay screens. *Environ. Health Perspect.* **2008**, *16*, 1203–1210. [CrossRef] [PubMed]
10. Schebb, N.H.; Inceoglu, B.; Ahn, K.C.; Morisseau, C.; Gee, S.J.; Hammock, B.D. Investigation of human exposure to triclocarban after showering and preliminary evaluation of its biological effects. *Environ. Sci. Technol.* **2011**, *45*, 3109–3115. [CrossRef] [PubMed]
11. Venkatesan, A.K.; Pycke, B.F.G.; Barber, L.B.; Lee, K.E.; Halden, R.U. Occurrence of triclosan, triclocarban, and its lesser chlorinated congeners in Minnesota freshwater sediments collected near wastewater treatment plants. *J. Hazard. Mater.* **2012**, *229–230*, 29–35. [CrossRef] [PubMed]
12. Scharpf, L.G., Jr.; Hill, I.D.; Maibach, H.I. Percutaneous penetration and disposition of triclocarban in man: Body showering. *Arch. Environ. Health* **1975**, *30*, 7–14. [CrossRef] [PubMed]
13. Schebb, N.H.; Buchholz, B.A.; Hammock, B.D.; Rice, R.H.J. Metabolism of the antibacterial triclocarban by human epidermal keratinocytes to yield protein adducts. *Biochem. Mol. Toxicol.* **2012**, *26*, 230–234. [CrossRef] [PubMed]
14. Xie, W.; Zhang, W.; Ren, J.; Li, W.; Zhou, L.; Cui, Y.; Chen, H.; Yu, W.; Zhuang, X.; Zhang, Z.; et al. Metabonomics indicates inhibition of fatty acid synthesis, β-oxidation, and tricarboxylic acid cycle in triclocarban-induced cardiac metabolic alterations in male mice. *J. Agric. Food. Chem.* **2018**, *66*, 1533–1542. [CrossRef] [PubMed]
15. Liu, J.; Qiu, H.; Morisseau, C.; Hwang, S.H.; Tsai, H.; Ulu, A.; Chiamvimonvat, N.; Hammock, B.D. Inhibition of soluble epoxide hydrolase contributes to the anti-inflammatory effect of antimicrobial triclocarban in a murine model. *Toxicol. Appl. Pharmacol.* **2011**, *255*, 200–206. [CrossRef] [PubMed]
16. Chalew, T.E.; Halden, R.U. Environmental exposure of aquatic and terrestrial biota to triclosan and triclocarban. *J. Am. Water Works Assoc.* **2009**, *45*, 4–13. [CrossRef] [PubMed]
17. Halden, R.U.; Paull, D.H. Analysis of triclocarban in aquatic samples by liquid chromatography electrospray ionization mass spectrometry. *Environ. Sci. Technol.* **2004**, *38*, 4849–4855. [CrossRef] [PubMed]
18. Ying, G.; Yu, X.; Kookana, R.S. Biological degradation of triclocarban and triclosan in a soil under aerobic and anaerobic conditions and comparison with environmental fate modelling. *Environ. Pollut.* **2007**, *150*, 300–305. [CrossRef] [PubMed]
19. Gledhill, W.E. Biodegradation of 3,4,4′-trichlorocarbanilide, TCC®, in sewage and activated sludge. *Water Res.* **1975**, *9*, 649–654. [CrossRef]
20. FDA Issues Final Rule on Safety and Effectiveness of Antibacterial Soaps. Available online: https://www.fda.gov/NewsEvents/Newsroom/PressAnnouncements/ucm517478.htm (accessed on 14 October 2018).

21. Hiles, R.A. Metabolism and toxicity of halogenated carbanilides: Absorption, distribution and excretion of radioactivity from 3,4,4′-trichloro[^{14}C]carbanilide (TCC) and 3-trifluoromethyl-4,4′-dichloro[^{14}C]carbanilide (TFC) in rats. *Food Cosmet. Toxicol.* **1977**, *15*, 205–211. [CrossRef]
22. Jeffcoat, A.R.; Handy, R.W.; Francis, M.T.; Willis, S.; Wall, M.E.; Birch, C.G.; Hiles, R.A. The metabolism and toxicity of halogenated carbanilides. Biliary metabolites of 3,4,4′-trichloro-carbanilide and 3-trifluoromethyl-4,4′-dichlorocarbanilide in the rat. *Drug Metab. Dispos.* **1977**, *5*, 157–166. [PubMed]
23. Markgraf, J.H.; Quinn, H. Antibacterial composition. U.S. Patent 3485919, 23 December 1969.
24. Savoie, P.R.; Welch, J.T. Preparation and utility of organic pentafluorosulfanyl-containing compounds. *Chem. Rev.* **2015**, *115*, 1130–1190. [CrossRef] [PubMed]
25. Altomonte, S.; Zanda, M. Synthetic chemistry and biological activity of pentafluorosulphanyl (SF_5) organic molecules. *J. Fuorine Chem.* **2012**, *143*, 57–93. [CrossRef]
26. Bassetto, M.; Ferla, S.; Pertusati, F. Polyfluorinated groups in medicinal chemistry. *Future Med. Chem.* **2015**, *7*, 527–546. [CrossRef] [PubMed]
27. Welch, J.T. Applications of pentafluorosulfanyl substitution in life sciences research. In *Fluorine in Pharmaceutical and Medicinal Chemistry: From Biophysical Aspects to Clinical Applications*; Gouverneur, V., Müller, K., Eds.; World Scientific: London, UK, 2012; pp. 175–207.
28. Saethre, L.J.; Berrah, N.; Bozek, J.D.; Boerve, K.J.; Carroll, T.X.; Kukk, E.; Gard, G.L.; Winter, R.; Thomas, T.D. Chemical insights from high-resolution X-ray photoelectron spectroscopy and ab initio theory: Propyne, trifluoropropyne, and ethynylsulfur pentafluoride. *J. Am. Chem. Soc.* **2001**, *123*, 10729–10737. [CrossRef] [PubMed]
29. Kanishchev, O.S.; Dolbier, W.R., Jr. Generation of ortho-SF_5-benzyne and its diels−alder reactions with furans: Synthesis of 1-SF_5-naphthalene, its derivatives, and 1,6(1,7)-bis-SF_5-naphthalenes. *J. Org. Chem.* **2016**, *81*, 11305–11311. [CrossRef] [PubMed]
30. Sheppard, W.A. Arylsulfur pentafluorides. *J. Am. Chem. Soc.* **1962**, *84*, 3072–3076. [CrossRef]
31. Westphal, M.V.; Wolfstädter, B.T.; Plancher, J.; Gatfield, J.; Carreira, E.M. Evaluation of *tert*-butyl isosteres: Case studies of physicochemical and pharmacokinetic properties, efficacies, and activities. *ChemMedChem.* **2015**, *10*, 461–469. [CrossRef] [PubMed]
32. Phillips, M.A.; Lotharius, J.; Marsh, K.; White, J.; Dayan, A.; White, K.L.; Njoroge, J.W.; El Mazouni, F.; Lao, Y.; Kokkonda, S.; et al. A long-duration dihydroorotate dehydrogenase inhibitor (DSM265) for prevention and treatment of malaria. *Sci. Transl. Med.* **2015**, *7*, 296ra111. [CrossRef] [PubMed]
33. Murphy, C.D. Microbial degradation of fluorinated drugs: Biochemical pathways, impacts on the environment and potential applications. *Appl. Microbiol. Biotechnol.* **2016**, *100*, 2617–2627. [CrossRef] [PubMed]
34. Jackson, D.A.; Mabury, S.A. Environmental properties of pentafluorosulfanyl compounds: Physical properties and photodegradation. *Environ. Toxicol. Chem.* **2009**, *28*, 1866–1879. [CrossRef] [PubMed]
35. Zarei, M.; Vázquez-Carrera, M.; Vázquez, S.; Leiva, R.; Pujol, E. HRI Activators Useful for the Treatment of Cardiometabolic Diseases. Patent PCT WO2018/010856A1, 18 January 2018.
36. Raasch, M.S. Ureido-Substituted Arylsulfur Pentafluorides. U.S. Patent 3073861, 15 January 1963.
37. Karagiannidis, L.E.; Haynes, C.J.E.; Holder, K.J.; Kirby, I.L.; Moore, S.J.; Wells, N.J.; Gale, P.A. Highly effective yet simple transmembrane anion transporters based upon *ortho*-phenylenediamine bis-ureas. *Chem. Commun.* **2014**, *50*, 12050–12053. [CrossRef] [PubMed]
38. Walsh, S.E.; Maillard, J.Y.; Russell, A.D.; Catrenich, C.E.; Charbonneau, D.L.; Bartolo, R.G. Activity and mechanisms of action of selected biocidal agents on Gram-positive and -negative bacteria. *J. Appl. Microbiol.* **2003**, *94*, 240–247. [CrossRef] [PubMed]
39. Hughes, D.; Karlén, A. Discovery and preclinical development of new antibiotics. *Upsala J. Med. Sci.* **2014**, *119*, 162–169. [CrossRef] [PubMed]
40. Kleemann, H.; Weck, R. *Ortho*-Substituted Pentafluorosulfanylbenzenes, Process for Their Preparation and Their Use as Valuable Synthetic Intermediates. U.S. Patent 7932416 B2, 26 April 2011.

41. Barniol-Xicota, M.; Escandell, A.; Valverde, E.; Julián, E.; Torrents, E.; Vázquez, S. Antibacterial activity of novel benzopolycyclic amines. *Bioorg. Med. Chem.* **2015**, *23*, 290–296. [CrossRef] [PubMed]

Sample Availability: Samples of the compounds are available from the authors.

ARTICLE 2

Novel Oleanolic and Maslinic Acid Derivatives as a Promising Treatment against Bacterial Biofilm in Nosocomial Infections: An in Vitro and in Vivo Study

Publicat a la revista *ACS Infectous Diseases* (Q1, IF_{2019} = 4.614)

DOI: 10.1021/acsinfecdis.9b00125

Juliol 2019

Autors: **Núria Blanco-Cabra**[1], Karina Vega-Granados[2], Laura Moya-Andérico[1], Marija Vukomanovic[1], Andrés Parra[2], Luis Álvarez de Cienfuegos[2,*], Eduard Torrents[1,*]

1: Bacterial infections and antimicrobial therapies group, Institute for Bioengineering of Catalonia (IBEC), The Barcelona Institute of Science and Technology (BIST). Baldiri Reixac 15-21. 08028 Barcelona. Spain.

2: Department of Organic Chemistry, Faculty of Science, University of Granada. Campus Universitario Fuentenueva s/n. 18071 Granada. Spain.

***:** Correspondència: Dr. Eduard Torrents (etorrents@ibecbarcelona.eu);
Dr. Luis Álvarez de Cienfuegos (lac@ugr.es)

ACS Infectious Diseases

Article

Cite This: *ACS Infect. Dis.* 2019, 5, 1581−1589

pubs.acs.org/journal/aidcbc

Novel Oleanolic and Maslinic Acid Derivatives as a Promising Treatment against Bacterial Biofilm in Nosocomial Infections: An in Vitro and in Vivo Study

Núria Blanco-Cabra,[†] Karina Vega-Granados,[‡] Laura Moya-Andérico,[†] Marija Vukomanovic,[†] Andrés Parra,[‡] Luis Álvarez de Cienfuegos,[*,‡,§] and Eduard Torrents[*,†]

[†]Bacterial Infections and Antimicrobial Therapies Group, Institute for Bioengineering of Catalonia (IBEC), The Barcelona Institute of Science and Technology (BIST), Baldiri Reixac 15-21, 08028 Barcelona, Spain

[‡]Department of Organic Chemistry, Faculty of Science, University of Granada, Campus Universitario Fuentenueva s/n, 18071 Granada, Spain

[§]Instituto de Investigación Biosanitaria ibs.GRANADA, Universidad de Granada, 18012 Granada, Spain

S *Supporting Information*

ABSTRACT: Oleanolic acid (OA) and maslinic acid (MA) are pentacyclic triterpenic compounds that abound in industrial olive oil waste. These compounds have renowned antimicrobial properties and lack cytotoxicity in eukaryotic cells as well as resistance mechanisms in bacteria. Despite these advantages, their antimicrobial activity has only been tested in vitro, and derivatives improving this activity have not been reported. In this work, a set of 14 OA and MA C-28 amide derivatives have been synthesized. Two of these derivatives, MA-HDA and OA-HDA, increase the in vitro antimicrobial activity of the parent compounds while reducing their toxicity in most of the Gram-positive bacteria tested, including a methicillin-resistant *Staphylococcus aureus*-MRSA. MA-HDA also shows an enhanced in vivo efficacy in a *Galleria mellonella* invertebrate animal model of infection. A preliminary attempt to elucidate their mechanism of action revealed that these compounds are able to penetrate and damage the bacterial cell membrane. More significantly, their capacity to reduce antibiofilm formation in catheters has also been demonstrated in two sets of conditions: a static and a more challenged continuous-flow *S. aureus* biofilm.

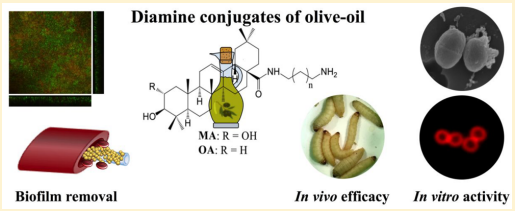

KEYWORDS: *maslinic and oleanolic acids, natural products, in vitro and in vivo antimicrobials, Galleria mellonella, antibiofilm, Staphylococcus aureus*

Staphylococcus aureus is a major global healthcare problem because it is a leading cause of infections in hospitals and the major cause of biofilm formation in catheters and other medical devices like prostheses.[1] Because the bacteria embedded in biofilms can be 100 or even 1000 times more resistant to antibiotics than planktonic-growing bacteria,[2] these *S. aureus* biofilms can generate dangerous infections such as endocarditis, prosthetic joint infection, and even sepsis. The only effective treatment against these biofilms is the removal of the medical device and long-term antibiotic therapy,[3] which can develop antibiotic-resistant bacteria such as methicillin-resistant *S. aureus* (MRSA) and a high increase in the overall treatment cost.[4−6] MRSA infections are more related to bacteremia cases and have poorer clinical outcomes.[4] As a result of the improper use of antibiotics, multiresistant bacteria are a worldwide worrying health problem and cause significant morbidity and mortality. Therefore, there is a critical need to find alternatives to common antibiotics with a smaller risk of resistance development.

Oleanolic acid (OA) and maslinic acid (MA) are pentacyclic triterpenic compounds that can be widely isolated from plants. The function of these triterpenes seems to be protection against dehydration and microbes, as has been noticed with an increase in plant infections when the synthesis of these compounds diminishes.[7,8] They are vastly present in the fruits of *Olea europaea* and consequently abound in industrial olive oil waste.[8,9]

OA and MA have been extensively used in ancestral medicine and have, among others, long-recognized anti-inflammatory, anti-hyperlipidemic, antitumor, and hepatoprotective properties in addition to their known antimicrobial activity.[7,8,10−17] Moreover, these triterpenes have no cytotoxicity on eukaryotic cells, and no resistance mechanisms in bacteria have been found yet.[12] Despite the fact that the exact antimicrobial mechanism of these compounds is still unknown,

Received: April 3, 2019
Published: July 3, 2019

DOI: 10.1021/acsinfecdis.9b00125
ACS Infect. Dis. 2019, 5, 1581−1589

Scheme 1. Synthesis of MA and OA Amine Derivatives

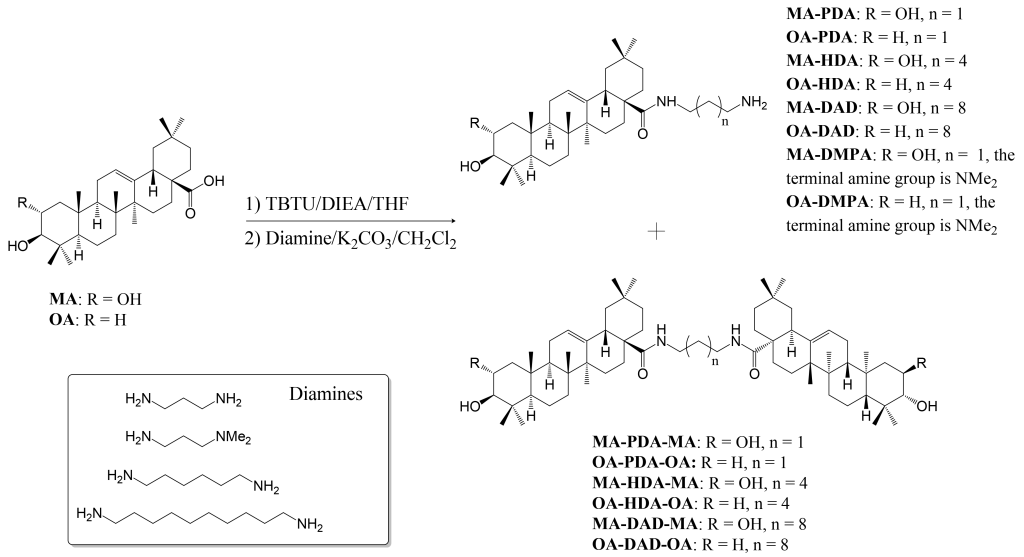

there are some works indicating the peptidoglycan synthesis as the principal target,[10,18] which can explain why these antimicrobial activities have been mostly seen in Gram-positive species, whereas the compounds were devoid of antimicrobial activity against the Gram-negative bacteria tested.[7,10−12,16,17] Despite the antimicrobial activity against Gram-positive bacteria and the lack of toxicity and resistance mechanisms, the activity of OA and MA has only been tested in vitro, and as far as we know, OA and MA derivatives with improved antimicrobial activity are not known.

In this respect, in this work, a set of 14 OA and MA C-28 amide derivatives (Scheme 1 and Table 1) have been synthesized and analyzed for their in vitro and in vivo antimicrobial efficacy and toxicity properties. Moreover, the antibiofilm activity in catheters and flow biofilms of the more active compounds has also been evaluated. The choice of these derivatives was proposed with the aim of simultaneously satisfying two essential criteria. The first one was to obtain two groups of molecules with very different polarities and molecular weights to study which factor could influence the antibacterial activity more. The second one was to obtain these derivatives by means of a simple and direct synthetic strategy which would allow us to obtain, on one hand, derivatives with minimal chemical modifications in order to maintain the low toxicity of the natural OA and MA and, on the other hand, their easy synthesis in large quantities. Furthermore, it has been recently shown that some OA and MA C-28 amide derivatives have enhanced anticancer activity with respect to the natural triterpenes.[13]

For the first time, two of these new derivatives (OA-HDA and MA-HDA) increase the in vitro antimicrobial activity and reduce the toxicity of the parent compounds by reducing the minimum inhibitory concentration (MIC) in most of the Gram-positive bacteria tested, highlighting the efficacy against *S. aureus* and MRSA. Remarkably, MA-HDA also shows enhanced activity in vivo in the *Galleria mellonella* animal model of infection. A preliminary attempt to investigate their mechanism of action shows that these compounds are able to damage the bacterial cell membrane. Their antimicrobial properties have also been evaluated by their antibiofilm capacity. Again, these two derivatives are more effective than their parent compounds in reducing *S. aureus* biofilms in a static and continuous-flow manner. These two derivatives can serve as a guide for the development of useful antimicrobial and antibiofilm agents based on easily accessible natural compounds that can be used alone or in combination with other antimicrobials to promote synergy.[17]

RESULTS AND DISCUSSION

Antibacterial Activity and In Vitro Toxicity. The amide derivatives of oleanolic acid (OA) and maslinic acid (MA) were tested for their antibacterial activity in planktonic bacterial growth. The antibacterial activity that can be seen in Table 1 is represented regarding minimal inhibitory concentration 50% (MIC_{50}) and defined as the compound concentration that inhibits bacterial growth by 50%.

As previously described,[7,10−12,16,17,19] OA and MA inhibited the Gram-positive bacterial growth, whereas no effect was detected against Gram-negative pathogens. Similarly, the amide derivatives tested in this work did not show antibacterial activity against any Gram-negative pathogen tested (Table 1). Cholesterol (C) was used as a negative control. No antimicrobial activity was detected when OA-PDA, OA-DMPA, MA-PDA-MA, OA-PDA-OA, and OA-DAD-OA were used. Furthermore, the diamine chemical precursors HDA and DAD alone did not exhibit any antimicrobial activity at the highest concentration tested (120 μg/mL, data not shown).

Among the 14 derivatives tested in this work, MA-HDA and OA-HDA showed the highest efficacy by maintaining or enhancing the antimicrobial activity of MA and OA in most of the strains tested with particular relevance against *S. aureus* and

DOI: 10.1021/acsinfecdis.9b00125
ACS Infect. Dis. 2019, 5, 1581−1589

Table 1. MIC_{50}, Cytotoxicity, and Selectivity Index (SI) of Compounds[a]

Compound	Formula	MIC_{50} (μg/ml)								
		Gram-Positive				Gram-Negative				
		S. aureus	*S. aureus*-MRSA	*S. epidermidis*	*S. mutans*	*E. faecalis*	*E. coli*	*P. aeruginosa*	CC_{50} (μg/ml)	LD_{50} (mg/kg)
C		NA	NA	NA	NA	NA	NA	NA	NT	>400
MA		**15 (20.9/504)**	75	**25 (12.5/302)**	**15 (20.9/504)**	**15 (20.9/504)**	NA	NA	314 ± 6	302.44 ± 67
OA		**30 (10.5/302)**	75	200	**30 (10.5/302)**	**30 (10.5/302)**	NA	NA	314 ± 9.8	361.8 ± 70
MA-PDA	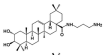	200	200	NA	NA	NA	NA	200	310 ± 5.4	
OA-PDA	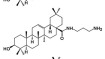	NA	NA	NA	NA	NA	NA	NA	312 ± 8.6	
MA-HDA	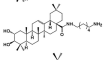	**15 (17.9/661)**	**25 (10.7/397)**	**20 (13.4/496)**	**50 (5.4/198)**	75	NA	NA	268 ± 5.3	396.56 ± 81.2
OA-HDA	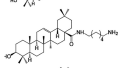	**4 (62.2/1313)**	**10 (24.9/525)**	**5 (49.8/1050)**	**5 (49.8/1050)**	**15 (16.6/350)**	NA	NA	249 ± 10.1	210.08 ± 69.9
MA-DAD	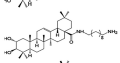	**20 (10.5)**	**25 (8.4)**	**10 (21)**	**25 (8.4)**	**25 (8.4)**	NA	NA	250 ± 10.9	
OA-DAD	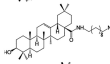	**30 (10.4)**	**30 (10.4)**	**7.5 (41.7)**	**25 (12.5)**	**25 (12.52)**	NA	NA	313 ± 5.3	
MA-DMPA	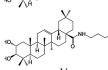	75	85	75	85	75	NA	NA	NT	
OA-DMPA		NA	NA	NA	NA	NA	NA	NA	NT	
MA-PDA-MA	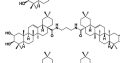	NA	NA	NA	NA	NA	NA	NA	120 ± 19.5	
OA-PDA-OA	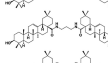	NA	NA	NA	NA	NA	NA	200	NT	
MA-HDA-MA	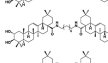	NA	NA	100	100	NA	NA	NA	312 ± 9.4	
OA-HDA-OA	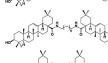	NA	NA	75	100	100	NA	NA	314 ± 12.8	
MA-DAD-MA	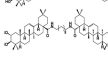	NA	NA	50	NA	NA	NA	NA	317.5 ± 2.9	
OA-DAD-OA	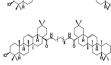	NA	NA	NA	NA	NA	NA	NA	912 ± 3.3	

[a]MIC_{50} was evaluated on: *S. aureus*, *Staphylococcus aureus*; *S. aureus*-MRSA, *Staphylococcus aureus* methicillin-resistant; *S. epidermidis*, *Staphylococcus epidermidis*; *S. mutans*, *Streptococcus mutans*; *E. faecalis*, *Enterococcus faecalis*; *E. coli*, *Escherichia coli*; *P. aeruginosa*, *Pseudomonas aeruginosa*; C, cholesterol. NA, no-activity or MIC_{50} > 250 μg/mL. Cytotoxicity (CC_{50}) was evaluated on human alveolar epithelial A459 cells. NT, non-cytotoxic or CC_{50} > 1000 μg/mL. Lethal doses (LD_{50}) were evaluated in *Galleria mellonella* larvae. Selectivity index (SI), calculated as CC_{50}/MIC_{50} and LD_{50}/MIC_{50}, are indicated in parentheses next to the MIC value.

Methicillin-Resistant *S. aureus* (MRSA). It is noteworthy that the HDA derivative compounds (MA-HDA and OA-HDA) increased their antimicrobial activity and reduced the MIC_{50} against MRSA by 66% and 87%, respectively (MIC_{50} of 25 and 10 μg/mL) compared to their original compounds (OA and MA, MIC_{50} 75 μg/mL). The same behavior was seen with the DAD derivative compounds (MA-DAD and OA-DAD), which reduced MRSA MIC_{50} by 66% and 60%, respectively. Since antibiotic-resistant bacteria like MRSA are nowadays a public health concern, it is crucial to find new antimicrobials that do not produce resistance mechanisms in these bacteria. Thus, the improved activity of HDA and DAD compounds and the fact that resistance mechanisms have not yet been found in the parent compounds MA and OA[12,16] identify these molecules as a possible good alternative for MRSA treatment.

Additional studies were performed to determine their in vitro toxicity using the A549 human epithelial pulmonary cell line. The in vitro toxicity in cells, expressed in Table 1 as the concentration that kills 50% of the cells (CC_{50}), demonstrates that the HDA and the DAD derivatives from MA and OA were not more toxic than their precursors, although they showed better antimicrobial activity in some bacterial strains.

DOI: 10.1021/acsinfecdis.9b00125
ACS Infect. Dis. 2019, 5, 1581−1589

In Vivo Toxicity and Efficacy in *Galleria mellonella*. *Galleria mellonella* was used to evaluate the toxicity (lethal dose) of the new antimicrobial compounds tested.[20] We evaluated the compound dose per kilogram of greater wax moth larvae that kills 50% of the animal population (lethal dose 50, LD_{50}). Using the MIC_{50} and the toxicity indexes CC_{50} and LD_{50}, the selectivity indexes (SI) were calculated. The selectivity indexes (in cells or *Galleria mellonella*) emphasize the improvement of the HDA derivatives' activity (OA-HDA, SI = 62.2 or 1313; MA-HDA, SI = 17.9 or 661) against *S. aureus* growth related to their toxicity, as seen with the 5-fold increase in the SI of OA-HDA compared to OA.

The use of *Galleria mellonella* as an invertebrate animal model to test in vivo toxicity and to calculate the SI is crucial because the selectivity index (SI) is increased considerably when calculated with the LD_{50} rather than with the CC_{50} (Table 1). In some cases, the toxicity in vivo can be significantly different; for example, the toxicity of the MA-HDA compound increased in vitro while the in vivo toxicity decreased in comparison to the predecessor MA. Our results highlight the use of an animal model for toxicity evaluation to better select a compound for further investigative steps or drug development. The use of *G. mellonella* is a cheap screening alternative for in vivo toxicity and efficacy prior to analysis in rodents or even more expensive options.

Additionally, *Galleria mellonella* larvae were used as a *S. aureus* model of infection to evaluate in vivo antibacterial efficacy of the best active amide derivatives (MA-HDA and OA-HDA). *G. mellonella* were infected with *S. aureus* at 1.5×10^9 cfu/mL into the hemocoel and treated twice with the compounds at 240 mg/kg (1 and 6 h post-infection). As illustrated in Figure 1, treatment with MA-HDA and MA

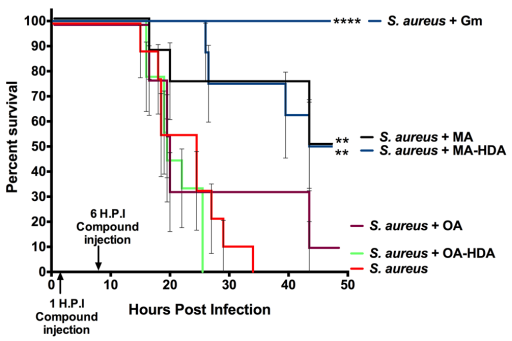

Figure 1. Kaplan–Meier survival curve of *Galleria mellonella* larvae infected with *S. aureus* and treated with the different compounds 1 and 6 h post-infection at a final concentration of 240 mg per kg of body weight. Gentamicin (Gm) at 20 mg/kg was used as a control. Asterisks: statistically significant difference versus *S. aureus* without treatment in a log-rank test, GraphPad 6.0 (**: *p*-value <0.005; ****: *p*-value <0.0001).

compounds resulted in 50% of the larvae surviving, whereas only 20% of *Galleria* survived the *S. aureus* infection after the treatment with OA. Nevertheless, no differences were seen between the untreated insects and the ones treated with OA-HDA, showing a lack of in vivo activity of this compound. As the in vivo toxicity diminished in the MA-HDA derivative, these results enhanced the antibacterial efficacy of MA-HDA by increasing the survival of *Galleria mellonella* infected with *S. aureus* by 50%.

Since these two new compounds (MA-HDA and OA-HDA) have high activity and selectivity index, they could be considered good antibacterial agents in a modern therapy context, especially useful in the treatment of multidrug resistant bacteria. As the antibiotics used in chemotherapy no longer appear to be as effective as they were when created, there is an urgent need for the discovery of new antibacterial drugs with different action mechanisms to tackle the growing drug resistance.

Effect on Bacterial Cell Membrane and Possible Mechanisms of Action. To identify a preliminary mechanism of action of the different compounds used in this work, Live/Dead and membrane damage staining analyses were first carried out. The Live/Dead analysis (Figure 2A) was performed by staining *S. aureus* cells after 4 h of treatment with the diverse compounds. This differential staining allowed discrimination of viable bacteria (stained with SYTO9 dye, green) from dead bacteria (stained with PI dye, red), as well as seeing the growth impairment that the treatment could cause. After 4 h of treatment, a notable decrease of viable cells could be detected when the OA, MA, OA-HDA, MA-HDA, OA-DAD, and MA-DAD compounds were used, as shown in Figure 2A with the average count in Table S1, while a persistence of these cells was seen when compounds without activity were used (MA-HDA-MA and MA-DMPA). Moreover, a specific membrane staining with FM 4-64 dye was performed. After staining for 10 min (Figure 2B), membrane impairment in the active compounds could be observed. Some dye accumulations could be appreciated in the membrane (red dots indicated by an arrow) when treated with the active antimicrobial compounds (OA, MA, OA-HDA, MA-HDA, OA-DAD, and MA-DAD). These accumulations reaffirmed the Live/Dead results and suggested a bacteriolytic mode of action.

Finally, scanning electron microscope (SEM) characterization of the treated *S. aureus* cells was carried out to validate our previous staining experiments. Figure 2C shows SEM images of *S. aureus* cells after exposure to the compounds. The images show that the bacteria's surface became rough and bubbly in many *S. aureus* treated cells while the nontreated cells' membrane remained smooth, thus suggesting membrane damage and further corroborating the results seen in the fluorescent microscope analysis.

Previous results show that MA and OA induced cell membrane destabilization and destruction.[12,21] Proteases, protein kinases, and transcription factors have been proposed as a target for these compounds,[10,22−25] but the exact molecular mechanism remains unknown. The mechanism of action of MA has not been reported in bacteria but only against protozoa, nematodes, viruses, and cancerogenic cells as a glycogen phosphorylase inhibitor,[26] regulator of transcription factors and protein kinases,[24] and inhibitor of proteases.[27,28] However, a nonstandard binding mechanism of MA to these proteins[29] has also been suggested.

Regarding the mechanism of action of OA against bacteria, it is well-known that it inhibits peptidoglycan metabolism and prevents cell division in *Listeria monocytogenes*.[18] Other studies demonstrate a similar effect of OA in the Gram-positive *Streptococcus mutans* by proving the effect in both the peptidoglycan metabolism at a transcriptional level[10] and the adherence to the tooth surface to form the cariogenic

DOI: 10.1021/acsinfecdis.9b00125
ACS Infect. Dis. 2019, 5, 1581−1589

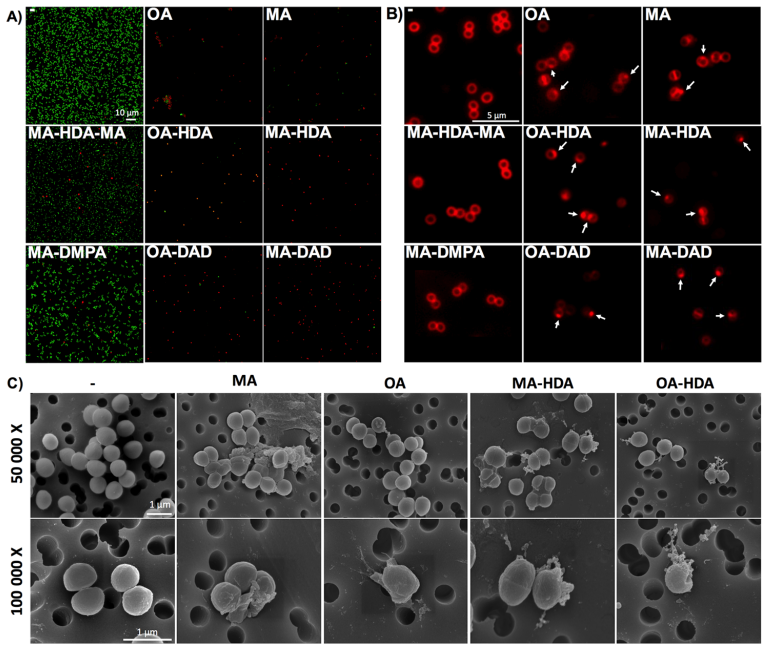

Figure 2. (A) Live/Dead analysis in *S. aureus*. Green fluorescence indicates live cells and red fluorescence indicates metabolically inactive (dead) cells. (B) Membrane damage analysis by FM 4-64 staining of *S. aureus*. The arrows show nonuniform stain accumulations in the membrane indicating cell damage. (C) SEM images of *S. aureus* cells after the compounds' treatment.

biofilm.[30] Despite not having antimicrobial activity in *Escherichia coli*, it has been demonstrated that OA affects the efflux of pumps in this bacteria[23] and acts as a stress inducer agent[22] that reduces the expression of the cysteine regulon and induces heat shock response with the DnaK synthesis.

Nevertheless, the different activity among the OA and MA derivatives and concerning the parent OA and MA compounds suggests that the mechanism of action of these derivatives might be different from the natural triterpenic acids. The only structural difference between all the derivatives is the length of the diamine residue. It seems that these compounds require a certain chain length to be active, and for this reason, only the longer chain (HDA and DAD) derivatives are active. This might have some justification if the mechanism of action is due to bacterial cell membrane interaction and posterior destabilization, as suggested by the Live/Dead and membrane damage staining analyses and the SEM characterization. Both Gram-positive and Gram-negative bacteria have a negatively charged envelope due to the negative charge of teichoic acids and lipopolysaccharides, respectively, but regarding the plasma membrane, Gram-positive bacteria contain a larger portion of negatively charged phospholipids than Gram-negative bacteria.[31] At a physiological pH, the terminal amine group is positively charged and can promote the interaction of the derivatives with the plasma membrane by electrostatic interactions which are going to be enhanced in the Gram-positive membrane. Once the derivatives are in contact with the membrane, they need to be inserted efficiently to produce membrane destabilization. This second step is where the length of the alkyl chain may have relevant importance. If the alkyl chain is short, the interaction is mainly superficial, and the derivatives do not have the possibility of being inserted into the cell membrane. On the other hand, if the length of the chain is long enough, the derivatives can be inserted into the cell membrane, thus provoking disruption. It is known that the alkyl chain length in small organic compounds which tackle bacterial cell membranes has a major impact on the activity of the compounds.[32−34] In our case, HDA-derivatives, having a diamine alkyl chain of 6 carbons, present the most effective combination.

Antibiofilm Activity against *Staphylococcus aureus* Static and Continuous Biofilms. Since bacteria within biofilms can be more resistant to antimicrobials than in planktonic state, the removal capacity of preformed *S. aureus* biofilms grown in static and continuous flow was tested.

First, we grew a *S. aureus* biofilm on catheter tubes for 72 h. Then, we treated them with different compounds at a concentration of 50 μg/mL for an additional 24 h. As we can see in Figure 3, the more active compounds (MA, MA-HDA, and OA-HDA) were able to remove more than 99% of the preformed biofilm when compared to the untreated biofilm. However, at the concentration tested, OA and MA-HDA-MA had subinhibitory concentration activity (Figure 3) without any ability to remove the biofilm, but they do enhance the formation of the biofilm[35] which could explain the increase in the biofilm growth produced. Note that the antibacterial activity was higher for the MA-HDA and OA-HDA compounds in contrast to the well-known antibiotic ciprofloxacin.

Second, we performed a continuous *S. aureus* flow biofilm to resemble the conditions in which this bacteria establishes a chronic infection. The *S. aureus* continuous biofilm was formed

DOI: 10.1021/acsinfecdis.9b00125
ACS Infect. Dis. 2019, 5, 1581−1589

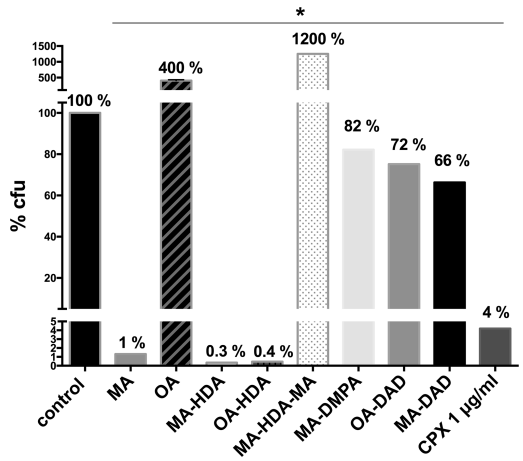

Figure 3. Antibacterial efficacy of compounds on *S. aureus* ATCC 12600 catheter biofilms. Bars indicate percentage (%) of viable biofilm cells (cfu) remaining on the catheter after 24 h treatment with the compounds. Cpx, ciprofloxacin. Asterisk (*): statistically significant difference versus control without treatment (p-value <0.05 in an unpaired t-test, GraphPad 6.0).

during 4 consecutive days and afterward treated with different compounds at a concentration of 50 μg/mL for an additional 24 h. The images of Figure 4A are confocal Z-projections with the corresponding orthogonal views of the biofilm after treatment and the plot in Figure 4B shows the average biofilm biomass. Clearly, the best antibiofilm activity was detected with the MA-HDA and OA-HDA compounds (30% and 45% reduction in biofilm biomass, respectively) with a corresponding decrease in thickness (around 10 μm) as seen in the orthogonal views (Figure 4A and B). It is important to point out that these compounds have better antimicrobial efficacy compared to the MA and OA original compounds.

CONCLUSIONS

For the first time, novel OA and MA derivatives outperform the known antimicrobial activity of their parent compounds. Of the 14 OA and MA C-28 amide derivatives studied, two derivatives, MA-HDA and OA-HDA, have shown better in vitro antimicrobial activity in all of the Gram-positive bacterial strains tested by significantly reducing the MIC_{50} against MRSA in 66% and 87%, respectively, when compared to the MA and OA compounds. In vitro toxicity studies also showed that these new derivatives did not increase the toxicity with respect to their parent compounds. Preliminary studies conducted to shed light on their mechanism of action revealed that these compounds were able to penetrate and damage the bacterial cellular membrane. These excellent in vitro results have also been validated in vivo in a *Galleria mellonella* animal model. In particular, MA-HDA showed the best results in terms of efficacy and toxicity, increasing the survival of *G. mellonella* infected with *S. aureus* by 50%.

Taken together, these results point out the relevance that natural feedstock has in providing bioactive compounds for therapeutic purposes. In this case, OA and MA are natural products obtained in large quantities from olive oil waste, and therefore, they are easily accessible and inexpensive. Through very few steps of very simple chemical transformations, we have obtained novel derivatives that are highly active in vitro and in vivo against dangerous Gram-positive bacterial strains including MRSA. Their mechanism of action suggests that these compounds could be used in combination with other antibiotics to promote synergy.

EXPERIMENTAL SECTION

Chemistry. Oleanolic (3β-hydroxyolean-12-en-28-oic acid, OA) and maslinic (2α,3β-dihydroxyolean-12-en-28-oic acid) acids were isolated from solid waste resulting from olive oil production, which were extracted in a Soxhlet with hexane and EtOAc successively.[36] Both acids were purified from these mixtures by flash chromatography over silica gel, eluting with CH_2Cl_2/acetone of increasing polarity.[37] The C-28 amide derivatives were prepared following a protocol previously described (see Scheme 1).[13] Very briefly, the carboxyl group of the OA and MA was first activated with *O*-(Benzotriazol-1-yl)-*N*,*N*,*N*′,*N*′-tetramethyluronium tetrafluoroborate (TBTU). The OA and MA-TBTU derivatives were obtained by the addition of TBTU in the presence of diisopropylethylamine (DIEA) in dry THF and at room temperature. Second, the OA and MA-TBTU derivatives were dissolved in CH_2Cl_2 and reacted with the corresponding diamine reagents [propane-1,3-

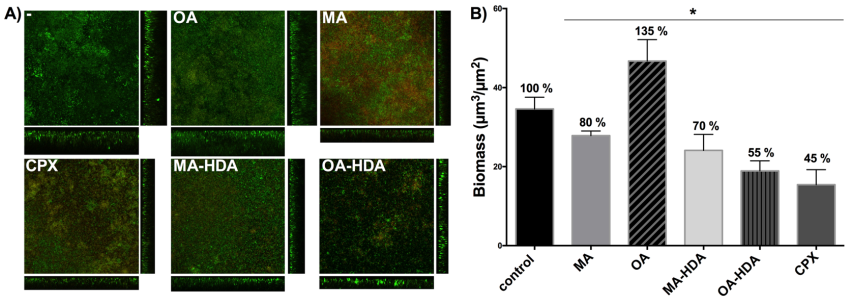

Figure 4. Antibiofilm efficacy of 24 h treatment of compounds against *S. aureus* biofilms grown on a continuous flow system for 96 h. (A) Confocal laser scanning microscope (CLSM) pictures (sum of stack images and orthogonal views) stained with LIVE/DEAD BacLight Bacterial Viability Kit. (B) Biomass ($\mu m^3/\mu m^2$) of the biofilms analyzed with COMSTAT2. Cpx, ciprofloxacin. Asterisk (*): statistically significant difference versus control without treatment (p-value <0.05 in an unpaired t-test, GraphPad 6.0).

DOI: 10.1021/acsinfecdis.9b00125
ACS Infect. Dis. 2019, 5, 1581−1589

diamine (PDA), hexane-1,6-diamine (HDA), and decane-1,10-diamine (DAD)] in the presence of K_2CO_3 to originate two products in all cases: monomers exceeding 60% yield (MA-PAD 63%, MA-HDA 64%, MA-DAD 62%, OA-PAD 65%, OA-HDA 62%, and OA-DAD 63%) and dimers close to 30% yield (MA-PAD-MA 27%, MA-HDA-MA 28%, MA-DAD-MA 30%, OA-PAD-OA 28%, OA-HDA-OA 29%, and OA-DAD-OA 29%).[13] The reaction of OA and MA-TBTU derivatives with *N,N*-dimethyl-1,3-propanediamine afforded only one compound (MA-DMPA and OA-DMPA) with a 90% yield in both cases. In all instances, the compounds were purified by column chromatography. The purity of the compounds was determined by a Waters Acquity UPLC system (ultra-performance liquid chromatography) coupled with a Waters Synapt G2 HRMS spectrometer (high resolution mass spectra), with ESI (electrospray ionization) being ⩾95%. Isolated compounds were characterized by ^{1}H NMR and HRMS, matching what has already been reported. MA-DMPA and OA-DMPA were characterized by ^{1}H and ^{13}C NMR and HRMS. Copies of NMR spectra and HRMS values are included in the Supporting Information.

Bacterial Strains and Growth Conditions. Wild-type *Staphylococcus aureus* CECT 86 (ATCC 12600), *Staphylococcus epidermidis* CECT 231 (ATCC 1798), *Streptococcus mutans* CECT 479 (ATCC 25175), *Enterococcus faecalis* CECT 481 (ATCC 19433), *Escherichia coli* K12 MG1655 CECT 433 (ATCC 700926), and *Pseudomonas aeruginosa* PAO1 CECT 4122 (ATCC 15692) were obtained from the Spanish Type Culture Collection (CECT). *Staphylococcus aureus* MRSA was from our laboratory stock.[38] *S. aureus* antimicrobial activity profiles are listed in Table S2. All strains were routinely cultivated in Tryptic Soy Broth (TSB) or Luria−Bertani (LB) medium (Scharlab) at 37 °C.

Antibacterial Susceptibility Testing (In Vitro Activity). The different compounds were tested against different bacterial strains as previously described.[38] Briefly, bacteria were grown in TSB or LB medium to an $O.D._{550} \approx 0.1$ ($\approx(4.3 \times 10^7) \pm (1.4 \times 10^6)$ cfu/mL) and plated in a 96-well microtiter plate (Corning 3596 Polystyrene Flat Bottom 96 Well, Corning NY) containing several concentrations of the compounds according to the Clinical Laboratory Standards Institute (CLSI) guidelines.[39] The plate was incubated at 37 °C with shaking at 120 rpm for 8 h and the absorbance at 550 nm was read every 15 min in a SPARK Multimode microplate reader (Tecan).

The minimal inhibitory concentration 50% (MIC_{50}) was defined as the compound concentration that inhibited the bacterial growth by 50%.

Mammalian Cytotoxicity Determination (In Vitro Toxicity). Human alveolar epithelial A549 cells (ATCC CCL-185) were set and allowed to sediment in a microtiter plate (Corning 3596 Polystyrene Flat Bottom 96 Well, Corning NY) at 2×10^4 cells/well and compounds were added at several concentrations. After 24 h, a 10% of MTT solution (3-[4,5-dimethylthiazol-2-yl]-2,5-diphenyltetrazolium bromide, Sigma-Aldrich) was added and the formazan that precipitated 3 h later was dissolved with acidic isopropanol. Absorbance was read at 550 nm in a SPARK multimode microplate reader (Tecan) to determine cell viability. CC_{50} was calculated with Prism 6.00 (GraphPad Software) as the concentration of the compound that diminished the cell population by 50%. Values ± standard deviation for 3 independent experiments are shown.

Animal Toxicity Determination (In Vivo Toxicity). *Galleria mellonella* larvae were reared on an artificial diet (15% corn flour, 15% wheat flour, 15% baby cereal, 11% powdered milk, 6% brewer's yeast, 25% honey, and 13% glycerol) at 34 °C in darkness prior to use. *G. mellonella* larvae were injected with 10 μL of each compound at 300 and 400 mg/kg with a microsyringe (Hamilton) into the hemocoel through the top left proleg. Five larvae (200−250 mg each) were injected per compound and concentration and larvae mortality was recorded daily. Control groups were injected with 10 μL of 1× PBS (Phosphate Saline Buffer) or the vehicle (DMSO) at the highest concentration used.

LD_{50} (median lethal dose) was calculated with Prism 6.00 (GraphPad Software) as the concentration of the compound that killed 50% of the larvae within 24 h. Values ± standard deviation for 3 independent experiments are shown.

Survival Assay in *Galleria mellonella* Animal Model (In Vivo Efficacy). An infective dose of *S. aureus* (1.5×10^9 cfu/mL) was injected in *Galleria mellonella* larvae into the hemocoel through the upper left proleg. One hour and six hours post-infection, 10 μL of the compound at 240 mg/kg were injected through a different proleg. Each compound was injected in a group of five larvae (200−250 mg each). Control groups were injected with 10 μL of 1× PBS (Phosphate Saline Buffer), the vehicle (DMSO), or gentamicin at 20 mg/kg. *G. mellonella* larvae were incubated at 37 °C and mortality was recorded daily. Survival curves were plotted using Kaplan−Meier analysis and differences in survival rates were analyzed by the log-rank test (GraphPad Prism 6.00). Differences with P values of <0.005 were considered statistically significant.

Fluorescent Microscopy Viability and Membrane Analysis. *S. aureus* was grown in TSB medium to an $O.D._{550} \approx 0.3$ ($\approx(1.3 \times 10^8) \pm (3 \times 10^7)$ cfu/mL) and the compounds were added at a concentration of 50 μg/mL for 4 h in the live−dead test and for 10 min in the membrane analysis.

The bacterial cells were harvested and stained with the LIVE/DEAD BactLight Bacterial Viability kit (Thermo Fisher Scientific) for the viability test and with 10 μg/mL of *N*-(3-triethylammoniumpropyl)-4-(6-(4-(diethylamino)phenyl)-hexatrienyl)pyridinium dibromide (FM 4−64, Thermo Fisher Scientific) for the membrane analysis, according to the manufacturer's specifications. Bacteria were then visualized with a Nikon inverted fluorescent microscope ECLIPSE Ti−S/L100 (Nikon) coupled with a DS-Qi2 Nikon camera (Nikon).

Scanning Electronic Microscopy (SEM) Bacterial Analysis. Morphological analysis of *S. aureus* after exposure to antimicrobial compounds was performed using field emission scanning electron microscopy (Nova NanoSEM FEISEM). *S. aureus* was grown in TSB medium to an $O.D._{550} \approx 0.6$ ($\approx(2 \times 10^8) \pm (4 \times 10^7)$ cfu/mL) and exposed to compounds at a concentration of 25 μg/mL for 30 min. Nonexposed bacteria were used as a reference. Immediately after exposure, bacteria were fixed in glutaraldehyde. For that purpose, 100 μL of treated culture were centrifuged for 5 min at 6000 rpm and TSB was replaced with 50 μL of glutaraldehyde solution (3 wt.%). After 3 h at room temperature, the fixative was replaced with the same volume of fresh fixative and left at 4 °C overnight. Fixed bacteria were deposited on the top of the porous membranes by filtration in soft vacuum. To remove the fixative, deposited bacteria were washed three times with 1× PBS (during 15 min for each replacement) and dehydrated in serially diluted ethanol (30,

DOI: 10.1021/acsinfecdis.9b00125
ACS Infect. Dis. 2019, 5, 1581−1589

50, 70, 90, and 100 wt.%) (30 min in each concentration). The cells in ethanol were finally dried using critical point technique (CPD Baltec 030). Before examination in SEM, bacteria deposited on membranes were sputtered with a thin layer of gold for better conductivity.

Antibacterial Effect of Compounds on Biofilms Growing on Catheters. Sterile silicone catheter pieces (2 mm diameter and 1 cm width) (SILT-002, SUDELAB) were placed in a 10 mL tube and covered with a *S. aureus* culture of $O.D._{\cdot 550} \approx 0.1$ ($\approx(4.3 \times 10^7) \pm (1.43 \times 10^6)$ cfu/mL) in TSB medium +0.2% glucose. The tubes were incubated at 37 °C without shaking. After 72 h, the catheter pieces were washed three times with 1× phosphate buffer saline (PBS) (Fisher BioReagents) to discard the planktonic growth (nonbiofilm forming bacteria) and were treated with the different compounds at a concentration of 50 μg/mL. After 24 h, the catheters were washed again and a solution of 1× PBS + TWEEN 0.05% was added. Then, the tubes were placed in an ultrasonic bath (USC100T, VWR) for 5 min and vortexed for 30 s to remove the bacteria growing in a biofilm. Serial dilutions were plated on TSB agar plates to determine the viable cells in the biofilm (cfu, colony forming units). The viable counts in the control experiment without treatment were $(4.4 \times 10^5) \pm (1.7 \times 10^5)$ cfu/mL.

Antibacterial Effect of Compounds on Continuous-Flow Biofilms. *S. aureus* continuous-flow biofilms were formed as previously described[40,41] with some modifications and with an initial bacteria inoculum of $O.D._{\cdot 550} \approx 0.1$ ($\approx(4.3 \times 10^7) \pm (1.43 \times 10^6)$ cfu/mL). The biofilms were grown in 2% (v/v) TSB + 0.2% glucose pumped through the flow cells chambers using a peristaltic pump ISM (Ismatec) at 42 μL/min. These flow cells (DTU) were previously coated with 20% bovine plasma (Biowest) overnight prior to the inoculation of the bacteria. After 4 days of growth, the flow was stopped and different compounds diluted in media, including ciprofloxacin as a control, were injected into the formed biofilms. After 24 h treatment, biofilms were stained with the Live/Dead BacLight Bacterial Viability Kit (Thermo Fisher Scientific) and visualized under a Zeiss LSM 800 confocal laser scanning microscope (CLSM) with the 20×/0.8 air objective. Analysis of the images obtained was performed to quantify the biomass and thickness of the biofilms using ImageJ FIJI and COMSTAT2 software.[42]

■ ASSOCIATED CONTENT

Supporting Information

The Supporting Information is available free of charge on the ACS Publications website at DOI: 10.1021/acsinfecdis.9b00125.

General information and copies of NMR spectra and HRMS values (PDF)

■ AUTHOR INFORMATION

Corresponding Authors

*E-mail: lac@ugr.es.
*E-mail: etorrents@ibecbarcelona.eu.

ORCID

Andrés Parra: 0000-0001-7485-8753
Luis Álvarez de Cienfuegos: 0000-0001-8910-4241
Eduard Torrents: 0000-0002-3010-1609

Author Contributions

The manuscript was written through contributions of all authors. All authors have given approval to the final version of the manuscript. Karina Vega Granados and Andrés Parra designed and synthesized the library of oleanolic and maslinic acid derivatives and wrote the manuscript. Núria Blanco-Cabra, Laura Moya-Andérico, and Marija Vukomanovic performed biological assays and wrote the manuscript. Eduard Torrents and Luis Alvarez de Cienfuegos directed the research, revised the experimental data, and wrote the manuscript. All authors have given approval to the final version of the manuscript.

Notes

The authors declare no competing financial interest.

■ ACKNOWLEDGMENTS

This study was partially supported by grants from the Ministerio de Economía, Industria y Competitividad, MINECO, and Agencia Estatal de Investigación, AEI, Spain, cofunded by Fondo Europeo de Desarrollo Regional, FEDER, European Union (BIO2015−63557-R, FIS2017−85954-R and RTI2018−098573-B-100), the CERCA program and *AGAUR-Generalitat de Catalunya* (2017SGR-1079), the European Regional Development Fund (FEDER), Catalan and Spanish cystic fibrosis federation, the EIT Health and Obra Social "La Caixa". K.V.G. thanks CONACYT (Consejo Nacional de Ciencia y Tecnología) Gobierno del estado de Baja California 2015 for her fellowship. The authors wish to thank Johanna Binding and Zoe Downer for technical assistance. L.A.C. wants to thank "Unidad de Excelencia Química aplicada a Biomedicina y Medioambiente" for support. Finally we would like to thank the Editor and reviewers whose suggestions greatly improved the manuscript.

■ REFERENCES

(1) Otto, M. (2018) Staphylococcal Biofilms. *Microbiol. Spectrum 6* (4), 1 DOI: 10.1128/microbiolspec.GPP3-0023-2018.
(2) Stewart, P. S., and Costerton, J. W. (2001) Antibiotic resistance of bacteria in biofilms. *Lancet 358* (9276), 135−8.
(3) Costerton, J. W., Stewart, P. S., and Greenberg, E. P. (1999) Bacterial biofilms: a common cause of persistent infections. *Science 284* (5418), 1318−22.
(4) Hassoun, A., Linden, P. K., and Friedman, B. (2017) Incidence, prevalence, and management of MRSA bacteremia across patient populations-a review of recent developments in MRSA management and treatment. *Crit Care 21* (1), 211.
(5) Tong, S. Y., Davis, J. S., Eichenberger, E., Holland, T. L., and Fowler, V. G., Jr. (2015) *Staphylococcus aureus* infections: epidemiology, pathophysiology, clinical manifestations, and management. *Clin. Microbiol. Rev. 28* (3), 603−61.
(6) Suresh, M. K., Biswas, R., and Biswas, L. (2019) An update on recent developments in the prevention and treatment of *Staphylococcus aureus* biofilms. *Int. J. Med. Microbiol. 309*, 1.
(7) Jesus, J. A., Lago, J. H., Laurenti, M. D., Yamamoto, E. S., and Passero, L. F. (2015) Antimicrobial activity of oleanolic and ursolic acids: an update. *Evid Based Complement Alternat Med. 2015*, 620472.
(8) Rufino-Palomares, E. (2015) Anti-cancer and Anti-angiogenic Properties of Various Natural Pentacyclic Tri-terpenoids and Some of their Chemical Derivatives. *Curr. Org. Chem. 19* (10), 1.
(9) Fernández-Hernández, A., Martinez, A., Rivas, F., García-Mesa, J. A., and Parra, A. (2015) Effect of the Solvent and the Sample Preparation on the Determination of Triterpene Compounds in Two-Phase Olive-Mill-Waste Samples. *J. Agric. Food Chem. 63* (17), 4269−4275.

DOI: 10.1021/acsinfecdis.9b00125
ACS Infect. Dis. 2019, 5, 1581−1589

(10) Park, S. N., Ahn, S. J., and Kook, J. K. (2015) Oleanolic acid and ursolic acid inhibit peptidoglycan biosynthesis in *Streptococcus mutans* UA159. *Braz J. Microbiol 46* (2), 613−7.
(11) Fontanay, S., Grare, M., Mayer, J., Finance, C., and Duval, R. E. (2008) Ursolic, oleanolic and betulinic acids: antibacterial spectra and selectivity indexes. *J. Ethnopharmacol. 120* (2), 272−6.
(12) Kim, S., Lee, H., Lee, S., Yoon, Y., and Choi, K. H. (2015) Antimicrobial action of oleanolic acid on *Listeria monocytogenes*, *Enterococcus faecium*, and *Enterococcus faecalis*. *PLoS One 10* (3), No. e0118800.
(13) Medina-O'Donnell, M., Rivas, F., Reyes-Zurita, F. J., Martinez, A., Lupianez, J. A., and Parra, A. (2018) Diamine and PEGylated-diamine conjugates of triterpenic acids as potential anticancer agents. *Eur. J. Med. Chem. 148*, 325−336.
(14) Liu, J. (1995) Pharmacology of oleanolic acid and ursolic acid. *J. Ethnopharmacol. 49* (2), 57−68.
(15) Lozano-Mena, G., Sanchez-Gonzalez, M., Juan, M. E., and Planas, J. M. (2014) Maslinic acid, a natural phytoalexin-type triterpene from olives–a promising nutraceutical? *Molecules 19* (8), 11538−59.
(16) Garcia-Salinas, S., Elizondo-Castillo, H., Arruebo, M., Mendoza, G., and Irusta, S. (2018) Evaluation of the Antimicrobial Activity and Cytotoxicity of Different Components of Natural Origin Present in Essential Oils. *Molecules 23* (6), 1399.
(17) Abreu, A. C., Paulet, D., Coqueiro, A., Malheiro, J., Borges, A., Saavedra, M. J., Choi, Y. H., and Simões, M. (2016) Antibiotic adjuvants from *Buxus sempervirens* to promote effective treatment of drug-resistant *Staphylococcus aureus* biofilms. *RSC Adv. 6* (97), 95000−95009.
(18) Kurek, A., Grudniak, A. M., Szwed, M., Klicka, A., Samluk, L., Wolska, K. I., Janiszowska, W., and Popowska, M. (2010) Oleanolic acid and ursolic acid affect peptidoglycan metabolism in *Listeria monocytogenes*. *Antonie van Leeuwenhoek 97* (1), 61−8.
(19) Pavel, I. Z., Danciu, C., Oprean, C., Dehelean, C. A., Muntean, D., Csuk, R., and Muntean, D. M. (2016) In Vitro Evaluation of the Antimicrobial Ability and Cytotoxicity on Two Melanoma Cell Lines of a Benzylamide Derivative of Maslinic Acid. *Anal. Cell. Pathol. 2016*, 2787623.
(20) Ignasiak, K., and Maxwell, A. (2017) *Galleria mellonella* (greater wax moth) larvae as a model for antibiotic susceptibility testing and acute toxicity trials. *BMC Res. Notes 10* (1), 428.
(21) Martin-Navarro, C. M., Lopez-Arencibia, A., Sifaoui, I., Reyes-Batlle, M., Fouque, E., Osuna, A., Valladares, B., Pinero, J. E., Hechard, Y., Maciver, S. K., and Lorenzo-Morales, J. (2017) Amoebicidal Activity of Caffeine and Maslinic Acid by the Induction of Programmed Cell Death in *Acanthamoeba*. *Antimicrob. Agents Chemother. 61* (6), 1 DOI: 10.1128/AAC.02660-16.
(22) Grudniak, A. M., Kurek, A., Szarlak, J., and Wolska, K. I. (2011) Oleanolic and ursolic acids influence affect the expression of the cysteine regulon and the stress response in *Escherichia coli*. *Curr. Microbiol. 62* (4), 1331−6.
(23) Martins, A., Vasas, A., Viveiros, M., Molnar, J., Hohmann, J., and Amaral, L. (2011) Antibacterial properties of compounds isolated from *Carpobrotus edulis*. *Int. J. Antimicrob. Agents 37* (5), 438−44.
(24) Sharma, H., Kumar, P., Deshmukh, R. R., Bishayee, A., and Kumar, S. (2018) Pentacyclic triterpenes: New tools to fight metabolic syndrome. *Phytomedicine 50*, 166−177.
(25) Liang, Z., Zhang, L., Li, L., Liu, J., Li, H., Zhang, L., Chen, L., Cheng, K., Zheng, M., Wen, X., Zhang, P., Hao, J., Gong, Y., Zhang, X., Zhu, X., Chen, J., Liu, H., Jiang, H., Luo, C., and Sun, H. (2011) Identification of pentacyclic triterpenes derivatives as potent inhibitors against glycogen phosphorylase based on 3D-QSAR studies. *Eur. J. Med. Chem. 46* (6), 2011−21.
(26) Mukaratirwa, S., Gcanga, L., and Kamau, J. (2016) Efficacy of maslinic acid and fenbendazole on muscle larvae of *Trichinella zimbabwensis* in laboratory rats. *J. Helminthol. 90* (1), 86−90.
(27) Moneriz, C., Marin-Garcia, P., Garcia-Granados, A., Bautista, J. M., Diez, A., and Puyet, A. (2011) Parasitostatic effect of maslinic acid. I. Growth arrest of *Plasmodium falciparum* intraerythrocytic stages. *Malar. J. 10*, 82.
(28) De Pablos, L. M., dos Santos, M. F., Montero, E., Garcia-Granados, A., Parra, A., and Osuna, A. (2010) Anticoccidial activity of maslinic acid against infection with *Eimeria tenella* in chickens. *Parasitol. Res. 107* (3), 601−4.
(29) Moneriz, C., Mestres, J., Bautista, J. M., Diez, A., and Puyet, A. (2011) Multi-targeted activity of maslinic acid as an antimalarial natural compound. *FEBS J. 278* (16), 2951−61.
(30) Kozai, K., Miyake, Y., Kohda, H., Kametaka, S., Yamasaki, K., Suginaka, H., and Nagasaka, N. (1987) Inhibition of glucosyltransferase from *Streptococcus mutans* by oleanolic acid and ursolic acid. *Caries Res. 21* (2), 104−8.
(31) Malanovic, N., and Lohner, K. (2016) Gram-positive bacterial cell envelopes: The impact on the activity of antimicrobial peptides. *Biochim. Biophys. Acta, Biomembr. 1858* (5), 936−46.
(32) Ghosh, C., Manjunath, G. B., Akkapeddi, P., Yarlagadda, V., Hoque, J., Uppu, D. S., Konai, M. M., and Haldar, J. (2014) Small molecular antibacterial peptoid mimics: the simpler the better! *J. Med. Chem. 57* (4), 1428−36.
(33) Hoque, J., Konai, M. M., Sequeira, S. S., Samaddar, S., and Haldar, J. (2016) Antibacterial and Antibiofilm Activity of Cationic Small Molecules with Spatial Positioning of Hydrophobicity: An in Vitro and in Vivo Evaluation. *J. Med. Chem. 59* (23), 10750−10762.
(34) Konai, M. M., and Haldar, J. (2017) Fatty Acid Comprising Lysine Conjugates: Anti-MRSA Agents That Display In Vivo Efficacy by Disrupting Biofilms with No Resistance Development. *Bioconjugate Chem. 28* (4), 1194−1204.
(35) Kaplan, J. B. (2011) Antibiotic-induced biofilm formation. *Int. J. Artif. Organs 34* (9), 737−51.
(36) Garcia-Granados, A. Process for the industrial recovery of oleanolic and maslinic acids contained in the olive milling byproducts. PCT Int. Appl. WO 9804331, 1998.
(37) Martinez, A., Perojil, A., Rivas, F., Parra, A., Garcia-Granados, A., and Fernandez-Vivas, A. (2015) Biotransformation of oleanolic and maslinic methyl esters by *Rhizomucor miehei* CECT 2749. *Phytochemistry 117*, 500−508.
(38) Barniol-Xicota, M., Escandell, A., Valverde, E., Julian, E., Torrents, E., and Vazquez, S. (2015) Antibacterial activity of novel benzopolycyclic amines. *Bioorg. Med. Chem. 23* (2), 290−6.
(39) Clinical and laboratory standards institute (2006) *Methods for dilution andtimicrobial susceptibility test for bacteria that grow aerobically; approved standard*, CLSI document M7-A7, 7th ed.;, Clinical and Laboratory Standards Institute, Wayne, PA.
(40) Baelo, A., Levato, R., Julian, E., Crespo, A., Astola, J., Gavalda, J., Engel, E., Mateos-Timoneda, M. A., and Torrents, E. (2015) Disassembling bacterial extracellular matrix with DNase-coated nanoparticles to enhance antibiotic delivery in biofilm infections. *J. Controlled Release 209*, 150−8.
(41) Crespo, A., Blanco-Cabra, N., and Torrents, E. (2018) Aerobic Vitamin B12 Biosynthesis Is Essential for *Pseudomonas aeruginosa* Class II Ribonucleotide Reductase Activity During Planktonic and Biofilm Growth. *Front. Microbiol. 9*, 986.
(42) Givskov, M., Hentzer, M., Ersbøll, B. K.ær, Heydorn, A., Sternberg, C., Nielsen, A. T., and Molin, Sør. (2000) Quantification of biofilm structures by the novel computer program COMSTAT. *Microbiology 146*, 2395−407.

DOI: 10.1021/acsinfecdis.9b00125
ACS Infect. Dis. 2019, 5, 1581−1589

Supporting Information

Table S1: Average ± standard deviation and ratio of green and red cells in the Live/Dead analysis.

	CONTROL	OA	MA	MA-HDA-MA	OA-HDA	MA-HDA	MA-DMPA	OA-DAD	MA-DAD
GREEN CELLS (alive)	4450 ± 296.6	15.17 ± 7.3	4 ± 2.8	1570.7 ± 20.8	0.8 ± 1.09	5 ± 2.55	1241 ± 153.9	6.67 ± 4	2.67 ± 3.05
RED CELLS (dead)	76 ± 8.485	68.8 ± 32.16	44.5 ± 14.1	144.33 ± 24.5	34.2 ± 7.12	68.7 ± 18.7	96.25 ± 19.2	31.67 ± 22.85	98 ± 13
RATIO (green/ red)	58.55	0.22	0.09	10.88	0.02	0.07	12.89	0.21	0.03

Table S2: Staphylococcus aureus antimicrobial activity profile.

	Antimicrobial activity profile (MIC_{50} µg/ml)	
Antibiotic	***S. aureus* CECT 86 (ATCC 12600)**	***S. aureus* MRSA**
Linezolid	2	4
Oxacillin	1	>250
Vancomycin	1	1
Daptomycin	0.25	0.5
Ciprofloxacin	0.25	

General Information

To obtain the extract of the raw material, n-Hexane (Merck, ref. 1.04374) and EtOAc (Fisher Scientific, ref. E/0900/17) solvents were used with previous distillation. The isolation of the amino compounds, maslinic and oleanolic acids was carried out by flash chromatography, using silica gel 60 (Merck, ref. 1.09385) as the stationary phase, and CH2Cl2 (Fisher Scientific, ref. D/1852/17), with increasing amounts of Me_2CO (Fisher Scientific, ref. A/0600/17) as the mobile phase. For the control of flash chromatography and reactions, silica gel 60 aluminum sheets (Merk. ref. 1.16835) were used, the compounds were made visible by spraying a mixture of H_2SO_4 and AcOH, followed by heating at 120 °C, and finally observed with UV light at 254 nm. For the amidation reactions were used DIEA (Sigma-Aldrich, ≥99%, ref. D125806), TBTU (Apollo Scientific, ref. PC0921), 3-(Dimethylamino)-1-propylamine (Sigma-Aldrich, ≥98.0%, ref. 39380), 1,3-Diaminopropane (Sigma-Aldrich, ≥98.0%, ref. 239984), 1,6-Diaminohexane (Sigma-Aldrich, 98%, ref. H11696), 1,10-Diaminodecane (ACROS Organics 97%, ref. 112130250), Na_2SO_4 Anhydrous (Fisher Chemical, 99+%, ref. S/6600/65), K_2CO_3 (PanReac AppliChem, ref. 141490), the solvents THF (Sigma-Aldrich, HPLC ≥99%, ref. 270385) with previous distillation, and CH_2Cl_2 (Fisher Scientific, ref. D/1852/17). The reagents were used without further purification. Measurements of NMR spectra were made in VARIAN direct drive (400 and 500 MHz ^1H NMR) spectrometers. The ^{13}C chemical shifts were assigned with the aid of distortion less enhancement by polarization transfer (DEPT) using a flip angle of 135.

MA-PDA

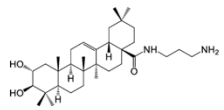

^{1}HNMR($CDCl_3$, 400 MHz): δ 6.43 (dd, 1H, *J*1 = *J*2 = 5.4 Hz), 5.35 (dd, 1H, *J*1 = *J*2 = 3.2 Hz), 3.70 (ddd, 1H, *J*1 = 4.8, *J*2 = 9.6, *J*3 = 14.0 Hz), 3.50–3.41 (m, 1H), 3.13–3.10 (m, 1H), 2.98 (d, 1H, *J* = 9.6 Hz), 2.75 (t, 1H, *J* = 6.4 Hz), 2.52 (dd, 1H, *J*1 = 3.6, *J*2 = 12.8 Hz), 1.15, 1.02, 0.97, 0.90, 0.90, 0.81, 0.75 (s, 3H); ESI-HRMS m/z calculated for $C_{33}H_{57}N_2O_3$ $[M+1]^+$ 529.4369, found 529.4336.

OA-PDA

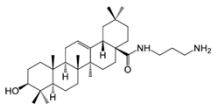

^{1}HNMR($CDCl_3$, 400 MHz): δ 6.41 (dd, 1H, *J*1 = *J*2 = 5.0 Hz), 5.35 (dd, 1H, *J*1 = *J*2 = 3.2 Hz), 3.49–3.44 (m, 1H), 3.21 (dd, 1H, *J*1 = 4.6, *J*2 = 8.8 Hz), 3.13–3.10 (m, 1H), 2.77 (t, 2H, *J* = 6.0 Hz), 2.52 (dd, 1H, *J*1 = 3.4, *J*2 = 13.0 Hz), 1.25, 1.15, 0.98, 0.90, 0.90, 0.78, 0.76 (s, 3H); ESI-HRMS m/z calculated for $C_{33}H_{57}N_2O_2$ $[M+1]^+$ 513.4420, found 513.4426.

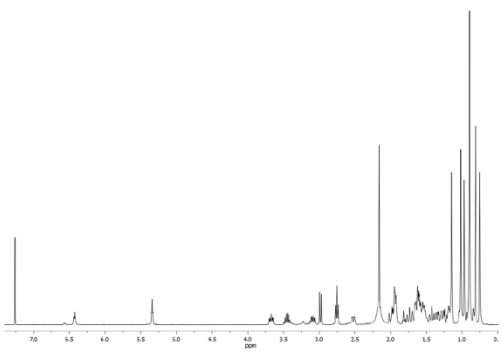

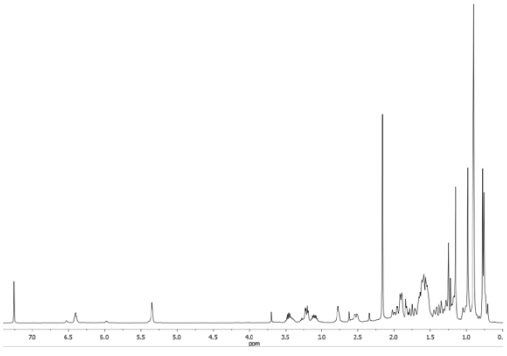

MA-HDA

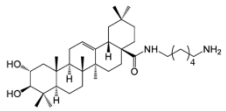

^{1}HNMR($CDCl_3$, 400 MHz): δ 5.90 (dd, 1H, *J*1 = *J*2 = 5.4 Hz), 5.36 (dd, 1H, *J*1 = *J*2 = 3.2 Hz), 3.68 (ddd, 1H, *J*1= 4.8, *J*2 = 9.2, *J*3 = 14.0 Hz), 3.35–3.32 (m, 1H), 3.19–3.15 (m, 1H), 2.98 (d, 1H, *J* = 9.2 Hz), 2.69 (t, 2H, *J* = 6.4 Hz), 2.49 (dd, 1H, *J*1 = 3.6, *J*2 = 12.8 Hz), 1.15, 1.02, 0.98, 0.90, 0.90, 0.82, 0.75 (s, 3H); ESI-HRMS m/z calculated for $C_{36}H_{63}N_2O_3$ [M+1]$^+$ 571.4839, found 571.4842.

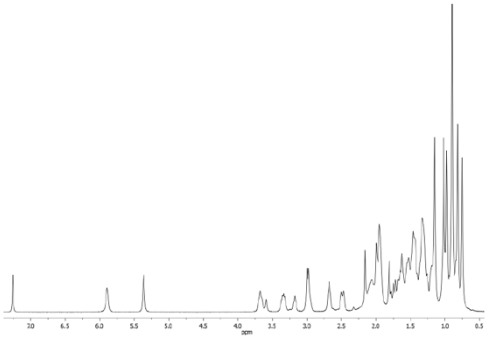

OA-HDA

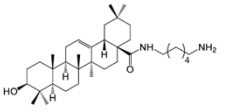

^{1}HNMR($CDCl_3$, 400 MHz): δ 5.96 (dd, 1H, *J*1 = *J*2 = 6.0 Hz), 5.37 (dd, 1H, *J*1 = *J*2 = 2.8 Hz), 3.37–3.32 (m, 1H), 3.21 (dd, 1H, *J*1 = 4.4, *J*2 = 10.8 Hz), 2.98–2.94 (m, 1H), 2.78 (t, 2H, *J* = 6.0 Hz), 2.50 (dd, 1H, *J*1 = 2.8, *J*2 = 13.2 Hz), 1.15, 0.98, 0.91, 0.90, 0.90, 0.78, 0.75 (s, 3H); ESI-HRMS m/z calculated for $C_{36}H_{63}N_2O_2$ [M+1]$^+$ 555.4890, found 555.4874.

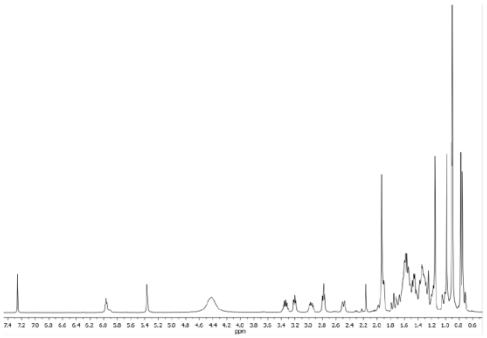

MA-DAD

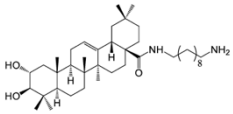

^{1}HNMR($CDCl_3$, 400 MHz): δ 5.91 (dd, 1H, *J*1 = *J*2 = 4.8 Hz), 5.36 (dd, 1H, *J*1 = *J*2 = 2.8 Hz), 3.68 (ddd, 1H, *J*1= 4.0, *J*2 = 9.6, *J*3 = 14.0 Hz), 3.36–3.28 (m, 1H), 3.06–2.99 (m, 1H), 3.00 (d, 1H, *J* = 9.6 Hz), 2.68 (t, 2H, *J* = 6.4 Hz), 2.50 (dd, 1H, *J*1 = 2.4, *J*2 = 12.4 Hz), 1.28, 1.16, 1.03, 0.99, 0.90, 0.82, 0.76 (s, 3H); ESI-HRMS m/z calculated for $C_{40}H_{71}N_2O_3$ [M+1]$^+$ 627.5386, found 627.5478.

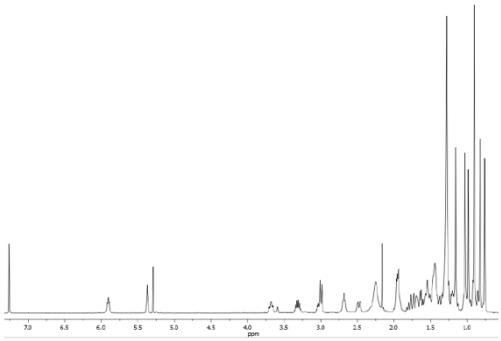

OA-DAD

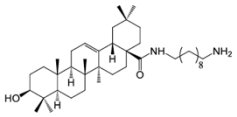

^{1}HNMR($CDCl_3$, 400 MHz): δ 6.41 (dd, 1H, *J*1 = *J*2 = 5.2 Hz), 5.35 (dd, 1H, *J*1 = *J*2 = 3.2 Hz), 3.49–3.39 (m, 1H), 3.21 (dd, 1H, *J*1 = 4.6, *J*2 = 11.1 Hz), 3.14–3.07 (m, 1H), 2.77 (t, 2H, *J* = 6.0 Hz), 2.52 (dd, 1H, *J*1 = 3.6, *J*2 = 13.2 Hz), 1.25, 1.15, 0.98, 0.91, 0.90, 0.78, 0.76 (s, 3H); ESI-HRMS m/z calculated for $C_{40}H_{71}N_2O_2$ [M+1]$^+$ 611.5516, found 611.5534.

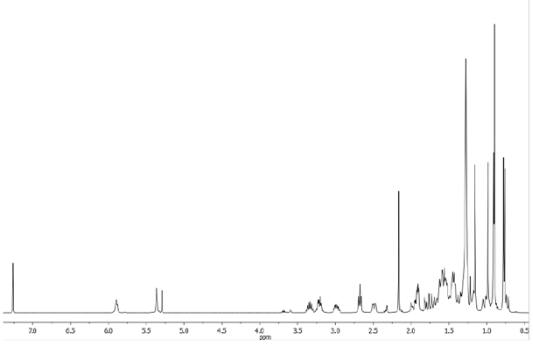

MA-DMPA

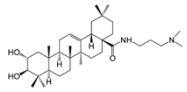

^{1}HNMR($CDCl_3$, 500 MHz): δ 7.01 (dd, 1H, *J*1 = *J*2 = 5.4 Hz), 5.30 (dd, 1H, *J*1 = *J*2 = 3.6 Hz), 3.66 (ddd, 1H, *J*1 = 4.8, *J*2 = 9.6, *J*3 = 14.0 Hz), 3.53–3.45 (m, 1H), 3.00–2.98 (m, 1H), 2.97 (d, 1H, *J* = 9.5 Hz), 2.51 (dd, 1H, *J*1 = 3.6, *J*2 = 12.8 Hz), 2.25, 2.25, 1.12, 1.01, 0.95, 0.89, 0.88, 0.80 0.73 (s, 3H). ^{13}CNMR ($CDCl_3$, 126 MHz): δ 178.10 (C), 144.80 (C), 122.53 (CH), 83.92 (CH), 68.90 (CH), 58.81(CH_2), 55.34(CH), 53.95(CH_2), 47.68(CH), 46.88 (CH_2), 46.44 (CH_2), 46.22 (C), 45.62 (CH), 42.04 (C), 41.99 (CH_3), 39.54 (C), 39.30 (CH_2), 38.32 (C), 34.24 (CH_2), 33.16 (CH_3), 32.99 (CH_2), 32.39 (CH_2), 31.86 (C), 30.84 (C), 29.39 (CH_3), 28.75 (CH_3), 27.44 (CH_2), 26.07 (CH_3), 26.05 (CH_2), 23.67 (CH_3), 23.63(CH_2), 18.44 (CH_2), 17.04 (CH_3), 16.90 (CH_3), 16.73 (CH_3). ESI-HRMS m/z calculated for $C_{35}H_{61}N_2O_3$ $[M+1]^+$ 557.4604, found 557.4682.

OA-DMPA

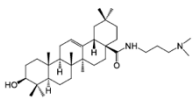

^{1}HNMR($CDCl_3$, 500 MHz): δ 6.78 (dd, 1H, *J*1 = *J*2 = 5.3 Hz), 5.34 (dd, 1H, *J*1 = *J*2 = 3.7 Hz), 3.47–3.40 (m, 1H), 3.18 (dd, 1H, *J*1 = 4.6, *J*2 = 11 Hz), 3.09–3.02 (m, 1H), 2.58 (dd, 1H, *J*1 = 3.4, *J*2 = 13.0 Hz), 2.37, 2.37, 1.13, 0.97, 0.90, 0.89, 0.89, 0.77, 0.73 (s, 3H). ^{13}CNMR ($CDCl_3$, 126 MHz): δ 178.44 (C), 144.80 (C), 122.75 (CH), 79.09 (CH), 57.17 (CH_2), 55.28 (CH), 47.71 (CH), 46.85(CH_2), 46.34 (C), 44.43 (CH), 42.04 (C), 41.95 (CH_3), 39.51(C), 38.89 (C), 38.57 (CH_2), 38.17 (CH_2), 37.13 (C), 34.28 (CH_2), 33.18 (CH_3), 33.03 (CH_2), 32.54 (CH_2), 30.86 (C), 28.23(CH_3), 27.50 (CH_2), 27.29 (CH_2), 26.03 (CH_3), 25.69 (CH_2), 23.73 (CH_3), 23.64 (CH_2), 23.60 (CH_2), 22.68 (CH_3), 18.44 (CH_2), 17.07 (CH_3), 15.71 (CH_3), 15.46 (CH_3).ESI-HRMS m/z calculated for $C_{35}H_{61}N_2O_2$ $[M+1]^+$ 541.4655, found 541.4733.

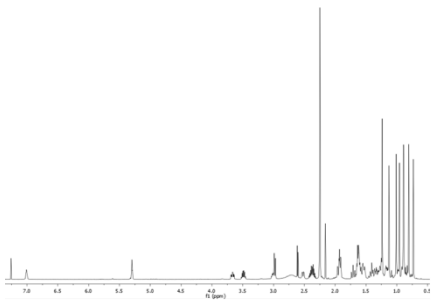

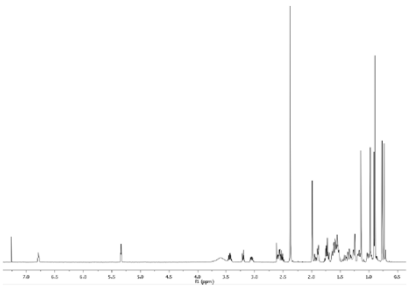

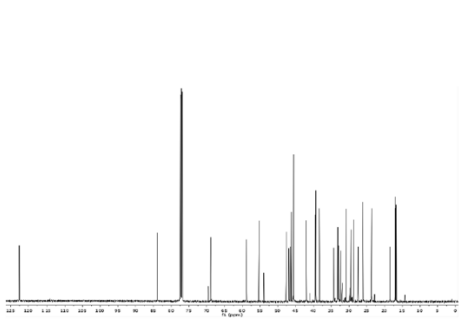

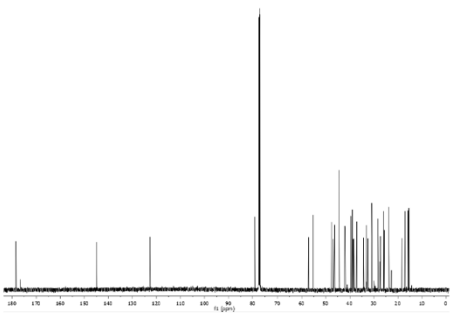

MA-PDA-MA

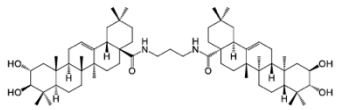

^{1}HNMR($CDCl_3$, 400 MHz): δ 6.43 (dd, 1H, *J*1 = *J*2 = 6.0 Hz), 5.35 (dd, 1H, *J*1 = *J*2 = 3.2 Hz), 3.70 (ddd, 1H, *J*1 = 4.0, *J*2 = 9.2, *J*3 = 14.0 Hz), 3.28–3.23 (m, 1H), 3.15–3.10 (m, 1H), 3.01 (d, 1H, *J* = 9.2 Hz), 2.65 (dd, 1H, *J*1 = 3.6, *J*2 = 13.2 Hz), 1.16, 1.03, 0.98, 0.92, 0.91, 0.83, 0.74 (s, 3H); ESI-HRMS m/z calculated for $C_{63}H_{103}N_2O_6$ $[M+1]^+$ 983.7816, found 983.7781.

OA-PDA-OA

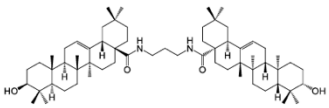

^{1}HNMR($CDCl_3$, 400 MHz): δ 6.41 (dd, 1H, *J*1 = *J*2 = 6.0 Hz), 5.40 (dd, 1H, *J*1 = *J*2 = 3.2 Hz), 3.28–3.24 (m, 1H), 3.21 (dd, 1H, *J*1 = 4.8, *J*2 = 11.21 Hz), 3.14–3.10 (m, 1H), 2.64 (dd, 1H, *J*1 = 3.2, *J*2 = 14.4 Hz), 1.25, 1.15, 0.98, 0.91, 0.90, 0.77, 0.74 (s, 3H); ESI-HRMS m/z calculated for $C_{63}H_{101}N_2O_4$ $[M+1]^+$ 949.7761, found 949.7772.

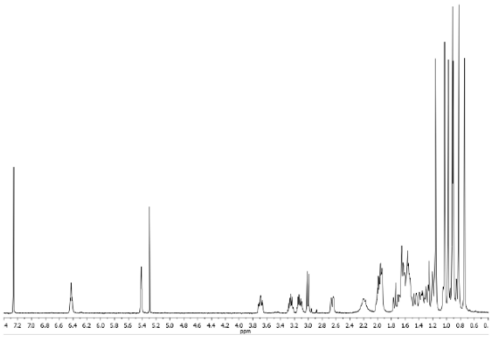

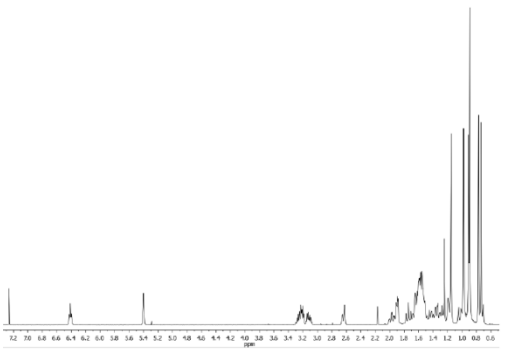

MA-HDA-MA

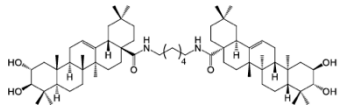

^{1}HNMR(CDCl3, 400 MHz): δ 5.94 (dd, 1H, *J*1 = *J*2 = 5.4 Hz), 5.38 (dd, 1H, *J*1 = *J*2 = 3.2 Hz), 3.70 (ddd, 1H, *J*1 = 4.4, *J*2 = 9.2, *J*3 = 13.6 Hz), 3.38–3.30 (m, 1H), 3.01–2.94 (m, 1H), 3.00 (d, 1H, *J* = 9.2 Hz), 2.50 (dd, 1H, *J*1 = 3.2, *J*2 = 12.8 Hz), 1.25, 1.16, 1.03, 0.99, 0.90, 0.83, 0.76 (s, 3H); ESI-HRMS m/z calculated for $C_{66}H_{109}N_2O_6$ $[M+1]^+$ 1025.8286, found 1025.8268.

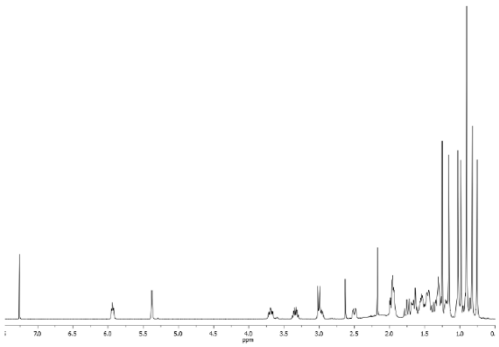

OA-HDA-OA

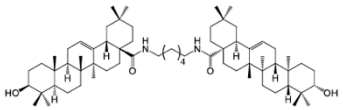

^{1}HNMR($CDCl_3$, 400 MHz): δ 5.95 (dd, 1H, *J*1 = *J*2 = 5.2 Hz), 5.36 (dd, 1H, *J*1 = *J*2 = 3.0 Hz), 3.35–3.30 (m, 1H), 3.20 (dd, 1H, *J*1 =4.2, *J*2 = 11.0 Hz), 3.00–2.93 (m, 1H), 2.48 (dd, 1H, *J*1 = 3.2, *J*2 = 13.2 Hz),1.14, 0.97, 0.89, 0.89, 0.88, 0.77, 0.74 (s, 3H); ESI-HRMS m/z calculated for $C_{66}H_{107}N_2O_4$ $[M+1]^+$ 991.8231, found 991.8235.

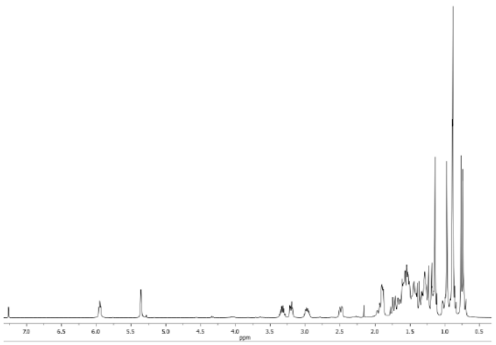

MA-DAD-MA

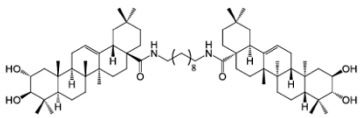

^{1}HNMR(CDCl3, 400 MHz): δ 5.94 (dd, 1H, *J*1 = *J*2 = 5.2 Hz), 5.37 (dd, 1H, *J*1 = *J*2 = 3.2 Hz), 3.69 (ddd, 1H, *J*1 = 4.4, *J*2 = 9.6, *J*3 = 14 Hz), 3.35–3.29 (m, 1H), 3.02–2.96 (m, 1H), 3.51 (d, 1H, *J* = 9.6 Hz), 2.47 (dd, 1H, *J*1 = 3.2, *J*2 = 12.4 Hz), 1.25, 1.16, 1.03, 0.98, 0.90, 0.83, 0.76 (s, 3H); ESI-HRMS m/z calculated for $C_{70}H_{117}N_2O_6$ $[M+1]^+$ 1081.8912, found 1081.8900.

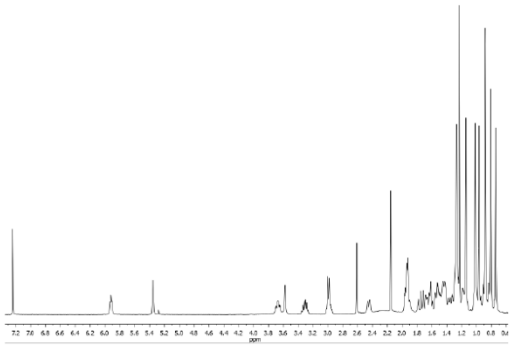

OA-DAD-OA

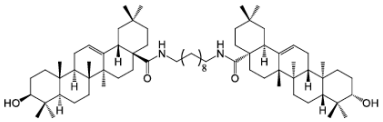

^{1}HNMR($CDCl_3$, 400 MHz): δ 5.90 (dd, 1H, *J*1 = *J*2 = 4.8 Hz), 5.36 (dd, 1H, *J*1 = *J*2 = 2.8 Hz), 3.37–3.32 (m, 1H), 3.21 (dd, 1H, *J*1 =4.4, *J*2 = 10.8 Hz), 3.00–2.93 (m, 1H), 2.49 (dd, 1H, *J*1 = 2.6, *J*2 = 12.6 Hz),1.25, 1.15, 0.98, 0.91, 0.90, 0.78, 0.76 (s, 3H); ESI-HRMS m/z calculated for $C_{70}H_{117}N_2O_4$ $[M+1]^+$ 1049.9013, found 1049.8990.

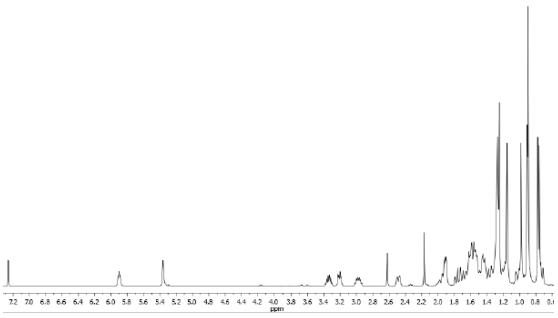

ARTICLE 3

A new BiofilmChip device as a personalized solution for testing biofilm antibiotic resistance.

Manuscrit

Autors: **Núria Blanco-Cabra**[1,#], Maria José López-Martínez[2,5,6,#], Betsy Verónica Arévalo-Jaimes[1], María Teresa Martin-Gómez[3], Josep Samitier[2,5,6] and Eduard Torrents[1,4,*]

1: Bacterial Infections and Antimicrobial Therapies, Institute for Bioengineering of Catalonia (IBEC) The Barcelona Institute of Science and Technology (BIST), Barcelona, Spain.

2: Nanobioengineering group. Institute for Bioengineering of Catalonia (IBEC), The Barcelona Institute of Science and Technology (BIST). Baldiri Reixac 15-21. 08028 Barcelona. Spain.

3: Microbiology Department, Hospital Universitari Vall d'Hebron, Barcelona, Spain.

4: Microbiology Section, Department of Genetics, Microbiology and Statistics, Faculty of Biology, University of Barcelona, 643 Diagonal Ave., 08028, Barcelona, Spain.

5: Networking Biomedical Research Center in Bioengineering, Biomaterials and Nanomedicine (CIBER-BBN) Monforte de Lemos 3-5, Pabellón 11, 28029 Madrid, Spain

6: Department of Electronics and Biomedical engineering, University of Barcelona, Martí i Franquès 1, 08028 Barcelona, Spain

#: Aquestes coautores han contribuït de manera igualitària en aquest article.

*: Correspondència: Dr. Eduard Torrents (etorrents@ibecbarcelona.eu)

Abstract

Currently, three major circumstances threaten the management of infections: increasing antimicrobial resistance, expansion of chronic biofilm-associated infections, and lack of an appropriate approach to treat them. To date, the development of accelerated drug susceptibility testing of biofilms and of new antibiofouling systems has not been achieved despite the availability of different methodologies. There is a need for easy-to-use methods of testing the antibiotic susceptibility of bacteria that form biofilms and for screening new possible antibiofilm strategies.

Here, we present a new easy method for testing antibiofilm susceptibility using a microfluidic device (BiofilmChip) that measures biofilm biomass by electrical impedance spectroscopy. BiofilmChip enables the growth of different bacterial species from clinically isolated strains and directly from sputum samples obtained from cystic fibrosis patients. Our results demonstrate that BiofilmChip is a useful tool for antimicrobial resistance testing in biofilms.

Introduction

Biofilms are communities of microorganisms that form on and attach to living and nonliving surfaces. Biofilms are ubiquitous, as they are found in natural, industrial and medical environments. Biofilms can be beneficial under some conditions, for example, for biodegradation in wastewater treatment, but they are often undesired because of their ability to cause infections, contamination, biofouling, and biocorrosion[1].

The attached microorganisms form microcolonies on a surface, where the bacteria are embedded in the extracellular polymeric substances (EPS) that form the biofilm matrix[2]. The matrix protects the microorganisms and makes biofilms very difficult to eradicate because it increases their resistance to biological, mechanical, physical, and chemical treatments[3]. Taking into account that approximately 80% of chronic infections in animals and humans are estimated to be biofilm-related[4], their formation presents a severe threat in the battle against antimicrobial resistance, and related treatments require several billions of US dollars each year worldwide[5,6]. Moreover, to date, no antibiotic that can successfully eradicate biofilms has been found, so there is a great need for new strategies to combat biofilms[7] while awaiting for the development of effective antibiofilm molecules.

Model systems of in vitro biofilms are essential in research laboratories for testing new antibiofilm compounds, as well as in clinical laboratories for determining the best treatment of biofilm-related infections. There is a wide selection of different monitoring techniques for biofilm growth and characterization, varying in the analysis scale, handling time, sensitivity and final detection technique employed[8]. Standard methods mostly rely on colorimetric measurements and are commercially available, i.e., the MBEC Assay®[9] and the Biofilm Ring Test[10]. These techniques allow

the screening of different antimicrobials in a high-throughput way, but they are generally destructive endpoint diagnostic tools and require removal of the formed biofilm from the growth substrate used. For this reason, these systems cannot be exploited for online monitoring characterization.

Other techniques require advanced microscopy systems to monitor biofilm growth, which is not always available in clinics and some research laboratories. Moreover, the majority of these high-throughput screening techniques involve the use of static devices with limited nutrients, which form biofilms that do not resemble the biofilms found during natural infections. In addition, dynamic devices that allow bacteria to grow under flow conditions can better mimic real in vivo infective conditions[11]. One of the recurrent problems with such flow conditions is the need for large volumes of media and tubing, which prevent high-throughput screening. Recently, Acea Bioscience released xCELLigence based on electrical impedance spectroscopy (EIS) measured on the basis of a defined Cell Index (CI) parameter[14]. This technique is based on the detection of changes in the diffusion coefficient of a redox solute, which is recorded as an electrochemical reaction on the electrode; thus, this technique provides an excellent nondestructive method for real-time and in situ measurements not based on confocal microscopy. Indeed, EIS was shown to be suitable for online monitoring of biofilm formation, although all the experiments were performed under static conditions and did not resemble all natural infections[15,16].

Microfluidics represents the next generation of fluidic platforms for biomedical research[12]. Microfluidic devices provide dynamic systems with significant control over the flow rate settings, potential for real-time analysis and, particularly for biofilms, greater similarity to the in vivo infective environments by creating the physical conditions encountered in natural environments[13].

Even though antibiotics that affect planktonic growth typically become useless when the bacteria form a biofilm, none of the abovementioned techniques are normally used in clinical laboratories to find appropriate treatments for a chronic biofilm infection, as they are too complicated and require costly and intricate equipment operated by experienced personnel. Instead, antibiotic efficacy is determined using planktonic bacteria. Furthermore, real biofilm-forming infections are known to be polymicrobial, which modify their antibiotic susceptibility[18], but conventional antimicrobial susceptibility test is performed on single isolates obtained from complex samples, thereby missing other important species and their interactions in clinical samples[17].

In this work, we developed a microfluidic system to determine the best therapeutic intervention for a patient suffering a chronic infection from bacteria growing in a biofilm or a treatment for antifouling in industry, among other applications. We proposed an innovative rapid method for studying new antibiofouling strategies, including drug susceptibility testing of different bacterial species using EIS. This microfluidic platform allows homogeneous biofilm growth that can be easily monitored without using a confocal microscope and enables the development and co-culture of polymicrobial biofilms that resemble the real biofilm infections found in complex matrixes such as sputum samples (e.g., cystic fibrosis infections).

Results

Chip fabrication and characterization

A microfluidic platform with an integrated interdigitated sensor (BiofilmChip) was designed to monitor the growth and treatment of a biofilm in a controlled manner (Fig. 1a-b). The chip was prepared by a combination of standard photolithography and soft lithography techniques. The final system setup is shown in Fig. 1c. Briefly, the medium bottle was connected through tubing to the microfluidic device. Medium was pumped through the system via a high-precision peristaltic pump (see the Material and Methods for details).

Following the experimental scheme shown in Fig. 1d and f, a biofilm formed and grew inside the chambers via irreversible attachment of bacterial cells to the cover glass. The biofilms could then be visualized under a confocal microscope after a specific staining procedure (Fig. 1c and f) or directly analyzed by impedance measurements (as shown in Fig. 1c and e).

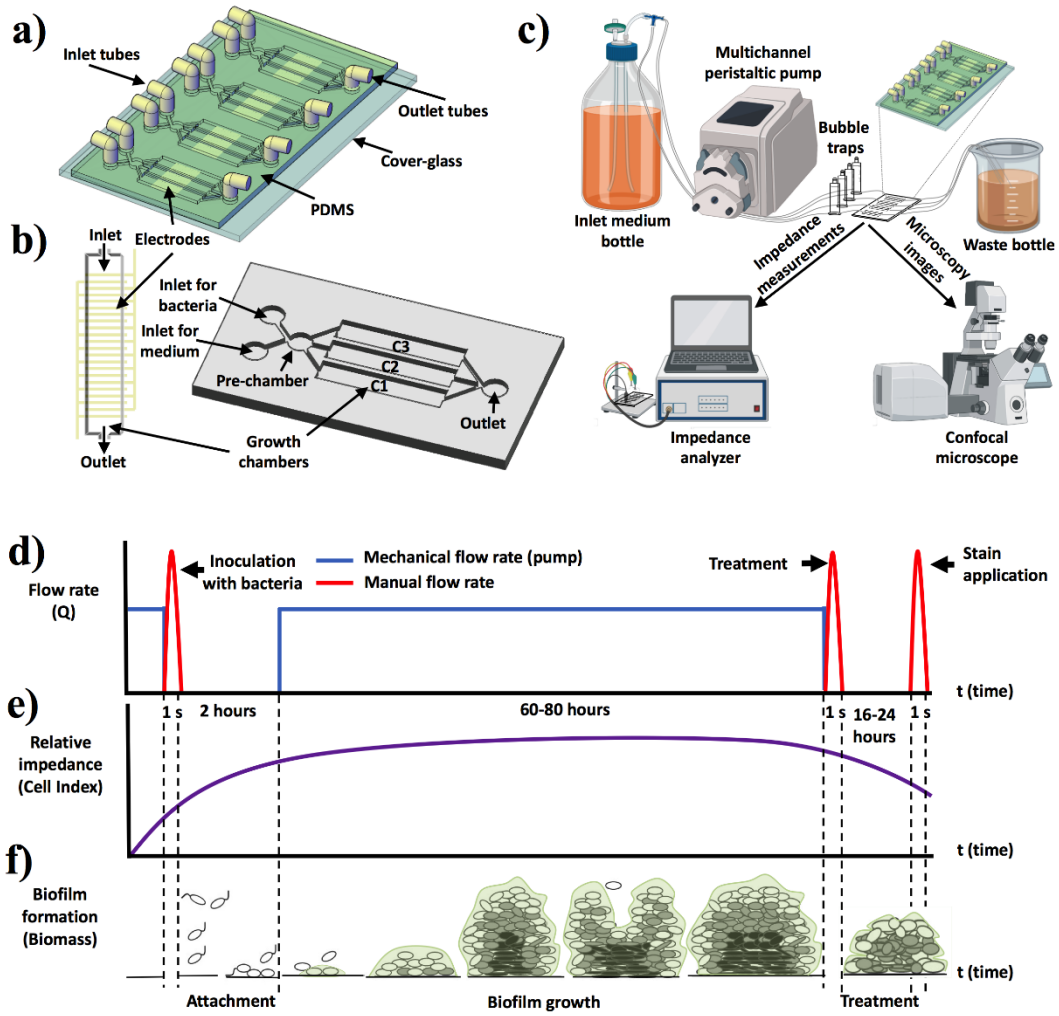

Fig. 1. **Biofilm chip design:** a) BiofilmChip 3D view, b) 3D view of one chamber with the electrodes and one set of 3 chambers, c) experimental setup, d) changes in the mechanical flow rate (in blue) and the manual flow rate (in red, only during the inoculation with bacteria and applications of treatment or stain), e) expected relative impedance and f) biofilm formation over time. Figure created in part with biorender.com.

Optimal parameters for uniform biofilm formation

Our primary goal was to design a BiofilmChip with optimized capacity for growing biofilms with maximal uniformity across the different chambers of the chip. First, several prototype designs with chambers that differed in dimension and shape were fabricated and tested by growing a *P. aeruginosa* PAO1 biofilm. The different prototypes manufactured and tested are shown in Fig. 2, and the formed biofilms were established as described in Fig. 1c, stained with LIVE/DEAD dyes, and visualized under a confocal microscope. As seen in Fig. 2, the chamber geometry and height clearly impacted the optimal biofilm formation: a rectangular morphology was preferred over a square morphology.

As observed in prototype b (Fig. 2b), the biofilm formed in the square chamber was nonhomogeneous, while that formed in the rectangular chamber (with a height of 150 µm) remained smooth (Fig. 2d).

P. aeruginosa cell division was impaired in the outer biofilm layers of the 50- and 100-µm height chambers, with evident cell filamentation and increased cell death (stained in red), indicated by a more significant proportion of red biomass (ratios of dead cell biomass to total biomass of 0.57, 0.26 and 0.37) (Fig. 2a-c). On the other hand, bacteria had a morphology characteristic of wild-type *Pseudomonas* in the chip with 150-µm height chambers and showed uniform green staining covering the entire surface area (a lower proportion of dead cells) (Fig. 2d-e).

Even though the optimal parameters (rectangular shape with 150 µm high) resulted in homogeneous biofilms with a low proportion of dead cells (ratio of 0.24), manual system manipulations (i.e., direct injection during inoculation and staining) caused disturbances in biofilm uniformity (Fig. 2d). There is a tremendous boost of the shear stress all along with the chamber due to the abrupt increase in the flow rate when injecting the bacteria for inoculation. (Fig. 1d). The pressure generated at the inlet was 363 ± 197 psi during manual injection[19]. At this specific pressure generated during injection, we simulated the influence of fluid velocity and chamber shape on biofilm formation using COMSOL Multiphysics software (COMSOL AB, Sweden). Supplementary Fig. 1 shows that the inclusion of a prechamber ahead of the biofilm growth chambers stabilized the flow and rendered a better distribution of velocity, minimizing the effect of sample loading. The results were confirmed by observing uniform biofilm growth in the chambers, as shown in Fig. 2e.

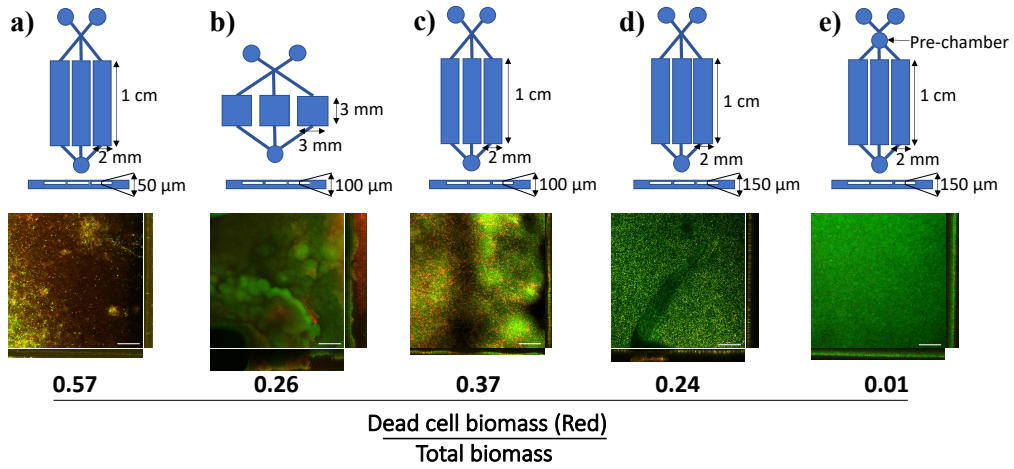

Fig. 2. BiofilmChip dimensions, geometry and functional characterization: schematic representations of the different manufactured chip geometries. The biofilm structure formed in each chip is shown in the confocal microscopy images (sum and orthogonal views). In all cases, the biofilm was grown for 72 hours and stained with the LIVE/DEAD BacLight Bacterial Viability Kit. At the bottom of the images, the proportion of dead cells (stained in red) in the total biofilm biomass is shown. Scale bar represents 50 µm.

BiofilmChip robustness

We next evaluated the robustness of the BiofilmChip with the optimized conditions (rectangular chambers 2 mm wide, 10 mm long, and 150 µm high with a 2-mm prechamber diameter) (Fig. 2e) by analyzing some biofilm parameters along with the biofilm growth chamber. For these experiments, we used laboratory strains of *Pseudomonas aeruginosa* PAO1 and *Staphylococcus aureus* (ATCC12600). We compared the biofilm biomass and thickness at different locations inside a chamber (close to the inlets, the middle part and the outlet, see Fig. 3a), across all three chambers (Fig. 3b) and finally among separate chambers of the same set (Fig. 3c). In all cases, we observed robust, homogenous biofilm formation with similar biomass and thickness values among the different locations and chambers, demonstrating the uniformity of the biofilm formed. Note that in Fig. 3c, we used two bacterial strains isolated from chronically infected cystic fibrosis patients (*P. aeruginosa* PAET1 and methicillin-resistant *S. aureus* MRSA).

As a proof of concept to evaluate the ability of our BiofilmChip to assess antimicrobial therapy, we determined the ability of the chip to sense a reduction in the biomass of biofilm formed after treating a mature biofilm (72 hours old) with a known antibiotic. As shown in Fig. 3d, the treatment of *P. aeruginosa* laboratory strain PAO1 and clinical *P. aeruginosa* isolate PAET1 with 2 and 20 µg/ml ciprofloxacin, respectively, produced a reduction in the biofilm biomass (35 and 71%) and thickness (12 and 14%) detected with our BiofilmChip. Therefore, BiofilmChip was suitable for use in inhibition experiments to observe changes in biofilm biomass after specific antibiotic treatment.

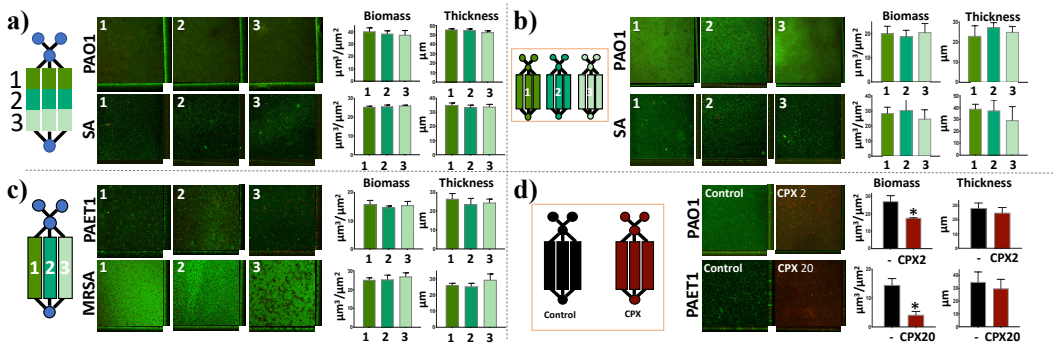

Fig. 3. BiofilmChip robustness evaluation: Uniformity in the established biofilm biomass and thickness across different chamber locations (a), between sets of chambers (b), and among chambers in the same set (c). Decreases in biomass and thickness after 24 hours of treatment of *P. aeruginosa* PAO1 and PAET1 with ciprofloxacin (d). In all cases, 72-hour-old biofilms were stained and visualized by confocal microscopy (CLSM). Images represent the sum of stacked CLSM images and their corresponding orthogonal views, and bars show the quantified biofilm biomass ($\mu m^3/\mu m^2$) and average thickness (µm). PAO1 (*P. aeruginosa* PAO1 laboratory strain), PAET1 (*P. aeruginosa* PAET1 clinical isolate strain), SA (*S. aureus* laboratory strain), MRSA (*S. aureus* MRSA clinical isolate strain). *: $p<0.05$ vs. control in a *t*-test.

BiofilmChip is a versatile system to grow biofilm directly from clinical sputum samples.

The BiofilmChip prototype has been tested with laboratory and clinical strains of *P. aeruginosa* and *S. aureus* (Fig. 3) and directly from patient samples.

Sputum samples from cystic fibrosis patients (Supplementary Table 1) at different stages of *P. aeruginosa* and/or *S. aureus* chronic infection were tested. First, the sputum samples were treated with hypotonic media as described in the Material and Methods section and inoculated directly into the BiofilmChip by injecting the sample through the inlet port while the medium flow was stopped. After 2 hours, the TSB media was allowed to flow for 72 hours. The formed biofilm was stained and visualized under a confocal microscope.

Interestingly, our system allowed the biofilm formation and growth of different bacterial species simultaneously from the sputum samples. Fig. 4 displays representative confocal microscopy images of the biofilms formed from four different sputa (I-IV) (Supplementary Table 1). Different bacterial shapes and morphologies can be seen in the enlarged image of biofilms a) and b) (Fig. 4, sputum I-II), stained with the LIVE/DEAD Viability Kit. Furthermore, the biofilms from sputum III and IV (Fig. 4c-d), stained with the Gram Stain Kit, can be distinguished on the basis of the Gram staining of the different bacteria found. Information concerning the identification and antibiotic susceptibility of the bacteria present in each sputum sample is presented in Supplementary Table 1. Sputum II and IV were found to contain *P. aeruginosa* and *S. aureus* (Supplementary Table 1), which could correspond to the bacilli and staphylococci found in the biofilm (Fig. 4b and d). However, other bacteria also grew, as observed in the confocal images. On the other hand, only *P. aeruginosa* was found in the planktonic cultures of sputum I and III (Fig 4a and c, Supplementary Table 1), which can correspond to the bacilli found in the biofilm from sputum I, but no signs of Gram-negative bacilli were found in the biofilm from sputum III, demonstrating the existing variability between the planktonic cells used for microbiological identification and those involved in biofilm growth.

The importance of growing the biofilms directly from sputum samples before analyzing them was corroborated by directly visualizing the sputum by confocal microscopy imaging (Supplementary Fig. 2), showing that it is not possible to directly observe diverse bacteria and their interactions due to the low bacterial concentrations, the presence of eukaryotic cells and the remaining mucus.

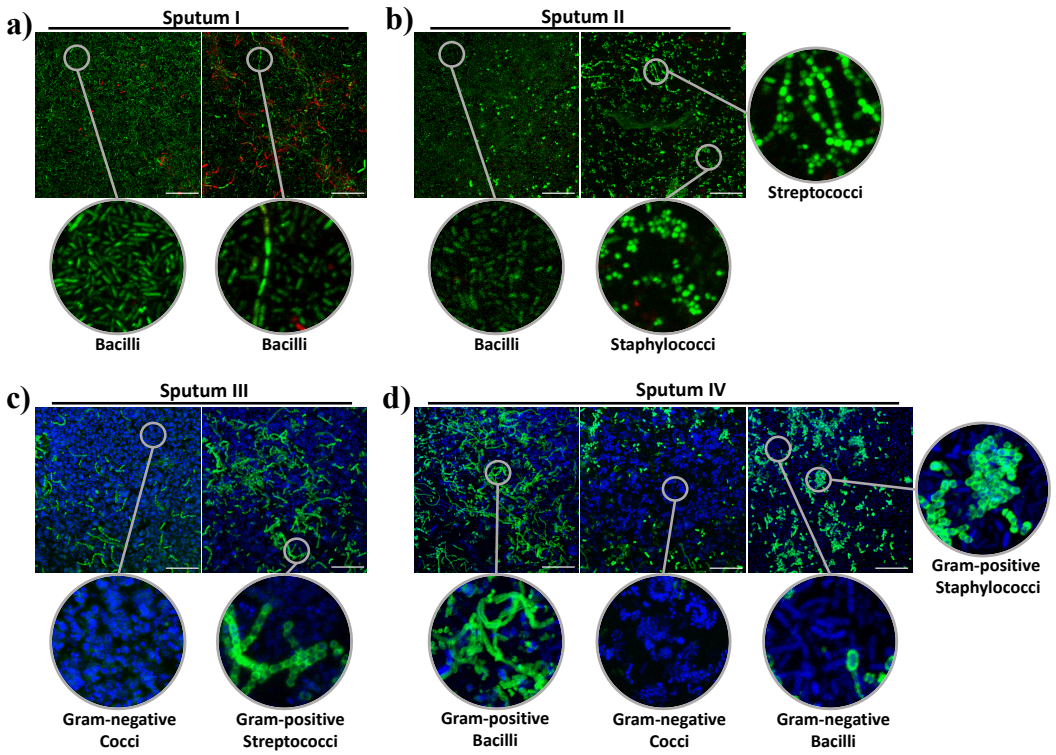

Fig. 4. Biofilms formed from four different sputum samples (I-IV) with enlarged images showing the different bacterial shapes found. Biofilms were stained with a LIVE/DEAD BacLight Bacterial Viability Kit (a and b) and with a Gram Stain Kit (c and d), which stains Gram-negative bacteria blue and Gram-positive bacteria green. Scale bar represents 20 μm.

Correlation of confocal microscopy and impedance measurements in the BiofilmChip.

To validate the use of the BiofilmChip in antibiofilm drug susceptibility tests, 3-day-old biofilms of *P. aeruginosa* PAO1 (wild-type strain) and *P. aeruginosa* PAET1 (clinically isolated strain) were treated for 24 hours with 2 μg/ml and 20 μg/ml ciprofloxacin, respectively. They were imaged with confocal microscopy to calculate the biofilm biomass. As shown in Fig. 3d, the treated biofilm biomass was significantly decreased compared to that of the control biofilm without treatment. Then, to evaluate whether impedance measurements could be correlated to the established confocal microscopy images for biofilm monitoring, a *P. aeruginosa* PAO1 strain encoding a green fluorescent protein (*GFP*) (MK171) was used to grow and easily visualize the biofilm during the time when staining it continuously was not necessary.

We next used BiofilmChip devices with integrated interdigitated sensors (see Fig. 1a-b and the Material and Methods). Initially, impedance was measured at frequency values between 4 Hz and 400 kHz every 12 hours during the entire biofilm growth period (from before inoculation until after treatment). Measures were plotted in a Bode diagram (shown in Supplementary Fig. 3). The results at 400 Hz frequency showed substantial differences in impedance at the different steps of the experiment. Then, impedance measurements at 400 Hz and confocal microscopy images were performed at the same time to calculate the cell index (CI) (see the Materials and Methods) and the biofilm biomass, respectively. In the early stages of biofilm formation, the cells can be imaged under a confocal microscope, but the calculated biomass is nearly zero. The CI, however, varied during the initial biofilm formation stages. Fig. 5 shows how the CI can reflect biofilm growth more accurately than confocal microscopy throughout the maturation process, whereas the biomass calculated from microscopy images can only be accurately detected in mature biofilms (65-72 hours old). Thereafter, 69 hours old biofilms were treated with ciprofloxacin at 5 μg/ml and 10 μg/ml for 16 hours, and the impedance and biomass were measured. Both the CI and biomass presented the same response to the antibiotic at the two concentrations (green and red lines, Fig. 5) or the lack of treatment (blue line, Fig. 5).

Considering the impedance changes on the basis of antibiotic treatment seen in Fig. 5, the applicability of these impedance measurements to the antibiotic sensitivity of real patient samples was tested (Supplementary Table 1, sputum V-VII). Biofilms were grown from different sputum samples having a pathogen with a known susceptibility profile, and they were treated with different antibiotics. Biofilm impedance diminished in the presence of an effective antimicrobial treatment, as proven by the difference in CI values calculated before and after antibiotic exposure of biofilms formed from sputa V-VII (Supplementary Table 1). This CI response agrees with the response found from Fig. 5, validating the use of BiofilmChip for biofilm susceptibility testing directly from clinical samples.

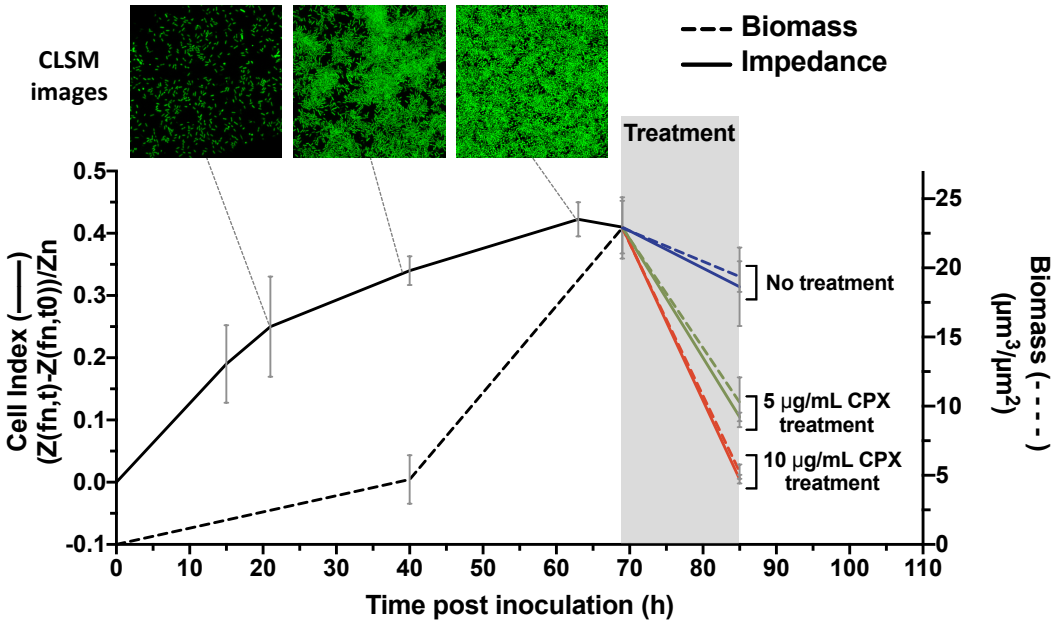

Fig. 5. Monitored *P. aeruginosa* MK171 (expressing eGFP) biofilm growth and effect of antibiotic treatment evaluated on the basis of electrical impedance (represented as the CI, left y-axis, solid line) and biomass calculated from confocal microscopy images (defined as $\mu m^3/\mu m^2$, right y-axis, dashed line). In the shaded part, corresponding to the treatment duration, green and red lines represent 5 µg/ml and 10 µg/ml ciprofloxacin treatment, respectively, and the blue line illustrates the control without treatment. Representative confocal images from three different time points are shown.

Discussion

Biofilm-related infections are currently a serious threat around the world. The overuse and misuse of antibiotics, along with the expansion of biofilm-associated chronic infections is leading to an increasing prevalence of multi-drug resistant bacteria, resulting in a rise in the morbidity and mortality of these infections, which are expected to cause the death of ten million people by 2050[20]. The susceptibility of bacteria embedded in a biofilm can significantly differ from that of the same free-living bacteria, as it is known that bacteria growing in biofilms have an intrinsically higher antibiotic resistance than their planktonic counterparts due to different mechanisms[21]. Nevertheless, currently, the treatment decisions for biofilm infections are based on susceptibility tests performed in planktonic bacteria immediately after individual bacterial isolation. This makes the treatment choice inappropriate for the effective management of biofilm-associated infections[22]. Moreover, standard antimicrobial susceptibility tests are performed on individual isolates considered relevant by the microbiologist among the full range of growing microorganisms, so in case more than one pathogen is isolated, multiple tests have to be carried out. Taken together, part of the antimicrobial misuse could be attributed to the lack of tools and readily implemented technologies applied in typical microbiology laboratories to easily determine the proper treatment for biofilm infections.

The tool we developed consists of a microfluidic chamber aligned to an interdigitated electrode on which the biofilm grows. It was designed to evaluate biomass formation during the establishment of a biofilm and test antimicrobial drugs and treatments using EIS. Due to the integration of EIS into this BiofilmChip, it is unnecessary to use sophisticated technology such as advanced confocal microscopy, making it suitable for typical microbiology laboratories or industry.

BiofilmChip has several advantages. For example, the microfluidics better mimic growth and resemble a naturally occurring biofilm and reduce the amount of medium and reagents needed to run these continuous biofilm experiments. We have optimized this chip's development by producing different variants of the growth chamber geometry and dimensions to enable optimal biofilm development. It has been documented that the flow cell geometry and the shear stress in the chambers affect biofilm growth[23]. In agreement with that, we observed that both the chamber shape and height were key factors to be considered when reproducing a homogeneous biofilm. It was found that a rectangular shape and 150 μm height were optimal for this purpose, as shown in Fig. 2.

Moreover, an important feature of our device is the inclusion of a prechamber in the design (Fig. 1a), which prevents biofilm disturbances caused by manual inoculations that suddenly increase the flow rate (and consequently the shear stress) inside the chambers. The simulations of the media flow velocity inside the chambers (Supplementary Fig. 1) demonstrated that the design with a prechamber enables a more homogeneous media distribution among the three chambers of the same set, leading to a more uniform biofilm and minimizing the impact of manual injection. Although

biofilms in nature are rather heterogeneous[24], homogeneity is a key factor for further reliable detection of susceptibility under different treatments. As Fig. 3d shows, significant decreases in *P. aeruginosa* PAO1 and PAET1 biofilm biomass were detected after treatment with 2 μg/ml and 20 μg/ml ciprofloxacin, respectively. To our knowledge, the prechamber is an innovative component that has never been published before; therefore, this new component represents a breakthrough in microfluidic devices, where flow rate control is critical.

It is well known that continuous biofilms produced in vitro are more reliable for antibiotic susceptibility studies[25], as they are more reproducible and similar to the in vivo infection than are in vitro static biofilms performed in microtiter plates. However, the analysis of these continuous biofilms by confocal microscopy is expensive, requires further staining and trained personnel and is extraordinarily time-consuming. We demonstrate an excellent correlation of the biofilm biomass measured via a standardized methodology involving confocal microscopy with the impedance results, which clearly validates the use of EIS to evaluate biofilm growth. One interesting observation from the use of impedance measurements at 400 Hz is that such measurements are more sensitive, as they can detect biofilms in the early stages of growth, when biomass measurements by confocal microscopy are not sensitive enough to distinguish the attachment of bacterial cells to the substrate (Fig. 5). Once a biofilm is mature, the measures under confocal microscopy are comparable to those under EIS.

Moreover, the impedimetric response can be used to measure the reaction of biofilms to antibiotic exposure. In the biofilms in Fig. 5, the CI has the same pattern as the quantified biomass. For the biofilms formed from sputum samples described in Supplementary Table 1 (V-VII), the impedimetric response of the biofilms to the antibiotic was on the same wavelength as the sensitivity reported from the sputum, demonstrating the applicability of the BiofilmChip for antibiofilm testing and choosing the right personalized therapy.

Interestingly, the BiofilmChip was designated to be used for growing biofilms with different characteristics, including biofilms composed of different bacterial species (from laboratory use or clinical isolates) and isolated directly from different samples obtained from patients suffering a biofilm infection (sputum from patients suffering from bronchiectasis, urinary infections, etc.) or hypothetically from contaminated surfaces such as medical devices (catheters, cardiac valves, infected joints, etc.) or samples from the food industry (surfaces, etc.), among others.

Under natural conditions, most of these biofilms are formed from a polymicrobial community of bacteria[26]. Specifically, a clear example is found in chronic infections in the cystic fibrosis lung, which is known as a polymicrobial consortium formed from different bacterial species[27,28]. Under these conditions, the antibiotic concentration needed to remove the formed biofilm is different from

the needed to treat isolated planktonic bacteria or even to treat bacteria grown in a monomicrobial biofilm.

Our BiofilmChip enables the growth of polymicrobial biofilms, as it makes the growth of a biofilm directly from a patient sputum sample possible and ensures that no species are excluded, and helps determine the best treatment needed for personalized therapy. For instance, the sputum samples used to form the biofilm shown in Fig. 4 b) and d) are reportedly from a CF patient suffering from a lung infection by *P. aeruginosa* and *S. aureus* (sputum II and IV in Supplementary Table 1). However, when these sputum samples were directly grown in the BiofilmChip, a diverse population of other microorganisms was found, and the polymicrobial nature of these infections was demonstrated. The antibiotic treatment prescribed for these patients has probably been determined from the individual susceptibility of *P. aeruginosa* and *S. aureus* grown in isolation and planktonically, but as we have previously reported[18], antibiotic resistance can significantly change in polymicrobial biofilms[29,30]. Therefore, the treatment chosen for these patients would have probably been more accurate if it had been based on the BiofilmChip, allowing personalized treatment.

Materials and Methods

Laboratory and clinically isolated bacterial strains and growth conditions

Wild-type *Pseudomonas aeruginosa* PAO1 strain CECT 4122 (ATCC 15692) and *Staphylococcus aureus* CECT 86 (ATCC 12600) were obtained from the Spanish Type Culture Collection (CECT). The *P. aeruginosa* PAET1 strain isolated from a cystic fibrosis patient suffering from persistant infection and *S. aureus* MRSA were from our laboratory stock[31,32]. *Pseudomonas aeruginosa* PAO1::eGFP (MK171) was kindly provided by Prof. Tim Tolker-Nielsen[33]. To obtain inocula for examination, the strains were cultured overnight at 37°C in Luria Bertani (LB) liquid medium (Scharlab, Spain) for *P. aeruginosa* and tryptic soy broth (TSB) medium (Scharlab, Spain) for *S. aureus*. Bacterial growth was measured by reading the absorbance at 550 nm (A_{550}).

Obtaining and Processing clinical sputum samples

Excess sputum samples (Supplementary Table 1) from cystic fibrosis patients were collected at the Hospital Universitari Vall d'Hebron Microbiology Department. Approval regarding human sample collection and manipulation was obtained from the Clinical Research Ethics Committee (Comitè Ètic d'Investigació Clínica, CEIC) under the number PR(AG)275/2019. Sputum samples were diluted in 10 mM Tris-HCl hypotonic buffer at pH 7.5 (Fisher Scientific, Spain) in a 1:1 ratio and incubated at 4°C for 5 minutes before inoculation.

Microfluidic device design and fabrication: Chip fabrication and electrode fabrication

The fabrication of the BiofilmChip (Fig. 1a) involved a multistep procedure using photolithographic and soft lithographic techniques carried out in the MicroFabSpace and Microscopy Characterization Facility, Unit 7 of ICTS "NANBIOSIS" from CIBER-BBN at IBEC. All solvents and chemicals were obtained from Sigma Aldrich unless otherwise specified. The SU-8 photoresist and developer were from MicroChem (Newton, MA). The Ordyl photoresist and developer were from Elga (Italy).

Microfluidic chambers were designed using CAD software (Autodesk, USA), and the master was built over a glass substrate (TED PELLA, Inc., USA) (75 mm x 25 mm). Briefly, the fabrication process started with three consecutive solvent baths (acetone, isopropanol, and ethanol) applied to the glass slide. Following this cleaning protocol, up to three layers of Ordyl SY 550 were laminated on top of the support material using a hot/cold laminator to obtain a smooth attached film surface (150 µm high). Then, the slide was exposed through an acetate photomask to UV light (5 s, 24 mW cm2, 345 nm) in the mask aligner and subsequently placed on a hot plate at 65 °C for 3 minutes.

The 3D master mold fabrication was finished by developing the Ordyl film using the developer solvent for 3 minutes. To replicate this mold, a poly(dimethylsiloxane) (PDMS) prepolymer mixture (a curing agent-to-PDMS ratio of 1:10, Sylgard®184, Dow Corning) was placed in a desiccator with a vacuum applied to remove bubbles. The mixture was then poured on top of the Ordyl master to fabricate a PDMS replica and heated overnight at 65 °C. The casted PDMS was peeled off carefully, and inlet and outlet holes were made using a Harris Uni-Core 0.5 mm puncher. A general view of the PDMS BiofilmChip used for biofilm growth and analysis is shown in Fig. 1a. The BiofilmChip includes several sets of independent chambers, each connected to two inlets (one for medium and one for bacterial inoculation), one prechamber, three different growth chambers (C1, C2, C3) and one outlet (Fig. 1b). Each growth chamber was 2 mm wide, 10 mm long and 150 µm high. The BiofilmChip unit was fabricated as three connected chambers (C1, C2 and C3) and considered representative with coherent replicates for straightforward analysis of a given sample.

Gold interdigitated sensors (Fig. 1b) were fabricated onto a glass coverslip to facilitate inspection under a confocal microscope and correlation to impedance measurements. The dimensions and characteristics of the interdigitated electrode were 16 pairs of gold fingers with 75 µm width and 75 µm gap between them. The design of these fingers was selected following the microfluidic chamber size (Fig. 1b). AZ5214 was spread using a spinner to create a uniform layer over the glass substrate. After that, the resin was exposed to UV light in the desired pattern. Then, it was reversed, followed by UV flood light exposure. Next, the glass coverslip was dipped into a solution of AZ Developer 400K. Then, 20 nm chromium and 80 nm gold were thermally evaporated on glass. After this step, the glass slip was dipped into an AZ Remover 100 solution to remove the photoresist, leaving only the desired pattern's gold/chromium layer. For bonding to the PDMS microfluidic chamber, an

O_2 plasma cleaner was used to activate both surfaces. PDMS slabs were carefully placed in contact with the glass slide and left on a hot plate to create permanent bonding. The PDMS microfluidic chamber chip was ready to use. Before every assay, the microfluidic device was exposed to UV/ozone for 15 minutes to make the surface hydrophilic and sterile. Then, the device was filled with sterile Milli-Q water.

Experimental setup

The BiofilmChip system operated in the three different biofilm formation stages (inoculation, growth and measurement). The final setup is shown in Fig. 1c. LB or TSB + 0.2% glucose was stored in a 100 ml bottle connected through Tygon E-3603 tubing (1.5 mm diameter) (DD BioLab) to the microfluidic device. Tubes were attached to the chip by insertion into the inlet and outlet access holes. The medium was pumped through the system with a high-precision Ismatec IPC16 ISM933 multichannel peristaltic pump (Ismatec). Bubble traps (DTU Systems Biology, Technical University of Denmark) were added to the system to avoid the formation of bubbles inside the growth chambers. A constant flow rate of 11.4 µl/min for each set of three chambers was established. The system was filled with media through one inlet, and then, at the inoculation stage, a solution of bacteria ($A_{550} \approx 0.1$) or diluted hypotonic buffer sputum sample was pumped into the chip chamber through the other inlet.

At the start of the growth stage, the peristaltic pump was stopped for two hours to allow cell adherence to the glass surface. Then, the medium flowed through the chambers for 65-72 hours. The system was previously sterilized with 0.5% v/v sodium hypochlorite in water as previously described[34], and experiments were carried out at room temperature.

Confocal laser scanning microscopy and image analysis

Pseudomonas aeruginosa and *Staphylococcus aureus* nonfluorescent biofilms were stained with the LIVE/DEAD BacLight Bacterial Viability Kit (Thermo Scientific), consisting of SYTO9 and propidium iodide. Staining of the biofilms formed from sputum was performed with the Bacterial Viability and Gram Stain Kit (Biotium), which differentiates Gram-positive and Gram-negative bacteria. This kit comprises wheat germ agglutinin (WGA) coupled to a CF™-488 fluorophore that stains the walls of Gram-positive bacteria and the dye DAPI, which stains both Gram-negative and Gram-positive bacteria. Biofilms formed with *Pseudomonas aeruginosa* MK171 (expressing eGFP) were visualized under the microscope directly without staining.

All biofilms were visualized under a Zeiss LSM 800 confocal scanning laser microscope (CSLM) using 20X/0.80 air or 63X/1.4 oil objectives. Simulated fluorescence projections and

orthogonal sections were generated using ImageJ software, and COMSTAT 2 software was used to quantify the biomass and thickness of the biofilms[35].

Biofilm treatment

Biofilms between 65 and 72 hours old were treated for 16 or 24 hours with different antibiotic concentrations while the medium flow was stopped. After the treatment, the flow was set at 11.4 µl/min for 30 minutes to wash and exclude detached bacteria affected by the antibiotic from the biofilm.

Impedance measurements and cell index calculation:

We based our monitoring on the cell index (CI) parameter[36], as we wanted to use an independent parameter to compare measurements among different samples. The measurements were performed at 400 Hz.

$CI(t)= (Z(fn,t)-Z(fn,t0))/Zn$

where Zn is the corresponding nominal impedance value of fn (without cells)

The device used to record EIS values was an Agilent 4294A 40 Hz-110 MHz precision impedance analyzer. This equipment allowed measuring the impedance along a range of frequencies with an oscilloscope level of 0.5 V. The impedance was measured in the module and phase format and plotted in Bode diagrams. Once the microfluidic device was connected, two impedance measurements were recorded each day, one during the morning and the second one during the afternoon.

References

1 Karunakaran, E., Mukherjee, J., Ramalingam, B. & Biggs, C. A. "Biofilmology": a multidisciplinary review of the study of microbial biofilms. *Appl Microbiol Biotechnol* **90**, 1869-1881, doi:10.1007/s00253-011-3293-4 (2011).

2 Flemming, H. C. & Wingender, J. The biofilm matrix. *Nat Rev Microbiol* **8**, 623-633, doi:10.1038/nrmicro2415 (2010).

3 Lebeaux, D., Chauhan, A., Rendueles, O. & Beloin, C. From in vitro to in vivo Models of Bacterial Biofilm-Related Infections. *Pathogens* **2**, 288-356, doi:10.3390/pathogens2020288 (2013).

4 Sharma, D., Misba, L. & Khan, A. U. Antibiotics versus biofilm: an emerging battleground in microbial communities. *Antimicrob Resist Infect Control* **8**, 76, doi:10.1186/s13756-019-0533-3 (2019).

5 Yebra, D. M., Kiil, S. & Dam-Johansen, K. Antifouling technology—past, present and future steps towards efficient and environmentally friendly antifouling coatings. *Progress in Organic Coatings* **50**, 75-104, doi:10.1016/j.porgcoat.2003.06.001 (2004).

6 Lebeaux, D., Ghigo, J. M. & Beloin, C. Biofilm-related infections: bridging the gap between clinical management and fundamental aspects of recalcitrance toward antibiotics. *Microbiol Mol Biol Rev* **78**, 510-543, doi:10.1128/MMBR.00013-14 (2014).

7 Wolfmeier, H., Pletzer, D., Mansour, S. C. & Hancock, R. E. W. New Perspectives in Biofilm Eradication. *ACS Infect Dis* **4**, 93-106, doi:10.1021/acsinfecdis.7b00170 (2018).

8 Haney, E. F., Trimble, M. J., Cheng, J. T., Valle, Q. & Hancock, R. E. W. Critical Assessment of Methods to Quantify Biofilm Growth and Evaluate Antibiofilm Activity of Host Defence Peptides. *Biomolecules* **8**, doi:10.3390/biom8020029 (2018).

9 Harrison, J. J. *et al.* Microtiter susceptibility testing of microbes growing on peg lids: a miniaturized biofilm model for high-throughput screening. *Nat Protoc* **5**, 1236-1254, doi:10.1038/nprot.2010.71 (2010).

10 Olivares, E. *et al.* The BioFilm Ring Test: a Rapid Method for Routine Analysis of *Pseudomonas aeruginosa* Biofilm Formation Kinetics. *J Clin Microbiol* **54**, 657-661, doi:10.1128/jcm.02938-15 (2016).

11 Azeredo, J. *et al.* Critical review on biofilm methods. *Crit Rev Microbiol* **43**, 313-351, doi:10.1080/1040841x.2016.1208146 (2017).

12 Sackmann, E. K., Fulton, A. L. & Beebe, D. J. The present and future role of microfluidics in biomedical research. *Nature* **507**, 181-189, doi:10.1038/nature13118 (2014).

13 Janakiraman, V., Englert, D., Jayaraman, A. & Baskaran, H. Modeling growth and quorum sensing in biofilms grown in microfluidic chambers. *Ann Biomed Eng* **37**, 1206-1216, doi:10.1007/s10439-009-9671-8 (2009).

14 van Duuren, J. *et al.* Use of Single-Frequency Impedance Spectroscopy to Characterize the Growth Dynamics of Biofilm Formation in *Pseudomonas aeruginosa*. *Sci Rep* **7**, 5223, doi:10.1038/s41598-017-05273-5 (2017).

15 Pires, L. *et al.* Online monitoring of biofilm growth and activity using a combined multi-channel impedimetric and amperometric sensor. *Biosens Bioelectron* **47**, 157-163, doi:10.1016/j.bios.2013.03.015 (2013).

16 Paredes, J., Becerro, S. & Arana, S. Comparison of real time impedance monitoring of bacterial biofilm cultures in different experimental setups mimicking real field environments. *Sensors and Actuators B: Chemical* **195**, 667-676, doi:https://doi.org/10.1016/j.snb.2014.01.098 (2014).

17 Hall-Stoodley, L. & Stoodley, P. Evolving concepts in biofilm infections. *Cell Microbiol* **11**, 1034-1043, doi:10.1111/j.1462-5822.2009.01323.x (2009).

18 Cendra, M. D. M., Blanco-Cabra, N., Pedraz, L. & Torrents, E. Optimal environmental and culture conditions allow the in vitro coexistence of *Pseudomonas aeruginosa* and *Staphylococcus aureus* in stable biofilms. *Sci Rep* **9**, 16284, doi:10.1038/s41598-019-52726-0 (2019).

19 Hayward, W. A. *et al.* Pressure generated by syringes: implications for hydrodissection and injection of dense connective tissue lesions. *Scand J Rheumatol* **40**, 379-382, doi:10.3109/03009742.2011.560892 (2011).

20 O'Neill, J. in *AMR Review.* (eds The Review on & Antimicrobial Resistance).

21 Hall, C. W. & Mah, T. F. Molecular mechanisms of biofilm-based antibiotic resistance and tolerance in pathogenic bacteria. *FEMS Microbiol Rev* **41**, 276-301, doi:10.1093/femsre/fux010 (2017).

22 Coenye, T., Goeres, D., Van Bambeke, F. & Bjarnsholt, T. Should standardized susceptibility testing for microbial biofilms be introduced in clinical practice? *Clin Microbiol Infect* **24**, 570-572, doi:10.1016/j.cmi.2018.01.003 (2018).

23 Salek, M. M., Jones, S. M. & Martinuzzi, R. J. The influence of flow cell geometry related shear stresses on the distribution, structure and susceptibility of Pseudomonas aeruginosa 01 biofilms. *Biofouling* **25**, 711-725, doi:10.1080/08927010903114603 (2009).

24 Wimpenny, J., Manz, W. & Szewzyk, U. Heterogeneity in biofilms. *FEMS Microbiol Rev* **24**, 661-671, doi:10.1111/j.1574-6976.2000.tb00565.x (2000).

25 Reichhardt, C. & Parsek, M. R. Confocal Laser Scanning Microscopy for Analysis of Pseudomonas aeruginosa Biofilm Architecture and Matrix Localization. *Front Microbiol* **10**, 677, doi:10.3389/fmicb.2019.00677 (2019).

26 Stacy, A., McNally, L., Darch, S. E., Brown, S. P. & Whiteley, M. The biogeography of polymicrobial infection. *Nature Reviews Microbiology* **14**, 93-105, doi:10.1038/nrmicro.2015.8 (2016).

27 Kidd, T. J. *et al.* Defining antimicrobial resistance in cystic fibrosis. *J Cyst Fibros*, doi:10.1016/j.jcf.2018.08.014 (2018).

28 Filkins, L. M. & O'Toole, G. A. Cystic Fibrosis Lung Infections: Polymicrobial, Complex, and Hard to Treat. *PLoS Pathog* **11**, e1005258, doi:10.1371/journal.ppat.1005258 (2015).

29 Orazi, G. & O'Toole, G. A. Pseudomonas aeruginosa Alters Staphylococcus aureus Sensitivity to Vancomycin in a Biofilm Model of Cystic Fibrosis Infection. *mBio* **8**, doi:10.1128/mBio.00873-17 (2017).
30 Orazi, G., Ruoff, K. L. & O'Toole, G. A. Pseudomonas aeruginosa Increases the Sensitivity of Biofilm-Grown Staphylococcus aureus to Membrane-Targeting Antiseptics and Antibiotics. *MBio* **10**, doi:10.1128/mBio.01501-19 (2019).
31 Crespo, A., Gavalda, J., Julian, E. & Torrents, E. A single point mutation in class III ribonucleotide reductase promoter renders *Pseudomonas aeruginosa* PAO1 inefficient for anaerobic growth and infection. *Sci Rep* **7**, 13350, doi:10.1038/s41598-017-14051-2 (2017).
32 Blanco-Cabra, N. *et al.* Novel Oleanolic and Maslinic Acids derivatives as a promising treatment against bacterial biofilm in nosocomial infections: An in Vitro and in Vivo study. *ACS Infect Dis*, doi:10.1021/acsinfecdis.9b00125 (2019).
33 Klausen, M. *et al.* Biofilm formation by *Pseudomonas aeruginosa* wild type, flagella and type IV pili mutants. *Mol Microbiol* **48**, 1511-1524 (2003).
34 Crespo, A., Blanco-Cabra, N. & Torrents, E. Aerobic Vitamin B12 Biosynthesis Is Essential for *Pseudomonas aeruginosa* Class II Ribonucleotide Reductase Activity During Planktonic and Biofilm Growth. *Front Microbiol* **9**, 986, doi:10.3389/fmicb.2018.00986 (2018).
35 Weiss Nielsen, M., Sternberg, C., Molin, S. & Regenberg, B. *Pseudomonas aeruginosa* and *Saccharomyces cerevisiae* biofilm in flow cells. *J Vis Exp*, doi:10.3791/2383 (2011).
36 Gutiérrez, D., Hidalgo-Cantabrana, C., Rodríguez, A., García, P. & Ruas-Madiedo, P. Monitoring in Real Time the Formation and Removal of Biofilms from Clinical Related Pathogens Using an Impedance-Based Technology. *PLoS One* **11**, e0163966, doi:10.1371/journal.pone.0163966 (2016).

Acknowledgements

We thank Prof. Tim Tolker-Nielsen from Costerton Biofilm Center, University of Copenhagen for providing the *P. aeruginosa* MK171 strain. This work was supported in part through grants to ET from the Ministerio de Ciencia, Innovación y Universidades (BIO2015-63557-R and RTI2018-098573-B-100) (MINECO / FEDER), the Generalitat de Catalunya (2017 SGR1079 and CERCA programme), and the Spanish Cystic Fibrosis Foundation and La Caixa Foundation.

Authors want to acknowledge MicroFabSpace and Microscopy Characterization Facility, Unit 7 of ICTS "NANBIOSIS" from CIBER-BBN at IBEC.

This research was supported by Networking Biomedical Research Center (CIBER), Spain. CIBER is an initiative funded by the VI National R&D&i Plan 2008–2011, Iniciativa Ingenio 2010, Consolider Program, CIBER Actions, and the Instituto de Salud Carlos III (RD16/0006/0012), with the support of the European Regional Development Fund. This work was funded by the CERCA Programme and by the Commission for Universities and Research of the Department of Innovation, Universities, and Enterprise of the Generalitat de Catalunya (2017 SGR 1079). This work has been developed in the context of AdvanceCat and Base3D with the support of ACCIÓ (Catalonia Trade and Investment; Generalitat de Catalunya) under the Catalonian ERDF operational program (European Regional Development Fund) 2014–2020. This work was funded by the Spanish Ministry of Economy and Competitiveness (MINECO) through the projects MINDS (Proyectos I+D Excelencia + FEDER): TEC2015-70104-P, CTQ2016-75870-P.

Supplementary Tables and Figures

Supplementary Table 1. Sputum samples from cystic fibrosis patients were used to grow the biofilms, and the cell index was calculated after antibiotic treatment. Information concerning the bacterial species identified and their antibiotic sensitivity was obtained from the Microbiology Service at the Vall d'Hebron Barcelona Hospital Campus.

Sputum sample	**Bacterial species identified**	**Antibiotic treatment (sensitivity)**	**Cell Index (CI) change after antibiotic treatment**
I	*P. aeruginosa*	(Not reported)	(Not used)
II	*P. aeruginosa* and *S. aureus*	(Not reported)	(Not used)
III	*P. aeruginosa*	(Not reported)	(Not used)
IV	*P. aeruginosa* and *S. aureus*	(Not reported)	(Not used)
V	*S. aureus*	Ciprofloxacin (Susceptible)	- 0.06
		Ampicillin (Resistant)	+ 0.07
VI	*S. aureus*	Ampicillin (Susceptible)	- 0.93
		Ciprofloxacin (Resistant)	+ 0.72
VII	*P. aeruginosa*	Colistin (Susceptible)	- 0.07
		Ampicillin (Resistant)	+ 0.04

Supplementary Fig. 1. Results of computational fluid dynamics (CFD) simulations to show the effect of a prechamber when loading the sample manually. Figures show contours of velocity (m/s) on the surface of the designed biofilm chip without (a) and with (b) a prechamber.

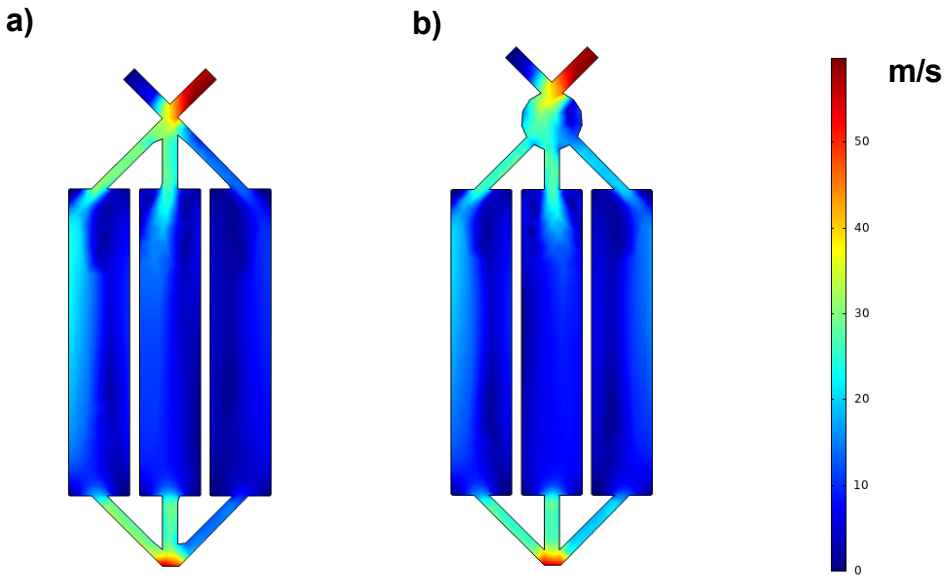

Supplementary Fig. 2. Confocal microscopy images of different sputum samples stained with the Bacterial Viability and Gram Stain Kit.

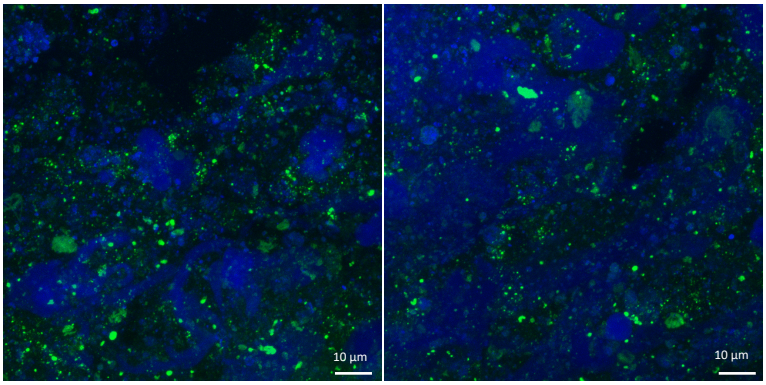

Supplementary Fig. 3. Bode diagram for a treated BiofilmChip chamber. Sweep frequency measurement was between 4 Hz - 400 kHz.

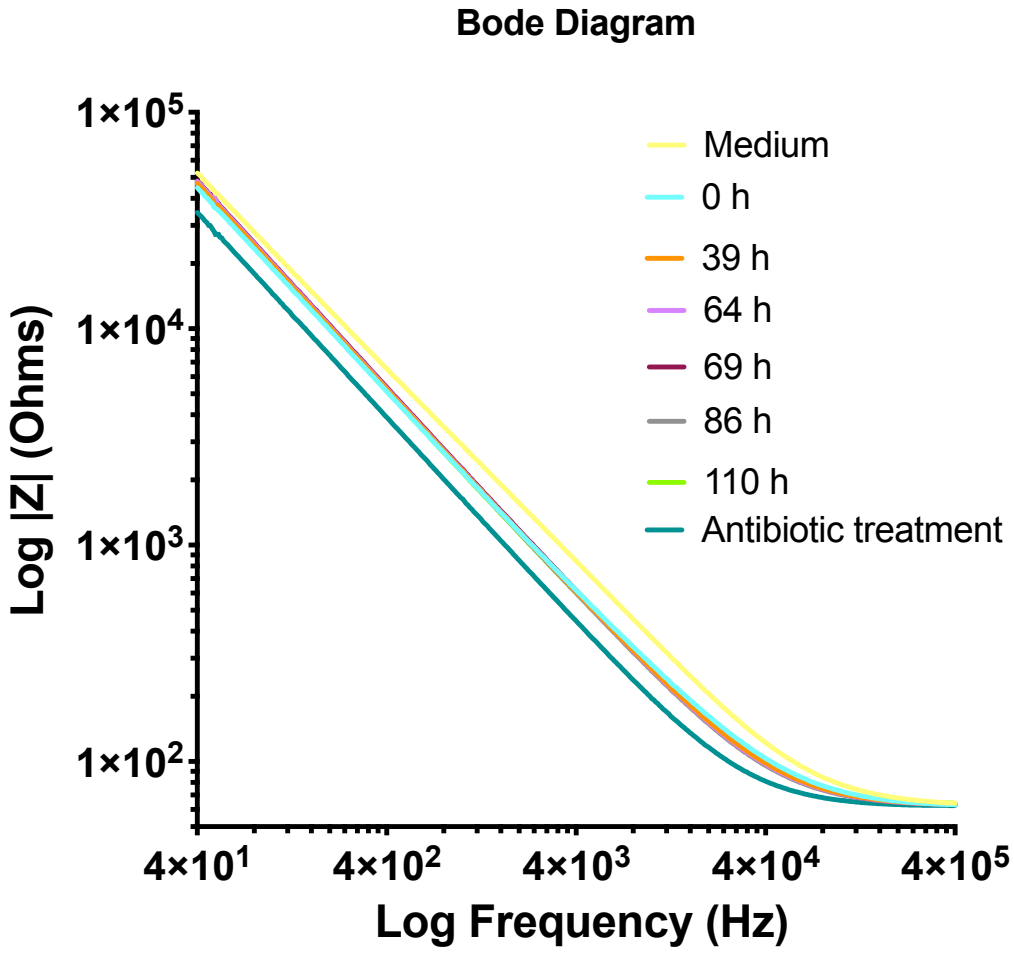

ARTICLE 4

Characterization of different alginate lyases for dissolving *Pseudomonas aeruginosa* biofilms

Publicat a la revista *Scientific Reports* (Q1, IF_{2019} = 3.998)

DOI: 10.1038/s41598-020-66293-2

Juny 2020

Autors: **Núria Blanco-Cabra**[1,#], Bernhard Paetzold[2,#], Tony Ferrar[3], Rocco Mazzolini[3], Eduard Torrents[1], Luis Serrano[3,4,5,*], Maria LLuch-Senar[3,*]

1: Bacterial Infections and Antimicrobial Therapies, Institute for Bioengineering of Catalonia (IBEC) The Barcelona Institute of Science and Technology (BIST), Barcelona, Spain.

2: S-Biomedic N.V. Turnhoutsweg 30 2340 Beerse (Belgium)

3: EMBL/CRG Systems Biology Research Unit, Centre for Genomic Regulation (CRG), The Barcelona Institute of Science and Technology, Dr Aiguader 88, Barcelona 08003, Spain.

4: Universitat Pompeu Fabra (UPF), 08003 Barcelona, Spain.

5: Institució Catalana de Recerca i Estudis Avançats (ICREA), 08010 Barcelona, Spain.

#: Aquests coautors han contribuït de manera igualitària en aquest article.

*: Correspondència: Dr. Maria Lluch-Senar (maria.lluch@crg.eu);
Dr. Luis Serrano (luis.serrano@crg.eu).

www.nature.com/scientificreports

SCIENTIFIC REPORTS
nature research

OPEN

Characterization of different alginate lyases for dissolving *Pseudomonas aeruginosa* biofilms

Núria Blanco-Cabra[1,6], Bernhard Paetzold[2,6], Tony Ferrar[3], Rocco Mazzolini[3], Eduard Torrents[1], Luis Serrano[3,4,5]✉ & Maria LLuch-Senar[3]✉

Aggregates of *Pseudomonas aeruginosa* form a protective barrier against antibiotics and the immune system. These barriers, known as biofilms, are associated with several infectious diseases. One of the main components of these biofilms is alginate, a homo- and hetero-polysaccharide that consists of β-D-mannuronate (M) and α-L-guluronate (G) units. Alginate lyases degrade this sugar and have been proposed as biotherapeutic agents to dissolve *P. aeruginosa* biofilms. However, there are contradictory reports in the literature regarding the efficacy of alginate lyases against biofilms and their synergistic effect with antibiotics. We found that most positive reports used a commercial crude extract from *Flavobacterium multivorum* as the alginate lyase source. By using anion exchange chromatography coupled to nano LC MS/MS, we identified two distinct enzymes in this extract, one has both polyM and polyG (polyM/G) degradation activities and it is similar in sequence to a broad-spectrum alginate lyase from *Flavobacterium sp*. S20 (Alg2A). The other enzyme has only polyG activity and it is similar in sequence to AlyA1 *from Zobellia galactanivorans*. By characterizing both of these enzymes together with three recombinant alginate lyases (a polyM, a polyG and a polyM/G), we showed that only enzymes with polyM/G activity such as Alg2A and A1-II' (alginate lyase from *Sphingomonas sp*.) are effective in dissolving biofilms. Furthermore, both activities are required to have a synergistic effect with antibiotics.

Biofilms are complex and dynamic structures formed by different pathogens that cause chronic persistent and recurrent infections. Among 65–80% of human infections are associated with biofilms[1–4]. They are especially frequent in pulmonary infectious diseases like cystic fibrosis (CF), chronic obstructive pulmonary disease (COPD), bronchiectasis and ventilator-associated pneumonia (VAP). The challenge of treating biofilm infections is the increased resistance of the bacteria within the biofilm to antimicrobial agents and host defense mechanisms[5]. The metabolic activity of the bacterial cells is low, resulting in slow-growing cells with radically downregulated cell division rates[6]. Therefore, antibiotics such as β-lactams, which are only active against dividing cells, are not very efficient at eradicating biofilm infections. These diseases are very difficult to manage therapeutically, as the minimum effective bactericidal concentration of antibiotics for biofilm eradication *in vivo* is impossible to reach without causing adverse effects and renal and/or hepatic injury. Moreover, many of the pathogenic bacterial strains are antibiotic resistant. In particular, critically ill patients who are intubated and on mechanical ventilation are at greater risk of developing VAP[7]. *P. aeruginosa* and *Staphylococcus aureus* are the primary causative pathogens of biofilm-associated pulmonary infections[7,8].

When these bacteria grow in biofilms, they form an extracellular matrix that acts as a barrier against antibiotics and the host immune system[9]. In the lung of CF patients, *P. aeruginosa* generally transitions to a mucoid phenotype characterized by the overproduction of the exopolysaccharide alginate[10]. Alginate is the most abundant extracellular matrix polysaccharide and consists of β-D-mannuronate (M) and α-L-guluronate (G) as monomeric units. These units can be linked in three different kinds of blocks, poly β-D-mannuronate (polyM), poly

[1]Bacterial infections and antimicrobial therapies, Institute for Bioengineering of Catalonia (IBEC), The Barcelona Institute of Science and Technology (BIST), Barcelona, Spain. [2]S-Biomedic N.V. Turnhoutsweg 30 2340, Beerse, Belgium. [3]EMBL/CRG Systems Biology Research Unit, Centre for Genomic Regulation (CRG), The Barcelona Institute of Science and Technology, Dr Aiguader 88, Barcelona, 08003, Spain. [4]Universitat Pompeu Fabra (UPF), 08003, Barcelona, Spain. [5]Institució Catalana de Recerca i Estudis Avançats (ICREA), 08010, Barcelona, Spain. [6]These authors contributed equally: Núria Blanco-Cabra and Bernhard Paetzold. ✉e-mail: luis.serrano@crg.eu; maria.lluch@crg.eu

α-L-guluronate (polyG) or the heteropolymer (polyM/G)[11]. The alginate is O-acetylated at the C-2 and/or C-3 positions in mannuronate residues[12–14]. The monomer composition and the acetylation change depend on the strains and the carbon source. Alginate is one of the most extensively studied *P. aeruginosa* virulence factors and it is associated with persistence in the chronically inflamed airway[15–17]. Therefore, when trying to identify possible drug targets, many studies have focused on the alginate production pathway or the degradation of alginate by enzymes[18–23].

Biochemical characterization of different alginate lyases[24–34] has revealed different polyM and polyG activities. The enzymes are classified into seven polysaccharide lyase (PL) families (PL5, 6, 7, 14, 15, 17, and 18) in the Carbohydrate-Active enzymes (CAZY) database[35]. Alginate lyases from family PL7 have been widely studied, and the crystal structures of several PL7 alginate lyases are solved[36–38]. Structural analysis shows that these lyases share a common β-sandwich fold consisting of two β-sheets, in which conserved amino acid residues compose a deep active cleft that is covered by two flexible lid loops[36–38]. This family comprises both endolytic and exolytic alginate lyases.

The substrate specificities of PL7 alginate lyases are also diverse, including polyG-specific, polyM-specific, and bifunctional enzymes. One example of a bifunctional PL7 alginate lyase from *Sphingomonas sp*. A1 is A1-II'[39]. With respect to the PL5 family, AlgL is a 40-kDa poly-β-D-mannuronate lyase from *P. aeruginosa* that preferentially degrades deacetylated polyM *via* a β-elimination reaction, resulting in disaccharides and trisaccharides as its major products[40,41]. Purified alginate lyases from *P. aeruginosa* strains (AlgL) have polyG/M activity and have been shown to dissolve *P. aeruginosa* PAO1 strain biofilms[25]. Alginate lyases A1-I (PL5 + 7 family), A1-II (PL7 family) and A1-III (PL5 family) from *Sphingomonas sp*. strain A1 can produce di- and trisaccharides as major final products from alginate[42]. In addition, an oligoalginate lyase of this bacterium can degrade alginate oligosaccharides into their respective constituent monosaccharides[43]. A1-I is active against acetylated and non-acetylated alginates. A1-II, on the other hand, prefers polyG and non-acetylated alginate. A1-III efficiently liquefies polyM and acetylated alginates produced by mucoid cells.

Alginate lyase treatment has been shown to reduce viscosity both in cultures of clinical isolates and in CF sputum[29]; it strips biofilms from abiotic surfaces[22,44], enhances phagocytosis of *P. aeruginosa* by human immune cells[20,23,45], and improves the efficacy of various antipseudomonal antibiotics[18,19,45,46]. However, although multiple studies have reported that the biofilm inhibitory concentration (BIC) of antibiotics against *P. aeruginosa* biofilm cultures is lowered when combined with alginate lyase activity[18–21,47], it was also shown that synergy between tobramycin and the A1-III and AlgL enzymes is completely decoupled from their catalytic activity[47]. This raises the question of whether it is their enzyme activity that is important for dissolving biofilms. Moreover, whilst different studies using commercial crude extracts containing alginate lyase activity have been shown to dissolve biofilms[18–20,23], recent studies have shown that the recombinant AlgL enzyme does not show a significant antibiofilm effect; its catalytic activity against alginate and acetylated alginate is not sufficiently high[48]. Thus, a careful reexamination of the alginate lyases responsible for the enzymatic activities present in these extracts could clarify whether these proteins can really be used to dissolve *P. aeruginosa* biofilms and reduce the required dose of antibiotics in CF patients.

Here, we purified five alginases. Four belong to the PL7 family: Alg2A and AlyA1 (both related to the ones found in the crude Sigma extract), A1-II' and A1-II; and one to the PL5 family (A1-III). We have characterized their activities against polyG, polyM and polyM/G substrates. We also tested their capacity to dissolve biofilms of two *P. aeruginosa* strains (PAO1 *wt* and PAO1Δ*mucA*) and evaluated their synergistic effect when used in combination with the antibiotic ciprofloxacin[49]. The efficacy of this fluoroquinolone in biofilms has been previously assessed by showing that antibiotic resistance of *P. aeruginosa* and *S. aureus* is critically increased during coculture biofilm growth[50].

Results

Isolation and identification of the alginate lyase activities from the crude extract of *Flavobacterium multivorum*. The crude extract of *Flavobacterium multivorum* from Sigma (A1603 Sigma) was first fractionated using anion exchange and gel filtration chromatography. Then, the enzymatic activity of the different fractions was examined in a halo test done with the *P. aeruginosa* PAO1 *wt* cells (HT, Fig. 1A; Material and methods) and in an activity assay with brown seaweed alginate as the substrate (time point of 4 h; Fig. 1B). With both methods, we identified two separate activities in samples covering the range of fractions from B2 to B5 (Fig. 1A and B). The B2 and B5 fractions, as well as the surrounding ones, were analyzed by SDS gel electrophoresis (Fig. 1C). An upper band of approximately 40 kDa was enriched in fraction B5-B4 and a lower band of about 30 kDa was enriched in fractions B3 to B1, both being consistent across two different samples fractionated the same way.

Both bands were analyzed separately by mass spectrometry (MS) after trypsin and chymotrypsin digestions (Table 1 and Tables S1 to S8). As the source of the extract was unknown, identified spectra were assigned to peptide sequences by performing a *de novo* search[51]. To find protein sequences that had regions of similarity to the peptides found by MS, we used Basic Local Alignment search Tool (BLAST)[52]. BLAST search revealed that the peptide sequences from the lower SDS band were found in five orthologue alginate lyases (Tables S1 to S4). Peptides from the upper band were found in an alginate lyase (*Zobellia galactanivorans* (AlyA1); PL7 family)[35] and in two proteins with no assigned function (hypothetical proteins; NCBI reference sequences: WP_012026046.1 and WP_012026879.1) (Tables S5 to S8). Alg2A protein from *Flavobacterium sp*. S20 (PL7 family[35]); was selected as representative of the five alginate lyases detected in the lower band since its sequence contained the higher number of MS unique peptides (Fig. S1). These results suggested that enzymes similar to Alg2A and/or AlyA1, as well as proteins belonging to the two hypothetical protein families, could be responsible for degrading *P. aeruginosa* alginate biofilms.

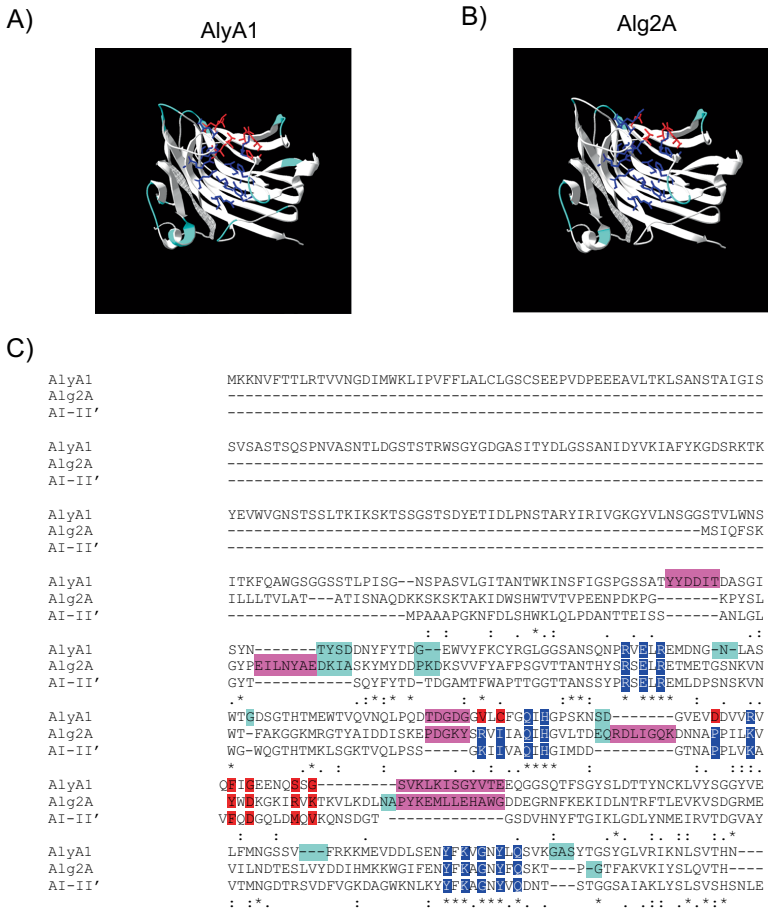

Figure 1. Activity of the Sigma extract fractions obtained after purification: (**A**) activity measured by the halo assay. We show images of the negative control (c-, no halo) and the halo formed with one representative fraction B2 of the Sigma extract (in blue, surrounding the disk). Scale bar corresponds to 10 mm (**B**) alginate lyase activity measured aafter 4 h of incubation and (**C**) SDS gel of the purified fractions that show activity. In the figure, a representative plot of two different experiments is shown.

	Lower Band		Upper Band	
Protease used for the digestion	**Nr of Peptides**	**Nr of Proteins**	**Nr of Peptides**	**Nr of Proteins**
Trypsin	529	157	134	73
Chymotrypsin	80	45	188	61

Table 1. Mass Spectrometry results of the two bands of the SDS gels run after the purification steps. The proteins extracted from the bands were digested with trypsin and chymotrypsin proteases. The table shows the number of peptides identified in each experiment and the Nr of proteins associated after Blast alignment.

Sequence analysis of AlyA1 and Alg2A. Alg2A (AEB69783.1) contains the highly conserved regions described for the PL7 family: (LIV)-XXWX-(LVI)-(TQN)LP, R-(SVA)-ELRE, NW, (IVLM)(IVLM)(AG)QIH, and YFKAG-X-G-Y-X-Q (Fig. S1), which compose the cavity of a jelly-roll β-sandwich structure where it is assumed to bind a suitable substrate (Fig. 2B). Alg2A has a QIH sequence in its catalytic center, which is a hallmark of polyM/G lyases[53]. It also contains the conserved YFKAGNYFQ motif that is essential for catalysis. The

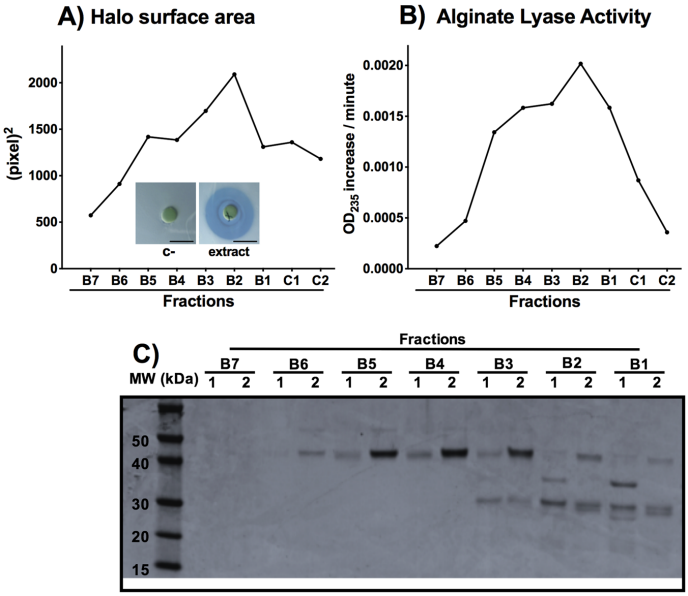

Figure 2. Modelling of AlyA1 and Alg2A based on A1-II' (2CWS) crystal structure. (**A**,**B**) Models of protein structures of AlyA1 and Alg2A, respectively. Loops involved in the interaction with the substrate are labeled in light blue. In dark blue we show the conserved residues in the cavity close to the putative active site. In red, non-conserved residues of the cavity. (**C**) ClustalW alignment of AlyA1 (WP_013992548.1), A1-II' and Alg2A (AEB69783.1) protein sequences. Shadowed in dark blue are the residues that form the conserved substrate cavity and in red the important but non-conserved residues of this cavity. Loops important for substrate binding are labelled in light blue. Highly conserved regions described for PL7 family are marked with an asterisk. In bright pink, we show the unique aa sequences present in Alg2A or AlyA1 sequences.

closest alginase in sequence which crystal structure has been determined (2CWS) is the A1-II' alginate lyase from *Sphingomonas sp. A1*[54].

Regarding AlyA1 (WP_013992548.1), sequence alignment shows that it is also a member of the PL7 family and it contains the same elements as Alg2A (Fig. 2C) plus an extra domain of the family 32 (CBM32) that is required for carbohydrate binding[55]. Moreover, AlyA1 contains the QIH sequence that is characteristic of polyM/G alginases. However, it was classified in the SF3 subfamily of the PL7 family, which in theory, should only hydrolyze polyG substrates.

In the Fig. 2C we show the sequence alignment of Alg2A, AlyA1 and A1-II'. Alg2A has four longer loops than AlyA1 – three of which are located around the predicted substrate-binding site (Fig. 2A) – suggesting that this enzyme could recognize or bind to a different polymer structure. With respect to the residues that line the cavity, the conserved ones were associated with the putative active site, but the residues on one side are quite divergent (Fig. 2C-labeled in red). This reinforces the idea that although the catalytic mechanism of A1-II' and Alg2A must be the same, Alg2A could recognize polymer structures of a different composition. Sequence analysis and comparison with A1-II' alginate lyase shows a similar picture for AlyA1. The loops surooounding the cavity in the jelly roll where the substrate should bind are of different length and sequence than Alg2A, and the residues surrounding the active site are conserved with those at one end being different (Fig. 2C-labeled in red). In this case the number of loops and residues that are different from the crystal structure is larger than Alg2A.

Characterization of the alginate-degrading activity of the identified proteins. Although we cloned both hypothetical proteins, we were only able to express and purify WP_012026046.1. Regarding the two alginate lyases (Alg2A (AEB69783.1) and AlyA1 (WP_013992548.1)) identified as possible orthologues of the alginate lyases from the extract, we were able to express and purify both. We also included other alginate lyases, namely A1-II', A1-II (both PL7 family), and A1-III (PL5 family), to compare the activity of different enzymes by measuring the degradation of different substrates: brown seaweed, polyM and polyG alginate (Fig. 3; Table 2 and Table 3). Alginate lyase activity was determined by following the increase in absorbance at 235 nm due to the formation of a carbon-carbon double bond at the end of the product generated from lyase-mediated cleavage of alginate. We also determined Kcat and Km constants for the different recombinant proteins with PolyG and PolyM substrates (Table 3; Fig. S2). No activity was found for the hypothetical protein (WP_012026046.1) against any of the studied substrates (data not shown).

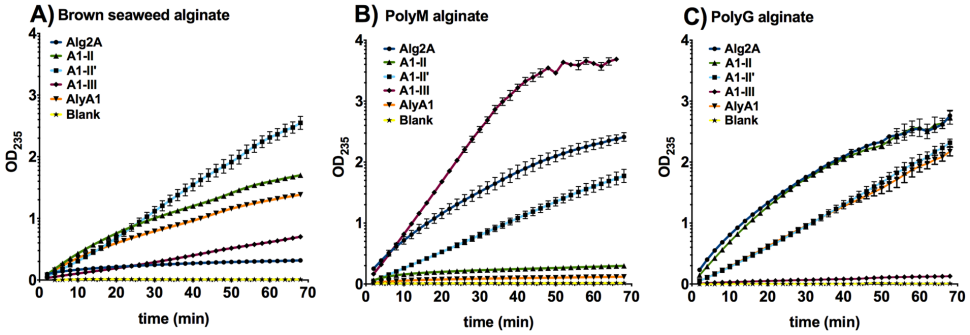

Figure 3. Enzyme activity against different substrates. Alginate lyase enzyme kinetic activity against different substrates: (**A**) brown seaweed alginate, (**B**) polyM alginate and (**C**) polyG alginate. Error bars represent the standard deviation of three different replicates. The blank sample was obtained by adding buffer instead of enzyme and it was subtracted in all the samples.

	Brown seaweed alginate		PolyM		PolyG	
	Slope	r2	Slope	r2	Slope	r2
Alg2A	0.0069	0.969	0.0523	0.995	0.064	0.9936
A1-II	0.0389	0.9965	0.0084	0.9303	0.0651	0.9988
A1-II′	0.0328	0.9985	0.0263	0.9999	0.0299	0.999
A1-III	0.088	0.9995	0.0834	0.9998	0.0024	0.9824
AlyA1	0.0304	0.9906	0.0034	0.9604	0.0312	0.999

Table 2. Slope values of the linear equations from the activity curves against different substrates for different enzymes. R-squared (r2) is the coefficient of determination, or the coefficient of multiple determination for the linear regression.

	PolyG			PolyM		
	Kcat	Km (mg/ml)	Kcat/Km	Kcat	Km (mg/ml)	Kcat/Km
AlyA1	19.68	3.083	6.38			
A1-II	20.55	1.866	11.01			
A1-II′	7.339	1.281	5.73			
A1-III	0.4732	1.248	0.38	85.37	5.36	15.94
Alg2A	18.13	5.531	3.28			

Table 3. Km and Kcat values of different enzimes in presence of PolyM and PolyG substrates.

The two polyM/G alginases, A1-II' and Alg2A, showed both polyG and polyM activity, but although having similar residues in the catalytic pocket, Alg2A showed more activity against both alginates than A1-II'. The specificity constant (Kcat/Km) calculated for each enzyme shows that A1-II' is more specific for PolyG than Alg2A. Regarding PolyM substrate, we could determine the Kcat/Km specificity constant only for the A1-III enzyme, since in the case of the other proteins, saturation by substrate was not reached under the different concentrations tested (Fig. S2). Moreover, A1-II' exhibited also activity against brown seaweed alginate, whereas Alg2A did not. AlyA1 has also the QIH sequence characteristic of polyM/G alginate lyases, but lacks activity against polyM alginate and revealed a similar activity to A1-II, displaying both enzymatic activities against polyG alginate and brown seaweed alginate. Regarding A1-III, it showed a great polyM activity a low activity against brown seaweed alginate and without any enzymatic activity against the polyG alginate.

This result confirms what was suggested by the sequence and structural analysis, that the loops surrounding the active site and the residues in the binding pocket far away from the active site play a role in substrate recognition.

Characterization of the alginate lyase activity of the candidate proteins on *P. aeruginosa* biofilms. The enzymatic activity of alginate lyases was evaluated in *P. aeruginosa* biofilms grown for 96 hours before treatment. The experiment was performed in flow cell chambers where disaggregation was followed by imaging with a confocal microscope (Fig. 4). After treatment with different alginate lyases for 12 hours,

www.nature.com/scientificreports/

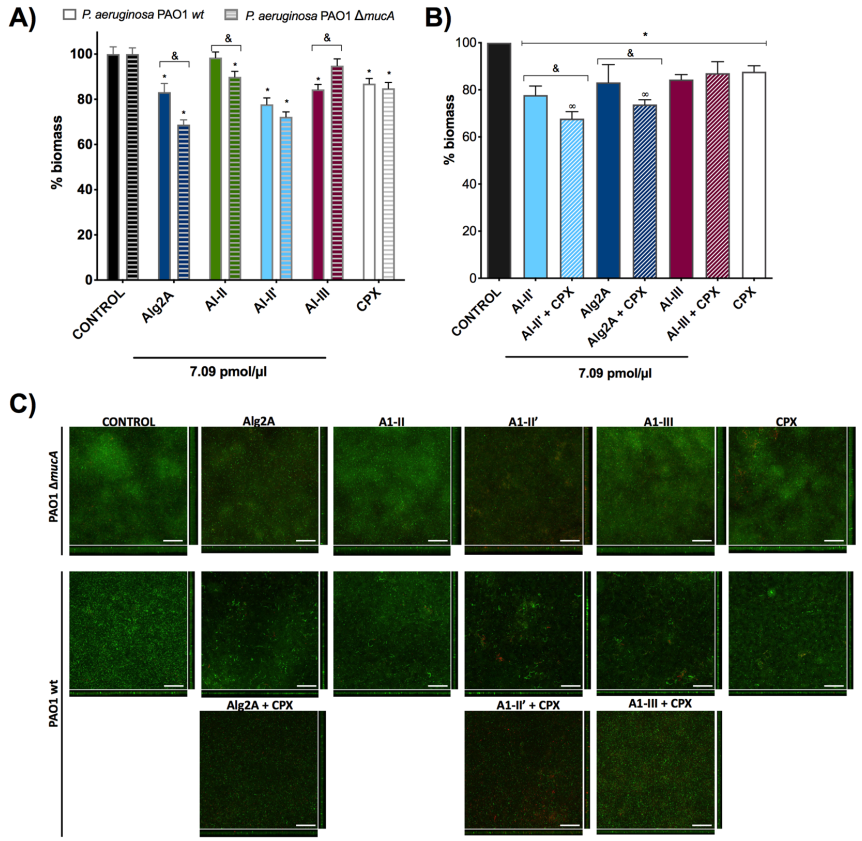

Figure 4. Biofilm degradation activity. (**A**) The histogram shows the ability of different enzymes to degrade biofilms formed by *P. aeruginosa* PAO1 *wt* (solid bars) and PAO1Δ*mucA* (striped bars). The concentration of enzyme was the same in each sample (7.09 pmol/µl), that corresponds to 0.32 mg/ml for Alg2A; 0.14 mg/ml for A1-II; 0.22 mg/ml for A1-II'; and 0.23 mg/ml for A1-III. The values are normalized against the control sample (non-treated biofilm) that has 100% biomass. The decrease in the percentage of biomass reflects the effect of the treatment. The asterisk (*) indicates a significant difference ($p < 0.05$) when the sample is compared with the control. The (&) indicates a significant difference ($p < 0.05$) when the PAO1 *wt* strain is compared with PAO1Δ*mucA*. (**B**) Synergism between antibiotics and the AlyA1, A1-III and Alg2A alginate lyase proteins. The asterisk (*) indicates a significant difference ($p < 0.05$) when the sample is compared with the control. The (&) indicates a significant difference ($p < 0.05$) when alginase is compared with alginase + ciprofloxacin. The (∞) indicates a significant difference ($p < 0.05$) when the sample is compared with ciprofloxacin. (**C**) Sum of stack images and the corresponding orthogonal views of the confocal microscopy images of *P. aeruginosa* PAO1 *wt* and PAO1 Δ*mucA* biofilms treated with 7.09 pmol/µl of the different alginate lyases and 1 µg/ml of ciprofloxacin (CPX). Red and green colors show the *P. aeruginosa* dead and alive cells detected by the LIVE/DEAD staining kit, respectively. Scale bar corresponds to 50 µm.

we measured the biomass, thickness and roughness of the biofilms formed by wild type *P. aeruginosa* PAO1 (non-mucoid) and PAO1Δ*mucA* (mucoid strain) (Table S9). By measuring the difference in biofilm biomass between the untreated and treated samples, we were able to estimate the level of biofilm degradation by different alginate lyases (Fig. 4). After 12 hours of treatment, the Alg2A and A1-II' proteins resulted in the highest reduction of biofilm biomass (around 30%) of both *P. aeruginosa* strains, confirming their degradation activity (Fig. 4A). Interestingly, Alg2A was more efficient at degrading the biofilm of PAO1Δ*mucA* than that of PAO1 *wt*. In contrast, A1-II' degraded the biofilms formed by both strains to a similar extent. Although some biomass decrease was observed for A1-II in the PAO1 Δ*mucA* strain biofilm, the same alginate lyase had no reduction activity in the PAO1 *wt* biofilm. In the case of the A1-III alginate lyase, the reduction of the biomass was only observed in the PAO1 *wt* strain. However, the activity of these two enzymes (A1-II and A1-III) was lower when compared to the activity of the rest of the studied proteins (Alg2A and A1-II'). Confocal microscopy images

corroborated the abovementioned decreases in biomass (Fig. 4C, Supplementary Fig. S4). The ability of these enzymes to degrade biofilms was also compared with ciprofloxacin (CPX) antibiotic treatment, a benchmark treatment that results in approximately 15% biofilm reduction (Fig. 4A). After 12 hours of biofilm formation, A1-II' is significantly more efficient at degrading the biofilm than pure CPX treatment.

In summary, we have shown that the broad spectrum polyM/G Alg2A and A1-II' alginate lyases (PL7 family), but not the polyM or polyG alginate lyases like A1-II, (PL7) A1-III (PL5) and AlyA1 (PL7), can dissolve biofilms formed by *P. aeruginosa*.

Synergistic effects between alginate lyases and antibiotic treatment in the degradation of biofilms. To gain insight into the role of alginate lyase activity in enhancing the effect of antibiotics, we treated *P. aeruginosa* PAO1 *wt* biofilms with Alg2A, A1-III or A1-II' together with CPX and studied the impact on biofilm biomass disaggregation. As shown in Fig. 4B, the combination of A1-II' or Alg2A with CPX produced a synergistic effect on biofilm disaggregation, with more than a 10% increase in the reduction of the biofilm biomass. Therefore, as previously shown, the combination of A1-III with CPX did not produced a synergistic effect (Fig. 4B). Thus, degradation of biofilm by enzymes with polyM/G activity is necessary to see an effect by CPX.

We discarded any antimicrobial activity by A1-II' and Alg2A because no effect on the viability of PAO1 *wt* and PAO1Δ*mucA* strains was observed when grown in planktonic culture (Supplementary Fig. S3). Altogether, these results reveal that using Alg2A or A1-II' alginate lyases to dissolve *P. aeruginosa* biofilms enhance antibiotic treatment.

Discussion

Alginate, one of the main virulence factors associated with *P. aeruginosa* biofilms, has been the main target over the last decades when attempting to uncover alternative treatments for CF. The alginate heterogeneity generated by different combinations of β-D-mannuronate (M) and α-L-guluronate (G), as well as their different acetylation profiles, make this exopolysaccharide very difficult to target.

Many studies demonstrating the antibiofilm activity of alginases have used crude cell extracts from *P. aeruginosa*[20,23,45]. Other groups used purified enzymes such as A1-III and AlgL, and concluded that the synergistic effects with antibiotics were independent of the enzyme activity[47].

Upon testing the ability to degrade the biofilms of two different *P. aeruginosa* strains (one of them mucoid), by different alginases, representing the two major families and with different substrate specificities, we consistently found that the broad spectra alginate lyases were the most active enzymes. In fact, only when polyM/G enzymes were combined with ciprofloxacin antibiotic, the synergistic effect was observed. In contrast, enzymes which only have polyG and polyM degradation activities respectively, showed less activity towards the biofilms and no synergistic effect with CPX. This agrees with previous results that showed polyG that A1-III did not amplify the effect of antibiotics against *P. aeruginosa* biofilms.

We also found that among polyM/G enzymes, A1-II' was able to degrade the brown seaweed substrate more efficiently than Alg2A. Altogether, these results suggest that A1-II' and Alg2A have a broad activity spectrum against different biofilms because they degrade a greater variety of alginate matrixes. In fact, a different endolytic reaction mode was assigned to the Alg2A enzyme because it produces a larger amount of penta-, hexa-, and hepta-saccharides from the hydrolysis products when compared with other alginate lyases.

In conclusion, we have unraveled the effect that different alginate lyases have on *P. aeruginosa* biofilm degradation and we have identified Alg2A and A1-II' as good disperal agents. We show an increase in the efficiency of antibiotic treatment when combined with Alg2A or A1-II'. Characterization of different alginate lyase proteins on biofilms reveled that Alg2A and A1-II', despite having similar polyG/M and different activity against seaweed brown algynate, are the best candidates to use for degrading biofilms formed by different *P. aeruginosa* strains.

Methods

Ionic exchange and gel filtration chromatography. For anion exchange chromatography we used a HiTrap Q HP column (GE Healthcare product # 17-1153-01) in conjunction with an ÄKTA-FPLC system. The alginate lyase sample (Sigma #A1603) was dissolved in 20 mM Tris pH 8 as buffer A and applied to the pre-equilibrated column. As buffer B, we used the same buffer with 1 M NaCl. After 20 ml, we increased the salt concentration to 500 mM over 50 ml and collected fractions of 1 ml.

For gel filtration chromatography a Superdex-75 column was used (GE Healthcare product # 17-5174-01) with 20 mM Tris pH 8 and 150 mM NaCl as running buffer. The fraction size was 0.5 ml.

To achieve the presented resolution of proteins in the crude extract, we first performed an anion exchange chromatography, pooled fractions 37–42, 48–51 and 55–60, concentrated them and performed subsequent gel filtration. After the chromatographic runs, all fraction were supplemented with 10% glycerol to ensure protein stability.

Mass spectrometry of fractions. All experimental proteomics procedures were performed by the UPF/CRG Proteomics Unit. We performed an initial tryptic digestion and peptide fingerprint MS analysis on the crude alginate lyase extract (Sigma A1603). Our aim was to screen for known toxins or other proteins with biofilm dissolving properties. We did not yield any reasonable lead from this. Therefore, we cut the protein bands identified as peaking using the halo activity test from an SDS gel. The bands were digested by trypsin or chymotrypsin and analyzed by nano-LC MS/MS. The resulting peaks were analyzed as DeNovo assembly using the software PEAKS (Bioinformatics solutions Inc.).

Bacterial strains. Wild type *P. aeruginosa* PAO1 (ATCC 15692) and its isogenic *mucA* mutant PAO1Δ*mucA* strain (lab strain) were grown in LB medium at 37 °C. As standard conditions, *E. coli* BL21 and TOP10 strains were cultured at 37 °C in LB with the respective antibiotics added (50 μg/ml kanamycin).

Proteins expression and purification. Synthetic genes encoding for Hypothetical protein (WP_012026046.1), Alg2A (AEB69783.1), AlyA1 (WP_013992548.1), A1-II (AGJ83952.1), A1-III (BAB03312.1) and A1-II´ (BAD16656.1) were ordered from GenScript. Then, they were cloned using Gibson assembly into pETM14, which results in a His-tag on the C-terminus of the protein. Expression was performed in *E. coli* BL21 and induction was performed at 16 °C with 1 mM of IPTG overnight. Two purification steps were performed: a nickel affinity chromatography followed by a desalting PD10 column, both in the 50 mM Tris pH 7.4, 300 mM NaCl, 10% glycerol, and 2 mM DTT. Proteins were analyzed by SDS gel electrophoresis.

Halo test assay. For the halo test the *P. aeruginosa* PAO1 *wt* cells were grown on agar plates with *Pseudomonas* isolation medium (PI medium) (Bactopeptone 20 g/l, $MgCl_2$ 1.4 g/l, K_2SO4 10 g/l, glycerol 1%, pH 7.2). First the Petri dish was seeded with 1 ml of a bacterial culture (OD_{600}=0.8) and paper disks (MDB-oxoid CT0998-B) were placed on the agar. Then, the disks were soaked with 10 µl of alginate lyase solution (17.5, 8.75 and 4.375 pmols) and the plates incubated for 16 hours at 37 °C. Formation of halos was then evaluated by visual inspection and direct measurement of halo diameter. Image J program was used to calculate the diameter of halos obtained from pictures and measured in pixels.

Measurements of activity by UV assay. Activity of the alginate lyase was determined by the increase in absorbance at 235 nm due to the formation of a carbon-carbon double bond at the end of the product generated from lyase-mediated cleavage of alginate. Three different substrates were tested: brown seaweed alginate (Sigma# W201502 A straight-chain, hydrophilic, colloidal, polyuronic acid composed of glucuronic and mannuronic acid residues), ELICITYL # DP25-DP45 Guluronate oligosaccharides (polyG) and ELICITYL # DP20-DP35 Mannuronate oligosaccharides (polyM).

The substrates were dissolved in a solution of 20% glycerol and 20 mM Tris pH 7.4 so as to reach a final alginate concentration of 0.2%. Then, 50 µL of these substrates were added to the wells containing 7.1 pmol of each enzyme. As positive control we used 10 pmols of Sigma A1603 alginase. Absorbance was measured at 235 nm every 2 minutes for 78 minutes using UV-star microplates, 96wells, (Greiner #655801).

Biofilm cultivation in flow cell chambers and microscopy. *P. aeruginosa* biofilms were grown in LB medium supplemented with 0.2% glucose at 20 °C in flow cell chambers as was previous described[56,57]. After 96 h the mature biofilm was treated with different alginate lyases for 12 h. For analysis, the biofilm was stained using the LIVE/DEAD BacLight Bacterial Viability kit (Thermo Scientific) and visualized with a Zeiss LSM 800 confocal laser scanning microscope (CSLM) using the 20×/0.8 objective with excitation wavelengths of 488 and 560 nm. Microscope images were processed with the ImageJ analysis software and COMSTAT 2, a specific biofilm analysis software was used to quantify the biofilm biomass, thickness and roughness[58].

Antimicrobial activity of alginate lyases. *P. aeruginosa* PAO1 *wt* and PAO1 Δ*mucA* were grown until an optical density (OD_{550} nm) of 0.1 was reached and then plated in a microtiter plate (Corning 3596 Polystyrene Flat Bottom 96 Well Corning, NY, USA). The different alginases were added at a similar concentration to the one used in the biofilm analysis (7.09 pmol/µl). Bacterial growth at 37 °C and 150 rpm was monitored for 8 hours, and the absorbance measured at 550 nm every 15 minutes in an SPARK Multimode microplate reader (Tecan, Männedorf, Switzerland).

Statistical analysis. Values are expressed as mean ± standard deviation (SD). Statistical analyses were performed using GraphPad Prism 6.00 (GraphPad Software, San Diego, CA, USA) software package. Single comparisons were performed with Welch's correction. A value of $p < 0.05$ was considered as statistically significant.

Received: 10 June 2019; Accepted: 15 May 2020;
Published online: 10 June 2020

References

1. Hoiby, N., Bjarnsholt, T., Givskov, M., Molin, S. & Ciofu, O. Antibiotic resistance of bacterial biofilms. *Int J Antimicrob Agents* **35**, 322–332, https://doi.org/10.1016/j.ijantimicag.2009.12.011 (2010).
2. Obst, U., Schwartz, T. & Volkmann, H. Antibiotic resistant pathogenic bacteria and their resistance genes in bacterial biofilms. *Int J Artif Organs* **29**, 387–394 (2006).
3. Smith, A. W. Biofilms and antibiotic therapy: is there a role for combating bacterial resistance by the use of novel drug delivery systems? *Adv Drug Deliv Rev* **57**, 1539–1550, https://doi.org/10.1016/j.addr.2005.04.007 (2005).
4. Stewart, P. S. Mechanisms of antibiotic resistance in bacterial biofilms. *Int J Med Microbiol* **292**, 107–113, https://doi.org/10.1078/1438-4221-00196 (2002).
5. del Pozo, J. L. & Patel, R. The challenge of treating biofilm-associated bacterial infections. *Clin Pharmacol Ther* **82**, 204–209, https://doi.org/10.1038/sj.clpt.6100247 (2007).
6. Ancion, P. Y., Lear, G. & Lewis, G. D. Three common metal contaminants of urban runoff (Zn, Cu & Pb) accumulate in freshwater biofilm and modify embedded bacterial communities. *Environ Pollut* **158**, 2738–2745, https://doi.org/10.1016/j.envpol.2010.04.013 (2010).
7. Torres, A. *et al.* International ERS/ESICM/ESCMID/ALAT guidelines for the management of hospital-acquired pneumonia and ventilator-associated pneumonia: Guidelines for the management of hospital-acquired pneumonia (HAP)/ventilator-associated pneumonia (VAP) of the European Respiratory Society (ERS), European Society of Intensive Care Medicine (ESICM), European Society of Clinical Microbiology and Infectious Diseases (ESCMID) and Asociacion Latinoamericana del Torax (ALAT). *Eur Respir J* 50, https://doi.org/10.1183/13993003.00582-2017 (2017).
8. Kalil, A. C. *et al.* Management of Adults With Hospital-acquired and Ventilator-associated Pneumonia: 2016 Clinical Practice Guidelines by the Infectious Diseases Society of America and the American Thoracic Society. *Clin Infect Dis* **63**, e61–e111, https://doi.org/10.1093/cid/ciw353 (2016).
9. Leid, J. G. *et al.* The exopolysaccharide alginate protects Pseudomonas aeruginosa biofilm bacteria from IFN-gamma-mediated macrophage killing. *J Immunol* **175**, 7512–7518 (2005).

10. Ramsey, D. M. & Wozniak, D. J. Understanding the control of Pseudomonas aeruginosa alginate synthesis and the prospects for management of chronic infections in cystic fibrosis. *Mol Microbiol* **56**, 309–322, https://doi.org/10.1111/j.1365-2958.2005.04552.x (2005).
11. Gacesa, P. Enzymic degradation of alginates. *Int J Biochem* **24**, 545–552 (1992).
12. Davidson, I. W., Lawson, C. J. & Sutherland, I. W. An alginate lysate from Azotobacter vinelandii phage. *J Gen Microbiol* **98**, 223–229, https://doi.org/10.1099/00221287-98-1-223 (1977).
13. Franklin, M. J. & Ohman, D. E. Identification of algF in the alginate biosynthetic gene cluster of Pseudomonas aeruginosa which is required for alginate acetylation. *J Bacteriol* **175**, 5057–5065 (1993).
14. Skjak-Braek, G., Grasdalen, H. & Larsen, B. Monomer sequence and acetylation pattern in some bacterial alginates. *Carbohydr Res* **154**, 239–250 (1986).
15. Davies, J. C. & Bilton, D. Bugs, biofilms, and resistance in cystic fibrosis. *Respir Care* **54**, 628–640 (2009).
16. Hentzer, M. *et al*. Alginate overproduction affects Pseudomonas aeruginosa biofilm structure and function. *J Bacteriol* **183**, 5395–5401 (2001).
17. May, T. B. *et al*. Alginate synthesis by Pseudomonas aeruginosa: a key pathogenic factor in chronic pulmonary infections of cystic fibrosis patients. *Clin Microbiol Rev* **4**, 191–206 (1991).
18. Alipour, M., Suntres, Z. E. & Omri, A. Importance of DNase and alginate lyase for enhancing free and liposome encapsulated aminoglycoside activity against Pseudomonas aeruginosa. *J Antimicrob Chemother* **64**, 317–325, https://doi.org/10.1093/jac/dkp165 (2009).
19. Alkawash, M. A., Soothill, J. S. & Schiller, N. L. Alginate lyase enhances antibiotic killing of mucoid Pseudomonas aeruginosa in biofilms. *APMIS* **114**, 131–138, https://doi.org/10.1111/j.1600-0463.2006.apm_356.x (2006).
20. Eftekhar, F. & Speert, D. P. Alginase treatment of mucoid Pseudomonas aeruginosa enhances phagocytosis by human monocyte-derived macrophages. *Infect Immun* **56**, 2788–2793 (1988).
21. Hatch, R. A. & Schiller, N. L. Alginate lyase promotes diffusion of aminoglycosides through the extracellular polysaccharide of mucoid Pseudomonas aeruginosa. *Antimicrob Agents Chemother* **42**, 974–977 (1998).
22. Lamppa, J. W., Ackerman, M. E., Lai, J. I., Scanlon, T. C. & Griswold, K. E. Genetically engineered alginate lyase-PEG conjugates exhibit enhanced catalytic function and reduced immunoreactivity. *PLoS One* **6**, e17042, https://doi.org/10.1371/journal.pone.0017042 (2011).
23. Mai, G. T., Seow, W. K., Pier, G. B., McCormack, J. G. & Thong, Y. H. Suppression of lymphocyte and neutrophil functions by Pseudomonas aeruginosa mucoid exopolysaccharide (alginate): reversal by physicochemical, alginase, and specific monoclonal antibody treatments. *Infect Immun* **61**, 559–564 (1993).
24. Dong, S. *et al*. Molecular insight into the role of the N-terminal extension in the maturation, substrate recognition, and catalysis of a bacterial alginate lyase from polysaccharide lyase family 18. *J Biol Chem* **289**, 29558–29569, https://doi.org/10.1074/jbc.M114.584573 (2014).
25. Ghadam, P., Akhlaghi, F. & Ali, A. A. One-step purification and characterization of alginate lyase from a clinical Pseudomonas aeruginosa with destructive activity on bacterial biofilm. *Iran J Basic Med Sci* **20**, 467–473, https://doi.org/10.22038/IJBMS.2017.8668 (2017).
26. Islan, G. A., Dini, C., Bartel, L. C., Bolzan, A. D. & Castro, G. R. Characterization of smart auto-degradative hydrogel matrix containing alginate lyase to enhance levofloxacin delivery against bacterial biofilms. *Int J Pharm* **496**, 953–964, https://doi.org/10.1016/j.ijpharm.2015.10.050 (2015).
27. Matsushima, R. *et al*. Analysis of extracellular alginate lyase and its gene from a marine bacterial strain, Pseudoalteromonas atlantica AR06. *Appl Microbiol Biotechnol* **86**, 567–576, https://doi.org/10.1007/s00253-009-2278-z (2010).
28. Matsushima, R., Watanabe, R., Tsuda, M. & Suzuki, T. Analysis of extracellular alginate lyase (alyA) expression and its regulatory region in a marine bacterial strain, Pseudoalteromonas atlantica AR06, using a gfp gene reporter system. *Mar Biotechnol (NY)* **15**, 349–356, https://doi.org/10.1007/s10126-012-9488-6 (2013).
29. Mrsny, R. J., Lazazzera, B. A., Daugherty, A. L., Schiller, N. L. & Patapoff, T. W. Addition of a bacterial alginate lyase to purulent CF sputum *in vitro* can result in the disruption of alginate and modification of sputum viscoelasticity. *Pulm Pharmacol* **7**, 357–366 (1994).
30. Rahman, M. M., Wang, L., Inoue, A. & Ojima, T. cDNA cloning and bacterial expression of a PL-14 alginate lyase from a herbivorous marine snail Littorina brevicula. *Carbohydr Res* **360**, 69–77, https://doi.org/10.1016/j.carres.2012.05.019 (2012).
31. Xu, F. *et al*. Novel Molecular Insights into the Catalytic Mechanism of Marine Bacterial Alginate Lyase AlyGC from Polysaccharide Lyase Family 6. *J Biol Chem* **292**, 4457–4468, https://doi.org/10.1074/jbc.M116.766030 (2017).
32. Maki, H., Mori, A., Fujiyama, K., Kinoshita, S. & Yoshida, T. Cloning, sequence analysis and expression in Escherichia coli of a gene encoding an alginate lyase from Pseudomonas sp. OS-ALG-9. *J Gen Microbiol* **139**, 987–993, https://doi.org/10.1099/00221287-139-5-987 (1993).
33. Lee, S. I., Choi, S. H., Lee, E. Y. & Kim, H. S. Molecular cloning, purification, and characterization of a novel polyMG-specific alginate lyase responsible for alginate MG block degradation in Stenotrophomas maltophilia KJ-2. *Appl Microbiol Biotechnol* **95**, 1643–1653, https://doi.org/10.1007/s00253-012-4266-y (2012).
34. Li, S., Wang, L., Han, F., Gong, Q. & Yu, W. Cloning and characterization of the first polysaccharide lyase family 6 oligoalginate lyase from marine Shewanella sp. *Kz7*. *J Biochem* **159**, 77–86, https://doi.org/10.1093/jb/mvv076 (2016).
35. Cantarel, B. L. *et al*. The Carbohydrate-Active EnZymes database (CAZy): an expert resource for Glycogenomics. *Nucleic Acids Res* **37**, D233–238, https://doi.org/10.1093/nar/gkn663 (2009).
36. Chen, X. L. *et al*. Characterization of a New Cold-Adapted and Salt-Activated Polysaccharide Lyase Family 7 Alginate Lyase from Pseudoalteromonas sp. *SM0524*. *Front Microbiol* **7**, 1120, https://doi.org/10.3389/fmicb.2016.01120 (2016).
37. Yamasaki, M. *et al*. Structure and function of a hypothetical Pseudomonas aeruginosa protein PA1167 classified into family PL-7: a novel alginate lyase with a beta-sandwich fold. *J Biol Chem* **279**, 31863–31872, https://doi.org/10.1074/jbc.M402466200 (2004).
38. Osawa, T., Matsubara, Y., Muramatsu, T., Kimura, M. & Kakuta, Y. Crystal structure of the alginate (poly alpha-l-guluronate) lyase from Corynebacterium sp. at 1.2 A resolution. *J Mol Biol* **345**, 1111–1118, https://doi.org/10.1016/j.jmb.2004.10.081 (2005).
39. Miyake, O., Ochiai, A., Hashimoto, W. & Murata, K. Origin and diversity of alginate lyases of families PL-5 and -7 in Sphingomonas sp. strain A1. *J Bacteriol* **186**, 2891–2896 (2004).
40. Wong, T. Y., Preston, L. A. & Schiller, N. L. ALGINATE LYASE: review of major sources and enzyme characteristics, structure-function analysis, biological roles, and applications. *Annu Rev Microbiol* **54**, 289–340, https://doi.org/10.1146/annurev.micro.54.1.289 (2000).
41. Linker, A. & Evans, L. R. Isolation and characterization of an alginase from mucoid strains of Pseudomonas aeruginosa. *J Bacteriol* **159**, 958–964 (1984).
42. Yoon, H. J. *et al*. Overexpression in Escherichia coli, purification, and characterization of Sphingomonas sp. A1 alginate lyases. *Protein Expr Purif* **19**, 84–90, https://doi.org/10.1006/prep.2000.1226 (2000).
43. Hashimoto, W., Miyake, O., Momma, K., Kawai, S. & Murata, K. Molecular identification of oligoalginate lyase of Sphingomonas sp. strain A1 as one of the enzymes required for complete depolymerization of alginate. *J Bacteriol* **182**, 4572–4577 (2000).
44. Strathmann, M., Wingender, J. & Flemming, H. C. Application of fluorescently labelled lectins for the visualization and biochemical characterization of polysaccharides in biofilms of Pseudomonas aeruginosa. *J Microbiol Methods* **50**, 237–248 (2002).
45. Bayer, A. S. *et al*. Functional role of mucoid exopolysaccharide (alginate) in antibiotic-induced and polymorphonuclear leukocyte-mediated killing of Pseudomonas aeruginosa. *Infect Immun* **59**, 302–308 (1991).

46. Bayer, A. S. *et al*. Effects of alginase on the natural history and antibiotic therapy of experimental endocarditis caused by mucoid Pseudomonas aeruginosa. *Infect Immun* **60**, 3979–3985 (1992).
47. Lamppa, J. W. & Griswold, K. E. Alginate lyase exhibits catalysis-independent biofilm dispersion and antibiotic synergy. *Antimicrob Agents Chemother* **57**, 137–145, https://doi.org/10.1128/AAC.01789-12 (2013).
48. Jang, C. H. *et al*. Modeling and Re-Engineering of Azotobacter vinelandii Alginate Lyase to Enhance Its Catalytic Efficiency for Accelerating Biofilm Degradation. *PLoS One* **11**, e0156197, https://doi.org/10.1371/journal.pone.0156197 (2016).
49. Follath, F. *et al*. Use of ciprofloxacin in the treatment of Pseudomonas aeruginosa infections. *Eur J Clin Microbiol* **5**, 236–240, https://doi.org/10.1007/bf02013997 (1986).
50. Cendra, M. D. M., Blanco-Cabra, N., Pedraz, L. & Torrents, E. Optimal environmental and culture conditions allow the *in vitro* coexistence of Pseudomonas aeruginosa and Staphylococcus aureus in stable biofilms. *Sci Rep* **9**, 16284, https://doi.org/10.1038/s41598-019-52726-0 (2019).
51. Seidler, J., Zinn, N., Boehm, M. E. & Lehmann, W. D. De novo sequencing of peptides by MS/MS. *Proteomics* **10**, 634–649, https://doi.org/10.1002/pmic.200900459 (2010).
52. Altschul, S. F., Gish, W., Miller, W., Myers, E. W. & Lipman, D. J. Basic local alignment search tool. *J Mol Biol* **215**, 403–410, https://doi.org/10.1016/S0022-2836(05)80360-2 (1990).
53. Zhu, B. & Yin, H. Alginate lyase: Review of major sources and classification, properties, structure-function analysis and applications. *Bioengineered* **6**, 125–131, https://doi.org/10.1080/21655979.2015.1030543 (2015).
54. Yamasaki, M., Ogura, K., Hashimoto, W., Mikami, B. & Murata, K. A structural basis for depolymerization of alginate by polysaccharide lyase family-7. *J Mol Biol* **352**, 11–21, https://doi.org/10.1016/j.jmb.2005.06.075 (2005).
55. Thomas, F. *et al*. Comparative characterization of two marine alginate lyases from Zobellia galactanivorans reveals distinct modes of action and exquisite adaptation to their natural substrate. *J Biol Chem* **288**, 23021–23037, https://doi.org/10.1074/jbc.M113.467217 (2013).
56. Baelo, A. *et al*. Disassembling bacterial extracellular matrix with DNase-coated nanoparticles to enhance antibiotic delivery in biofilm infections. *J Control Release* **209**, 150–158, https://doi.org/10.1016/j.jconrel.2015.04.028 (2015).
57. Crespo, A., Blanco-Cabra, N. & Torrents, E. Aerobic Vitamin B12 Biosynthesis Is Essential for Pseudomonas aeruginosa Class II Ribonucleotide Reductase Activity During Planktonic and Biofilm Growth. *Front Microbiol* **9**, 986, https://doi.org/10.3389/fmicb.2018.00986 (2018).
58. Heydorn, A. *et al*. Quantification of biofilm structures by the novel computer program COMSTAT. *Microbiology* **146**(Pt 10), 2395–2407, https://doi.org/10.1099/00221287-146-10-2395 (2000).

Acknowledgements

We acknowledge support of the European Research Council (ERC) under the European Union's Horizon 2020 research and innovation program under agreement No 670216 (MYCOCHASSIS), the Spanish Ministry of Economy and Competitiveness and *Fondo Europeo de Desarrollo Regional* (MINECO-FEDER) (BIO2015-63557-R), 'Centro de Excelencia Severo Ochoa 2013-2017', FEDER project from Instituto Carlos III (ISCIII, Acción Estratégica en Salud 2016) (reference CP16/00094) and "Secretaria d'Universitats i Recerca del Departament d'Economia i Coneixement de la Generalitat de Catalunya / CERCA programme" (2014SGR678 and 2017SGR1079). The CRG/UPF Proteomics Unit is part of the "Plataforma de Recursos Biomoleculares y Bioinformáticos (ProteoRed)" supported by grant PT13/0001 of Instituto de Salud Carlos III from the Spanish Government.

Author contributions

B.P. did the purification of the protein from Sigma extract. MLS identified by analysis of M.S. data the novel alginate lyase. L.S. did the structure analysis of different alginate lyases. T.F. did the recombinant expression and purification of different enzymes. R.M. did the characterization of alginate lyase activity in the halo test. N.B.C. did the characterization of all enzymes by confocal microscopy. M.L.S. and L.S. conceived the idea, wrote the manuscript and supervised the work. E.T. was supervising biofilm experiments.

Competing interests

Bernhard Paetzold is employed by the S-Biomedic N.V. S-Biomedic N.V. focussed on the skin microbiome and is neither holding any IP rights on the described research results nor active in a related field. All other authors declare no competing interests.

Additional information

Supplementary information is available for this paper at https://doi.org/10.1038/s41598-020-66293-2.

Correspondence and requests for materials should be addressed to L.S. or M.L.-S.

Reprints and permissions information is available at www.nature.com/reprints.

Publisher's note Springer Nature remains neutral with regard to jurisdictional claims in published maps and institutional affiliations.

SUPPLEMENTARY FIGURES AND TABLES

Figure S1. Identification of alginate lyases by MS. Peptides associated with AlyA1 and Alg2A proteins, identified by MS are labeled in blue in the amino acid sequences of the proteins.

>Alg2A
MSIQFSKILLLTVLATATISNAQDKKSKSKTAKIDWSHWTVTVPEENPDKPGKPYSLGYPEILNYAEDKI
ASKYMYDDPKDKSVVFYAFPSGVTTANTHYSRSELRETMETGSNKVNWTFAKGGKMRGTYAIDDISKEPD
GKYSRVIIAQIHGVLTDEQRDLIGQKDNNAPPILKVYWDKGKIRVKTKVLKDLNAPYKEMLLEHAWGDDE
GRNFKEKIDLNTRFTLEVKVSDGRMEVILNDTESLVYDDIHMKKWGIFENYFKAGNYFQSKTPGTFAKVK
IYSLQVTH

>AlyA1
MKKNVFTTLRTVVNGDIMWKLIPVFFLALCLGSCSEEPVDPEEEAVLTKLSANSTAIGISSVSASTSQSP
NVASNTLDGSTSTRWSGYGDGASITYDLGSSANIDYVKIAFYKGDSRKTKYEVWVGNSTSSLTKIKSKTS
SGSTSDYETIDLPNSTARYIRIVGKGYVLNSGGSTVLWNSITKFQAWGSGGSSTLPISGNSPASVLGITA
NTWKINSFIGSPGSSATYYDDITDASGISYNTYSDDNYFYTDGEWVYFKCYRGLGGSANSQNPRVELREM
DNGNLASWTGDSGTHTMEWTVQVNQLPQDTDGDGGVLCFGQIHGPSKNSDGVEVDDVVRVQFIGEENQSS
GSVKLKISGYVTEEQGGSQTFSGYSLDTTYNCKLVYSGGYVELFMNGSSVFRKKMEVDDLSENYFKVGNY
LQSVKGASYTGSYGLVRIKNLSVTHN

Figure S2. Michaelis–Menten saturation curves for the different alginate lyases reactions. The A and B graphs show the relation between the substrate concentration and reaction rate for Poly G and Poly M substrates, respectively. Different colors represent the curves adjusted for different enzymes: AlyA1 (blue), A1-II (red), A1-II' (green), A1-III (violet) and Alg2A (orange).

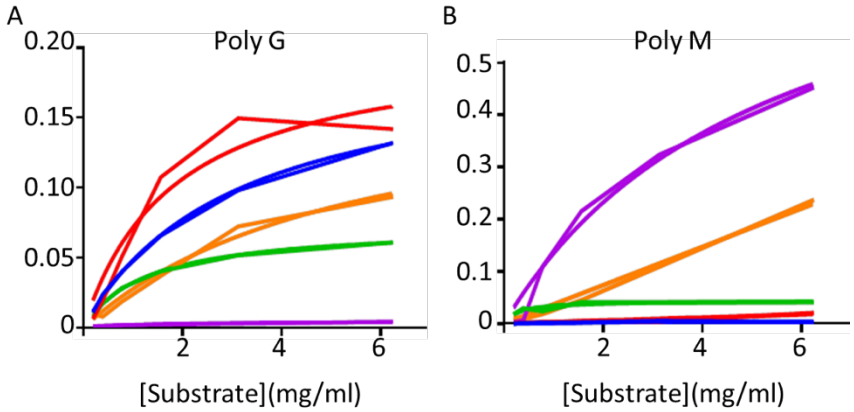

Figure S3. Growth curves of *P. aeruginosa* PAO1 wt and PAO1Δ*mucA* strains treated with different alginate lyases. Antimicrobial activity of different alginate lyases was tested by studying the growth effect of adding the different proteins at 7.09 pmol/µl after 8 hours of growth. No effect in the exponential growth of different strains was observed. As a control, ciprofloxacin was added at 0.5 µg/ml.

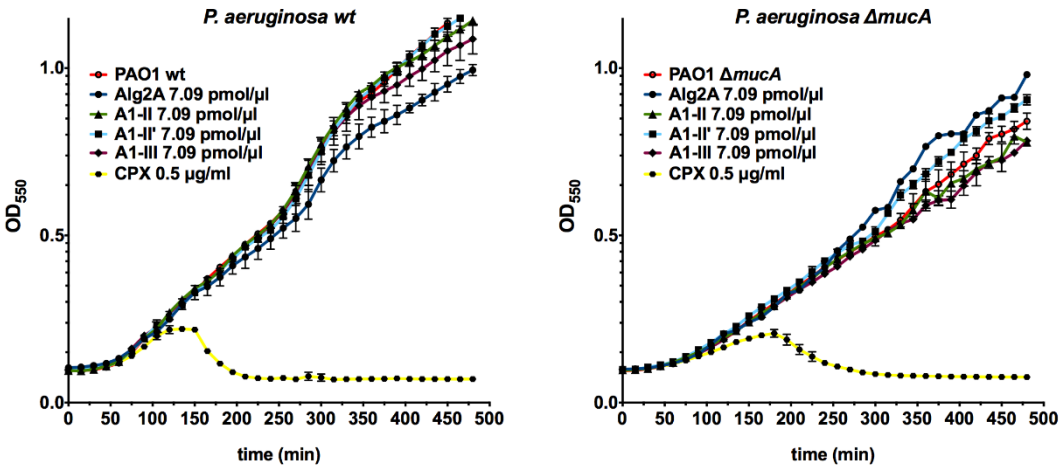

Figure S4. Sum of stack images and the corresponding orthogonal views of the confocal microscopy images of *P. aeruginosa* PAO1 *wt* and PAO1 Δ*mucA* 92-hour biofilms treated for 12 hours with 7.09 pmol/µl of the different alginate lyases and 1 µg/ml of ciprofloxacin (CPX). Red and green colors show the *P. aeruginosa* dead and alive cells detected by the LIVE/DEAD staining kit, respectively. Scale bar corresponds to 50 µm.

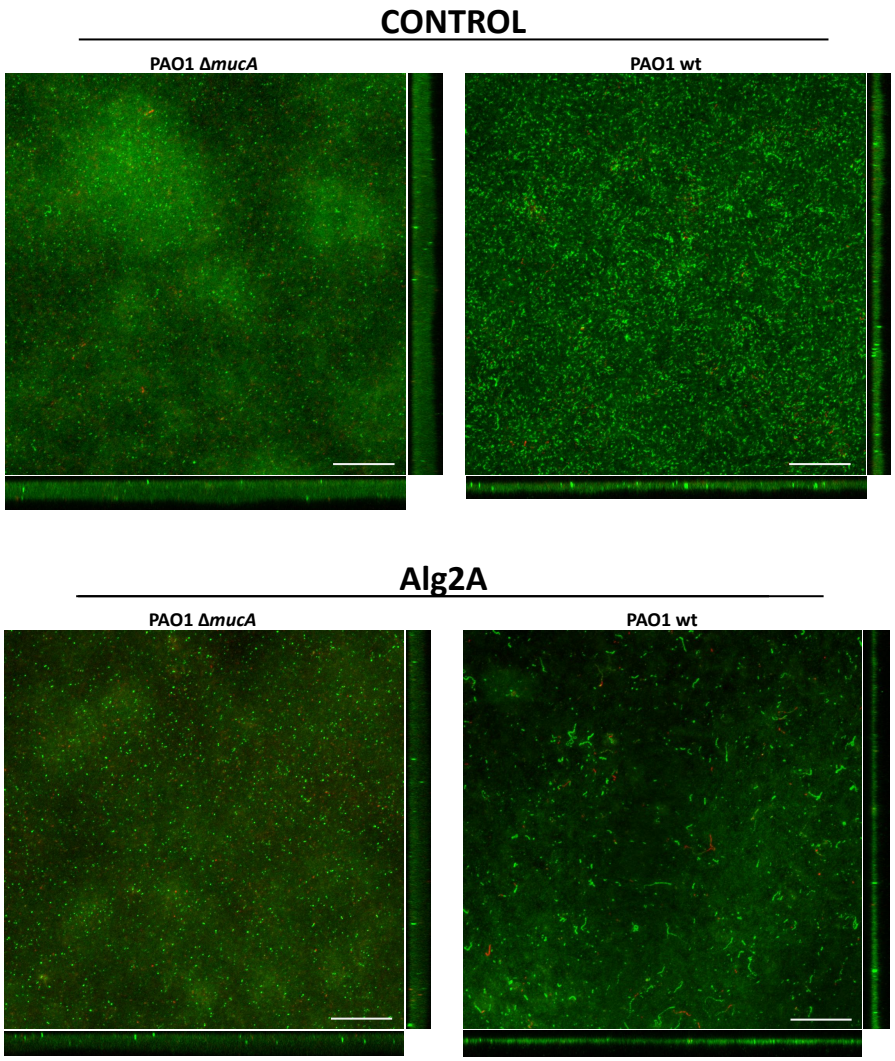

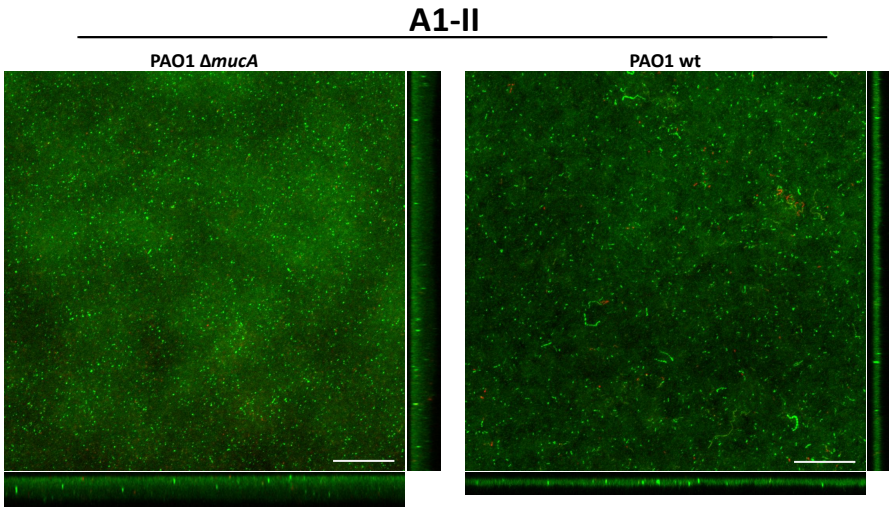
A1-II
PAO1 Δ*mucA*
PAO1 wt

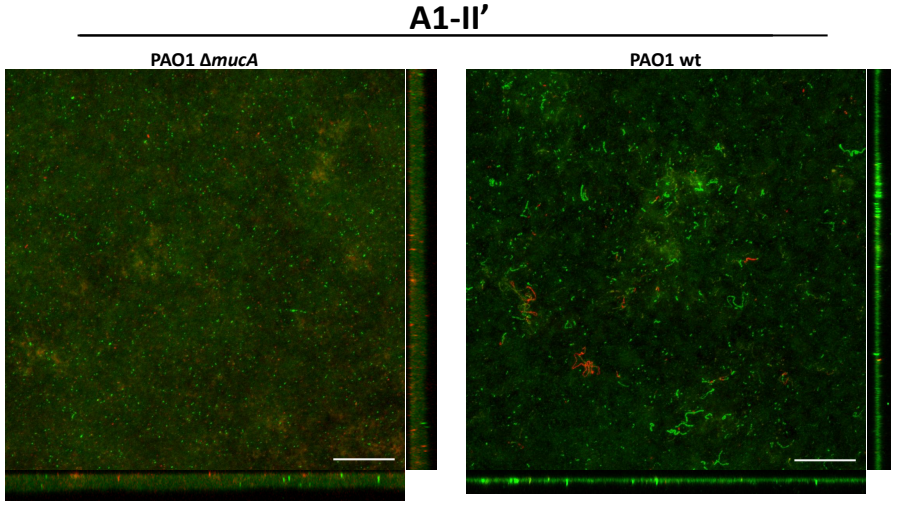
A1-II'
PAO1 Δ*mucA*
PAO1 wt

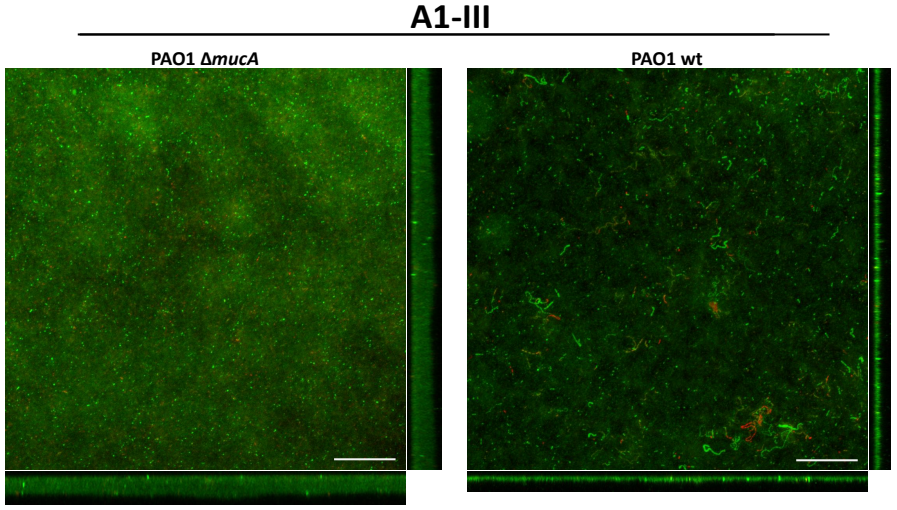
A1-III
PAO1 Δ*mucA*
PAO1 wt

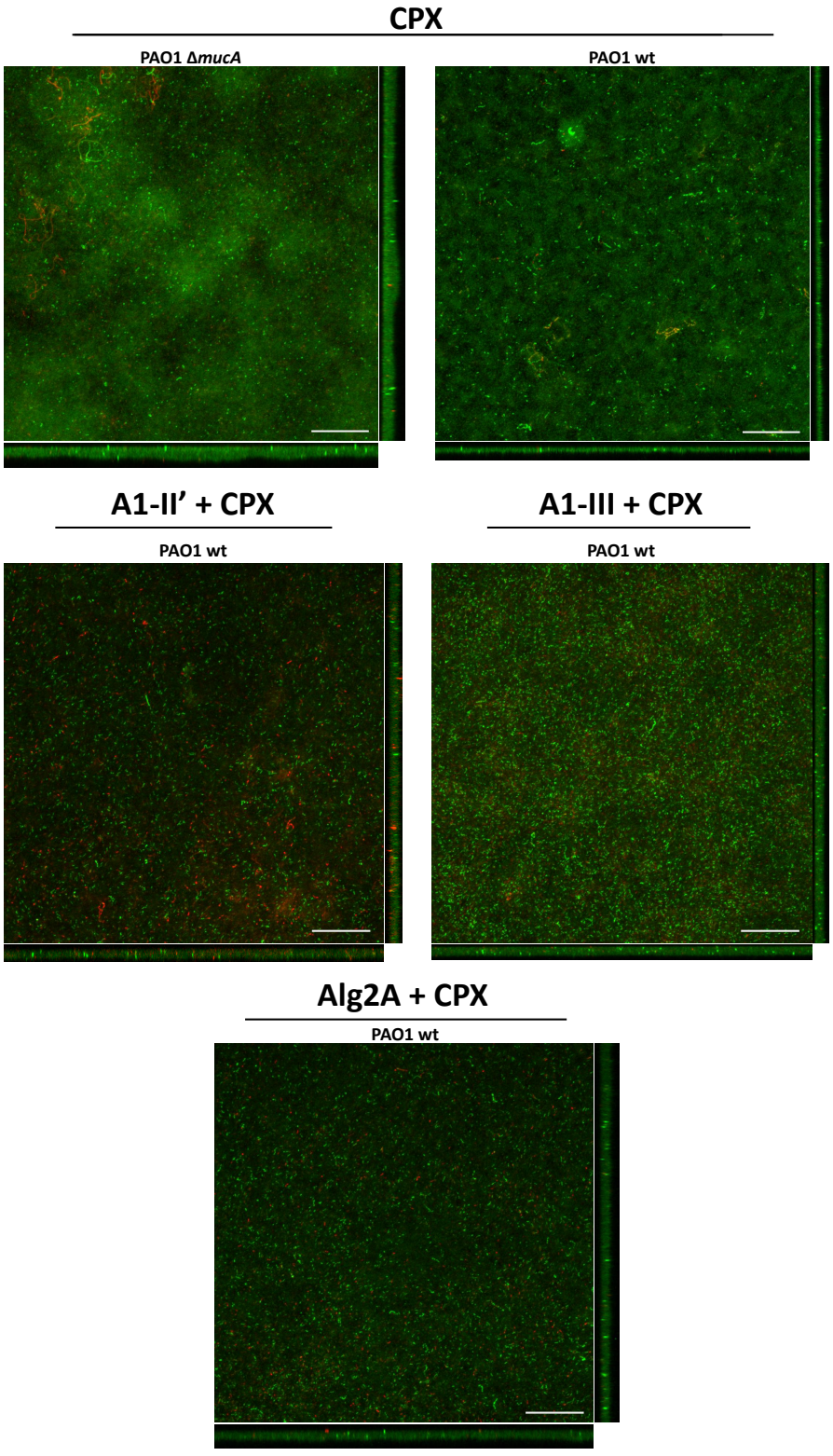
CPX
PAO1 ΔmucA
PAO1 wt
A1-II' + CPX
PAO1 wt
A1-III + CPX
PAO1 wt
Alg2A + CPX
PAO1 wt

Table S9. Values of confocal microscopy assays: Values of biomass, thickness and roughness ± SD

PAO1	CONTROL	Alg2A	AI-II	AI-II'	AI-III	CPX
BIOMASS ($\mu m^3/\mu m^2$)	11.09 ± 0.43	9.22 ± 0.84	10.92 ± 0.26	8.63 ± 0.43	9.36 ± 0.23	9.64 ± 0.24
THICKNESS (µm)	12.72 ± 0.92	12.37 ± 1.18	12.58 ± 0.8	12.18 ± 0.93	10.11 ± 0.51	11.64 ± 0.90
ROUGHNESS COEFFICIENT (variation of thickness)	0.19 ± 0.07	0.12 ± 0.02	0.09 ± 0.09	0.09 ± 0.00	0.13 ± 0.01	0.10 ± 0.01

PAO1 Δ*mucA*	CONTROL	Alg2A	AI-II	AI-II'	AI-III	CPX
BIOMASS ($\mu m^3/\mu m^2$)	21.54 ± 0.72	14.81 ± 0.87	19.37 ± 0.75	15.56 ± 0.97	20.43 ± 1.04	18.28 ± 1.05
THICKNESS (µm)	21.14 ± 0.73	15.57 ± 1.50	19.25 ± 0.95	15.67 ± 0.47	20.16 ±1.14	18.33 ± 1.09
ROUGHNESS COEFFICIENT (variation of thickness)	0.08 ± 0.02	0.11 ± 0.03	0.08 ± 0.03	0.09 ± 0.01	0.07 ± 0.01	0.10 ± 0.01

PAO1	CONTROL	Alg2A + CPX	AI-II' + CPX
BIOMASS ($\mu m^3/\mu m^2$)	14.39 ± 2.11	10.62 ± 0.29	9.76 ± 0.42
THICKNESS (µm)	16.68 ± 2.57	13.04 ± 0.60	11.34 ±1.21
ROUGHNESS COEFFICIENT (variation of thickness)	0.10 ± 0.02	0.07 ± 0.00	0.10 ±0.02

PAO1	CONTROL	AI-III + CPX
BIOMASS ($\mu m^3/\mu m^2$)	22.10 ± 1.5	19.24 ± 1.10
THICKNESS (µm)	22.77 ± 1.8	19.25 ± 1.34
ROUGHNESS COEFFICIENT (variation of thickness)	0.05 ± 0.01	0.06 ± 0.01

ARTICLE 5

Tobramycin and DNase I dextran-based single-chain nanoparticles interaction with *Pseudomonas aeruginosa* extracellular biofilm matrix.

Manuscrit

Autors: **Núria Blanco-Cabra**[1], Julie Movellan[2], Marco Marradi[2,3], Raquel Gracia[2], Damien Dupin[2], Iraida Loinaz[2], Eduard Torrents[1,4]*

1: Bacterial Infections and Antimicrobial Therapies, Institute for Bioengineering of Catalonia (IBEC) The Barcelona Institute of Science and Technology (BIST), Barcelona, Spain

2: CIDETEC, Basque Research and Technology Alliance (BRTA), Parque Científico y Tecnológico de Gipuzkoa, Miramon Pasealekua, 196, Donostia-San Sebastián 20014, Spain.

3: Department of Chemistry "Ugo Schiff", University of Florence, via della Lastruccia 13, 50019 Sesto Fiorentino (FI), Italy.

4: Microbiology Section, Department of Genetics, Microbiology, and Statistics, Biology Faculty, Universitat de Barcelona, Barcelona, Spain

*: Correspondència: Dr. Eduard Torrents (etorrents@ibecbarcelona.eu)

Abstract

The extracellular matrix protects the biofilm cells by reducing the penetration of the antimicrobials. Tobramycin is an antibiotic extensively used for the treatment of *P. aeruginosa* biofilms, but due to its positive charges, it is sequestered in the biofilm periphery by the negative charges of the extracellular matrix, losing efficacy significantly. Several nano-based formulations have been designed and are nowadays used to increase the final concentration of the antibiotics at the infection site, but alternatives to increment the diffusion of this antibiotic into the biofilm are necessary. Dispersal of the biofilm extracellular matrix with enzymes like DNase I is another used therapy against biofilms that can increment antibiotic penetration and diffusion to reach the internal bacterial cells. Here, we combine the charge neutralization effect that the dextran-based single-chain polymer nanoparticles (DXT-SCPNs) provide to the tobramycin with aid of the DNase I to break the matrix. The effect of these DXT-SCPNs against continuous and mature *P. aeruginosa* and *S. aureus* biofilms is studied. Moreover, the specific interaction of DXT-SCPN with the different extracellular matrix components of the *P. aeruginosa* biofilm was analyzed, characterized, and their interactions were studied, showing an improvement of the activity of the tobramycin and the DNase I.

Introduction

Antibiotics are the principal therapy against acute bacterial infections. However, when a bacterial community attaches to a surface and grows in a biofilm form, the infections produced become chronic, and the antibiotics are much less effective [1]. Bacteria form a biofilm by building an extracellular matrix, which creates a physical and chemical barrier that is the leading cause of antibiotic inefficiency. This extracellular biofilm matrix comprises polysaccharides, lipids, proteins, and extracellular DNA (eDNA) [2].

Pseudomonas aeruginosa and *Staphylococcus aureus* are bacteria that usually form biofilms in the lungs affected by Cystic Fibrosis (CF) or Chronic Obstructive Pulmonary Disease (COPD), being the primary cause of morbidity and mortality in these illnesses [3]. *S. aureus* is frequently associated with *P. aeruginosa*, and this co-infection worsens the outcome of the disease [4]. eDNA is a key part of *P. aeruginosa* and *S. aureus* extracellular biofilm matrix, as it promotes bacterial adhesion on the surface in the early stages and maintains its structural stability in mature biofilms [5, 6]. eDNA was thought to be only a residual material of bacterial lysis until it was reported that the enzyme deoxyribonuclease (DNase I) could inhibit biofilm formation and dissolve established biofilms [7]. Nowadays, this enzyme is used in CF patients in aerosol form to help mucus clearance by reducing its viscosity and improving antibiotic chemotherapy [8].

When a pulmonary infection of *P. aeruginosa* becomes chronic and forms a biofilm, it frequently converts to a mucoid phenotype by overproducing the anionic polysaccharide alginate in the extracellular matrix [9]. Alginate protects bacteria from the immune system by inhibiting the complement system and reducing the neutrophils and macrophages' phagocytosis. Together with the eDNA, this negatively charged polysaccharide can bind to a positively charged antibiotic, thus diminishing the antibiotic diffusion throughout the biofilm [10, 11]. For example, tobramycin, an aminoglycoside extensively used in the treatment of CF lung infections caused by *P. aeruginosa*, has a considerably reduced biofilm diffusion [12]. It is also administrated via aerosol, as it mitigates the toxicity of tobramycin and increases the final concentration at the infection site, compensating for the low diffusion into the biofilm [13]. However, this is not enough, and the tobramycin and other antibiotics require enhanced biofilm diffusion and penetration to increase its antimicrobial efficacy, especially in CF chronic infections.

Drug nanocarriers can be used to effectively overcome these barriers and transport the drug to the site of interest. Nanoparticles protect the antimicrobial agent from degradation or deactivation, prevent interactions between the drug and the biofilm extracellular polymeric substances (EPS), and release the antibiotic locally and in a controlled manner to enhance antimicrobial activity. Many nano-based formulations for delivering antibiotics in chronic pulmonary infections have been investigated [14-16] and include inorganic nanoparticles, liposomes, polymeric nanoparticles, and hybrid systems. Some nanosystems like Arikayce®, a liposome amikacin nanocarrier for non-tuberculous mycobacterial pulmonary infections, are already commercialized [17]. These nanocarriers must provide enough concentration of the antibiotic at the infection site, avoiding accumulation and toxicity in undesired parts of the body [18].

The nanocarriers' rational design for pulmonary administration is key to reach the biofilm and deliver its cargo at the infection site. Previous works have demonstrated that to cross the mucus layer surrounding the infection, the delivery system size and surface charge are critical. Nanoparticles below 500 nm in diameter and neutral or negatively charged are considered the best candidates [19-22]. For the treatment of *P. aeruginosa* biofilms, it has been shown that the diffusion rate is size-dependent, and a nanosystem size below 100 nm is essential [23]. Moreover, the mobility and diffusion rate of the negatively-charged nanoparticles is higher than the positively charged ones, which are retained by the eDNA in the EPS [24] via electrostatic interactions.

The most studied polymeric nanoparticles are based on chitosan and polylactic-co-glycolic acid (PLGA). Despite the biocompatibility, degradability, and antimicrobial nature of chitosan that make it a promising vector, its hydrophobicity, which promotes its aggregation under biological conditions, hinders its use. On the other hand, PLGA nanoparticles have the disadvantage of

generating acidic degradation products and having low encapsulation efficiencies. Nevertheless, it is worth mentioning that PLGA loaded with ciprofloxacin/DNase I and colistin reduce formed biofilms considerably [25, 26]. However, in both cases, the amount of antibiotic encapsulated was not higher than 1 wt%, which would imply a considerable work in the nanoformulation for real patient therapy.

In addition, it is important to highlight that most of the antibiofilm studies using nanoparticles were produced using biofilms formed in static manner, which results in a weaker biofilm compared to the mature biofilm present in CF patients.

Recently, Single-Chain Polymer Nanoparticles (SCPNs) based on Dextran natural polysaccharides (DXT-SCPNs) have been used to carry antimicrobial peptides to fight infections from antimicrobial-resistant bacteria [27]. SCPNs [28-32] are obtained by collapsing a single polymer chain resulting into a small nanoparticle with sizes generally reported in the range of 1 to 20 nm, thus comparable to the ones of proteins and viruses. They are easily modulated either during their preparation or by posterior functionalization. Such DXT-SCPNs have shown ideal characteristics to be used as nanocarriers for imaging and immunotherapy, as they are size-controlled, biocompatible, biodegradable, and water-dispersible [33, 34]. Thanks to their small hydrodynamic size (20 nm), homogenous lung distribution was observed by SPECT-CT after intra-tracheal administration using Penn Century Microsprayer® aerosolizer, indicating that DXT-SCPNs are a suitable nanocarrier for lung administration [27, 34-36].

In this work, DXT-SCPNs carrying tobramycin via electrostatic interactions and formulated with DNase I are used for disaggregating mature *P. aeruginosa* and *S. aureus* biofilms. First, the maximum loading of the antibiotic and the characterization of the nanoformulated nanoantibiotic were investigated. The antimicrobial activity of the final candidates was studied in vitro in the presence of *Pseudomonas aeruginosa* and *Staphylococcus aureus*. Finally, the interactions of DXT-SCPNs, loaded and unloaded with Tobramycin and/or DNase I, with a mature *Pseudomonas* biofilm matrix grown under continuous conditions, are studied through time-lapse imaging by laser scanning confocal microscope.

Results and Discussion

SCPN characterization and activity against planktonic bacteria

DXT-SCPN were prepared as previously described [34] by the controlled collapse of single polymer chains into nanoparticles through intrachain cross-linking. The Intermediate I (Fig. S1) obtained after the intracross-linking of a single DXT polymer chain was then labelled with rhodamine *via* an esterification reaction. The progress of the reaction was followed by TLC, and the non-reacted rhodamine was removed using a PD-10 Sephadex column. ^{1}H NMR analysis of rhodamine-labelled SCPN, Intermediate II, showed the absence of hydrolysis of the ester groups and confirmed the presence of the rhodamine dye (Fig. S2). The amount of rhodamine covalently attached to the SCPN (18 μg Rh/mg Intermediate II) was calculated by UV-Vis spectroscopy using a previously prepared calibration curve (Fig. S3). Finally, the remaining methacrylate groups were functionalized with mercaptopropionic acid via thio-Michael addition to provide carboxylate functionality to SCPN (Fig. S1). The nanoantibiotic, SCPN with tobramycin (Tob-SCPN) was simply prepared by mixing the aqueous dispersion of SCPN with an aqueous solution of tobramycin, both at pH 7 (Fig. 1A). At such neutral pH, the tobramycin, positively charged *via* its amine groups (pKa = 7.4, 7.4, 6.2, 8.6, 7.6) [37], was electrostatically attached to SCPNs, which are negatively charged due to the presence of carboxylate groups (pKa = 5, determined experimentally). The addition of tobramycin to SCPN was monitored by aqueous electrophoresis, and a maximum loading of 40 wt% of the antibiotic in Tob-SCPN was achieved until reaching neutral charge, i.e. a zeta potential at around -5 (±2) mV for Tob-SCPN. Thus, the increase of zeta potential observed from -21 (±1) mV obtained for SCPN, up to quasi-neutral charge for Tob-SCPN, confirmed the electrostatic interactions between the cationic antibiotic and the anionic nanocarrier (Table 1, Fig. 1D). Nowadays, to treat infections, a relatively high loading of tobramycin is required to fight bacteria successfully and to avoid using a very high concentration of nanoparticles. DNase I was also simply formulated with SCPN and Tob-SCPN to avoid any chemical modification of the enzyme that could affect its activity (Fig. 1A). Large aggregates were observed for DNase I-SCPN nanosystems with Z-average of 102 nm, as judged by DLS (Dynamic Light Scattering) (Fig. 1C). Actually, the corresponding size distribution shows the presence of smaller particles (5 nm and 15 nm) which might indicate the presence of free DNase I (6 nm particles) as well as DNase I-SCPN as single particles (15 nm particles) or aggregates (100 nm particles). It is important to mention that the DLS technique overestimates the particle size in the presence of aggregates as an intensity-average technique. In addition, with a polydispersity index of 0.52, DLS is not the most suitable technique, and an electron microscopy technique is more indicated in this case. As can be seen in Fig. 1E, TEM analysis of DNase I-SCPN confirms that the main particle

population is composed by small particles of 21 ± 5 nm. On the other hand, a smaller particle size of Tob-DNase I-SCPN at 11 nm was observed by DLS, which could indicate some type of interactions between the nanoparticles and the enzyme. The exact interaction mechanism remains unclear but the different particles overall charge, negative for SCPN and close to neutral for Tob-SCPN, might suggest additional electrostatic interactions (Fig. 1D).

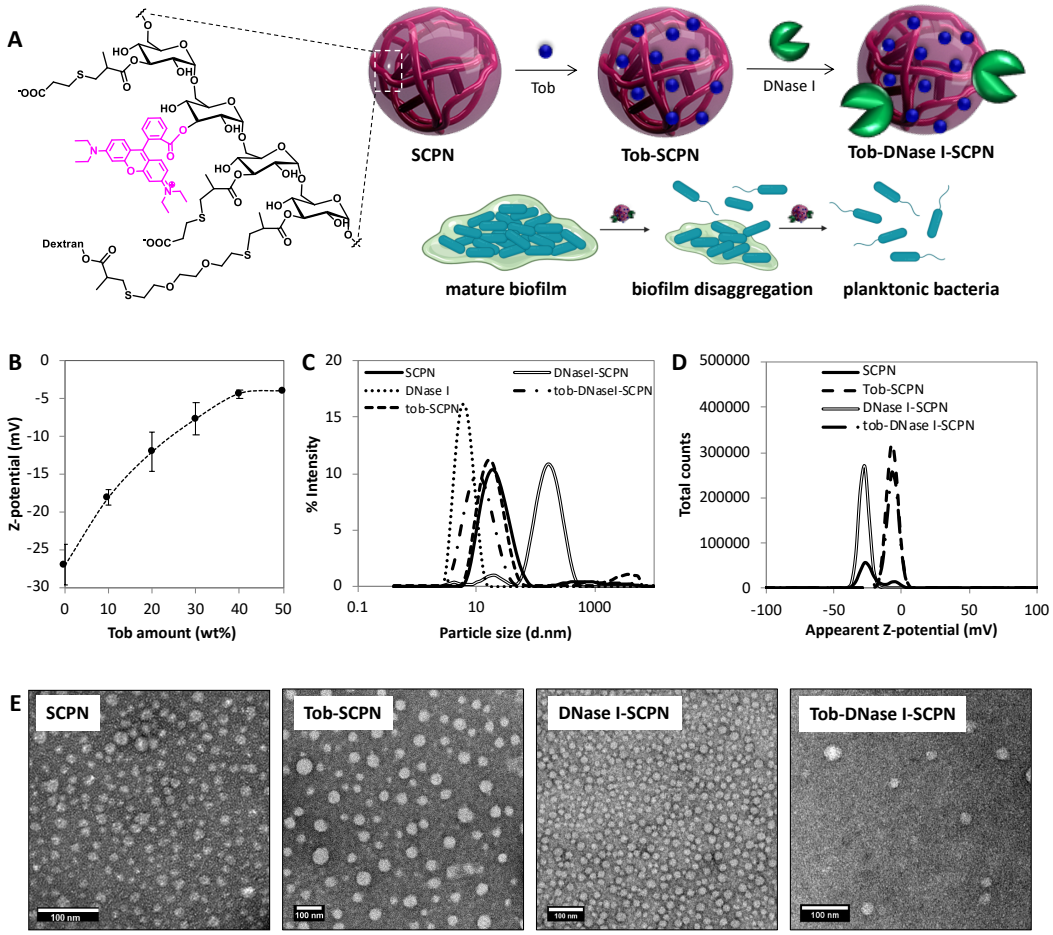

Fig. 1: A) Negatively charged SCPN labelled with Rhodamine (SCPN) and its functionalization with tobramycin (Tob) and DNase I; B) Zeta-potential in function of tobramycin wt% in Tob-SCPN formulation; C) Size distribution (DLS, 10 mg/ml in PBS); D) Z-potential distribution (10 mg/ml, 1 mM NaCl); E) TEM images of the different formulations, scale bar : 100 nm.

DXT-SCPN type	Tobramycin content[a] (µg tob/mg SCPN)[b]	DNase I content[a] (µg DNase I/mg SCPN)[b]	Dn average[c]	Z-average (d.nm)/ PdI[d]	Z-potential (mV)[d]
SCPN	-	-		19 ± 1 / 0.26 ± 0.04	-21 ± 1
Tob-SCPN	400 µg/mg (400 µg/mg active)	-	37 ± 13 nm	17 ± 1 / 0.27 ± 0.01	-5 ± 2
DNase I-SCPN	-	530 µg/mg (30 µg/mg active)	21 ± 5 nm	102 ± 2 / 0.52 ± 0.01	-28 ± 1
Tob-DNase I-SCPN	230 µg/mg (230 µg/mg active)	410 µg/mg (30 µg/mg active)	37 ± 13 nm	11 ± 1 / 0.27 ± 0.07	-6 ± 1

Table 1: Composition of the different formulations. (SCPN: nude nanoparticles; Tob-SCPN: nanoparticles with 40 wt % tobramycin; DNase I-SCPN: nanoparticles that have DNase I; Tob-DNase I-SCPN: nanoparticles that contain 23 wt % tobramycin and DNase I). [a)] tobramycin concentration measured by LC-MS; [b)] tobramycin and DNase I activity measured by comparing with the free drug and soluble enzyme; [c)] TEM measurements (at least 100 particles counted); [d)] analyzed using zetasizer nano (DLS)

The tobramycin and DNase I active concentration in the nanoformulations was further validated in two different experiments. On the one hand, the tobramycin activity was measured by comparing it with the same soluble tobramycin concentration in an 8-hour bacteria growth curve. As seen in Fig. 2, the planktonic growth curves of the *P. aeruginosa* and *S. aureus* treated with SCPN containing tobramycin have the same growth pattern as the ones treated with free soluble tobramycin at equivalent concentrations. These results indicated that the antibiotic concentration loaded in the SCPN synthesized in this work was active. Moreover, the innocuousness of the SCPN and DNase I-SCPN against planktonic bacteria could also be confirmed, as the growth curve with the treatment at high concentration of these nanoparticles (50 µg/ml) did not differ from the one without any treatment.

On the other hand, the activity of DNase I formulated within the nanoparticles was verified by quantifying the DNA degradation activity in an agarose gel electrophoresis and comparing it with

the activity of soluble DNase I (see Material and Methods). In contrast to the 100 % tobramycin activity inside the nanoparticles, the active DNase I is only 5.6 % and 7.3 % of the total loaded DNase I in the DNase I-SCPN and Tob-DNase I-SCPN, respectively (data not shown). It is well known that enzyme inactivation by nanomaterials can also originate from large changes in protein structure following absorption or covalent binding [38, 39].

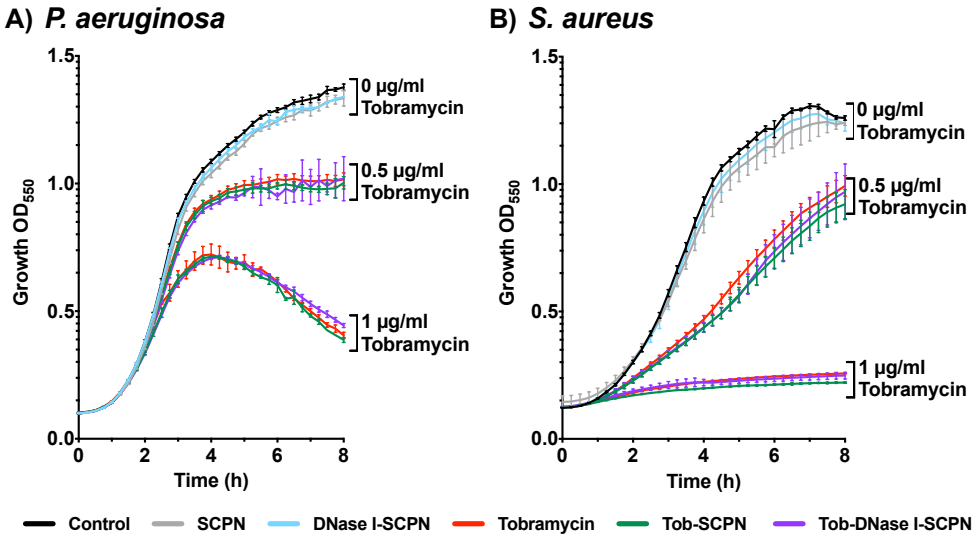

Fig. 2: 8-hour bacterial growth curves of A) *P. aeruginosa* and B) *S. aureus* treated with soluble tobramycin (red) and the different nanoparticles containing: 0 µg/ml of tobramycin (grey, 50 µg/ml of SCPN; blue, 50 µg/ml of DNase I-SCPN), 0.5 µg/ml of tobramycin (green, 1.25 µg/ml of Tob-SCPN; purple, 2.2 µg/ml of Tob-DNase I-SCPN) and 1 µg/ml of tobramycin (green, 2.5 µg/ml of Tob-SCPN; purple, 4.3 µg/ml of Tob-DNase I-SCPN). Black lines represent growth without any treatment.

SCPN enhance the tobramycin and DNase I activity against continuous P. aeruginosa and S. aureus biofilm

Continuous biofilms of *P. aeruginosa* PAO1 and *S. aureus* were grown for 72 hours in flow-cell chambers (see Material and Methods) and then treated for 16 hours with 0.26 µg/ml of DNase I, 2 µg/ml of tobramycin and with both treatments. At the same time, we treated the biofilms with SCPNs containing equivalent tobramycin and DNase I concentrations. The treated biofilm was stained and imaged in a confocal microscope, and different biofilm parameters were calculated (biomass and thickness). As seen in Fig. 3A and B, the most effective treatment for the *P. aeruginosa* and *S. aureus* biofilms were the use of Tob-DNase I-SCPN, containing both DNase I and tobramycin (purple striped bars), which were able to reduce the biofilms by 34 % and 16 % compared to the non-treated *P. aeruginosa* and *S. aureus*, respectively. Tob-DNase I-SCPN can reduce 5 % more of the established biofilm, compared to the corresponding treatment with soluble DNase I and tobramycin

(Fig. 3A and B, solid purple bars). Also, the treatment with nanoparticles containing tobramycin is more effective than the soluble free tobramycin (green striped and green solid bars), obtaining higher reduction (6 and 5 % in the *Pseudomonas* and *Staphylococcus* biofilms, respectively). Besides the biomass percentage reduction in the *Pseudomonas* biofilms treated with Tob-SCPN and Tob-DNase I-SCPN, it is also noticed a rise in the dead bacteria (stained in red) in the CLSM images of Fig 3C. Even though the reduction in the biofilms of *Staphylococcus* treated with these nanoparticles is not enough to see an increase in the red cells, it can be appreciated some cell-detachment that the treatment produced (Fig. 3D).

Treatment with DNase I-SCPN has, however, brought different results in the two biofilms tested. While in the *P. aeruginosa* biofilm, the established biofilm was reduced up to 33 %, in the *S. aureus*, the same treatment increased the biomass up to 129 % (Fig. 3B, blue striped bars). Moreover, it is worth mentioning that none of the biofilms treated with SCPN, without DNase I or tobramycin, significantly affect the biofilm, confirming the innocuousness of the dextran SCPN carrier (Fig. 3A and B black striped bars).

It is well known that eDNA plays an essential role in *P. aeruginosa* and *S. aureus* biofilms development [40, 41]. In the *S. aureus* case, eDNA promotes bacteria aggregation, since it has been previously seen that these structures decrease their size with the addition of DNase I and increase with exogenous DNA [42]. When *S. aureus* biofilm is treated with the DNase I-SCPN, there is an increase of the micro-colonies found in the computational analysis with COMSTAT (data not shown), indicating that the big bacterial clumps of the *S. aureus* biofilms are disaggregated, and smaller clusters are formed. The biofilm architecture becomes then loosened, thus producing an increase in the biomass quantification (Fig. 3B, blue striped bars). This can be clearly seen in the increase of the orthogonal views (thickness) and the 3D representation of Fig. 3D and E. Even though all SCPN tested are increasing the activity of the soluble treatment by about a 5 %, SCPNs are undoubtedly improving the activity of DNase I drastically, because DNase I-SCPN, even if not all the DNase I is localized on the SCPN as indicated by DLS studies, achieve a substantial detachment of the *S. aureus* biofilm and also cause the most significant reduction of *P. aeruginosa* biofilm compared to the soluble treatment (15% of improvement, Fig. 3A, striped compared to solid blue bars). A synergistic effect between free DNase I and DNase I-SCPN could explain such unexpected performances.

It is important to mention that in addition to being continuous, the biofilm formation during 72h allow the bacteria to grow in different layers making the whole study closer to the *in vivo* conditions and making the biofilm more challenging to treat. Most of the results published before outcome from studies carried out on static biofilms [43-49] or continuous biofilms grown for less than

24h [50], which implicates that they contain fewer bacteria in the biofilm state, often in monolayer and need less treatment to be eradicated.

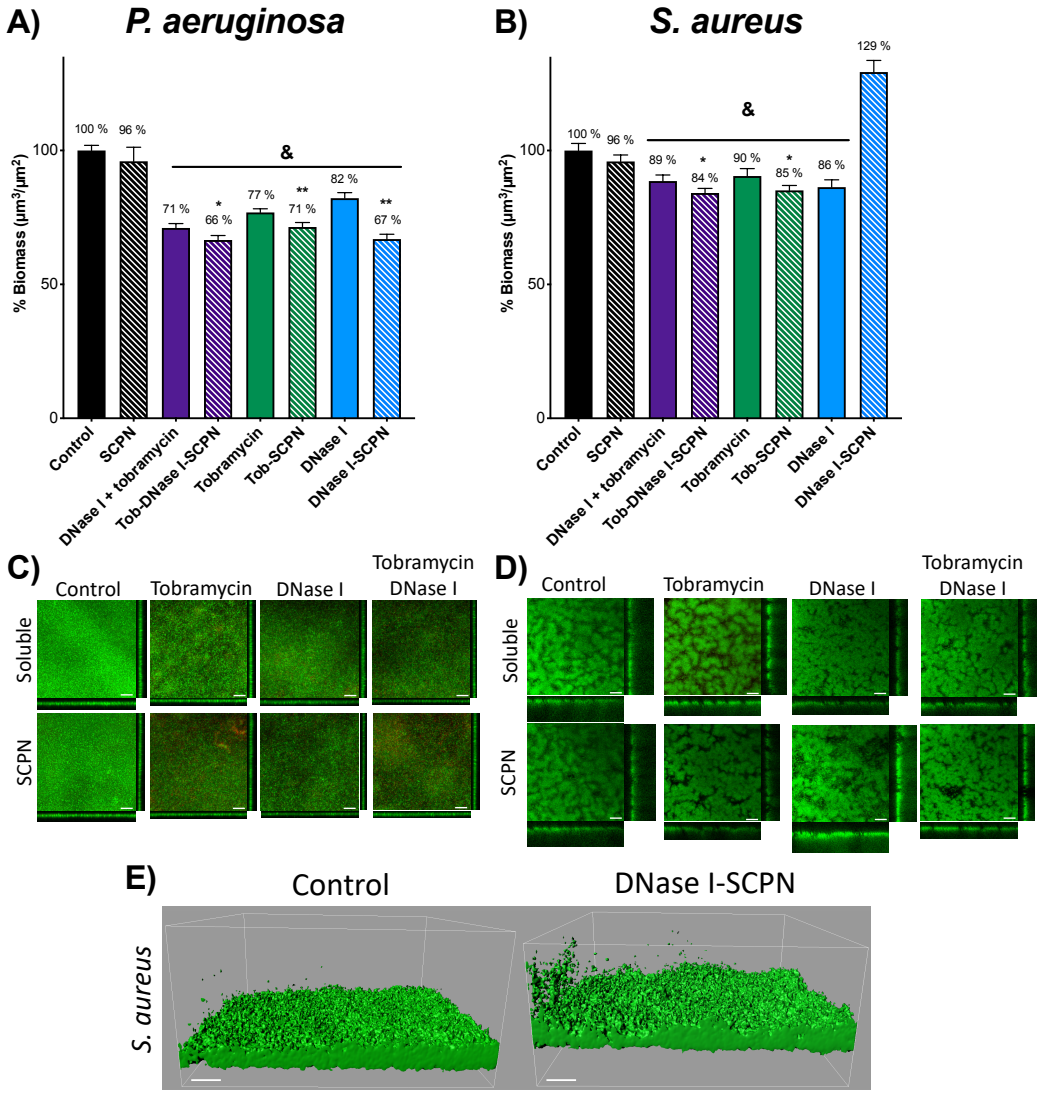

Fig. 3: Degradation of A) *P. aeruginosa* PAO1 and B) *S. aureus* 72 hours old biofilms treated for 16 hours with 0.26 µg/ml of DNase I and/or 2 µg/ml of tobramycin (solid bars), and with SCPN with equivalent encapsulated concentration of both treatments (striped bars). Blue bars correspond to DNase I treatment, green bars correlate to the antibiotic tobramycin, and both treatments together are represented in purple bars. Control (non-treated biofilm) and SCPN (without tobramycin and DNase I) are stated in black bars. All values are normalized against the control sample. Confocal Laser Scanning Microscope images (Sum of the stack and orthogonal views) of Live/Dead stained C) *P. aeruginosa* PAO1 and D) *S. aureus* biofilms. E) 3D view representation of the *S. aureus* biofilm without treatment and treated with DNase I-SCPN. The statistical analysis to determine significance was performed using the Student Unpaired *t*-Test (&: $p < 0.005$ vs Control. *: $p < 0.05$ and **: $p < 0.005$ vs treatment without SCPN). Scale bar represents 40 µm.

SCPN does not alter the biofilm growth

The experiment performed in Fig. 3 allows the SCPN efficacy to be identified by analyzing biofilm biomass change from the starting point (time 0) and after 16 hours of treatment but does not describe the dynamics and alterations at the biofilm extracellular matrix level. Also, neither shows the progression of the treatment nor the interaction of the nanoparticle with the biofilm. To further investigate this behavior, we studied how the different SCPN interact with an established 72-hour old *P. aeruginosa* PAO1 continuous biofilm by imaging their behavior during a time-lapse confocal microscopy experiment. During the 16-hour experiment, the bacterial cells, the eDNA, and the alginate as a representative component of the sugars present at the extracellular matrix, were differentially stained. Three different nanoparticles (SCPN, Tob-SCPN and Tob-DNase I-SCPN) were labelled with the rhodamine dye and inoculated inside the biofilm flow-cell chamber, all at the same concentration (100 µg SCPN/ml). At this concentration, which is ten times higher than the one used in Fig. 3, part of the nanoparticles are forming aggregates of about 2 µm of diameter after contact with the biofilm. With the different preliminary test experiments done (data not shown) we chose a variety of 2 µm as the optimal nanoparticle aggregate size to be tracked in the confocal microscope along the 16 hours of the time-lapse experiment. In contrast, smaller aggregates end up dissolved before the 16 hours (see Fig. S5 video A).

SCPN and the different dyes were simultaneously injected into a mature biofilm (see Material and Methods), and different regions with a 2 µm aggregate of nanoparticles were actively selected in the confocal microscope for tracking and imaging. The areas of interest were imaged for 16 hours with the programmable acquisition algorithm of the Zen software at multi-position time series (Zeiss). During the imaging, the focus was maintained, and the artefacts caused by the thermal drift or vibrations were avoided by using the Definite Focus equipment (Zeiss) coupled to the confocal microscope.

After the 16-hour treatment, a determined 13x13 µm region of interest surrounding the nanoparticle aggregate was created to analyze the behavior in the biofilm components with time (see Materials and Methods). Fig. 4 depicts the changes in matrix biomass, cells, and eDNA of the area surrounding the nanoparticle aggregate. This figure demonstrates the innocuousness of the SCPN, as it illustrates how the bacteria grow exponentially, becoming stationary at 6-9 hours when the planktonic bacteria cover 100 % of the region and cannot spread anymore (black line of Fig. 4B). Fig.4A also shows the increase of the extracellular matrix biomass achieved during the 16 hours of the time-lapse experiment (black line). When the continuous biofilm was formed, the constant media flow through the chamber expels the non-attached bacteria [51]. During the time-lapse imaging,

however, the flow was stopped, and the non-attached bacteria were allowed to grow planktonically while the attached bacteria continue to form the biofilm.

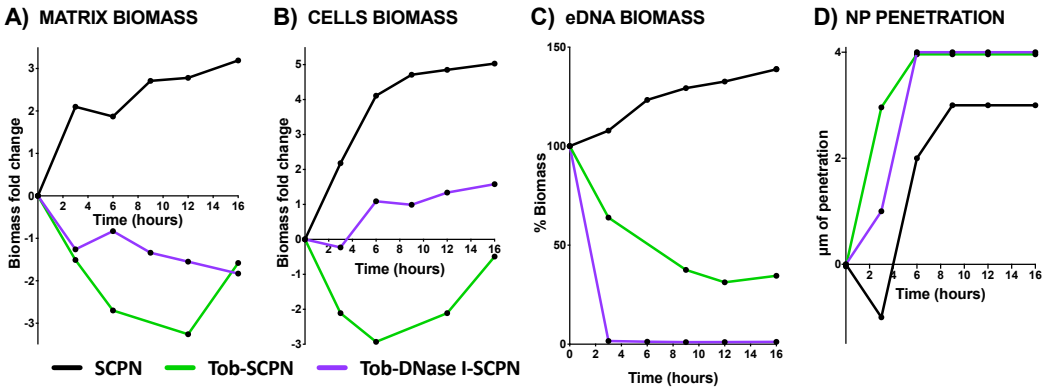

Fig. 4: Biomass variation during the time in A) matrix, B) cells, and C) extracellular DNA (eDNA) in a biofilm treated with SCPN (without tobramycin and DNase I) (black line), Tob-SCPN (green line) and Tob-DNase I-SCPN (purple line). Variation of the biomass in A) and B) is represented in fold change, while variation in C) is described in percentage. D) Position of the nanoparticle aggregate concerning the biofilm matrix.

With the data recovered from the microscopy images, a graphical representation of the distribution changes in the biofilm matrix (alginate staining), cells, eDNA and the nanoparticle aggregate was also developed (Fig. 5 and Fig. S5). In this figure, the changes in the percentage of biofilm area that covers each slice are represented. To normalize the biofilms, all plots start at the x-axis in the upper part of the biofilm, when the area covered by cells and the extracellular matrix begins to decrease. On the other hand, the area covered by nanoparticles was also normalized by assigning 100 % at the slice with the most significant part of the nanoparticle aggregate imaged. With SCPN (Fig. 5A), it can be seen that the bacterial cells are growing planktonically, as the percentage of area occupied by the cells (dark blue line) was increasing through time, reaching the whole area occupation after 9 hours. The 3D representation below the graphs depicts this planktonic growth with an increase of the dark blue at the top of the biofilm. In the Fig. 5A plots, the progression of the biofilm formation was also detected, as the light blue line was also growing during the time.

DNase I prevent the regrowth of the P. aeruginosa biofilm during 16 hours of treatment

In the biofilm treated with the SCPNs loaded with only tobramycin or in combination with DNase I (Fig. 5B and C), the biofilm cell behavior and the extracellular matrix were sensitive and suffered apparent modifications by the antibiotic and enzyme activity directly derived from the SCPN used. In both cases, it can be noticed that the matrix biofilm formation was impaired in the first hours, as the light blue line is occupying less space in the graph compared to the control SCPN (Fig. 5A). However, the green line shown in Fig. 4A and B indicates that the biofilm treated with Tob-SCPN was first decreasing its total biomass, but after some hours there was an increase in cell numbers and extracellular matrix (observed after 6 and 12 hours, respectively). Thus, enough quantity of tobramycin was available to fight bacteria at the start of the experiment, but the quantity was not enough at long term, and the living biofilm cells start to grow and build up the biofilm and all the extracellular matrix again. Such results might indicate that repeated doses (every 6-8 hours) of Tob-SCPN will be required for an efficient biofilm removal and treatment.

On the other hand, the biofilm treated with the SCPN containing both tobramycin and DNase I undergo a progressive decrease in the extracellular matrix and a slight increase in the free bacterial cells (Fig. 4A and B, purple line). The tobramycin released from these SCPN seems to be effective in the first three hours of treatment when the cells biomass starts to decrease (Fig. 4B, purple line). Still, afterwards, there is a sudden increase in the bacterial cells, due to the delay effect of the DNase I, that starts to disperse the biofilm by breaking down the internal eDNA network and releasing the bacterial cells. If compared to the SCPN (Fig. 4B, black line), we can observe that the tobramycin inside the nanoparticles was actively killing the free cells, as the rise of the purple line is much less pronounced than the black line. However, the dose should be increased, or the concentration of tobramycin should be higher to avoid the spread of the biofilm [52].

To have an equivalent SCPN aggregate size, the same amount of the different SCPNs were added to the biofilm to perform the time-lapse. However, at the same nanoformulation weight, the Tob-SCPN has a higher concentration of antibiotic than Tob-DNase I-SCPN (Table 1). This higher tobramycin concentration elucidates the reason for the faster decrease of the biomass for Tob-SCPN in Fig. 4A, compared to Tob-DNase I-SCPN. Nevertheless, even the higher concentration of tobramycin, after 12 hours, the biofilm treated with Tob-SCPN suffered a regrowth of the biofilm. However, the biofilm treated with Tob-DNase I-SCPN continues decreasing with time. The treatment with enzymes that degrade and break down the biofilm matrix, together with antibiotics that destroy the bacterial cells liberated from the biofilm, has been extensively studied, not only with deoxyribonucleases but also with proteases and glycoside hydrolases, and allows the reduction of the

antibiotic dose necessary to eradicate the biofilm, reducing the chance of antibiotic resistance acquisition [53].

Tob-DNase I SCPN enhance the eDNA dispersion and the interaction and penetrability to the P. aeruginosa biofilm matrix

The produced SCPNs are too small to be monitored with a confocal microscope (due to technical limitations), so the time-lapse experiment was carried out with SCPN aggregates that have ~2 μm of diameter. Such aggregates are not representative of the SCPN behavior but allow to study the approach and interaction with the extracellular matrix. The grey numbers in Fig. 5 and the Fig. 4D illustrate the position of the nanoparticle aggregate in the matrix during the time. In all the cases, the nanoparticle aggregate was close to the biofilm surface, but in the Tob-SCPN and Tob-DNase I-SCPN (Fig.4D, green and purple lines, 5B and 5C), the nanoparticle aggregate moves 1 μm deeper inside the biofilm than the SCPN. These nanoparticles without tobramycin or DNase I are negatively charged and thus repelled by the highly negatively charged extracellular matrix (Fig. 4D, black line and 5A).

Tobramycin is a positively charged antibiotic that is sequestered in the biofilm periphery by ionic interactions [12]. The neutralization of these charges when formulated with a negatively charged SCPN, together with the DNase I released could boost this penetration inside the biofilms. Although the real penetration of non-aggregated SCPN inside the biofilm cannot be determined, some authors conclude that the nanoparticle size is the key factor for the diffusion inside the matrix [26]. It has been seen penetration of nanoparticles up to 70 nm, but the perfect size seems to be between 10 and 30 nm [54]. Since the dextran-based single-chain nanoparticles of this study have an average size of 20 nm (Table 1), they have the ideal size to penetrate inside the matrix.

Finally, the concentration of eDNA surrounding the nanoparticle aggregate was also calculated through time. It is completely removed in less than 3 hours in the biofilm treated with Tob-DNase I-SCPN (Fig. 4C, purple line), while in the biofilm treated with Tob-SCPN, the eDNA decreases progressively due to the matrix degradation (Fig. 4C, green line). On the contrary, as the biofilm treated with SCPN continues to grow and build the extracellular matrix, the eDNA keeps gradually increasing over time (Fig. 4C, black line).

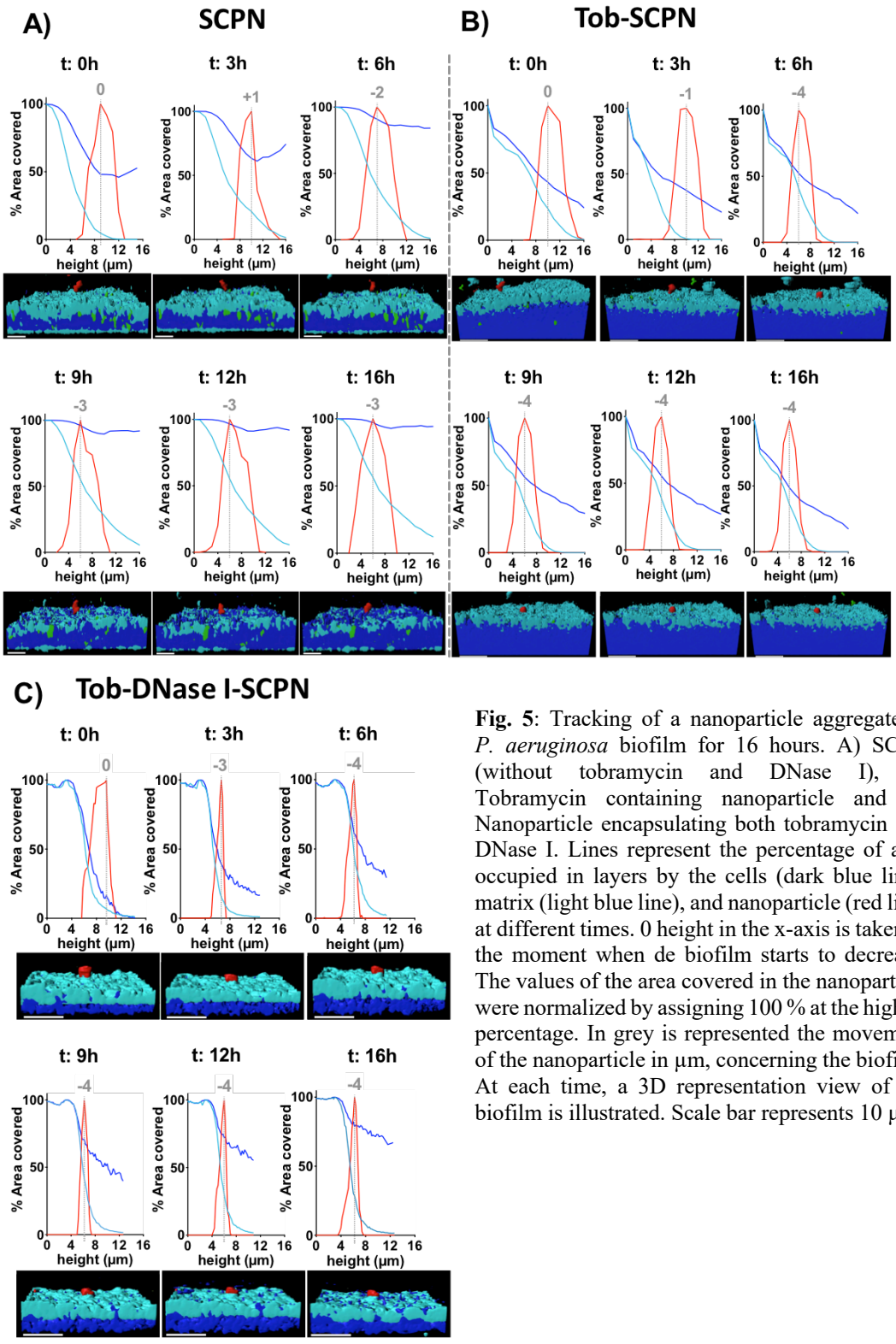

Fig. 5: Tracking of a nanoparticle aggregate in *P. aeruginosa* biofilm for 16 hours. A) SCPN (without tobramycin and DNase I), B) Tobramycin containing nanoparticle and C) Nanoparticle encapsulating both tobramycin and DNase I. Lines represent the percentage of area occupied in layers by the cells (dark blue line), matrix (light blue line), and nanoparticle (red line) at different times. 0 height in the x-axis is taken as the moment when de biofilm starts to decrease. The values of the area covered in the nanoparticle were normalized by assigning 100 % at the highest percentage. In grey is represented the movement of the nanoparticle in µm, concerning the biofilm. At each time, a 3D representation view of the biofilm is illustrated. Scale bar represents 10 µm.

Material and Methods

Materials

3-mercaptopropionic acid (≥99%), 4-(4,6-dimethoxy-1,3,5-triazin-2-yl)-4-methylmorpholinium chloride (DMTMM·HCl) (96%) and Rhodamine B (97%) were purchased from Aldrich. Phosphate-buffered saline (PBS) was purchased from Scharlau. 4-(Dimethylamino)pyridine (DMAP) and tobramycin (97%) were purchased from Acros-Organics. DNase I was purchased from Panreac, Applichem. Water (H_2O) used in the syntheses was deionized water from a MilliQ A10 Gradient equipment (Millipore).

SCPN: Dextran based single-chain polymer nanoparticles labelled with rhodamine

DXT-SCPN (100 mg, 222 μmol methacrylated glucose) were dispersed into PBS pH 7.4 at 10 mg/ml for 1h. Then, a mixture of DMTMM.Cl (4.6 mg, 16.7 μmol) and Rhodamine B (5.3 mg, 11 μmol) in PBS was added, and the reaction was stirred overnight at room temperature. The reaction was monitored by TLC in methanol to ensure the correct functionalization of the particles by rhodamine. The particles' methacrylate groups were functionalized by reaction with 3-mercaptopropionic acid (117 mg, 1.11 mmol) at pH 9 for 5 h. The crude was purified by dialysis (3.5 kDa MWCO RC membranes) against water. Water was refreshed twice a day until water conductivity reached values below 1 μS/cm. The final product was freeze-dried and kept at 4ºC until further analysis. Yield: 93 %. Glucose substitution degree DS = 45%. Crosslinking degree CL = 5%. Mw = 59 kDa. Rhodamine content: 18 μg/mg nanocarrier. Dh (DLS) = 19 ± 1 nm; PdI = 0.26 ± 0.04, Zeta-potential (pH = 7, 25 °C) = -21 ± 1 mV.

^{1}H NMR (500 MHz, D_2O) δ ppm: 8.55-6.74 (m, 0.3H, rhodamine H_{ar}), 5.54-4.86 (2.6H, including H-1 and H-2/3 substituted Glc), 4.25-3.33 (11.6H, m, rest of Glc and CH_2 Rhod), 1.28 (s, 3H, CH_3 Gluc and CH_3 rhod) (Fig. S4).

DNase I-SCPN

SCPN (10 mg, 0.2 μmol) and DNase I (11.3 mg, 0.4 μmol) were dispersed into water at 10 mg/ml at pH 7 and mixed for 1 h at room temperature. Sample was freeze-dried before further analysis. Dh (DLS) = 102 ± 2 nm; PdI = 0.52 ± 0.01, Zeta-potential (pH = 7, 25 °C) = -28 ± 1 mV. D (TEM, uranyl staining) = 20 ± 5 nm

Tob-SCPN

SCPN (6 mg, 0.1 μmol) and tobramycin (4 mg, 8.6 μmol) were respectively dispersed and dissolved into water at 10 mg/ml separately and pH was adjusted to 7. Then, both were mixed and stirred for 1 h at room temperature. The sample was freeze-dried and kept at 4ºC until further analysis. Dh (DLS) = 17 ± 1 nm; PdI = 0.27 ± 0.01, Zeta-potential (pH = 7, 25 °C) = -5 ± 2 mV. D (TEM, uranyl staining) = 37 ± 13 nm

Tob-DNase I-SCPN

Tob-SCPN (12.4 mg) and DNase I (11.2 mg) were dispersed into NaCl 1 mM at 10 mg/ml at pH 7 and gently mixed for 1h at RT. Dh (DLS) = 11 ± 1 nm; PdI = 0.27 ± 0.07, Zeta-potential (pH = 7, 25 °C) = -6 ± 1 mV. D (TEM, uranyl staining) = 37 ± 13 nm

Dynamic Light Scattering (DLS)

DLS analyses were conducted using a Zetasizer Nano ZS, ZEN3600 Model (Malvern Instruments Ltd). All measurements were performed in disposable sizing cuvettes at a laser wavelength of 633 nm and a scattering angle of 173°, while the zeta-potential measurements were performed in disposable zeta potential cells (pH 7.4, 25 °C). Before the measurement, the samples were dispersed in PBS solution for size measurements and 1 mM NaCl for zeta-potential measurements at a concentration of 10 mg/ml. Each measurement was repeated for thrice per sample at 25 °C.

Nuclear magnetic resonance (1H NMR)

NMR spectra were recorded on a Bruker AVANCE III spectrometer at 500 MHz and 25 °C. Chemical shifts (δ) are given in ppm relative to the residual signal of the solvent. Splitting patterns: b, broad; s, singlet; d, doublet; t, triplet; q, quartet; m, multiplet.

UV-vis

UV-vis measurements to determine rhodamine loading were carried out at 1 mg/ml in PBS using UV-2401PC UV-vis recording spectrophotometer from Shimadzu. Rhodamine content was calculated using a calibration curve of rhodamine in PBS.

Liquid Chromatography – Mass Spectroscopy (LC-MS)

LC-MS data were recorded using a UPLC Acquity instrument equipped with a Acquity C18 100*2.1mm*1.7µm coupled to a LCT Premier XT ESI-TOF mass spectrometer (source: electrospray positive mode/w mode m/z range 50-1000, capilar vol: 1000 / cone volt: 50) and analyzed using Masslynx 4.1 software from Waters. The mobile phases used were A: 0.1% HFBA in water and B: 0.1% HFBA in acetonitrile. Tobramycin elution was carried out as an isocratic of 95% A for 2 minutes and a gradient from 5% to 1% A in 15 minutes. Tobramycin was detected after 6.7 min elution (m/z = 468).

Transmission Electron Microscopy (TEM)

TEM analyses were performed in a TECNAI G2 20 TWIN microscope (FEI, Eindhoven, The Netherlands), operating at an accelerating voltage of 200 KeV in a bright-field image mode. One drop of the sample dispersion in water (~3 µL, 0.1 mg/mL) was deposited on a carbon film supported on a copper grid (300 mesh), hydrophilized by a glow discharge process just prior to use. After staining for 20 seconds with a uranyl acetate aqueous solution (1% w/v), the sample was dried at room temperature overnight. Number average diameter was calculated by ImageJ platform analysis using a Gaussian curve fitting after counting at least 300 nanoparticles.

Bacterial strains and growth conditions

Wild-type *Pseudomonas aeruginosa* PAO1 CECT 4122 (ATCC 15692) and *Staphylococcus aureus* CECT 86 (ATCC 12600) were obtained from the Spanish Type Culture Collection (CECT) and cultivated at 37 ºC in Luria-Bertani broth medium (LB) (Scharlab) or Tryptic Soy Broth (TSB) (Scharlab), respectively. The bacterial growth was measured by reading the Optical Density (O.D.) at 550 nm.

Antibacterial activity against planktonic bacteria

P. aeruginosa PAO1 and *S. aureus* were grown planktonically to initial exponential log phase ($O.D._{550\ nm} \approx 0.1$) and plated in a microtiter plate (Corning 3596 Polystyrene Flat Bottom 96 Well) supplemented with different SCPN and antibiotic concentrations following the Clinical Laboratory Standards Institute (CLSI) guidelines [55]. As previously described [56], the microtiter plate was incubated at 37 ºC in a SPARK Multimode microplate reader (Tecan) with a 150 rpm shaking. The bacterial growth was monitored for 8 hours by reading the $O.D._{550\ nm}$ every 15 minutes.

DNase I activity testing

DNase I-SCPN and a known concentration of DNase I (Panreac Applichem, ref A3778) were incubated with 100 ng of *P. aeruginosa* genomic DNA for 30 minutes at 37 ºC. Samples were then loaded into a 0.8 % agarose gel plus ethidium bromide (0.25 µg/ml) and visualized under U.V. light in a Gel Doc™ XR+ (Bio-Rad Laboratories). DNase I activity was estimated with the DNA degradation quantification performed with the software Quantity One (Bio-Rad Laboratories).

Antibacterial activity against continuous-flow biofilms

Continuous biofilms were grown using a Flow-Cell system, as previously reported [56, 57]. *P. aeruginosa* biofilms were grown with LB medium, and *S. aureus* biofilms were grown with 2% TSB medium. In both cases, 0.2 % glucose was added to the medium to stimulate biofilm formation. Before the inoculation of *S. aureus*, the flow cells (DTU Systems Biology) were coated with 20% of bovine plasma (Biowest) overnight. These flow cells were inoculated with 350 µl of *P. aeruginosa* PAO1 or *S. aureus* at $O.D._{550\ nm} \approx 0.1$. After allowing the bacteria to attach for 2 hours, the specific medium for each bacterium was pumped through the system at 42 µl/min employing an Ismatec ISM 943 peristaltic pump (Ismatec). Bubble traps (DTU Systems Biology) were placed in the system to avoid biofilm disturbances. Biofilms were grown for 3 days (72 hours) at room temperature, and then the treatment (0.26 µg/ml of DNase I, 2 µg/ml of tobramycin or the same concentration inside the nanoformulation) was injected into the mature biofilms. After 16 hours of treatment, biofilms were stained with SYTO9 and propidium iodide (Live/Dead BacLight Bacterial Viability Kit, Thermo Fisher Scientific) following manufacturer instructions and visualized using a Zeiss LSM 800 confocal laser scanning microscope (CLSM) with the 20 X/0.8 air objective. Biomass and thickness quantification of the images obtained was performed using FIJI and COMSTAT2 software [58].

Time-lapse experiments

P. aeruginosa PAO1 continuous biofilms were grown in the flow-cell chambers as previously explained. To perform the time-lapse images, a concentration of 100 µg/ml of nanoparticles were injected into the mature-grown *P. aeruginosa* PAO1 biofilms (72 hours old) with specific biofilm staining: DAPI at 300 nM (Life Technologies) for the intracellular DNA (biomass), TOTO™-1 Iodide at 1 µM (Thermofisher) to stain the extracellular DNA, and Concanavalin A AlexaFluor™ 647 conjugate at 100 mg/ml (Life Technologies) to dye the extracellular matrix of the biofilm (alginate). Microscopic images were taken approximately every 3 hours with the 63X/1.4 oil objective mounted in a Zeiss LSM 800 CLSM, using the multi-position Time Series module of the ZEN software and the Definite Focus.2 system implemented in our confocal microscope (Zeiss).

Analysis of matrix, cells, extracellular DNA, and nanoparticle variation was made by creating a specific ROI (region of interest) of 13x13 μm around the nanoparticle and quantifying the biomass and area occupied by layers using FIJI and COMSTAT2 software. 3D representation was created using IMARIS software (Bitplane AG).

Acknowledgements

This study was partially supported by grants from the Ministerio de Economía, Industria y Competitividad, MINECO, and Agencia Estatal de Investigación (AEI), Spain, co-funded by Fondo Europeo de Desarrollo Regional, FEDER, European Union (RTI2018-098573-B-100), the CERCA programme and AGAUR-Generalitat de Catalunya (2017SGR-1079), the European Regional Development Fund (FEDER), Catalan Cystic Fibrosis association and Obra Social "La Caixa".

CIDETEC kindly acknowledged the Basque Government for funding this work (ELKARTEK/BMG19 ref KK-2019/00015, ELKARTEK/BMG18 ref KK-2018/00038).

Bibliography

1. **Wolfmeier, H., et al.,** *New Perspectives in Biofilm Eradication.* ACS Infect Dis, 2018. 4(2): p. 93-106.
2. **Flemming, H.C. and J. Wingender,** *The biofilm matrix.* Nat Rev Microbiol, 2010. 8(9): p. 623-33.
3. **Ciofu, O., C.R. Hansen, and N. Høiby,** *Respiratory bacterial infections in cystic fibrosis.* Curr Opin Pulm Med, 2013. 19(3): p. 251-8.
4. **Cendra, M.D.M., et al.,** *Optimal environmental and culture conditions allow the in vitro coexistence of Pseudomonas aeruginosa and Staphylococcus aureus in stable biofilms.* Sci Rep, 2019. 9(1): p. 16284.
5. **Okshevsky, M. and R.L. Meyer,** *The role of extracellular DNA in the establishment, maintenance and perpetuation of bacterial biofilms.* Crit Rev Microbiol, 2015. 41(3): p. 341-52.
6. **Boles, B.R. and A.R. Horswill,** *Staphylococcal biofilm disassembly.* Trends Microbiol, 2011. 19(9): p. 449-55.
7. **Whitchurch, C.B., et al.,** *Extracellular DNA required for bacterial biofilm formation.* Science, 2002. 295(5559): p. 1487.
8. **Shire, S.J.**, *Stability Characterization and Formulation Development of Recombinant Human Deoxyribonuclease I [Pulmozyme®, (Dornase Alpha)]*, in *Formulation, Characterization, and Stability of Protein Drugs: Case Histories: Case Histories*, R. Pearlman and Y.J. Wang, Editors. 2002, Springer US: Boston, MA. p. 393-426.
9. **Folkesson, A., et al.,** *Adaptation of Pseudomonas aeruginosa to the cystic fibrosis airway: an evolutionary perspective.* Nat Rev Microbiol, 2012. 10(12): p. 841-51.
10. **Gordon, V., L. Bakhtiari, and K. Kovach,** *From molecules to multispecies ecosystems: the roles of structure in bacterial biofilms.* Phys Biol, 2019. 16(4): p. 041001.
11. **Chiang, W.C., et al.,** *Extracellular DNA shields against aminoglycosides in Pseudomonas aeruginosa biofilms.* Antimicrob Agents Chemother, 2013. 57(5): p. 2352-61.
12. **Tseng, B.S., et al.,** *The extracellular matrix protects Pseudomonas aeruginosa biofilms by limiting the penetration of tobramycin.* Environ Microbiol, 2013. 15(10): p. 2865-78.
13. **Deacon, J., et al.,** *Antimicrobial efficacy of tobramycin polymeric nanoparticles for Pseudomonas aeruginosa infections in cystic fibrosis: formulation, characterisation and functionalisation with dornase alfa (DNase).* J Control Release, 2015. 198: p. 55-61.
14. **Lim, Y.H., et al.,** *Polymeric nanoparticles in development for treatment of pulmonary infectious diseases.* Wiley Interdiscip Rev Nanomed Nanobiotechnol, 2016. 8(6): p. 842-871.
15. **Yhee, J.Y., J. Im, and R.S. Nho,** *Advanced Therapeutic Strategies for Chronic Lung Disease Using Nanoparticle-Based Drug Delivery.* J Clin Med, 2016. 5(9).
16. **Han, C., et al.,** *Recent developments in the use of nanoparticles for treatment of biofilms.* Nanotechnology Reviews, 2017. 6(5): p. 383-404.
17. **Zhang, J., et al.,** *Amikacin Liposome Inhalation Suspension (ALIS) Penetrates Non-tuberculous Mycobacterial Biofilms and Enhances Amikacin Uptake Into Macrophages.* Front Microbiol, 2018. 9: p. 915.
18. **Riehemann, K., et al.,** *Nanomedicine--challenge and perspectives.* Angew Chem Int Ed Engl, 2009. 48(5): p. 872-97.
19. **Chen, E.Y., et al.,** *Functionalized positive nanoparticles reduce mucin swelling and dispersion.* PLoS One, 2010. 5(11): p. e15434.
20. **Forier, K., et al.,** *Transport of nanoparticles in cystic fibrosis sputum and bacterial biofilms by single-particle tracking microscopy.* Nanomedicine (Lond), 2013. 8(6): p. 935-49.

21. **Dawson, M., D. Wirtz, and J. Hanes,** *Enhanced viscoelasticity of human cystic fibrotic sputum correlates with increasing microheterogeneity in particle transport.* J Biol Chem, 2003. 278(50): p. 50393-401.
22. **Sanders, N.N., et al.,** *Cystic fibrosis sputum: a barrier to the transport of nanospheres.* Am J Respir Crit Care Med, 2000. 162(5): p. 1905-11.
23. **Meers, P., et al.,** *Biofilm penetration, triggered release and in vivo activity of inhaled liposomal amikacin in chronic Pseudomonas aeruginosa lung infections.* J Antimicrob Chemother, 2008. 61(4): p. 859-68.
24. **Messiaen, A.S., et al.,** *Transport of nanoparticles and tobramycin-loaded liposomes in Burkholderia cepacia complex biofilms.* PLoS One, 2013. 8(11): p. e79220.
25. **Baelo, A., et al.,** *Disassembling bacterial extracellular matrix with DNase-coated nanoparticles to enhance antibiotic delivery in biofilm infections.* J Control Release, 2015. 209: p. 150-8.
26. **Wan, F., et al.,** *Ultrasmall TPGS-PLGA Hybrid Nanoparticles for Site-Specific Delivery of Antibiotics into Pseudomonas aeruginosa Biofilms in Lungs.* ACS Appl Mater Interfaces, 2020. 12(1): p. 380-389.
27. **Falciani, C., et al.,** *Antimicrobial Peptide-Loaded Nanoparticles as Inhalation Therapy for Pseudomonas aeruginosa Infections.* Int J Nanomedicine, 2020. 15: p. 1117-1128.
28. **Pomposo, J.A.,** *Single-Chain Polymer Nanoparticles: Synthesis, Characterization, Simulations, and Applications*. Single-Chain Polymer Nanoparticles, ed. J.A. Pomposo. 2017.
29. **Kroger, A.P.P. and J.M.J. Paulusse,** *Single-chain polymer nanoparticles in controlled drug delivery and targeted imaging.* J Control Release, 2018. 286: p. 326-347.
30. **Mavila, S., et al.,** *Intramolecular Cross-Linking Methodologies for the Synthesis of Polymer Nanoparticles.* Chem Rev, 2016. 116(3): p. 878-961.
31. **Hanlon, A.M., C.K. Lyon, and E.B. Berda,** *What Is Next in Single-Chain Nanoparticles?* Macromolecules, 2016. 49(1): p. 2-14.
32. **Pomposo, J.A.,** *Bioinspired single-chain polymer nanoparticles.* 2014. 63(4): p. 589-592.
33. **Gracia, R., et al.,** *Biocompatible single-chain polymer nanoparticles loaded with an antigen mimetic as potential anticancer vaccine.* ACS Macro Letters, 2018. 7(2): p. 196-200.
34. **Gracia, R., et al.,** *Synthesis and functionalization of dextran-based single-chain nanoparticles in aqueous media.* J Mater Chem B, 2017. 5(6): p. 1143-1147.
35. **van der Weide, H., et al.,** *Therapeutic Efficacy of Novel Antimicrobial Peptide AA139-Nanomedicines in a Multidrug-Resistant Klebsiella pneumoniae Pneumonia-Septicemia Model in Rats.* Antimicrob Agents Chemother, 2020. 64(9).
36. **Ritter, D., et al.,** *In vitro inhalation cytotoxicity testing of therapeutic nanosystems for pulmonary infection.* Toxicol In Vitro, 2020. 63: p. 104714.
37. **Walter, F., Q. Vicens, and E. Westhof,** *Aminoglycoside-RNA interactions.* Curr Opin Chem Biol, 1999. 3(6): p. 694-704.
38. **Lira, A.L., et al.,** *Allosteric inhibition of alpha-thrombin enzymatic activity with ultrasmall gold nanoparticles.* Nanoscale Adv, 2019. 1(1): p. 378-388.
39. **Sizochenko, N., D. Leszczynska, and J. Leszczynski,** *Modeling of Interactions between the Zebrafish Hatching Enzyme ZHE1 and A Series of Metal Oxide Nanoparticles: Nano-QSAR and Causal Analysis of Inactivation Mechanisms.* Nanomaterials (Basel), 2017. 7(10).
40. **Mann, E.E., et al.,** *Modulation of eDNA release and degradation affects Staphylococcus aureus biofilm maturation.* PLoS One, 2009. 4(6): p. e5822.
41. **Okshevsky, M., V.R. Regina, and R.L. Meyer,** *Extracellular DNA as a target for biofilm control.* Curr Opin Biotechnol, 2015. 33: p. 73-80.
42. **Dengler, V., et al.,** *An Electrostatic Net Model for the Role of Extracellular DNA in Biofilm Formation by Staphylococcus aureus.* J Bacteriol, 2015. 197(24): p. 3779-87.

43. **d'Angelo, I., et al.,** *Overcoming barriers in Pseudomonas aeruginosa lung infections: Engineered nanoparticles for local delivery of a cationic antimicrobial peptide.* Colloids Surf B Biointerfaces, 2015. 135: p. 717-725.
44. **Pompilio, A., et al.,** *Electrochemically Synthesized Silver Nanoparticles Are Active Against Planktonic and Biofilm Cells of Pseudomonas aeruginosa and Other Cystic Fibrosis-Associated Bacterial Pathogens.* Front Microbiol, 2018. 9: p. 1349.
45. **Patel, K.K., et al.,** *Alginate lyase immobilized chitosan nanoparticles of ciprofloxacin for the improved antimicrobial activity against the biofilm associated mucoid P. aeruginosa infection in cystic fibrosis.* Int J Pharm, 2019. 563: p. 30-42.
46. **Al-Obaidi, H., R. Kalgudi, and M.G. Zariwala,** *Fabrication of inhaled hybrid silver/ciprofloxacin nanoparticles with synergetic effect against Pseudomonas aeruginosa.* Eur J Pharm Biopharm, 2018. 128: p. 27-35.
47. **Al-Nemrawi, N.K., et al.,** *Low Molecular Weight Chitosan-Coated PLGA Nanoparticles for Pulmonary Delivery of Tobramycin for Cystic Fibrosis.* Pharmaceuticals (Basel), 2018. 11(1).
48. **Gao, Y., et al.,** *Size and Charge Adaptive Clustered Nanoparticles Targeting the Biofilm Microenvironment for Chronic Lung Infection Management.* ACS Nano, 2020. 14(5): p. 5686-5699.
49. **Ho, D.K., et al.,** *Squalenyl Hydrogen Sulfate Nanoparticles for Simultaneous Delivery of Tobramycin and an Alkylquinolone Quorum Sensing Inhibitor Enable the Eradication of P. aeruginosa Biofilm Infections.* Angew Chem Int Ed Engl, 2020. 59(26): p. 10292-10296.
50. **Ernst, J., et al.,** *Polyester-based particles to overcome the obstacles of mucus and biofilms in the lung for tobramycin application under static and dynamic fluidic conditions.* Eur J Pharm Biopharm, 2018. 131: p. 120-129.
51. **Macia, M.D., E. Rojo-Molinero, and A. Oliver,** *Antimicrobial susceptibility testing in biofilm-growing bacteria.* Clin Microbiol Infect, 2014. 20(10): p. 981-90.
52. **Fleming, D. and K. Rumbaugh,** *The Consequences of Biofilm Dispersal on the Host.* Sci Rep, 2018. 8(1): p. 10738.
53. **Fleming, D. and K.P. Rumbaugh,** *Approaches to Dispersing Medical Biofilms.* Microorganisms, 2017. 5(2).
54. **Miller, K.P., et al.,** *Inorganic nanoparticles engineered to attack bacteria.* Chem Soc Rev, 2015. 44(21): p. 7787-807.
55. **CLSI**, *Methods for Dilution Antimicrobial Susceptibility Tests for Bacteria That Grow Aerobically*, in *CLSI standard M07*. 2018, Clinical and Laboratory Standards Institute: Wayne, PA.
56. **Blanco-Cabra, N., et al.,** *Novel Oleanolic and Maslinic Acid Derivatives as a Promising Treatment against Bacterial Biofilm in Nosocomial Infections: An in Vitro and in Vivo Study.* ACS Infect Dis, 2019. 5(9): p. 1581-1589.
57. **Blanco-Cabra, N., et al.,** *Characterization of different alginate lyases for dissolving Pseudomonas aeruginosa biofilms.* Sci Rep, 2020. 10(1): p. 9390.
58. **Heydorn, A., et al.,** *Quantification of biofilm structures by the novel computer program comstat.* Microbiology, 2000. 146(10): p. 2395-2407.

SUPPLEMENTARY MATERIAL

Fig. S1: Functionalization of DXT-SCPN with Rhodamine and 3-mercaptopropionic acid (MPA).

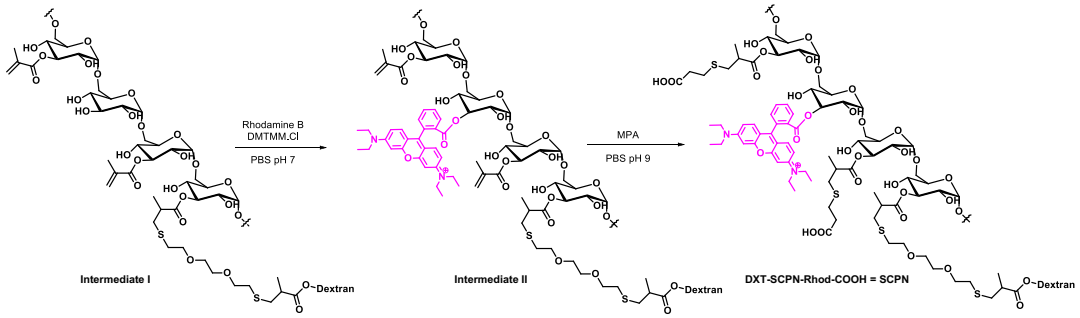

Fig. S2: ^{1}H NMR spectrum of rhodamine-labelled SCPN in D_2O

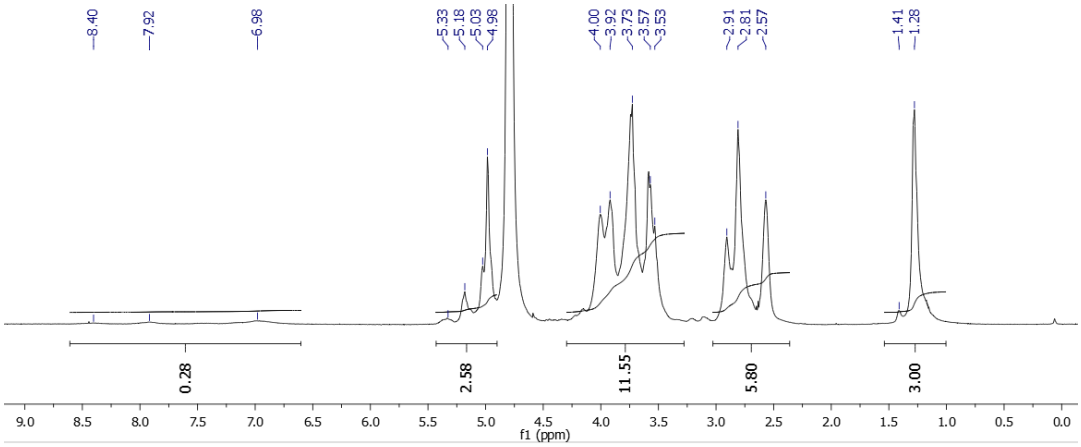

Fig. S3: UV-vis Rodamine calibration curve in PBS.

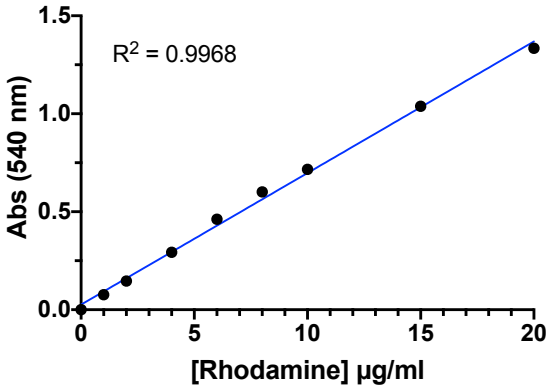

Fig. S4: ^{1}H NMR spectra of SCPN, DNase I-SCPN, Tob-SCPN, Tob-DNase I-SCPN, DNase I, and Tobramycin in D_2O.

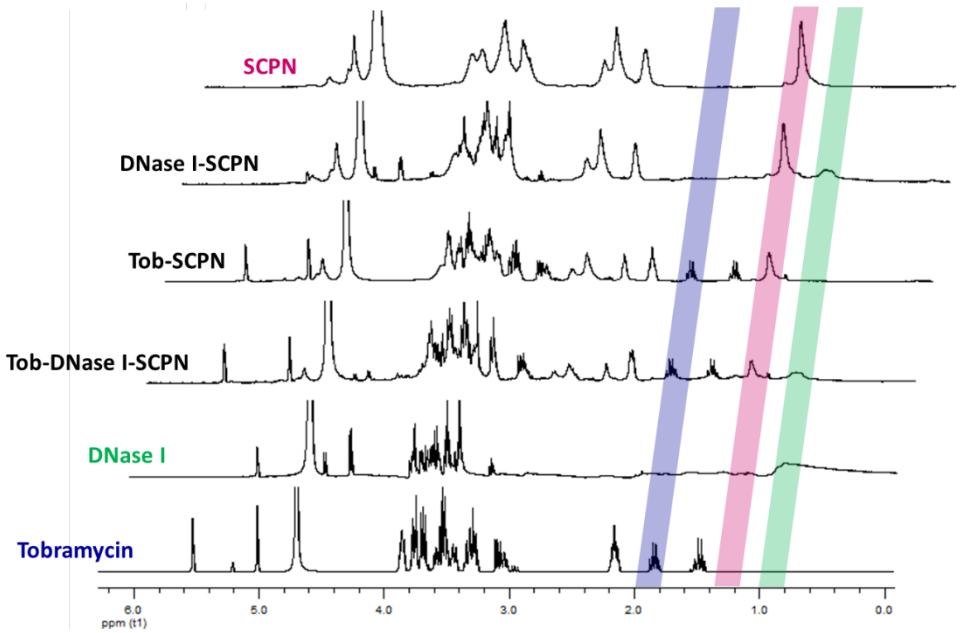

Fig. S5: Videos of the biofilm time-lapse can be found at: bit.ly/figureS5

- A: Example of an SCPN aggregate dissolved during the time-lapse
- B: SCPN
- C: Tob-SCPN
- D: Tob-DNase I-SCPN

RESUM GLOBAL DELS RESULTATS

1. Determinar l'activitat antimicrobiana i antibiofilm de noves molècules.

Els resultats corresponents a aquest primer objectiu s'exposen als articles ja publicats 1 i 2. En aquests treballs, s'analitza l'activitat antimicrobiana i antibiofilm de dos tipus de molècules, diferents entre elles, que han sigut modificades per tal de millorar el seu potencial com a fàrmacs antimicrobians. En ambdós casos també s'analitza la seva toxicitat i el possible mecanisme d'acció.

En el primer treball, titulat ***"Pentafluorosulfanyl-containing Triclocarban Analogs with Potent Antimicrobial Activity"***, s'analitzen els derivats de la molècula del triclocarban (TCC) obtinguts al laboratori de química farmacèutica de la facultat de Farmàcia de la UB, liderat pel Dr. Santiago Vázquez. El triclocarban és una urea molt utilitzada en la producció de sabons antimicrobians que conté en la seva estructura tres àtoms de clor [180]. En el treball presentat s'analitzen catorze compostos resultants de modificar la molècula del TCC reduint la quantitat d'àtoms de clor, per tal de disminuir la seva toxicitat i incrementar l'activitat antimicrobiana (Figura 2 de l'article 1).

Primerament, es va analitzar l'activitat antimicrobiana dels compostos en cultius planctònics, tant en bacteris Gram-positius (*S. aureus*, *S. aureus* MRSA, *S. epidermidis*, *S. mutants* i *E. faecalis*) com en Gram-negatius (*E. coli* i *P. aeruginosa*). Es va calcular la concentració de compost necessària per a inhibir el 50 % del creixement (*minimum inhibitory concentration*, MIC_{50}) (Taula 1 de l'article 1). Tal i com succeeix amb la molècula TCC, que només és activa amb bacteris del gènere *Staphylococcus,* cap dels catorze compostos derivats va mostrar activitat antimicrobiana contra els bacteris Gram-negatius analitzats, però sí contra els Gram-positius. La majoria dels derivats, a més de tenir efecte en la viabilitat dels bacteris del gènere *Staphylococcus*, amplien l'espectre d'acció i també tenen activitat contra altres Gram-positius com *S. mutants* i *E. faecalis.* D'aquesta anàlisi d'activitat en creixement planctònic, cal destacar dos compostos derivats que milloren l'activitat contra els *S. aureus* i *S. aureus* resistent a meticil·lina (MRSA); el compost núm. 12, que millora quasi dues vegades l'activitat en la soca MRSA i el compost núm. 10, que millora deu vegades l'activitat en les dues soques de *S. aureus* respecte a la molècula de TCC sense modificar.

També es va avaluar la toxicitat d'aquests compostos en cèl·lules eucariotes (macròfags murins J-774A.1), calculant la dosi necessària per a eliminar el 50 % de la població de cèl·lules (*citotoxic concentration*, CC_{50}). Amb la MIC i la CC es van poder determinar els seus índexs de selectivitat

(*selectivity index*, SI). Aquest índex es calcula dividint la CC entre la MIC i per tant mesura el marge de seguretat del fàrmac, com més alt és el SI, menys risc de patir intoxicació amb la dosi terapèutica. Moltes de les molècules derivades del TCC van presentar l'índex de selectivitat millor que el del TCC, ja sigui perquè la toxicitat dels derivats és menor (compostos núm. 3, 4, 11 i 13) o perquè, a més, també és menor la MIC (compostos núm. 10 i 12) (Taula 1 de l'article 1).

Posteriorment, es van fer dos assajos per veure de quina manera afecten els compostos a la viabilitat dels bacteris i intentar entendre els seus mecanismes d'acció, un assaig amb la tinció "*Live/Dead*" i una tinció específica de membrana. La tinció "*Live/Dead*" consta de dos colorants que tenyeixen el DNA, un que és capaç de travessar les membranes de les cèl·lules vives i les tenyeix de color verd i l'altre que només travessa les membranes molt danyades (de les cèl·lules mortes o molt perjudicades) i tenyeix les cèl·lules de vermell. D'aquesta manera, els bacteris vius es veuen de color verd i els morts de color vermell. En realitzar aquesta tinció després de tractar un cultiu de *S. aureus* durant quatre hores amb els compostos més actius, es va comprovar que el nombre total de cèl·lules disminuïa molt, i que la proporció de cèl·lules mortes o no viables (tenyides de vermell) augmentava, particularment en els compostos núm. 3, 5, 6 i 12 (Figura 3A de l'article 1). Per altra banda, la tinció de membrana es va realitzar després de deu minuts de tractament amb els compostos, per tal de poder veure si aquests afecten la membrana cel·lular de *S. aureus*. En la Figura 3B de l'article 1 es pot veure clarament com les membranes dels bacteris tractats estan afectades, ja que hi ha acumulació del colorant en certes zones on hi ha desestructuració de la membrana.

Com que el compost TCC es fa servir com a desinfectant [180], es va provar la capacitat dels compostos derivats de desinfectar superfícies contaminades. Per aquest motiu es va infectar una superfície amb *S. aureus* i es va rentar amb els compostos. En aquest cas, es va demostrar que el compost núm. 9 té la mateixa potència com a desinfectant que el TCC, i que els compostos núm. 10, 12 i 13, a més de tenir també el mateix poder desinfectant, són menys tòxics que el TCC. (Figura 4A de l'article 1, Taula 1 de l'article 1).

Una altra de les comprovacions d'aquest treball va ser veure si aquests compostos, a més de ser efectius per a erradicar *S. aureus* en creixement planctònic, també són efectius erradicant bacteris creixents en forma de biofilm. Per aquest motiu, es va fer un model de catèter contaminat amb un biofilm i es va tractar amb alguns dels compostos. Es va corroborar així que els compostos núm. 10 i 12 tenen la mateixa capacitat d'eliminar el biofilm del catèter que el TCC, presentant, a més, menor toxicitat que aquest (Figura 4B de l'article 1).

Per últim, es va realitzar un assaig per tal de saber la taxa de mutació espontània que provoca resistència en aquests nous compostos, ja que és important per a nous antimicrobians que no permetin l'adquisició de resistències en bacteris. Després de sembrar un cultiu de *S. aureus* en plaques d'agar que contenien els compostos, es va veure que el compost núm. 12 té una taxa de mutació similar a la del TCC, i que els compostos núm. 3, 9, 10 i 13 no indueixen mutació espontània en *S. aureus* (Taula 2 de l'article 1), la qual cosa els postula com a bons possibles antimicrobians.

En el segon treball presentat, titulat "***Novel Oleanolic and Maslinic Acid Derivatives as a Promising Treatment against Bacterial Biofilm in Nosocomial Infections: An in vitro and in vivo Study***", s'analitzen unes amines derivades de l'àcid oleanòlic (*oleanolic acid*, OA) i l'àcid maslínic (*maslinic acid*, MA) sintetitzades al grup de "Química Organometálica y Electrónica Molecular" de la Universidad de Granada (UGR). Aquests àcids són uns triterpens pentacíclics amb reconegudes propietats antimicrobianes [181, 182]. En aquest segon treball presentat s'analitza l'activitat antimicrobiana *in vitro* i *in vivo* de catorze compostos sintetitzats a la UGR afegint diferents diamines a l'OA i a l'MA (Esquema 1 de l'article 2).

En primer lloc, igual que amb els compostos derivats del TCC, es va estudiar la concentració necessària per a inhibir el creixement planctònic bacterià en 50% (MIC_{50}) en diferents bacteris Gram-positius i Gram-negatius. Amb aquest experiment es va esbrinar que els derivats mantenen i, en alguns casos milloren l'activitat dels terpens originals, ja que l'OA i l'MA són actius contra el bacteri *S. aureus*, però tenen molt poca activitat contra la soca multiresistent MRSA. En concret, quatre de les catorze amines derivades, l'MA-HDA, l'OA-HDA, l'MA-DAD i l'OA-DAD disminueixen la MIC contra MRSA en un 66%, 87%, 66% i 60% respectivament. En cap dels casos, però, hi ha activitat contra els bacteris Gram-negatius investigats (*E. coli* i *P. aeruginosa*) (Taula 1 de l'article 2).

En aquest treball, la toxicitat es va assajar no només en cèl·lules epitelials pulmonars A549 (*in vitro*), sinó també *in vivo* (en larves de *Galleria mellonella*), i es va calcular la dosi necessària per a eliminar el 50 % de la població de cèl·lules o larves (CC_{50}, *citotòxic concentration* o LD_{50} *lethal dose*). Amb aquesta anàlisi es va demostrar que els derivats són menys tòxics que els compostos parentals, cosa que fa augmentar l'índex de selectivitat (increment de fins a 5 vegades en el derivat OA-HDA) (Taula 1 de l'article 2).

En aquestes amines derivades de l'OA i l'MA també es va visualitzar al microscopi l'efecte que provoquen en els bacteris. Igual que en els derivats del TCC, en l'assaig "*Live/Dead*" després de

quatre hores de tractament es va veure una disminució de cèl·lules viables de *S. aureus* en els compostos més actius (Figura 2A de l'article 2). La tinció de membrana i l'anàlisi amb el microscopi electrònic de rastreig (SEM) també van confirmar que la membrana està afectada en les cèl·lules de *S. aureus* tractades amb aquests compostos (Figura 2B i 2C de l'article 2).

L'eficàcia antibiofilm d'aquestes amines també es va examinar amb dos mètodes, en un sistema estàtic que mimetitza la formació de biofilm en els catèters infectats i en un sistema de biofilm en continu. En el primer sistema es va comprovar que l'MA-HDA i l'OA-HDA erradiquen més del 99% el biofilm de *S. aureus* preformat en catèters (Figura 3 de l'article 2) i, en el segon sistema, els mateixos compostos derivats MA-HDA i OA-HDA van ser capaços d'eliminar el 30 i el 45 % respectivament del biofilm en continu (Figura 4 de l'article 2). En els dos tipus de biofilm aquests derivats van ser més eficaços que els compostos parentals MA i OA.

Per últim, es va estudiar l'eficàcia d'aquests compostos en el tractament d'infeccions *in vivo*, amb el model animal de *Galleria mellonella*. Les larves d'aquest insecte es van infectar amb *S. aureus* i posteriorment es van tractar amb dues dosis dels compostos. Aquest tractament va permetre la recuperació del 50 % de la població de larves tractades amb el compost parental MA i també amb l'amina derivada MA-HDA (Figura 1 de l'article 2).

2. Desenvolupar una tecnologia que permeti determinar la sensibilitat antibiòtica dels biofilms amb precisió.

Els resultats corresponents a aquest segon objectiu s'exposen a l'article 3. En aquest treball, titulat "**A new BiofilmChip device as a personalized solution for testing biofilm antibiotic resistance**" es desenvolupa el dispositiu "BiofilmChip", que és una estructura microfluídica que possibilita el creixement de biofilms de manera senzilla i l'anàlisi de la seva sensibilitat antibiòtica sense necessitar l'ús del microscopi confocal ni de personal altament qualificat en altres tecnologies presents en els laboratoris de recerca.

Aquest dispositiu s'ha dissenyat en col·laboració amb el grup de "Nanobioenginyeria" de l'Institut de Bioenginyeria de Catalunya (IBEC). Consta d'una carcassa de la silicona polidimetilsiloxà (PDMS) amb un cobreobjectes de vidre adherit. El PDMS té unes concavitats que, segellades amb el cobreobjectes, constitueixen les cambres on creixerà el biofilm i uns orificis per connectar els tubs

que permetran que el medi circuli a través d'aquestes cambres (Figura 1a, b i c de l'article 3). Un conjunt de tubs connecta tot el sistema hermèticament i el medi de cultiu circula des de l'ampolla de reservori a l'ampolla de residus, passant per les cambres a on hi ha el biofilm, gràcies a una bomba peristàltica que l'arrossega a una velocitat determinada i constant. Per tal de minimitzar l'aparició de bombolles que podrien irrompre el biofilm, abans de passar per les cambres, el medi travessa unes trampes de bombolles (Figura 1c de l'article 3).

El primer pas per al disseny d'aquest dispositiu va ser determinar els millors paràmetres per a la correcta formació del biofilm. Així, es van arribar a crear cinc prototips diferents, millorant les mides i formes de les cambres fins a aconseguir un creixement homogeni del biofilm i un baix percentatge de mort cel·lular en visualitzar-lo al microscopi confocal (Figura 2 de l'article 3). El prototip final inclou diferents conjunts de tres cambres amb una pre-cambra, que controla les variacions de flux dins de cada cambra. D'aquesta manera, s'ha demostrat que el creixement de biofilm és homogeni dins de la cambra, entre les diferents cambres del conjunt i entre els diferents conjunts de cambres, la qual cosa dóna robustesa per a la seva utilització (Figura 3a, b i c de l'article 3). També s'ha detectat que el BiofilmChip possibilita la detecció de canvis en la biomassa del biofilm quan s'hi aplica un tractament antibiòtic, permetent el seu ús com a eina diagnòstica (Figura 3d de l'article 3).

Per altra banda, el BiofilmChip ha permès fer créixer biofilms de soques clíniques (Figura 3c de l'article 3) i biofilms a partir d'aïllats clínics d'esputs de pacients amb infecció crònica pulmonar. A més, els biofilms creats a partir d'aquests esputs són polimicrobians, ja que mitjançant microscòpia confocal s'ha pogut visualitzar diferents espècies dins del mateix biofilm (Figura 4 de l'article 3).

Un cop comprovat, amb el microscopi confocal, el correcte funcionament del BiofilmChip, l'últim pas va ser afegir un sistema que permetés monitoritzar el creixement de biofilms sense l'ús de cap eina microscòpica. Per aquest motiu, en col·laboració amb el grup de "Nanobioenginyeria" de l'IBEC, es van incorporar uns elèctrodes interdigitats d'or a la zona del cobreobjectes on hi ha el creixement del biofilm (Figura 3a i b de l'article 3). Aquests elèctrodes possibiliten la monitorització del creixement i tractament del biofilm utilitzant mesures d'impedància electrònica. L'eficàcia d'aquest sistema es va comprovar monitoritzant el creixement i el tractament d'un biofilm de *P. aeruginosa* fluorescent (que expressa una proteïna fluorescent verda (*GFP, green fluorescent protein*)). L'anàlisi es va dur a terme simultàniament amb el microscopi confocal i amb les mesures d'impedància. Aquesta anàlisi ha evidenciat que la mesura de la impedància té la mateixa resposta que les mesures de biomassa quantificades amb el microscopi confocal. A més, aquestes mesures es correlacionen

quan es tracten els biofilms amb diferents concentracions d'antibiòtic. En estadis primerencs del biofilm, la mesura del creixement amb la impedància és molt més acurada que amb la biomassa calculada mitjançant el microscopi confocal (Figura 5 de l'article 3).

3. Desenvolupar noves tecnologies pel tractament de biofilms amb enzims disgregadors del biofilm.

Els resultats corresponents al tercer objectiu s'exposen en els articles 4 i 5.

En el quart treball, titulat *"**Characterization of different alginate lyases for dissolving Pseudomonas aeruginosa biofilms**"* s'analitza l'activitat disgregadora de biofilm de cinc alginat liases caracteritzades al laboratori del grup "Design of Biological Systems" del Centre de Recerca Genòmica (CRG). Les alginat liases són uns enzims que degraden l'alginat i que es classifiquen en set famílies PL, segons la seva estructura. Aquests enzims poden tenir diferent especificitat pels polímers que formen l'alginat (PolyM i PolyG) [183].

En aquest treball, s'analitza l'activitat de cinc alginat liases (Alg2A, AlyA1, A1-II, A1-II' i A1-III) pertanyents a dues famílies diferents (PL-5 i PL-7) i amb diferent especificitat pel substrat. Dues d'aquestes alginat liases (Alg2A i AlyA1) pertanyen a la família PL-7 i es van purificar a partir d'un extracte cru comercial (A1603 de Sigma). L'origen d'aquestes alginases són els bacteris *Flavobacterium multivorum* i *Zobellia galactanivorans* respectivament. Les altres alginat liases (A1-II, A1-II' i A1-III) provenen de la soca A1 del bacteri *Sphingomonas sp.* Les dues primeres també pertanyen a la família PL-7 i l'A1-III pertany a la PL-5. D'entre les cinc alginat liases analitzades, només una té especificitat per substrat PolyM (A1-III), dues per substrat PolyG (AlyA1 i A1-II) i dues degraden els dos polímers per igual (A1-II' i Alg2A), tal com resumeix la següent taula:

Alginat liasa	Família	Especificitat	Origen
Alg2A	PL7	PolyM i PolyG	*F. multivorum*
AlyA1	PL7	PolyG	*Z. galactanivorans*
A1-II'	PL7	PolyM i PolyG	*Sphingomonas sp.* A1
A1-II	PL7	PolyG	*Sphingomonas sp.* A1
A1-III	PL5	PolyM	*Sphingomonas sp.* A1

Al laboratori del CRG es van analitzar les seqüències de les diferents alginat liases, es van comparar amb la seva activitat i també es va caracteritzar l'especificitat de cada una per PolyM i PolyG. Posteriorment, al laboratori de l'IBEC es va comprovar que aquests enzims no tenen cap efecte en cultius planctònics de *Pseudomonas* (Figura S3 de l'article 4) i es va analitzar l'activitat degradadora en biofilms madurs crescuts en continu. Aquests biofilms eren de dues soques diferents de *P. aeruginosa,* la soca PAO1 *wild-type* i la soca PAO1 mutant *ΔmucA*, que té un fenotip mucoide, amb una sobreexpresió del polisacàrid alginat. En examinar el poder disgregador de les cinc alginat liases es va veure que els enzims que degraden els dos polímers de l'alginat per igual, Alg2A i A1-II', són els que més eficaçment degraden el biofilm, tot i que l'Alg2A degrada més la soca mucoide i l'A1-II' degrada les dues soques de la mateixa manera (Figura 4A i 4C de l'article 4). Pel que fa als enzims específics per a un tipus de polímer (A1-II i A1-III) no són tan efectius, i també difereixen en l'activitat contra les dues soques de *P. aeruginosa*. La primera degrada més el biofilm format per la soca mucoide i la segona, el format per la soca PAO1 *wild-type* (Figura 4A i 4C de l'article 4). Finalment, es va determinar que l'enzim AlyA1 no tenia activitat antibiofilm, ja que no va produir degradació en cap dels biofilms.

També es va assajar la possible sinergia de les alginat liases més actives amb l'antibiòtic ciprofloxacina, i es va veure que tant l'Alg2A com l'A1-II' milloren l'acció de l'antibiòtic (Figura 4B i 4C de l'article 4).

En el cinquè treball, titulat "***Tobramycin and DNase I dextran-based single-chain nanoparticles interaction with Pseudomonas aeruginosa extracellular biofilm matrix***.", s'han provat unes noves nanopartícules de cadena única de dextrà (*single-chain polymer nanoparticles*, SCPN) fabricades al centre d'investigació CIDETEC, al País Basc. Aquest tipus de nanopartícules són biocompatibles, biodegradables, solubles en aigua i, a més, poden carregar grans quantitats d'antibiòtic [184]. En el centre CIDETEC, aquestes SCPN han estat carregades amb l'antibiòtic tobramicina i/o funcionalitzades amb l'enzim DNasa I (Figura 1 de l'article 5).

Primerament, per tal de comprovar la concentració activa de tobramicina carregada en les SCPN, es va comparar l'eficàcia contra bacteris en creixement planctònic. En tractar els cultius de *P. aeruginosa* i *S. aureus* amb les SCPN carregades amb tobramicina i amb la mateixa concentració d'aquest antibiòtic lliure (soluble), es va veure que la corba de creixement era exactament igual, la qual cosa confirma que tot l'antibiòtic carregat dins de les SCPN és actiu i té capacitat de sortir de la nanopartícula (Figura 2 de l'article 5). També es va comprovar que les SCPN sense carregament i les

que només estan funcionalitzades amb DNasa I són innòcues per al creixement bacterià (Figura 2 de l'article 5).

Tanmateix, al tractar biofilms madurs crescuts en continu d'aquests mateixos bacteris amb les diferents SCPN, el resultat ha estat diferent. Les SCPN que contenen tobramicina sola i les que contenen tobramicina i DNasa I són significativament més eficaces disgregant el biofilm de *P. aeruginosa* i *S. aureus* que el mateix tractament de forma soluble (Figura 3 de l'article 5). En el cas de les SCPN que contenen DNasa I sola, però, hi ha diferències entre l'actuació en els biofilms de *P. aeruginosa* i els de *S. aureus*. Així com en els biofilms de *Pseudomonas* el tractament amb SCPN de DNasa I millora considerablement l'actuació d'aquest enzim, en els biofilms de *Staphylococcus* aquestes nanopartícules fan augmentar la biomassa del biofilm un 129 % (Figura 3B, D i E de l'article 5). D'altra banda, també s'ha demostrat que el dextrà que forma les SCPN no és el causant d'aquesta millora en el tractament, ja que el tractament amb les SCPN que no carreguen ni tobramicina ni DNasa I no té efecte en cap dels biofilms (Figura 3 de l'article 5).

Com que l'experiment de tractament de biofilms no permet veure l'alteració de la matriu extracel·lular del biofilm ni la interacció amb aquesta, es va afegir un fluoròfor (rodamina) a les SCPN, per a poder-les veure al microscopi confocal i així determinar quina és la interacció que tenen amb els diferents components del biofilm. Per aquest motiu es va fer una tinció diferencial dels diferents components de la matriu extracel·lular del biofilm de *P. aeruginosa* (cèl·lules, alginat i DNA extracel·lular) i es va realitzar un experiment en continu ("time-lapse"), visualitzant al microscopi confocal biofilms tractats amb SCPN durant setze hores i realitzant imatges d'aquests aproximadament cada tres hores. Amb aquest experiment s'ha pogut veure un clar creixement de la matriu extracel·lular i les cèl·lules bacterianes quan el biofilm es tracta amb les SCPN sense carregament, mentre que en les SCPN amb antibiòtic i/o enzim aquests dos paràmetres es troben afectats (Figura 4A i B de l'article 5).

A causa de la petita mida que tenen aquestes nanopartícules, que no permet realitzar un seguiment durant setze hores sense que les SCPN es desfacin o es perdin en el biofilm durant el time-lapse, aquest experiment s'ha fet amb agregats de SCPN d'aproximadament 2 µm de diàmetre i, per tant, no es pot determinar si les SCPN individuals (que tenen un diàmetre de 19 ± 1 nm) penetren a dins el biofilm. Tanmateix, en analitzar la posició de l'agregat de SCPN respecte a la matriu extracel·lular en el temps, s'ha pogut veure que les SCPN que contenen tobramicina i/o DNasa I s'introdueixen més a dins de la matriu del biofilm que les SCPN sense carregament (Figures 4D i 5 de l'article 5).

Finalment, pel que fa al DNA extracel·lular (eDNA), aquest es veu molt reduït en les SCPN que contenen DNasa I, tot i que també es redueix en el temps amb el tractament amb SCPN que només contenen tobramicina. Les SCPN control, però no tenen cap efecte en l'eDNA (Figura 4C de l'article 5).

4. Optimitzar la formació i anàlisi de biofilms *in vitro* de diferents espècies i soques bacterianes.

Pel que fa a l'últim objectiu, aquest s'ha dut a terme de manera transversal en tots els treballs anteriorment citats i també en els que s'inclouen als annexos.

En els treballs dels articles 1 i 2 s'ha optimitzat la formació de biofilms de *S. aureus* en un model en estàtic que simula un catèter infectat (Figura 4B de l'article 1 i figura 3 de l'article 2) i, específicament en l'article 2, en un model en continu (Figura 4 de l'article 2). En aquest últim model, el medi passa contínuament per les *flow-cells* on es forma el biofilm, enduent-se els bacteris que creixen planctònicament i que no en formen part. Un dels problemes que provoca en els biofilms de *S. aureus* és que es necessita que aquest bacteri creï unions fortes amb el substrat, per tal d'impedir que el medi se l'endugui. Com que el bacteri *S. aureus* s'uneix a proteïnes com el fibrinogen en les etapes primerenques de formació de biofilm, les *flow-cells* es van omplir amb plasma boví que conté aquestes proteïnes dotze hores abans d'afegir-hi el bacteri. Així, les cèl·lules de *S. aureus* es van poder unir al substrat, evitant que el medi se les endugués. Per altra banda, *S. aureus* creix molt ràpidament en un medi ric, i el creixement planctònic podria provocar l'obturació dels tubs abans de poder ser retirat pel medi que passa. Per aquest motiu va ser necessari provar diferents medis de cultiu que poguessin evitar un creixement massa ràpid. Finalment el procediment òptim va ser diluir el medi de cultiu al 2 % en aigua.

En el treball de l'article 6, titulat "***Aerobic Vitamin B12 Biosynthesis Is Essential for Pseudomonas aeruginosa Class II Ribonucleotide Reductase Activity During Planktonic and Biofilm Growth***" inclòs a l'annex 1 i també en els treballs dels articles 3 i 4 s'han optimitzat els biofilms de diferents soques clíniques i mutants (Figura 5 de l'article 6, figura 3 de l'article 3 i figura 4 de l'article 4). En aquestes soques cal optimitzar sobretot el medi i temps necessari per a formar un biofilm madur i homogeni, que normalment difereix entre les soques de laboratori i les *wild-type*.

En l'article 3, al dispositiu BiofilmChip, també s'optimitza la formació de biofilms directament des d'esputs provinents de malalts de FQ (Figura 4 de l'article 3). Aquests esputs solen tenir moltes cèl·lules eucariotes com neutròfils que impedeixen desenvolupar el biofilm. Per això, el procediment òptim va ser fer un xoc hipotònic durant deu minuts que va reduir el nombre de neutròfils i va permetre als bacteris presents formar el biofilm.

En el treball de l'article 5 es va optimitzar el mètode d'anàlisi dels biofilms (Figures 4 i 5 de l'article 5). Per una banda amb els diferents colorants que tenyeixen les parts del biofilm, i per l'altra amb l'anàlisi de la zona que envolta l'agregat de SCPN i que permet veure el moviment d'aquestes respecte al biofilm.

En el treball inclòs a l'annex 2, l'article 7, titulat "***Optimal environmental and culture conditions allow the in vitro coexistence of Pseudomonas aeruginosa and Staphylococcus aureus in stable biofilms***" s'han optimitzat les condicions per al creixement de biofilms en continu de *P. aeruginosa* i *S. aureus*, provant diferents medis que permetessin la coexistència de les dues espècies (Figura 6 de l'article 7).

DISCUSSIÓ

Les infeccions provocades pels biofilms constitueixen un greu problema de salut a escala mundial, ja que la seva resistència als antibiòtics pot arribar a ser mil vegades més alta que en els bacteris que viuen en forma lliure (planctònics) [6]. Actualment, els bacteris resistents provoquen la mort de vint-i-cinc mil persones l'any a la Unió Europea i unes set-centes mil arreu del món. L'organització mundial de la salut (OMS) estima que, cap a l'any 2050, la xifra mundial de morts per aquesta causa augmentarà fins als deu milions cada any, sent la principal causa de mort a tot el món [185]. Com que cap dels antibiòtics que actualment estan al mercat està dissenyat específicament per erradicar biofilms [186], és necessari buscar noves metodologies i eines per a l'estudi i tractament de biofilms, des de modificar molècules ja existents fins a trobar noves dianes d'acció, passant per nous dispositius de formació de biofilm.

1. Modificació i millora d'antimicrobians contra els biofilms de *S. aureus*

Els bacteris del gènere *Staphylococcus* són els principals causants de la formació de biofilms en dispositius mèdics. Concretament, l'espècie *S. aureus* provoca infeccions amb alta mortalitat i morbiditat, a causa de la constant aparició de soques multiresistents, com la soca MRSA (*Staphylococcus aureus* resistent a meticil·lina). La formació d'aquests biofilms pot generar diverses infeccions i acabar en sèpsia [187], i l'únic tractament possible sol ser la substitució del dispositiu [67]. En els treballs presentats als articles 1 i 2 s'han provat unes molècules, que han sigut modificades per a millorar el seu potencial contra els biofilms de *S. aureus*. Una part d'aquestes molècules són derivades del triclocarban (TCC) i unes altres, són derivades de l'àcid oleanòlic (OA) i l'àcid maslínic (MA).

El TCC és una diarilurea que té acció antibacteriana contra *S. aureus*, però en contenir tres àtoms de clor en la seva estructura, és un compost molt contaminant que pot persistir en l'ambient durant molts anys. A més, tot i que només es fa servir en ús tòpic, és potencialment tòxic per als humans, ja que s'absorbeix i es pot arribar a detectar al plasma sanguini. A causa de tot això, l'any 2017, l'Administració d'Aliments i Fàrmacs (*Food and Drug Administration,* FDA) va prohibir l'ús del TCC en productes de consum, juntament amb una molècula molt semblant, el triclosan [188, 189]. Els derivats presentats en aquest treball es van sintetitzar canviant de posició els àtoms de clor de la molècula TCC i també reemplaçant-los per altres grups com el pentafluorur de sofre (SF_5), grup que

s'usa molt en la fabricació de fàrmacs gràcies a les seves característiques que aporten estabilitat, alta electronegativitat i lipofília [190]. Gràcies a la reducció de grups de clor en la seva estructura, els derivats són menys tòxics per a les persones i per al medi ambient. A més de la reducció de la toxicitat, els derivats del TCC amplien l'espectre d'acció d'aquest compost, ja que són actius contra més bacteris Gram-positius, a part dels del gènere *Staphylococcus* (Taula 1 de l'article 1).

Per altra banda, els triterpens OA i MA es troben en diverses plantes, on fan una funció de protecció contra la deshidratació i les infeccions microbianes. Com que es troben en abundància en els fruits de l'olivera (*Olea europaea*), se'n pot extreure una gran quantitat en els residus procedents de la producció de l'oli d'oliva. Aquests dos compostos, molt usats en medicina ancestral, tenen propietats antiinflamatòries, anti-hiperlipidèrmiques, antitumorals i hepatoprotectives, a més d'antimicrobianes [191, 192]. Tot i que no s'han trobat mecanismes de resistència en bacteris, l'eficàcia d'aquests dos compostos només s'ha provat *in vitro*, i no s'han trobat derivats que en millorin l'activitat [193]. Els catorze compostos derivats de l'OA i l'MA d'aquest treball s'han sintetitzat afegint diferents diamines a les molècules OA i MA. Aquestes diamines difereixen entre elles en el grup terminal i la llargària de la seva cadena (Esquema 1 de l'article 2), per tal de poder estudiar què podria millorar l'activitat antimicrobiana. Els triterpens MA i OA tenen una toxicitat molt baixa i s'ha demostrat que l'addició de les diamines no n'augmenta la toxicitat, tot i que sí que millora l'activitat antimicrobiana contra alguns bacteris Gram-positius (Taula 1 de l'article 2).

En ambdós treballs s'han trobat derivats que milloren l'activitat antimicrobiana contra la soca de *S. aureus* resistent a meticil·lina (MRSA) (Taula 1 de l'article 1 i Taula 1 de l'article 2). Les soques MRSA són un greu problema hospitalari, ja que la resistència a la meticil·lina és causada per elements mòbils genètics que es transfereixen entre bacteris. A més, la majoria de soques MRSA tenen resistència a múltiples antibiòtics i només són sensibles als antibiòtics glicopèptids com la vancomicina, tot i que recentment ja estan apareixent soques MRSA amb menys sensibilitat a aquests antibiòtics [194]. Per tant, els compostos derivats del TCC núm. 10 i 12 i els compostos derivats dels triterpens MA-HDA i OA-HDA podrien ser una bona alternativa per al tractament de les soques MRSA, ja que milloren l'activitat dels compostos parentals contra la soca MRSA. A més, s'ha vist que els derivats més actius del TCC disminueixen o eliminen l'aparició de resistències (Taula 2 de l'article 1), i encara no s'han trobat resistències en els triterpens OA i MA [193].

Pel que fa a l'activitat antibiofilm, els compostos més actius dels dos treballs s'han provat en biofilms de *S. aureus* preformats en catèters de manera estàtica i, en el cas de les diamines derivades de l'OA

i l'MA, també s'han provat contra biofilms creixent en continu. Aquests últims representen un biofilm més similar al que es forma *in vivo* i, per tant, més difícil d'erradicar, motiu pel qual l'eficàcia per a erradicar aquest biofilm és més baixa, tot i que també millora respecte als triterpens parentals (Figura 4 de l'article 2). Per altra banda, en els anàlegs del TCC també s'ha provat la seva eficàcia per a netejar superfícies contaminades per *S. aureus*, i s'ha vist que la potència desinfectant, igual que l'activitat antibiofilm, és similar a les del TCC (Figura 4 de l'article 1).

Tant en el treball de l'article 1 com en el de l'article 2, s'ha intentat discernir el mecanisme molecular de la seva activitat antimicrobiana i, per això, s'han visualitzat al microscopi les cèl·lules de *S. aureus* tractades amb els compostos més actius, després de tenyir-les amb dues tincions diferents. Les tincions han confirmat que els compostos tenen un mode d'acció bacteriolític, ja que, després de quatre hores de tractament, hi ha un gran descens del nombre total de cèl·lules i un augment de les no viables (Figura 3A de l'article 1 i Figura 2A de l'article 2). La tinció de membrana per altra banda ha confirmat que els compostos afecten la membrana (Figura 3B de l'article 1 i Figura 2B de l'article 2). A més, en el cas dels derivats terpènics també s'han observat els bacteris al microscopi electrònic de rastreig (SEM), on també s'observen danys en la membrana de les cèl·lules tractades (Figura 2C de l'article 2). Cap dels derivats provats té un gran efecte en els bacteris Gram-negatius.

En el cas dels derivats del TCC, no s'ha arribat a discernir per què només afecta bacteris Gram-positius i, tot i semblar que l'addició del pentafluorur de sofre disminueix la toxicitat del compost i en millora l'activitat, no s'ha trobat una relació directa entre l'estructura i l'activitat dels nous compostos. Estudis posteriors al nostre confirmen que el TCC afecta la membrana dels bacteris i suggereixen que el mètode d'acció és similar al del triclosan, i que està relacionat amb el transport de precursors del peptidoglicà, la síntesi d'isoprenoides que donen estabilitat a la membrana [195] i la reducció de l'activitat de les bombes de reflux [196].

Amb els derivats de l'OA i l'MA, s'ha vist que els únics actius són els que tenen el grup terminal carregat positivament a pH fisiològic i una certa llargària en la cadena d'aquest grup terminal (Esquema 1 i Taula 1 de l'article 2). Aquesta característica estructural fa que tinguin afinitat per la membrana dels bacteris Gram-positius, la qual està més negativament carregada que la dels Gram-negatius [197].

Les larves de l'insecte *Galleria mellonella* són un bon model d'infecció perquè disposen d'un sistema immune innat similar al dels mamífers i són capaces de viure a la temperatura del cos humà, a més

de no requerir aprovació ètica i ser accessibles i fàcils de mantenir [198]. Ja que l'eficàcia dels compostos OA i MA només s'havia provat *in vitro*, en aquest treball s'ha pogut comprovar que el triterpè MA i l'amina derivada MA-HDA rescaten un 50 % de les larves infectades per *S. aureus* amb la injecció de només dues dosis d'aquests compostos (Figura 1 de l'article 2). A més, l'ús d'aquestes larves per a calcular l'índex de selectivitat ha fet que aquest augmenti considerablement, comparat amb el calculat a partir de la toxicitat en cèl·lules epitelials pulmonars (Taula 1 de l'article 2), gràcies al fet que la toxicitat és molt més baixa en el model *in vivo*.

2. Microfluídica per a l'estudi de biofilms

Actualment, en la majoria de laboratoris de microbiologia dels hospitals es fan servir paràmetres que determinen l'eficàcia antibiòtica usant bacteris en creixement planctònic (MIC), ja que els mètodes provats fins ara per a veure l'eficàcia antibiòtica en biofilms de mostres clíniques no han demostrat fer una predicció del tractament més acurada que les MIC [72]. Això pot ser per culpa que aquests mètodes emprats per a analitzar la sensibilitat en biofilms estan basats en sistemes en estàtic (tancats i amb uns nutrients limitats). Els "dispositius dinàmics", en canvi, són dispositius on contínuament hi ha un subministrament de medi de cultiu al biofilm, i això fa que el creixement es pugui considerar més semblant a la infecció que es dóna al cos humà, ja que proporcionen un *shear stress* (força mecànica que exerceix el medi) que mimetitza les condicions *in vivo*, com per exemple les que es donen en les vies respiratòries [58, 199]. El problema dels dispositius dinàmics és la despesa de medi de cultiu i la mida de la infraestructura que necessita, fent-lo pràcticament inutilitzable en un laboratori de diagnòstic microbiològic d'un hospital.

Són necessaris, per tant, nous mètodes que puguin servir per a determinar la sensibilitat antibiòtica de manera eficaç en mostres clíniques i així millorar el tractament antibiòtic de pacients amb infeccions cròniques. A més, els mètodes haurien de ser simples, sense el requeriment d'equipament sofisticat ni personal altament qualificat. Els sistemes de microfluídica, amb canals on el volum és molt petit, requereixen menys espai i permeten un gran control de la despesa dels reactius i medis necessaris i, per tant, són un bon model per als laboratoris de microbiologia dels hospitals.

El BiofilmChip, presentat al treball de l'article 3, és un dispositiu de microfluídica per a determinar el creixement bacterià en forma de biofilm i la seva sensibilitat antibiòtica. Aquest dispositiu compta amb un mínim de tres conjunts de tres cambres a on creixen els biofilms, i aquestes cambres han

estat optimitzades en mida i forma per al creixement de biofilms de forma homogènia en tots els conjunts de cambres, així com dins de la mateixa cambra (Figura 3 de l'article 3). Això s'ha aconseguit gràcies a l'addició d'una pre-càmara que estabilitza i controla les variacions en el *shear stress*. D'aquesta manera, és possible la comparació entre les diferents cambres i sets de cambres, podent detectar així canvis en el biofilm quan s'aplica un tractament antibiòtic (Figura 3d de l'article 3).

El BiofilmChip s'ha fet servir no només per fer créixer soques de laboratori de *P. aeruginosa* i *S. aureus*, sinó que també permet el creixement de biofilms de soques clíniques, molt més difícils de fer créixer en dispositius *in vitro* (Figura 3c de l'article 3). A més, també s'han pogut fer créixer biofilms directament des d'esputs de pacients amb infecció crònica pulmonar, en concret malalts de fibrosi quística (Figura 4 de l'article 3). Aquestes infeccions són sempre polimicrobianes [200] i això també provoca que la resistència antibiòtica sigui diferent de les infeccions per biofilm monomicrobianes [201]. Fer créixer els biofilms directament des de l'esput fa que sigui més fàcil mantenir les condicions que es donen en la infecció i tots els bacteris que en formen part. Així, en el nostre treball hem pogut comprovar com els biofilms crescuts en el BiofilmChip són polimicrobians i, per tant, la sensibilitat antibiòtica que es mesuri amb el BiofilmChip serà molt més acurada que si es mesura amb les tècniques tradicionals, on només s'estudia l'activitat antimicrobiana d'un monocultiu.

Tots aquests experiments s'han realitzat amb la caracterització dels biofilms crescuts al microscopi confocal, però aquesta és una eina que rarament està disponible en un laboratori de microbiologia d'un hospital, ja que és un equipament car i necessita personal especialitzat per a fer-lo servir. Per això, en el BiofilmChip s'han afegit uns elèctrodes a la zona on el biofilm creix que permeten monitoritzar aquest creixement aplicant un voltatge i mesurant la impedància, sense la necessitat de visualitzar-lo al microscopi. En fer mesures paral·lelament en biomassa i resposta d'impedància del biofilm durant el creixement i el tractament amb diferents dosis d'antibiòtics, s'ha vist com la impedància permet monitoritzar el creixement del biofilm en continu i, a més, és més sensible que les mesures amb el microscopi confocal (Figura 5 de l'article 3). Altres dispositius també han demostrat que la impedància permet monitoritzar el creixement en forma de biofilm. En alguns d'aquests dispositius, però, el biofilm creix de manera estàtica en pous de microplaques i el creixement no es mesura a la interfase aire-líquid que és on es forma realment [98, 99]. Altres dispositius no permeten un creixement a llarg termini o homogeni del biofilm [202, 203]. El BiofilmChip, per tant, és un bon instrument per a analitzar la sensibilitat antibiòtica dels biofilms de manera acurada i fàcil.

3. La disgregació de la matriu extracel·lular com a diana antibiofilm.

L'increment de la resistència als antibiòtics en combinació amb la falta d'eficiència en biofilms ha provocat que el focus se centri en la barrera que forma la matriu extracel·lular i, actualment, s'estan estudiant diversos agents antibiofilm que disgreguen la matriu en biofilms madurs i d'aquesta manera permeten que l'antibiòtic trobi els bacteris [179], com els enzims alginat liasa i DNasa I. En els treballs presentats als articles 4 i 5, s'analitza l'activitat disgregadora de biofilms d'aquests dos enzims, sols i en combinació amb antibiòtics.

Les alginat liases són uns enzims que degraden l'alginat i que es classifiquen, segons la seva estructura, en set famílies PL (*Polysaccharide Lyase*): PL-5, -6, -7, -14, -15, -17 i -18. L'alginat és un dels components de la matriu extracel·lular dels biofilms de *P. aeruginosa* i està compost per dos polímers (β-D-manuronat (M) i α-L-guluronat (G)) disposats en diferents blocs d'un dels polímers (polyM o polyG) o de seqüències dels dos polímers (polyMG) [204]. Les alginat liases actuen trencant l'enllaç glicosídic i poden tenir especificitat per un dels dos polímers (polyM, polyG) o degradar els dos indistintament [183]. L'alginat és considerat un dels factors de virulència en els biofilms de *P. aeruginosa*, ja que defensa aquest bacteri contra la fagocitosi i alguns antibiòtics com la tobramicina [21], per això és una bona diana per a combatre els biofilms. En el treball de l'article 3 s'ha comprovat la innocuïtat de les alginat liases en creixement planctònic (Figura S3 de l'article 4) i l'activitat contra biofilms en una soca de *P. aeruginosa wild-type* i una soca sobreproductora d'alginat (*ΔmucA*). S'ha demostrat l'activitat específica d'aquests enzims contra l'alginat, en veure que les alginat liases d'ampli espectre Alg2A i A1-II' són més efectives disgregant el biofilm de la soca mutant *ΔmucA* que el de la soca *wild-type* (Figura 4A i 4C de l'article 4).

Tot i que els enzims són una bona ajuda per a disgregar els biofilms, és important administrar-los conjuntament amb agents antimicrobians que eliminin els bacteris que s'alliberen en la disgregació, ja que si no, aquests poden colonitzar altres zones del cos i propagar més la infecció [140]. En el cas de les alginat liases, però, s'ha vist anteriorment que la sinergia d'aquests enzims amb antibiòtic és independent de la seva activitat disgregadora [205]. En l'article 4 es verifica com les alginat liases que degraden els dos polímers de l'alginat per igual (Alg2A i A1-II') són les úniques que tenen un efecte sinèrgic amb l'antibiòtic ciprofloxacina (Figura 4B i 4C de l'article 4).

En el treball que es presenta a l'article 5, a més de combinar l'acció de l'antibiòtic tobramicina i l'enzim DNasa I, aquests es troben simultàniament a dins de la mateixa nanopartícula de cadena

única de dextrà (SCPN). Els nanosistemes, com per exemple les NP, són una teràpia emergent en la lluita contra els biofilms i en els últims anys se n'han creat molts que incrementen la penetració a dins del biofilm per a alliberar els components antimicrobians, evitant la barrera protectora que forma la matriu extracel·lular [206]. No obstant això, tot i que aquests nanosistemes tenen bons resultats *in vitro*, a l'hora de la translació clínica hi ha molts problemes de biocompatibilitat i acumulació en certes parts del cos. Actualment, només dues formulacions de liposomes que contenen antibiòtics estan en la fase III d'assajos clínics: l'Arikace®, que conté l'antibiòtic amikacina, i el Pulmaquin®, que conté ciprofloxacina [207]. Les SCPN usades en l'article 5, en canvi, ja han demostrat ser biocompatibles i reduir la toxicitat dels principis actius que incorporen, a més d'aconseguir una bona distribució dins del pulmó usant l'aerosolitzador "Penn Century Microsprayer®" [184, 208-211]. En aquest últim article, les SCPN contenen, a més d'antibiòtic, l'enzim DNasa I. L'enzim DNasa I ja es fa servir actualment com a teràpia en malalts de FQ, en forma d'aerosol (amb el nom comercial de *Pulmozyme®*), per a reduir la viscositat de l'esput i ajudar així a l'eliminació del moc i per tant del biofilm format a les vies respiratòries [143]. Al nostre grup "Infeccions Bacterianes i Teràpies Antimicrobianes" de l'IBEC, es va treballar amb unes nanopartícules en les quals l'acció de l'enzim DNasa I millora la funció de l'antibiòtic ciprofloxacina en l'eliminació de biofilms de *P. aeruginosa*, ja que permeten l'actuació constant dels enzims disgregadors i l'alliberament progressiu dels antibiòtics [141].

En el cas de l'article 5, les SCPN que es fan servir contenen tobramicina, a més de la DNasa I, i s'han provat en biofilms de *S. aureus*, a més dels de *Pseudomonas*. S'ha vist que, tot i que aquestes SCPN tenen la mateixa acció que l'antibiòtic lliure en bacteris en creixement planctònic, milloren molt l'acció de l'antibiòtic en els biofilms formats per les dues espècies bacterianes (Figura 3 de l'article 5). L'alginat que forma part de la matriu extracel·lular dels biofilms de *Pseudomonas* protegeix aquest bacteri contra el sistema immune de l'organisme. A més, aquest polisacàrid i també l'eDNA estan carregats negativament i redueixen l'actuació de l'antibiòtic tobramicina, que està carregat positivament i es queda atrapat en la perifèria del biofilm [212]. L'ús de les SCPN amb tobramicina neutralitza la càrrega de l'antibiòtic i, juntament amb la degradació de l'eDNA per part de la DNasa I, permet disgregar la matriu del biofilm gradualment per tal que la tobramicina pugui accedir als bacteris.

El fet que aquestes SCPN estiguin marcades amb un fluoròfor permet visualitzar més en detall, al microscopi confocal, la seva forma d'actuació. En els experiments de *time-lapse* realitzats es va poder demostrar com la matriu extracel·lular i les cèl·lules del biofilm segueixen creixent si es tracta

amb SCPN sense carregament (Figura 4A i B de l'article 5), mentre que disminueix amb les SCPN que contenen tobramicina o les que també contenen DNasa I. La resposta del biofilm al tractament, però, és diferent entre les dues SCPN. En el tractament amb SCPN que només conten tobramicina, es produeix una recidiva en el creixement dels bacteris i del biofilm quan l'efecte de l'antibiòtic ha acabat, mentre que amb el tractament amb les SCPN que també contenen DNasa I, aquest enzim impedeix que el biofilm torni a formar-se quan l'efecte de l'antibiòtic ha acabat. A més, aquestes SCPN també demostren la necessitat d'afegir antibiòtic als tractaments amb enzims, ja que, com es pot veure a les Figures 4 i 5 de l'article 5, les SCPN que contenen ambdós components eviten la formació de biofilm, però els bacteris que s'alliberen gràcies a la DNasa I continuen creixent de forma planctònica. Com ja s'ha dit abans, l'ús d'enzims disgregadors en biofilms provoca la dispersió de la infecció i, per tant, és necessari combinar-los amb l'ús d'antimicrobians [140]. La incorporació d'aquests dos components dins de les SCPN permet que els enzims disgregadors i els antimicrobians actuïn simultàniament millorant la seva activitat contra els biofilms.

Pel que fa a la concentració de l'eDNA en els biofilms de *P. aeruginosa*, en l'experiment de *time-lapse* s'ha vist que aquest es degrada totalment amb les SCPN que contenen DNasa I. Tot i que no s'erradica totalment, aquest component de la matriu també disminueix progressivament amb el tractament de les SCPN que només contenen tobramicina (Figura 4C de l'article 5), gràcies a la degradació progressiva del biofilm.

L'eDNA també és una part important dels biofilms de *S. aureus*, on promou l'apilament i formació d'agregats [213]. En el tractament del biofilm d'aquest bacteri amb SCPN que contenen únicament DNasa I provoca un increment en la biomassa del biofilm (Figura 3B, D i E de l'article 5), a causa que redueix l'apilament i els agregats de cèl·lules es fan més petits, transformant el biofilm en més esponjós i fent que el càlcul de biomassa augmenti.

En aquests experiments de *time-lapse* també s'ha observat com les SCPN interaccionen amb la matriu del biofilm. Les SCPN són massa petites per a poder ser visualitzades individualment al microscopi confocal i, per això, els experiments de *time-lapse* es van realitzar amb agregats d'aquestes SCPN d'aproximadament 2 µm. Aquesta mida és massa gran per determinar si hi ha penetració dins del biofilm, però s'ha pogut observar com les SCPN que contenen tobramicina i les que també inclouen DNasa I s'acosten 4 µm respecte a la matriu durant les setze hores de l'experiment, mentre que les SCPN sense carregament s'acosten 1 µm menys, a causa segurament

de la seva càrrega negativa que és repel·lida per les càrregues negatives de la matriu extracel·lular del biofilm de *P. aeruginosa*.

Diversos estudis conclouen que la dimensió de les nanopartícules és un factor clau per la penetració d'aquestes dins del biofilm [214], i que la mida perfecta és entre 10 i 30 nm [215]. Les SCPN usades en l'article 5 tenen un diàmetre mitjà de 19 ± 1 nm i per tant són perfectes per a penetrar dins de l'estructura del biofilm.

CONCLUSIONS

1. Les diarilurees número 10 (*1,3-bis(4-(Pentafluoro-λ^6-sulfanyl)phenyl)*) i 12 (*1,3-bis(4-Chloro-3-(trifluoromethyl)phenyl)*) derivades del triclocarban amplien l'espectre d'acció contra bacteris Gram-positius, són menys tòxiques en cèl·lules eucariotes i, ambdues, milloren en deu i dues vegades respectivament la seva acció contra el bacteri *Staphylococcus aureus* resistent a meticil·lina.

2. Les diarilurees número 10 (*1,3-bis(4-(Pentafluoro-λ^6-sulfanyl)phenyl)*) i 12 (*1,3-bis(4-Chloro-3-(trifluoromethyl)phenyl)*) derivades del triclocarban tenen un mode bacteriolític d'acció i afecten la membrana dels bacteris, causen menys adquisicions de resistència que el triclocarban i tenen la mateixa eficàcia com a desinfectants i erradicant biofilms de *S. aureus* formats en catèters.

3. Les amines OA-HDA, OA-DAD, MA-HDA i MA-DAD, derivades dels triterpens àcid oleanòlic (OA) i àcid maslínic (MA), tenen un mode bacteriolític d'acció i afecten la membrana dels bacteris, no són més tòxiques que els compostos parentals i, a més, milloren l'acció contra el bacteri *S. aureus* resistent a meticil·lina en un 87, 60, 66 i 60 %, respectivament.

4. Les amines OA-HDA i MA-HDA, derivades dels triterpens àcid oleanòlic (OA) i àcid maslínic (MA) milloren l'acció antibiofilm dels compostos parentals i erradiquen els biofilms preformats de *S. aureus* un 99 % en biofilms de catèters i un 30 i 45 % respectivament en biofilms en continu.

5. El triterpè MA i la seva amina derivada MA-HDA recuperen en dues dosis un 50 % de larves de *Galleria mellonella* infectades amb *S. aureus*.

6. El dispositiu BiofilmChip permet un creixement homogeni del biofilm entre les diferents cambres que el conformen, gràcies a la precambra inclosa en el disseny.

7. El dispositiu BiofilmChip possibilita el creixement de biofilms de soques clíniques i biofilms polimicrobians provinents directament d'esputs de malalts d'infecció crònica pulmonar.

8. El dispositiu BiofilmChip facilita la monitorització del creixement i l'anàlisi de sensibilitat antibiòtica dels biofilms sense la necessitat de visualitzar-los al microscopi confocal i gràcies a la mesura d'impedància.

9. Les alginat liases d'ampli espectre Alg2A i A1-II' tenen sinergia amb l'antibiòtic ciprofloxacina i són més eficaces disgregant el biofilm de *P. aeruginosa* que les que només degraden PolyM o PolyG (A1-II, A1-III i AlyA1).

10. Les alginat liases d'ampli espectre Alg2A i A1-II' són més efectives disgregant el biofilm de *P. aeruginosa* de la soca sobreproductora d'alginat *ΔmucA* que el de la soca *wild-type,* demostrant així la seva especificitat per a l'alginat.

11. Les nanopartícules de cadena única de dextrà (SCPN) carregades amb l'antibiòtic tobramicina i/o l'enzim DNasa I milloren l'activitat de la tobramicina i/o DNasa I en la disgregació i erradicació dels biofilms de *P. aeruginosa* i *S. aureus*.

12. Les SCPN carregades amb l'antibiòtic tobramicina i l'enzim DNasa I erradiquen el biofilm de *P. aeruginosa* i eviten les recidives en el creixement dels bacteris i del biofilm quan l'efecte de l'antibiòtic ha finalitzat.

13. Les SCPN carregades amb l'antibiòtic tobramicina i les SCPN que també contenen l'enzim DNasa I entren 1 µm més en la matriu extracel·lular del biofilm de *P. aeruginosa* que les SCPN sense carregament.

14. El medi òptim per al creixement de biofilms en continu de *S. aureus* és TSB (*Tryptic Soy Broth*) diluït al 2 %, mentre que la vitamina B_{12} és necessària en el medi de cultiu per a la formació de biofilms en continu de *P. aeruginosa*.

15. El medi DMEM (*Dulbecco's Modified Eagle Medium*), juntament amb aportació d'oxigen, permet la coexistència de *P. aeruginosa* i *S. aureus* en els biofilms i, quan aquest medi és suplementat amb BSA (albúmina de sèrum boví), es produeix un augment en la proliferació de *S. aureus*.

BIBLIOGRAFIA

1. **Stewart, P.S. and M.J. Franklin,** *Physiological heterogeneity in biofilms.* Nat Rev Microbiol, 2008. 6(3): p. 199-210.
2. **Høiby, N.,** *A personal history of research on microbial biofilms and biofilm infections.* Pathog Dis, 2014. 70(3): p. 205-11.
3. **Costerton, J.W., G.G. Geesey, and K.J. Cheng,** *How bacteria stick.* Sci Am, 1978. 238(1): p. 86-95.
4. **Lappin-Scott, H., S. Burton, and P. Stoodley,** *Revealing a world of biofilms--the pioneering research of Bill Costerton.* Nat Rev Microbiol, 2014. 12(11): p. 781-7.
5. **Gordon, V., L. Bakhtiari, and K. Kovach,** *From molecules to multispecies ecosystems: the roles of structure in bacterial biofilms.* Phys Biol, 2019. 16(4): p. 041001.
6. **Stewart, P.S. and J.W. Costerton,** *Antibiotic resistance of bacteria in biofilms.* Lancet, 2001. 358(9276): p. 135-8.
7. **Miquel, S., et al.,** *Anti-biofilm Activity as a Health Issue.* Front Microbiol, 2016. 7: p. 592.
8. **Kanematsu, H. and D.M. Barry**, *Biofilm Problems and Environments*, in *Formation and Control of Biofilm in Various Environments*. 2020, Springer Singapore: Singapore. p. 173-200.
9. **Velmourougane, K., R. Prasanna, and A.K. Saxena,** *Agriculturally important microbial biofilms: Present status and future prospects.* J Basic Microbiol, 2017. 57(7): p. 548-573.
10. **Galié, S., et al.,** *Biofilms in the Food Industry: Health Aspects and Control Methods.* Front Microbiol, 2018. 9: p. 898.
11. **Flemming, H.C. and J. Wingender,** *The biofilm matrix.* Nat Rev Microbiol, 2010. 8(9): p. 623-33.
12. **Tseng, B.S., et al.,** *The extracellular matrix protects Pseudomonas aeruginosa biofilms by limiting the penetration of tobramycin.* Environ Microbiol, 2013. 15(10): p. 2865-78.
13. **Karunaratne, D.N.,** *The Complex World of Polysaccharides*. 2012: IntechOpen.
14. **Zogaj, X., et al.,** *The multicellular morphotypes of Salmonella typhimurium and Escherichia coli produce cellulose as the second component of the extracellular matrix.* Mol Microbiol, 2001. 39(6): p. 1452-63.
15. **Wingender, J., et al.,** *Isolation and biochemical characterization of extracellular polymeric substances from Pseudomonas aeruginosa.* Methods Enzymol, 2001. 336: p. 302-14.
16. **Danese, P.N., L.A. Pratt, and R. Kolter,** *Exopolysaccharide production is required for development of Escherichia coli K-12 biofilm architecture.* J Bacteriol, 2000. 182(12): p. 3593-6.
17. **Ma, L., et al.,** *Assembly and development of the Pseudomonas aeruginosa biofilm matrix.* PLoS Pathog, 2009. 5(3): p. e1000354.
18. **Sutherland, I.W.,** *The biofilm matrix--an immobilized but dynamic microbial environment.* Trends Microbiol, 2001. 9(5): p. 222-7.
19. **Götz, F.,** *Staphylococcus and biofilms.* Mol Microbiol, 2002. 43(6): p. 1367-78.
20. **Izano, E.A., et al.,** *Differential roles of poly-N-acetylglucosamine surface polysaccharide and extracellular DNA in Staphylococcus aureus and Staphylococcus epidermidis biofilms.* Appl Environ Microbiol, 2008. 74(2): p. 470-6.
21. **Moradali, M.F., S. Ghods, and B.H.A. Rehm,** *Pseudomonas aeruginosa Lifestyle: A Paradigm for Adaptation, Survival, and Persistence.* Frontiers in Cellular and Infection Microbiology, 2017. 7(39).
22. **Hentzer, M., et al.,** *Alginate overproduction affects Pseudomonas aeruginosa biofilm structure and function.* J Bacteriol, 2001. 183(18): p. 5395-401.
23. **Crespo, A., et al.,** *Regulation of ribonucleotide synthesis by the Pseudomonas aeruginosa two-component system AlgR in response to oxidative stress.* Sci Rep, 2017. 7(1): p. 17892.
24. **Colvin, K.M., et al.,** *The Pel and Psl polysaccharides provide Pseudomonas aeruginosa structural redundancy within the biofilm matrix.* Environ Microbiol, 2012. 14(8): p. 1913-28.
25. **Jennings, L.K., et al.,** *Pel is a cationic exopolysaccharide that cross-links extracellular DNA in the Pseudomonas aeruginosa biofilm matrix.* Proc Natl Acad Sci U S A, 2015. 112(36): p. 11353-8.
26. **Kaplan, J.B.,** *Biofilm dispersal: mechanisms, clinical implications, and potential therapeutic uses.* J Dent Res, 2010. 89(3): p. 205-18.

27. **Vacca, I.,** *Biofilms: Building up the matrix.* Nat Rev Microbiol, 2017. 15(9): p. 512-513.
28. **Reichhardt, C. and M.R. Parsek,** *Confocal Laser Scanning Microscopy for Analysis of Pseudomonas aeruginosa Biofilm Architecture and Matrix Localization.* Frontiers in microbiology, 2019. 10: p. 677-677.
29. **Otto, M.,** *Staphylococcal Biofilms.* Microbiol Spectr, 2018. 6(4).
30. **Joo, H.S. and M. Otto,** *Molecular basis of in vivo biofilm formation by bacterial pathogens.* Chem Biol, 2012. 19(12): p. 1503-13.
31. **van Schaik, E.J., et al.,** *DNA binding: a novel function of Pseudomonas aeruginosa type IV pili.* Journal of bacteriology, 2005. 187(4): p. 1455-1464.
32. **Whitchurch, C.B., et al.,** *Extracellular DNA required for bacterial biofilm formation.* Science, 2002. 295(5559): p. 1487.
33. **Okshevsky, M. and R.L. Meyer,** *The role of extracellular DNA in the establishment, maintenance and perpetuation of bacterial biofilms.* Crit Rev Microbiol, 2015. 41(3): p. 341-52.
34. **Das, T., et al.,** *DNA-mediated bacterial aggregation is dictated by acid–base interactions.* Soft Matter, 2011. 7(6): p. 2927-2935.
35. **Olivares, E., et al.,** *Clinical Impact of Antibiotics for the Treatment of.* Front Microbiol, 2019. 10: p. 2894.
36. **Allesen-Holm, M., et al.,** *A characterization of DNA release in Pseudomonas aeruginosa cultures and biofilms.* Mol Microbiol, 2006. 59(4): p. 1114-28.
37. **Wilton, M., et al.,** *Extracellular DNA Acidifies Biofilms and Induces Aminoglycoside Resistance in Pseudomonas aeruginosa.* Antimicrob Agents Chemother, 2016. 60(1): p. 544-53.
38. **Alhede, M., et al.,** *The origin of extracellular DNA in bacterial biofilm infections in vivo.* Pathog Dis, 2020. 78(2).
39. **Davey, M.E., N.C. Caiazza, and G.A. O'Toole,** *Rhamnolipid surfactant production affects biofilm architecture in Pseudomonas aeruginosa PAO1.* J Bacteriol, 2003. 185(3): p. 1027-36.
40. **Lau, P.C., et al.,** *Differential lipopolysaccharide core capping leads to quantitative and correlated modifications of mechanical and structural properties in Pseudomonas aeruginosa biofilms.* J Bacteriol, 2009. 191(21): p. 6618-31.
41. **O'Toole, G., H.B. Kaplan, and R. Kolter,** *Biofilm formation as microbial development.* Annu Rev Microbiol, 2000. 54: p. 49-79.
42. **Kaplan, J.B.,** *Antibiotic-induced biofilm formation.* Int J Artif Organs, 2011. 34(9): p. 737-51.
43. **Stoodley, P., et al.,** *Biofilms as complex differentiated communities.* Annu Rev Microbiol, 2002. 56: p. 187-209.
44. **Hall-Stoodley, L., J.W. Costerton, and P. Stoodley,** *Bacterial biofilms: from the natural environment to infectious diseases.* Nat Rev Microbiol, 2004. 2(2): p. 95-108.
45. **Klapper, I. and J. Dockery,** *Mathematical Description of Microbial Biofilms.* SIAM Review, 2010. 52: p. 221-265.
46. **Gross, M., et al.,** *Key role of teichoic acid net charge in Staphylococcus aureus colonization of artificial surfaces.* Infect Immun, 2001. 69(5): p. 3423-6.
47. **Romeo, T.,** *Bacterial Biofilms*. Vol. 322. 2008.
48. **Guttenplan, S.B. and D.B. Kearns,** *Regulation of flagellar motility during biofilm formation.* FEMS microbiology reviews, 2013. 37(6): p. 849-871.
49. **Klausen, M., et al.,** *Biofilm formation by Pseudomonas aeruginosa wild type, flagella and type IV pili mutants.* Mol Microbiol, 2003. 48(6): p. 1511-24.
50. **Sakuragi, Y. and R. Kolter,** *Quorum-sensing regulation of the biofilm matrix genes (pel) of Pseudomonas aeruginosa.* J Bacteriol, 2007. 189(14): p. 5383-6.
51. **Collins, A.J., et al.,** *From Input to Output: The Lap/c-di-GMP Biofilm Regulatory Circuit.* Annu Rev Microbiol, 2020.
52. **Solano, C., M. Echeverz, and I. Lasa,** *Biofilm dispersion and quorum sensing.* Curr Opin Microbiol, 2014. 18: p. 96-104.

53. **Jensen, P., et al.,** *Rapid necrotic killing of polymorphonuclear leukocytes is caused by quorum-sensing-controlled production of rhamnolipid by Pseudomonas aeruginosa.* Microbiology, 2007. 153(Pt 5): p. 1329-1338.
54. **Diggle, S.P., et al.,** *The Pseudomonas aeruginosa quinolone signal molecule overcomes the cell density-dependency of the quorum sensing hierarchy, regulates rhl-dependent genes at the onset of stationary phase and can be produced in the absence of LasR.* Mol Microbiol, 2003. 50(1): p. 29-43.
55. **Boles, B.R., M. Thoendel, and P.K. Singh,** *Rhamnolipids mediate detachment of Pseudomonas aeruginosa from biofilms.* Mol Microbiol, 2005. 57(5): p. 1210-23.
56. **Dunman, P.M., et al.,** *Transcription profiling-based identification of Staphylococcus aureus genes regulated by the agr and/or sarA loci.* J Bacteriol, 2001. 183(24): p. 7341-53.
57. **Periasamy, S., et al.,** *How Staphylococcus aureus biofilms develop their characteristic structure.* Proc Natl Acad Sci U S A, 2012. 109(4): p. 1281-6.
58. **Bahamondez-Canas, T.F., L.A. Heersema, and H.D.C. Smyth,** *Current Status of In Vitro Models and Assays for Susceptibility Testing for Wound Biofilm Infections.* Biomedicines, 2019. 7(2).
59. **Hall, C.W. and T.F. Mah,** *Molecular mechanisms of biofilm-based antibiotic resistance and tolerance in pathogenic bacteria.* FEMS Microbiol Rev, 2017. 41(3): p. 276-301.
60. **Brauner, A., et al.,** *Distinguishing between resistance, tolerance and persistence to antibiotic treatment.* Nat Rev Microbiol, 2016. 14(5): p. 320-30.
61. **Lebeaux, D. and J.M. Ghigo,** *[Management of biofilm-associated infections: what can we expect from recent research on biofilm lifestyles?].* Med Sci (Paris), 2012. 28(8-9): p. 727-39.
62. **Ratjen, F. and G. Döring,** *Cystic fibrosis.* The Lancet, 2003. 361(9358): p. 681-689.
63. **Høiby, N., O. Ciofu, and T. Bjarnsholt,** *Pseudomonas aeruginosa biofilms in cystic fibrosis.* Future Microbiol, 2010. 5(11): p. 1663-74.
64. **Ciofu, O., C.R. Hansen, and N. Høiby,** *Respiratory bacterial infections in cystic fibrosis.* Curr Opin Pulm Med, 2013. 19(3): p. 251-8.
65. **Folkesson, A., et al.,** *Adaptation of Pseudomonas aeruginosa to the cystic fibrosis airway: an evolutionary perspective.* Nat Rev Microbiol, 2012. 10(12): p. 841-51.
66. **Martínez-Solano, L., et al.,** *Chronic Pseudomonas aeruginosa infection in chronic obstructive pulmonary disease.* Clin Infect Dis, 2008. 47(12): p. 1526-33.
67. **Zheng, Y., et al.,** *Colonization of medical devices by staphylococci.* Environ Microbiol, 2018. 20(9): p. 3141-3153.
68. **Attinger, C. and R. Wolcott,** *Clinically Addressing Biofilm in Chronic Wounds.* Adv Wound Care (New Rochelle), 2012. 1(3): p. 127-132.
69. **Fleming, D., L. Chahin, and K. Rumbaugh,** *Glycoside Hydrolases Degrade Polymicrobial Bacterial Biofilms in Wounds.* Antimicrob Agents Chemother, 2017. 61(2).
70. **Arweiler, N.B. and L. Netuschil**, *The Oral Microbiota*, in *Microbiota of the Human Body: Implications in Health and Disease*, A. Schwiertz, Editor. 2016, Springer International Publishing: Cham. p. 45-60.
71. **Kolenbrander, P.E., et al.,** *Oral multispecies biofilm development and the key role of cell-cell distance.* Nat Rev Microbiol, 2010. 8(7): p. 471-80.
72. **Coenye, T., et al.,** *Should standardized susceptibility testing for microbial biofilms be introduced in clinical practice?* Clin Microbiol Infect, 2018. 24(6): p. 570-572.
73. **O'Toole, G.A. and R. Kolter,** *Initiation of biofilm formation in Pseudomonas fluorescens WCS365 proceeds via multiple, convergent signalling pathways: a genetic analysis.* Mol Microbiol, 1998. 28(3): p. 449-61.
74. **Azeredo, J., et al.,** *Critical review on biofilm methods.* Crit Rev Microbiol, 2017. 43(3): p. 313-351.
75. **Ceri, H., et al.,** *The Calgary Biofilm Device: new technology for rapid determination of antibiotic susceptibilities of bacterial biofilms.* J Clin Microbiol, 1999. 37(6): p. 1771-6.
76. **Chavant, P., et al.,** *A new device for rapid evaluation of biofilm formation potential by bacteria.* J Microbiol Methods, 2007. 68(3): p. 605-12.
77. **Sønderholm, M., et al.,** *Pseudomonas aeruginosa Aggregate Formation in an Alginate Bead Model System Exhibits.* Appl Environ Microbiol, 2017. 83(9).

78. **Sun, Y., et al.,** *In vitro multispecies Lubbock chronic wound biofilm model.* Wound Repair Regen, 2008. 16(6): p. 805-13.
79. **Jaśkiewicz, M., et al.,** *Methods Used for the Eradication of Staphylococcal Biofilms.* Antibiotics (Basel), 2019. 8(4).
80. **Nickel, J.C., et al.,** *Tobramycin resistance of Pseudomonas aeruginosa cells growing as a biofilm on urinary catheter material.* Antimicrob Agents Chemother, 1985. 27(4): p. 619-24.
81. **Goeres, D.M., et al.,** *A method for growing a biofilm under low shear at the air-liquid interface using the drip flow biofilm reactor.* Nat Protoc, 2009. 4(5): p. 783-8.
82. **Lawrence, J.R., G.D. Swerhone, and T.R. Neu,** *A simple rotating annular reactor for replicated biofilm studies.* J Microbiol Methods, 2000. 42(3): p. 215-24.
83. **Teodósio, J., M. Simões, and F. Mergulhão**, *Platforms for in-vitro biofilm studies*. 2013. p. 45-62.
84. **Tolker-Nielsen, T. and C. Sternberg,** *Methods for studying biofilm formation: flow cells and confocal laser scanning microscopy.* Methods Mol Biol, 2014. 1149: p. 615-29.
85. **Benoit, M.R., et al.,** *New device for high-throughput viability screening of flow biofilms.* Appl Environ Microbiol, 2010. 76(13): p. 4136-42.
86. **Le Norcy, T., et al.,** *A new method for evaluation of antifouling activity of molecules against microalgal biofilms using confocal laser scanning microscopy-microfluidic flow-cells.* International Biodeterioration & Biodegradation, 2019. 139: p. 54-61.
87. **Pletzer, D., et al.,** *New Mouse Model for Chronic Infections by Gram-Negative Bacteria Enabling the Study of Anti-Infective Efficacy and Host-Microbe Interactions.* mBio, 2017. 8(1).
88. **Klinger, J.D., et al.,** *Protective immunization against chronic Pseudomonas aeruginosa pulmonary infection in rats.* Infect Immun, 1983. 39(3): p. 1377-84.
89. **Cole, S.J., et al.,** *Catheter-associated urinary tract infection by Pseudomonas aeruginosa is mediated by exopolysaccharide-independent biofilms.* Infect Immun, 2014. 82(5): p. 2048-58.
90. **Nagata, T., et al.,** *Effect of erythromycin on chronic respiratory infection caused by Pseudomonas aeruginosa with biofilm formation in an experimental murine model.* Antimicrob Agents Chemother, 2004. 48(6): p. 2251-9.
91. **Bayes, H.K., et al.,** *A murine model of early Pseudomonas aeruginosa lung disease with transition to chronic infection.* Sci Rep, 2016. 6: p. 35838.
92. **Mall, M., et al.,** *Increased airway epithelial Na+ absorption produces cystic fibrosis-like lung disease in mice.* Nat Med, 2004. 10(5): p. 487-93.
93. **Bragonzi, A.,** *Murine models of acute and chronic lung infection with cystic fibrosis pathogens.* Int J Med Microbiol, 2010. 300(8): p. 584-93.
94. **Li, L., et al.,** *The importance of the viable but non-culturable state in human bacterial pathogens.* Front Microbiol, 2014. 5: p. 258.
95. **Chen, N.T. and C.W. Chang,** *Rapid quantification of viable legionellae in water and biofilm using ethidium monoazide coupled with real-time quantitative PCR.* J Appl Microbiol, 2010. 109(2): p. 623-34.
96. **Peeters, E., H.J. Nelis, and T. Coenye,** *Comparison of multiple methods for quantification of microbial biofilms grown in microtiter plates.* J Microbiol Methods, 2008. 72(2): p. 157-65.
97. **Sabaeifard, P., et al.,** *Optimization of tetrazolium salt assay for Pseudomonas aeruginosa biofilm using microtiter plate method.* J Microbiol Methods, 2014. 105: p. 134-40.
98. **van Duuren, J.B.J.H., et al.,** *Use of Single-Frequency Impedance Spectroscopy to Characterize the Growth Dynamics of Biofilm Formation in Pseudomonas aeruginosa.* Sci Rep, 2017. 7(1): p. 5223.
99. **Gutiérrez, D., et al.,** *Monitoring in Real Time the Formation and Removal of Biofilms from Clinical Related Pathogens Using an Impedance-Based Technology.* PLoS One, 2016. 11(10): p. e0163966.
100. **Haney, E.F., et al.,** *Critical Assessment of Methods to Quantify Biofilm Growth and Evaluate Antibiofilm Activity of Host Defence Peptides.* Biomolecules, 2018. 8(2).
101. **Adav, S.S. and D.J. Lee,** *Extraction of extracellular polymeric substances from aerobic granule with compact interior structure.* J Hazard Mater, 2008. 154(1-3): p. 1120-6.
102. **Lilledahl, M.B. and B.T. Stokke,** *Novel imaging technologies for characterization of microbial extracellular polysaccharides.* Front Microbiol, 2015. 6: p. 525.

103. **Hu, Y., J. Zhang, and J. Ulstrup,** *Investigation of Streptococcus mutans biofilm growth on modified Au(111)-surfaces using AFM and electrochemistry.* Journal of Electroanalytical Chemistry, 2011. 656(1): p. 41-49.
104. **Schlafer, S. and R.L. Meyer,** *Confocal microscopy imaging of the biofilm matrix.* J Microbiol Methods, 2017. 138: p. 50-59.
105. **Strathmann, M., J. Wingender, and H.C. Flemming,** *Application of fluorescently labelled lectins for the visualization and biochemical characterization of polysaccharides in biofilms of Pseudomonas aeruginosa.* J Microbiol Methods, 2002. 50(3): p. 237-48.
106. **Baird, F.J., M.P. Wadsworth, and J.E. Hill,** *Evaluation and optimization of multiple fluorophore analysis of a Pseudomonas aeruginosa biofilm.* J Microbiol Methods, 2012. 90(3): p. 192-6.
107. **Okshevsky, M. and R.L. Meyer,** *Evaluation of fluorescent stains for visualizing extracellular DNA in biofilms.* J Microbiol Methods, 2014. 105: p. 102-4.
108. **Stiefel, P., et al.,** *Critical aspects of using bacterial cell viability assays with the fluorophores SYTO9 and propidium iodide.* BMC Microbiol, 2015. 15: p. 36.
109. **Thurnheer, T., R. Gmür, and B. Guggenheim,** *Multiplex FISH analysis of a six-species bacterial biofilm.* J Microbiol Methods, 2004. 56(1): p. 37-47.
110. **Heydorn, A., et al.,** *Quantification of biofilm structures by the novel computer program comstat.* Microbiology, 2000. 146(10): p. 2395-2407.
111. **Ciofu, O., et al.,** *Antibiotic treatment of biofilm infections.* APMIS, 2017. 125(4): p. 304-319.
112. **Eleraky, N.E., et al.,** *Nanomedicine Fight against Antibacterial Resistance: An Overview of the Recent Pharmaceutical Innovations.* Pharmaceutics, 2020. 12(2).
113. **Barrasa-Villar, J.I., et al.,** *Impact on Morbidity, Mortality, and Length of Stay of Hospital-Acquired Infections by Resistant Microorganisms.* Clin Infect Dis, 2017. 65(4): p. 644-652.
114. **Kamaruzzaman, N.F., et al.,** *Targeting the Bacterial Protective Armour; Challenges and Novel Strategies in the Treatment of Microbial Biofilm.* Materials (Basel), 2018. 11(9).
115. **Koo, H., et al.,** *Targeting microbial biofilms: current and prospective therapeutic strategies.* Nat Rev Microbiol, 2017. 15(12): p. 740-755.
116. **Brackman, G. and T. Coenye,** *Quorum sensing inhibitors as anti-biofilm agents.* Curr Pharm Des, 2015. 21(1): p. 5-11.
117. **Huber, B., et al.,** *The cep quorum-sensing system of Burkholderia cepacia H111 controls biofilm formation and swarming motility.* Microbiology, 2001. 147(Pt 9): p. 2517-2528.
118. **Hentzer, M. and M. Givskov,** *Pharmacological inhibition of quorum sensing for the treatment of chronic bacterial infections.* J Clin Invest, 2003. 112(9): p. 1300-7.
119. **Hanzelka, B.L. and E.P. Greenberg,** *Quorum sensing in Vibrio fischeri: evidence that S-adenosylmethionine is the amino acid substrate for autoinducer synthesis.* J Bacteriol, 1996. 178(17): p. 5291-4.
120. **Brackman, G., et al.,** *Quorum sensing inhibitors increase the susceptibility of bacterial biofilms to antibiotics in vitro and in vivo.* Antimicrob Agents Chemother, 2011. 55(6): p. 2655-61.
121. **Anandan, K. and R.R. Vittal,** *Quorum quenching activity of AiiA lactonase.* Microb Pathog, 2019. 132: p. 230-242.
122. **Geske, G.D., M.E. Mattmann, and H.E. Blackwell,** *Evaluation of a focused library of N-aryl L-homoserine lactones reveals a new set of potent quorum sensing modulators.* Bioorg Med Chem Lett, 2008. 18(22): p. 5978-81.
123. **Brackman, G., et al.,** *The Quorum Sensing Inhibitor Hamamelitannin Increases Antibiotic Susceptibility of Staphylococcus aureus Biofilms by Affecting Peptidoglycan Biosynthesis and eDNA Release.* Scientific Reports, 2016. 6(1): p. 20321.
124. **Brackman, G., et al.,** *Cinnamaldehyde and cinnamaldehyde derivatives reduce virulence in Vibrio spp. by decreasing the DNA-binding activity of the quorum sensing response regulator LuxR.* BMC Microbiol, 2008. 8: p. 149.
125. **Albano, M., et al.,** *Antibacterial and anti-biofilm activities of cinnamaldehyde against S. epidermidis.* Microb Pathog, 2019. 126: p. 231-238.

126. **Rehman, Z.U. and T. Leiknes,** *Quorum-Quenching Bacteria Isolated From Red Sea Sediments Reduce Biofilm Formation by.* Front Microbiol, 2018. 9: p. 1354.
127. **Utari, P.D., J. Vogel, and W.J. Quax,** *Deciphering Physiological Functions of AHL Quorum Quenching Acylases.* Front Microbiol, 2017. 8: p. 1123.
128. **Haney, E.F., S.C. Mansour, and R.E.W. Hancock**, *Antimicrobial Peptides: An Introduction*, in *Antimicrobial Peptides: Methods and Protocols*, P.R. Hansen, Editor. 2017, Springer New York: New York, NY. p. 3-22.
129. **Yasir, M., M.D.P. Willcox, and D. Dutta,** *Action of Antimicrobial Peptides against Bacterial Biofilms.* Materials (Basel), 2018. 11(12).
130. **Pletzer, D., S.R. Coleman, and R.E. Hancock,** *Anti-biofilm peptides as a new weapon in antimicrobial warfare.* Curr Opin Microbiol, 2016. 33: p. 35-40.
131. **Overhage, J., et al.,** *Human host defense peptide LL-37 prevents bacterial biofilm formation.* Infect Immun, 2008. 76(9): p. 4176-82.
132. **Shahrour, H., et al.**, *AMPs as Anti-biofilm Agents for Human Therapy and Prophylaxis*, in *Antimicrobial Peptides: Basics for Clinical Application*, K. Matsuzaki, Editor. 2019, Springer Singapore: Singapore. p. 257-279.
133. **Fleming, D. and K.P. Rumbaugh,** *Approaches to Dispersing Medical Biofilms.* Microorganisms, 2017. 5(2).
134. **de la Fuente-Núñez, C., et al.,** *D-enantiomeric peptides that eradicate wild-type and multidrug-resistant biofilms and protect against lethal Pseudomonas aeruginosa infections.* Chem Biol, 2015. 22(2): p. 196-205.
135. **de la Fuente-Núñez, C., et al.,** *Broad-spectrum anti-biofilm peptide that targets a cellular stress response.* PLoS Pathog, 2014. 10(5): p. e1004152.
136. **Ansari, J.M., et al.,** *Anti-Biofilm Activity of a Self-Aggregating Peptide against Streptococcus mutans.* Front Microbiol, 2017. 8: p. 488.
137. **Brancatisano, F.L., et al.,** *Inhibitory effect of the human liver-derived antimicrobial peptide hepcidin 20 on biofilms of polysaccharide intercellular adhesin (PIA)-positive and PIA-negative strains of Staphylococcus epidermidis.* Biofouling, 2014. 30(4): p. 435-46.
138. **Libardo, M.D.J., et al.,** *Nuclease activity gives an edge to host-defense peptide piscidin 3 over piscidin 1, rendering it more effective against persisters and biofilms.* FEBS J, 2017. 284(21): p. 3662-3683.
139. **Heinbockel, L., et al.**, *Anti-Infective Polypeptides for Combating Bacterial and Viral Infections*. 2014. p. 3-31.
140. **Fleming, D. and K. Rumbaugh,** *The Consequences of Biofilm Dispersal on the Host.* Sci Rep, 2018. 8(1): p. 10738.
141. **Baelo, A., et al.,** *Disassembling bacterial extracellular matrix with DNase-coated nanoparticles to enhance antibiotic delivery in biofilm infections.* J Control Release, 2015. 209: p. 150-8.
142. **Shah, P.I., et al.,** *Recombinant human DNase I in cystic fibrosis patients with severe pulmonary disease: a short-term, double-blind study followed by six months open-label treatment.* Eur Respir J, 1995. 8(6): p. 954-8.
143. **Shire, S.J.**, *Stability Characterization and Formulation Development of Recombinant Human Deoxyribonuclease I [Pulmozyme®, (Dornase Alpha)]*, in *Formulation, Characterization, and Stability of Protein Drugs: Case Histories: Case Histories*, R. Pearlman and Y.J. Wang, Editors. 2002, Springer US: Boston, MA. p. 393-426.
144. **Nemoto, K., et al.,** *Effect of Varidase (streptodornase) on biofilm formed by Pseudomonas aeruginosa.* Chemotherapy, 2003. 49(3): p. 121-5.
145. **Shields, R.C., et al.,** *Efficacy of a marine bacterial nuclease against biofilm forming microorganisms isolated from chronic rhinosinusitis.* PLoS One, 2013. 8(2): p. e55339.
146. **Okshevsky, M., V.R. Regina, and R.L. Meyer,** *Extracellular DNA as a target for biofilm control.* Curr Opin Biotechnol, 2015. 33: p. 73-80.
147. **Kovach, K.N., et al.,** *Specific Disruption of Established P. aeruginosa Biofilms Using Polymer-Attacking Enzymes.* bioRxiv, 2019: p. 598979.

148. **Waryah, C.B., et al.,** *In Vitro Antimicrobial Efficacy of Tobramycin Against Staphylococcus aureus Biofilms in Combination With or Without DNase I and/or Dispersin B: A Preliminary Investigation.* Microb Drug Resist, 2017. 23(3): p. 384-390.
149. **Loughran, A.J., et al.,** *Impact of individual extracellular proteases on Staphylococcus aureus biofilm formation in diverse clinical isolates and their isogenic sarA mutants.* Microbiologyopen, 2014. 3(6): p. 897-909.
150. **Nguyen, U.T. and L.L. Burrows,** *DNase I and proteinase K impair Listeria monocytogenes biofilm formation and induce dispersal of pre-existing biofilms.* International Journal of Food Microbiology, 2014. 187: p. 26-32.
151. **Kumar Shukla, S. and T.S. Rao,** *Dispersal of Bap-mediated Staphylococcus aureus biofilm by proteinase K.* J Antibiot (Tokyo), 2013. 66(2): p. 55-60.
152. **Pelgrift, R.Y. and A.J. Friedman,** *Nanotechnology as a therapeutic tool to combat microbial resistance.* Advanced Drug Delivery Reviews, 2013. 65(13): p. 1803-1815.
153. **Dos Santos Ramos, M.A., et al.,** *Nanotechnology-based drug delivery systems for control of microbial biofilms: a review.* Int J Nanomedicine, 2018. 13: p. 1179-1213.
154. **Rukavina, Z. and Ž. Vanić,** *Current Trends in Development of Liposomes for Targeting Bacterial Biofilms.* Pharmaceutics, 2016. 8(2).
155. **Zhang, J., et al.,** *Amikacin Liposome Inhalation Suspension (ALIS) Penetrates Non-tuberculous Mycobacterial Biofilms and Enhances Amikacin Uptake Into Macrophages.* Front Microbiol, 2018. 9: p. 915.
156. **Clancy, J.P., et al.,** *Phase II studies of nebulised Arikace in CF patients with Pseudomonas aeruginosa infection.* Thorax, 2013. 68(9): p. 818-25.
157. **Beaulac, C., S. Sachetelli, and J. Lagace,** *In-vitro bactericidal efficacy of sub-MIC concentrations of liposome-encapsulated antibiotic against gram-negative and gram-positive bacteria.* J Antimicrob Chemother, 1998. 41(1): p. 35-41.
158. **Jones, M.N., et al.,** *Antibacterial reactive liposomes encapsulating coupled enzyme systems.* International Journal of Pharmaceutics, 1998. 162(1): p. 107-117.
159. **Halwani, M., et al.,** *Co-encapsulation of gallium with gentamicin in liposomes enhances antimicrobial activity of gentamicin against Pseudomonas aeruginosa.* J Antimicrob Chemother, 2008. 62(6): p. 1291-7.
160. **Sandreschi, S., et al.,** *Perspectives on polymeric nanostructures for the therapeutic application of antimicrobial peptides.* Nanomedicine (Lond), 2016. 11(13): p. 1729-44.
161. **Gaspar, M.C., et al.,** *Development of levofloxacin-loaded PLGA microspheres of suitable properties for sustained pulmonary release.* Int J Pharm, 2019. 556: p. 117-124.
162. **Patel, K.K., et al.,** *Alginate lyase immobilized chitosan nanoparticles of ciprofloxacin for the improved antimicrobial activity against the biofilm associated mucoid P. aeruginosa infection in cystic fibrosis.* Int J Pharm, 2019. 563: p. 30-42.
163. **Liu, Y., et al.,** *Surface-Adaptive, Antimicrobially Loaded, Micellar Nanocarriers with Enhanced Penetration and Killing Efficiency in Staphylococcal Biofilms.* ACS Nano, 2016. 10(4): p. 4779-89.
164. **Martin-Serrano, Á., et al.,** *Nanosystems as Vehicles for the Delivery of Antimicrobial Peptides (AMPs).* Pharmaceutics, 2019. 11(9).
165. **Hassani Sangani, M., M. Nakhaei Moghaddam, and M.M. Forghanifard,** *Inhibitory effect of zinc oxide nanoparticles on pseudomonas aeruginosa biofilm formation.* Nanomedicine Journal, 2015. 2(2): p. 121-128.
166. **Gurunathan, S., et al.,** *Enhanced antibacterial and anti-biofilm activities of silver nanoparticles against Gram-negative and Gram-positive bacteria.* Nanoscale Res Lett, 2014. 9(1): p. 373.
167. **Tasia, W., et al.,** *Enhanced eradication of bacterial biofilms with DNase I-loaded silver-doped mesoporous silica nanoparticles.* Nanoscale, 2020. 12(4): p. 2328-2332.
168. **Barraud, N., et al.,** *Nitric oxide: a key mediator of biofilm dispersal with applications in infectious diseases.* Curr Pharm Des, 2015. 21(1): p. 31-42.

169. **Barraud, N., et al.,** *Nitric oxide signaling in Pseudomonas aeruginosa biofilms mediates phosphodiesterase activity, decreased cyclic di-GMP levels, and enhanced dispersal.* J Bacteriol, 2009. 191(23): p. 7333-42.
170. **Babaei, S., et al.,** *Role of nitric oxide in the angiogenic response in vitro to basic fibroblast growth factor.* Circ Res, 1998. 82(9): p. 1007-15.
171. **Gusarov, I., et al.,** *Endogenous nitric oxide protects bacteria against a wide spectrum of antibiotics.* Science, 2009. 325(5946): p. 1380-4.
172. **Yasbolaghi, J., et al.,** *Advanced strategies for combating bacterial biofilms.* Journal of Cellular Physiology, 2019.
173. **Fong, S., et al.,** *Activity of Bacteriophages in Removing Biofilms of Pseudomonas aeruginosa Isolates from Chronic Rhinosinusitis Patients.* Frontiers in Cellular and Infection Microbiology, 2017. 7: p. 418.
174. **Novotny, L.A., et al.,** *Monoclonal antibodies against DNA-binding tips of DNABII proteins disrupt biofilms in vitro and induce bacterial clearance in vivo.* EBioMedicine, 2016. 10: p. 33-44.
175. **Campana, R., et al.,** *Activity of essential oil-based microemulsions against Staphylococcus aureus biofilms developed on stainless steel surface in different culture media and growth conditions.* Int J Food Microbiol, 2017. 241: p. 132-140.
176. **Kerekes, E.B., et al.,** *Anti-Biofilm Effect of Selected Essential Oils and Main Components on Mono- and Polymicrobic Bacterial Cultures.* Microorganisms, 2019. 7(9).
177. **Liu, M.Y., et al.,** *Rifampicin-Manuka Honey Combinations Are Superior to Other Antibiotic-Manuka Honey Combinations in Eradicating Staphylococcus aureus Biofilms.* Frontiers in Microbiology, 2018. 8(2653).
178. **May, R.M., et al.,** *An engineered micropattern to reduce bacterial colonization, platelet adhesion and fibrin sheath formation for improved biocompatibility of central venous catheters.* Clin Transl Med, 2015. 4: p. 9.
179. **Pinto, R.M., et al.,** *Innovative Strategies Toward the Disassembly of the EPS Matrix in Bacterial Biofilms.* Frontiers in Microbiology, 2020. 11(952).
180. **Ahn, K.C., et al.,** *In vitro biologic activities of the antimicrobials triclocarban, its analogs, and triclosan in bioassay screens: receptor-based bioassay screens.* Environ Health Perspect, 2008. 116(9): p. 1203-10.
181. **Park, S.N., S.J. Ahn, and J.K. Kook,** *Oleanolic acid and ursolic acid inhibit peptidoglycan biosynthesis in Streptococcus mutans UA159.* Braz J Microbiol, 2015. 46(2): p. 613-7.
182. **Pavel, I.Z., et al.,** *In Vitro Evaluation of the Antimicrobial Ability and Cytotoxicity on Two Melanoma Cell Lines of a Benzylamide Derivative of Maslinic Acid.* Anal Cell Pathol (Amst), 2016. 2016: p. 2787623.
183. **Zhu, B. and H. Yin,** *Alginate lyase: Review of major sources and classification, properties, structure-function analysis and applications.* Bioengineered, 2015. 6(3): p. 125-31.
184. **Gracia, R., et al.,** *Biocompatible single-chain polymer nanoparticles loaded with an antigen mimetic as potential anticancer vaccine.* ACS Macro Letters, 2018. 7(2): p. 196-200.
185. **O'Neill, J.** *Tackling drug-resistant infections globally: final report and recommendations*. in *AMR Review*. 2016. London, UK.
186. **Wolfmeier, H., et al.,** *New Perspectives in Biofilm Eradication.* ACS Infect Dis, 2018. 4(2): p. 93-106.
187. **Hassoun, A., P.K. Linden, and B. Friedman,** *Incidence, prevalence, and management of MRSA bacteremia across patient populations-a review of recent developments in MRSA management and treatment.* Crit Care, 2017. 21(1): p. 211.
188. **Schebb, N.H., et al.,** *Investigation of human exposure to triclocarban after showering and preliminary evaluation of its biological effects.* Environ Sci Technol, 2011. 45(7): p. 3109-15.
189. **Halden, R.U., et al.,** *The Florence Statement on Triclosan and Triclocarban.* Environ Health Perspect, 2017. 125(6): p. 064501.
190. **Altomonte, S. and M. Zanda,** *Synthetic chemistry and biological activity of pentafluorosulphanyl (SF5) organic molecules.* Journal of Fluorine Chemistry, 2013. 143: p. 57–93.

191. **Jesus, J.A., et al.,** *Antimicrobial activity of oleanolic and ursolic acids: an update.* Evid Based Complement Alternat Med, 2015. 2015: p. 620472.
192. **Rufino-Palomares, E.,** *Anti-cancer and Anti-angiogenic Properties of Various Natural Pentacyclic Triterpenoids and Some of their Chemical Derivatives.* Curr Org Chem, 2015. 19(10).
193. **Kim, S., et al.,** *Antimicrobial action of oleanolic acid on Listeria monocytogenes, Enterococcus faecium, and Enterococcus faecalis.* PLoS One, 2015. 10(3): p. e0118800.
194. **Enright, M.C., et al.,** *The evolutionary history of methicillin-resistant Staphylococcus aureus (MRSA).* Proc Natl Acad Sci U S A, 2002. 99(11): p. 7687-92.
195. **Zhong, Q., et al.,** *Metabolic network and recovery mechanism of Escherichia coli associated with triclocarban stress.* Ecotoxicol Environ Saf, 2020. 206: p. 111140.
196. **Maiden, M.M. and C.M. Waters,** *Triclosan depletes the membrane potential in Pseudomonas aeruginosa biofilms inhibiting aminoglycoside induced adaptive resistance.* PLoS Pathog, 2020. 16(10): p. e1008529.
197. **Malanovic, N. and K. Lohner,** *Gram-positive bacterial cell envelopes: The impact on the activity of antimicrobial peptides.* Biochim Biophys Acta, 2016. 1858(5): p. 936-46.
198. **Kay, S., et al.,** *Galleria mellonella Infection Model Identifies Both High and Low Lethality of Clostridium perfringens Toxigenic Strains and Their Response to Antimicrobials.* Front Microbiol, 2019. 10: p. 1281.
199. **Jaskiewicz, M., et al.,** *Methods Used for the Eradication of Staphylococcal Biofilms.* Antibiotics (Basel), 2019. 8(4).
200. **Filkins, L.M. and G.A. O'Toole,** *Cystic Fibrosis Lung Infections: Polymicrobial, Complex, and Hard to Treat.* PLoS Pathog, 2015. 11(12): p. e1005258.
201. **Kidd, T.J., et al.,** *Defining antimicrobial resistance in cystic fibrosis.* J Cyst Fibros, 2018.
202. **Paredes, J., S. Becerro, and S. Arana,** *Comparison of real time impedance monitoring of bacterial biofilm cultures in different experimental setups mimicking real field environments.* Sensors and Actuators B: Chemical, 2014. 195: p. 667-676.
203. **Pires, L., et al.,** *Online monitoring of biofilm growth and activity using a combined multi-channel impedimetric and amperometric sensor.* Biosens Bioelectron, 2013. 47: p. 157-63.
204. **Gacesa, P.,** *Enzymic degradation of alginates.* Int J Biochem, 1992. 24(4): p. 545-52.
205. **Lamppa, J.W. and K.E. Griswold,** *Alginate lyase exhibits catalysis-independent biofilm dispersion and antibiotic synergy.* Antimicrob Agents Chemother, 2013. 57(1): p. 137-45.
206. **Fulaz, S., et al.,** *Nanoparticle-Biofilm Interactions: The Role of the EPS Matrix.* Trends Microbiol, 2019.
207. **Makabenta, J.M.V., et al.,** *Nanomaterial-based therapeutics for antibiotic-resistant bacterial infections.* Nat Rev Microbiol, 2020.
208. **Gracia, R., et al.,** *Synthesis and functionalization of dextran-based single-chain nanoparticles in aqueous media.* J Mater Chem B, 2017. 5(6): p. 1143-1147.
209. **Falciani, C., et al.,** *Antimicrobial Peptide-Loaded Nanoparticles as Inhalation Therapy for Pseudomonas aeruginosa Infections.* Int J Nanomedicine, 2020. 15: p. 1117-1128.
210. **Ritter, D., et al.,** *In vitro inhalation cytotoxicity testing of therapeutic nanosystems for pulmonary infection.* Toxicol In Vitro, 2020. 63: p. 104714.
211. **van der Weide, H., et al.,** *Therapeutic Efficacy of Novel Antimicrobial Peptide AA139-Nanomedicines in a Multidrug-Resistant Klebsiella pneumoniae Pneumonia-Septicemia Model in Rats.* Antimicrob Agents Chemother, 2020. 64(9).
212. **Chiang, W.C., et al.,** *Extracellular DNA shields against aminoglycosides in Pseudomonas aeruginosa biofilms.* Antimicrob Agents Chemother, 2013. 57(5): p. 2352-61.
213. **Dengler, V., et al.,** *An Electrostatic Net Model for the Role of Extracellular DNA in Biofilm Formation by Staphylococcus aureus.* J Bacteriol, 2015. 197(24): p. 3779-87.
214. **Wan, F., et al.,** *Ultrasmall TPGS-PLGA Hybrid Nanoparticles for Site-Specific Delivery of Antibiotics into Pseudomonas aeruginosa Biofilms in Lungs.* ACS Appl Mater Interfaces, 2020. 12(1): p. 380-389.
215. **Miller, K.P., et al.,** *Inorganic nanoparticles engineered to attack bacteria.* Chem Soc Rev, 2015. 44(21): p. 7787-807.

ANNEXOS

ANNEX 1: ARTICLE 6

Aerobic Vitamin B_{12} Biosynthesis Is Essential for *Pseudomonas aeruginosa* Class II Ribonucleotide Reductase Activity During Planktonic and Biofilm Growth

Publicat a la revista *Frontiers in Microbiology* (Q1, IF_{2018} = 4.259)

DOI: 10.3389/fmicb.2018.00986

Maig 2018

Autors: Anna Crespo[1], **Núria Blanco-Cabra**[1], Eduard Torrents[1]*

1 Bacterial Infections and Antimicrobial Therapies, Institute for Bioengineering of Catalonia (IBEC) The Barcelona Institute of Science and Technology (BIST), Barcelona, Spain.

* Correspondència: Dr. Eduard Torrents (etorrents@ibecbarcelona.eu);

frontiers in Microbiology

ORIGINAL RESEARCH
published: 15 May 2018
doi: 10.3389/fmicb.2018.00986

Aerobic Vitamin B_{12} Biosynthesis Is Essential for *Pseudomonas aeruginosa* Class II Ribonucleotide Reductase Activity During Planktonic and Biofilm Growth

*Anna Crespo, Núria Blanco-Cabra and Eduard Torrents**

Bacterial Infections and Antimicrobial Therapies, Institute for Bioengineering of Catalonia, Barcelona Institute of Science and Technology, Barcelona, Spain

Pseudomonas aeruginosa is a major pathogenic bacterium in chronic infections and is a model organism for studying biofilms. *P. aeruginosa* is considered an aerobic bacterium, but in the presence of nitrate, it also grows in anaerobic conditions. Oxygen diffusion through the biofilm generates metabolic and genetic diversity in *P. aeruginosa* growth, such as in ribonucleotide reductase activity. These essential enzymes are necessary for DNA synthesis and repair. Oxygen availability determines the activity of the three-ribonucleotide reductase (RNR) classes. Class II and III RNRs are active in the absence of oxygen; however, class II RNRs, which are important in *P. aeruginosa* biofilm growth, require a vitamin B_{12} cofactor for their enzymatic activity. In this work, we elucidated the conditions in which class II RNRs are active due to vitamin B_{12} concentration constraints (biosynthesis or environmental availability). We demonstrated that increased vitamin B_{12} levels during aerobic, stationary and biofilm growth activate class II RNR activity. We also established that the *cobN* gene is essentially responsible for B_{12} biosynthesis under planktonic and biofilm growth. Our results unravel the mechanisms of dNTP synthesis by *P. aeruginosa* during biofilm growth, which appear to depend on the bacterial strain (laboratory-type or clinical isolate).

Keywords: Vitamin B_{12}, adenosylcobalamin, ribonucleotide reductases, *Pseudomonas aeruginosa*, NrdJ, bacterial growth, biofilm, anaerobiosis

OPEN ACCESS

Edited by:
Ivan Mijakovic, Chalmers University of Technology, Sweden

Reviewed by:
Paraskevi Papaioannidou, Aristotle University of Thessaloniki, Greece
Dinesh Sriramulu, Shres Consultancy (Life Sciences), India

****Correspondence:***
Eduard Torrents
etorrents@ibecbarcelona.eu

Specialty section:
This article was submitted to Microbial Physiology and Metabolism, a section of the journal Frontiers in Microbiology

Received: *09 January 2018*
Accepted: *26 April 2018*
Published: *15 May 2018*

Citation:
Crespo A, Blanco-Cabra N and Torrents E (2018) Aerobic Vitamin B_{12} Biosynthesis Is Essential for Pseudomonas aeruginosa Class II Ribonucleotide Reductase Activity During Planktonic and Biofilm Growth. Front. Microbiol. 9:986. doi: 10.3389/fmicb.2018.00986

INTRODUCTION

Pseudomonas aeruginosa is an opportunistic pathogen that causes severe chronic infections in immunocompromised patients and other risk groups, such as cystic fibrosis (CF) or chronic obstructive pulmonary disease (COPD) patients. The key to *P. aeruginosa* survival in environments that range from soil to various living host organisms is its metabolic versatility. It subsists on various carbon sources for energy, uses nitrogen as a terminal electron acceptor under anaerobic conditions, requires minimal nutrients, and grows at temperatures up to 42°C. *P. aeruginosa* uses anaerobic metabolism to reduce nitrogen (N_2) via the denitrification process (Schobert and Jahn, 2010; Arat et al., 2015), as an essential metabolic condition during chronic infection and biofilm growth (Yoon et al., 2006; Hassett et al., 2009; Crespo et al., 2016).

During *P. aeruginosa* infections, bacteria must multiply inside the infected organisms (plant, animal, insect, etc.), requiring active DNA synthesis for bacterial cell division. Ribonucleotide reductase (RNR) enzymes provide all living organisms with deoxyribonucleotide triphosphates (dNTP) supplying the monomers for DNA synthesis. Three different RNR classes exist (class I, subdivided into Ia, Ib, and Ic; class II and class III) that differ in their overall protein structure and cofactor requirements, but all possess allosteric regulation and use organic radicals to initiate catalysis through free radical chemistry (Jordan and Reichard, 1998; Cotruvo Jr and Stubbe, 2011; Hofer et al., 2012; Torrents, 2014). *P. aeruginosa* is one of the few organisms that encode three different RNR classes; the oxygen-dependent class Ia (encoded by the *nrdAB* genes), the oxygen-independent class II (encoded by the *nrdJab* genes) and the oxygen-sensitive class III (encoded by the *nrdDG* genes). Specifically, class II RNR activity depends on an external cofactor, adenosylcobalamin (AdoCob) or vitamin B_{12}, to generate its radical independently of oxygen to reduce the different ribonucleotides to their corresponding deoxyribonucleotides.

Vitamin B_{12} is one of the most structurally complex cofactors synthesized by bacteria (Warren et al., 2002); however, not all microorganisms encode for the ∼25 genes needed for the complete biosynthetic pathway. In nature, two vitamin B_{12} biosynthesis pathways exist: the aerobic, or late cobalt insertion pathway and the anaerobic, or early cobalt insertion pathway (Warren et al., 2002). One of the genes involved in the aerobic pathway that participates in cobalt insertion is the *cobN* gene described extensively in *Pseudomonas denitrificans* (Warren et al., 2002). The most studied anaerobic biosynthetic pathway involved in early cobalt insertion was described in *Salmonella typhymurium* (Roth et al., 1993).

Pseudomonas synthesizes vitamin B_{12} for different metabolic reactions, such as methionine synthesis, cobalamin biosynthesis, and RNR enzymes. One essential reaction is ribonucleotide synthesis by RNR. *P. aeruginosa* PAO1 has been demonstrated to grow in a filament cell morphology due to cellular stress by RNR activity depletion, such as the low expression levels of class III RNR under anaerobic conditions (Lee et al., 2012; Crespo et al., 2017) or the high nitric oxide levels in the denitrification process, which interacts with a cobalamin precursor of the vitamin B_{12} pathway (Broderick et al., 2005; Yoon et al., 2011; Sullivan et al., 2013). Therefore, this cell filamentation results from DNA replication impairment that affects *P. aeruginosa* PAO1 cell division, thus affecting infection (Sjöberg and Torrents, 2011; Crespo et al., 2017), anaerobic growth (Torrents et al., 2005; Torrents, 2014) and biofilm growth (Crespo et al., 2016). Class II and III RNR enzymes reduce ribonucleotides under these conditions. Thus, their activity is essential for cell division (Crespo et al., 2016, 2017).

Class II RNR (NrdJab) activity is oxygen independent, but it strictly depends on vitamin B_{12} availability. To date, the link between internal vitamin B_{12} biosynthesis or availability from the environment and the real class II RNR activity is unknown. Therefore, in this work, we analyzed *P. aeruginosa* vitamin B_{12} biosynthesis during aerobic growth, anaerobic growth and biofilm formation. We also determined the relationship between vitamin B_{12} biosynthesis and class II RNR activity under different growing conditions.

MATERIALS AND METHODS

Bacterial Strains and Growth Conditions

Pseudomonas aeruginosa and *Escherichia coli* strains, listed in **Table 1**, were grown in Luria-Bertani broth (LB) or minimum medium (MM) (Kjaergaard et al., 2000) at 37°C. MM containing 1% KNO_3 (MMN) was used for anaerobic liquid growth in screw-cap tubes (Hungate tubes) (Garriga et al., 1996; Crespo et al., 2016) or in anaerobic plates using the GENbag system (bioMérieux) according to the manufacturer's instructions.

The medium was supplemented, when necessary, with the following antibiotics: 100 μg/ml or 50 μg/mL gentamicin, 300 μg/ml carbenicillin and 40 μg/ml tetracycline for *P. aeruginosa*, and 10 μg/ml gentamicin and 50 μg/ml ampicillin for *E. coli.*

Construction of *cobN* Deletion Mutant Strain

Pseudomonas aeruginosa PAO1 with a mutation in the *cobN* gene (ETS126; Δ*cobN*) was constructed by inserting the gentamicin-resistance gene (*aacC1*) into the *cobN* gene by homologous recombination using the pEX18Tc vector, as previously described (Quenee et al., 2005; Sjöberg and Torrents, 2011). Briefly, two 400-bp areas surrounding the *P. aeruginosa* PAO1 *cobN* gene were amplified by PCR using the High-Fidelity PCR Enzyme Mix (Thermo Scientific) with the primer pairs, CobN1HIII-up/CobN2BI-low and CobN3BI-up/CobN4SI-low, listed in **Table 2**. The two amplicons were cloned separately into the pJET1.2 vector (Thermo Scientific). A plasmid containing both fragments was generated by *BamHI*/*SacI* digestion. The gentamicin resistance gene *aacC1* was obtained using *Bam*HI digestion of pUCGmlox, and the corresponding cassette was ligated to the two fragments. The construct was cloned into the *sac*B gene-based counter-selection pEX18Tc vector and transferred into the S17.1λ*pir* strain for *P. aeruginosa* PAO1 conjugation as previously described (Crespo et al., 2016). Transconjugants were selected by plating them with tetracycline, gentamicin and sucrose (5%), used for *sacB*-mediated plasmid counter selection. *aacC1* insertion was screened and verified by PCR with the primer pair CobN1HIII-up/CobN5-low and later confirmed by DNA sequencing.

Quantitative Real-Time PCR (qRT-PCR)

Transcripts of RNR genes (*nrdA, nrdJ* and *nrdD)* were quantified using quantitative real-time PCR (qRT-PCR). *P. aeruginosa* was grown in planktonic conditions at the mid-exponential growth phase in which samples were treated with RNAprotect Bacterial Reagent (Qiagen). The RNeasy Mini Kit (Qiagen) was used to isolate and purify total RNA, and extra DNA was removed using DNase I (Turbo DNA-free, Applied Biosystems) per the manufacturer's instructions.

TABLE 1 | Strains and plasmids used in this study.

Strain or plasmid	Description	Source
PLASMIDS		
pJET1.2/blunt	*Blunt-end vector, AmpR*	*Thermo Scientific*
pUCGmlox	Ap^R, Gm^R; source of Gm^R cassette	Hoang et al., 1998
pEX18Tc	*sac*B based counter-selection vector, Tc^R	Hoang et al., 1998
pETS160	pBBR1 derivative carrying *nrdDG* operon, Gm^R	Sjöberg and Torrents, 2011
pETS134	pETS130 derivative carrying *nrdA* promoter, Gm^R	Sjöberg and Torrents, 2011
pETS136	pETS130 derivative carrying *nrdD* promoter, Gm^R	Sjöberg and Torrents, 2011
pETS180	pETS130 derivative carrying *nrdJ* promoter, Gm^R	Crespo et al., 2015
STRAINS		
E. coli		
DH5α	*recA1 endA1 hsdR17 supE44 thi-1 relA1 Δ(lacZYA-argF)U169 deoR Φ80dlacZM15*	Lab stock
S17.1 λ*pir*	*recA thi pro hsdR- M+RP4::2-Tc::Mu::Km Tn7 Tpr Smr Xpir*	de Lorenzo et al., 1993
P. aeruginosa		
PAO1	Wild-type (ATCC 15692 / CECT 4122)- Spanish Type Culture Collection	Lab strain
PA14	Wild-type *P. aeruginosa* PA14	Lab strain
PAET1	*CF strain isolated from chronic patient*	Lab strain, (Crespo et al., 2017)
ETS102 (Δ***nrdJ***)	*P. aeruginosa* PAO1 *nrdJ*::ΩTc; Tc^R	Sjöberg and Torrents, 2011
ETS103 (Δ***nrdD***)	*P. aeruginosa* PAO1 *nrdD*::ΩTc; Tc^R	Sjöberg and Torrents, 2011
ETS125 (Δ***nrdJ*Δ*nrdD***)	*P. aeruginosa* PAO1 *nrdD*::ΩTc; Tc^R, *nrdJ*::ΩGm; Gm^R	Crespo et al., 2016
ETS126 (Δ***cobN***)	*P. aeruginosa* PAO1 *cobN*::ΩGm, Gm^R	This work

TABLE 2 | Oligonucleotides and probes used in this study.

Name	Sequence (5′ → 3′)	Application
pJET-rev	AAGAACATCGATTTTCCATGGCAG	Check-Cloning
pJET-up	CGACTCACTATAGGGAGAGCGGC	Check-Cloning
CobN1HIII-up	AAGCTTATGCACCTGTTGCGCACCC	Cloning
CobN2BI-low	GGATCCCAGAAGCGCTCGGCCTGCT	Cloning
CobN3BI-up	GGATCCTGAATCCGAAGTGGATCGC	Cloning
CobN4SI-low	GAGCTCCTATTCCTCTTCCGACGTCCA	Cloning
CobN5-low	CAGGCCAGGCCCTTGAAAC	Cloning
gapTaqM-low	GAGGTTCTGGTCGTTGGT	qRT-PCR
nrdATaqM2-low	TGTTCATGTCGTGGGTACG	qRT-PCR
nrdJTaqM2-low	GTAAACACCCGCACCACTTC	qRT-PCR
nrdDTaqM2-low	CCGAGTTGAGGAAGTTCTGG	qRT-PCR
Univ-Res-Gen-lw	AAGAATTCACGCGTCGCTCATGAGACAATA	Cloning
Univ-Res-Gen-up	AAGAATTCACGCGTATATATGAGTAAACTT	Cloning
nrdA-FAM	CTGGCACCTGGACATC	qRT-PCR probe
nrdJ-FAM	TCGGCTCGGTCAACCT	qRT-PCR probe
nrdD-FAM	CCCGACCTACAACATC	qRT-PCR probe
gap-FAM	CCTGCACCACCAACTG	qRT-PCR probe

DNA contaminations were verified by PCR. cDNA was synthetized using 0.5 μg of RNA with SuperScript III Reverse Transcriptase (Thermo Scientific). The primers used are listed in **Table 2** (Crespo et al., 2016). RNA was quantified using a NanoDrop 1000 spectrophotometer (Thermo Scientific). The *gapA* gene was used to normalize the transcript gene levels.

Green Fluorescent Protein Gene Reporter Assay

GFP fluorescence expressed in plasmids, pETS134 (P*nrdA*), pETS180 (P*nrdJ*) and pETS136 (P*nrdD*), was measured to determine each RNR gene's promoter activity. *P. aeruginosa* containing the *nrd* promoter fusion was grown to exponential phase, and three independent 1-ml samples were analyzed. Cells were fixed with 1 ml of freshly prepared PBS 1x solution containing 2% formaldehyde (Sigma) and stored in the dark at 4°C. GFP fluorescence was measured in a 96-well plate (Costar® 96-Well Black Polystyrene Plate, Corning) on an Infinite 200 Pro Fluorescence Microplate Reader (Tecan), as previously described (Crespo et al., 2015). Three measurements were performed per independent sample.

Continuous-Flow Biofilm Formation

Continuous-flow cell biofilms were grown in MM + 0.2% glucose and performed as previously described (Baelo et al., 2015; Crespo et al., 2016). These *in vitro* formed biofilms are a more natural, mature biofilm with clear oxygen concentration stratification (Stewart and Franklin, 2008). Briefly, biofilms were grown in a three-channel flow cell with a constant flow rate of 42 μl per minute for each channel using an Ismatec ISM 943 pump (Ismatec). After 5 days of growth, biofilms were stained with the LIVE/DEAD BacLight Bacterial Viability Kit (Thermo Scientific) and visualized using a Zeiss LSM 800 confocal laser scanning microscope (CSLM). Images were generated using ImageJ Fiji software, and COMSTAT 2 software was used to quantify biomass and biofilm thickness (Heydorn et al., 2000).

Vitamin B_{12} Quantification by HPLC-MS

Pseudomonas aeruginosa PAO1, PAET1, and PA14 strains were grown in MM or MMN medium for 20 h in aerobic or anaerobic conditions or for 5 days in a continuous-flow cell biofilm growth system. Cells were lysed using lysozyme (50 mg/ml) (Sigma) and sonicated five times on ice using a 6-mm sonication probe at 32% power for 20 s (Digital Sonifier, Branson). After centrifugation (4,000 × g at 4°C), the supernatants were filtrated with a 10-kDa Centricon column (Millipore). Samples were manipulated in the dark to avoid vitamin B_{12} degradation. Finally, 1% ammonium formate was added to each sample before HPLC-MS quantification. Samples of 10 µl were injected into the Luna 5-µm C18 100 Å (150 × 2 mm) column for HPLC-MS [4000 QTRAP (AB SCIEX) in an Aligent 1,200 Series] at the Separation Techniques platform of the Scientific Center Services of the Scientific Park of Barcelona (PCB). A calibration curve was constructed for vitamin B_{12} (Sigma) measured in the range of 0.1–100 ng/ml. Values were normalized, and the protein concentration was measured using a Bradford assay (Bio-Rad).

Fluorescence Microscopic Imaging and Analysis

Pseudomonas aeruginosa strain cultures were stained using the LIVE/DEAD BacLight viability kit (Thermo Scientific) for 15 min at room temperature in the dark. Fluorescent bacteria were visualized with a Nikon ECLIPSE Ti-S/L 100 inverted fluorescence microscope (Nikon) coupled with a Nikon DS-Qi2 camera. Live cells were visualized in green (SYTO 9 dye), and dead cells were visualized in red (propidium iodide dye). ImageJ software was used for image analysis.

RESULTS AND DISCUSSION

Vitamin B_{12} Availability Is Essential for Class II RNR Activity in *P. aeruginosa* Growth

Vitamin B_{12}, or adenosylcobalamin (AdoCob), acts as a radical generator for class II RNR enzyme activity, but the link between vitamin B_{12} biosynthesis and class II RNR (NrdJ) activity in *P. aeruginosa* is poorly understood, and further investigations are required, especially during bacterial biofilm growth.

We first analyzed the essentiality and role of the class II RNR enzyme under aerobic and anaerobic conditions depending on vitamin B_{12} availability. We used diverse *P. aeruginosa* PAO1 strains deficient for different RNR classes (ETS102, Δ*nrdJ*; ETS103, Δ*nrdD*, and ETS125, Δ*nrdJ*Δ*nrdD*) (see **Table 1**). We also used a specific mutant strain for the vitamin B_{12} biosynthesis pathway involved in cobalt insertion under aerobic conditions (ETS126, Δ*cobN*). As the *nrdA* mutation is unviable (Sjöberg and Torrents, 2011), we added 30 mM hydroxyurea (HU) to mimic an *nrdA* mutant strain. Hydroxyurea interferes with *P. aeruginosa* PAO1 growth, arresting DNA replication by inhibiting NrdA activity (Gale et al., 1964; Sjöberg and Torrents, 2011; Lee et al., 2012; Julian et al., 2015).

Aerobically, class Ia RNR inhibition by HU decreased *P. aeruginosa* PAO1 wild-type growth in minimal medium, as previously described (Jordan et al., 1999; Torrents et al., 2005), but after 48 h of aerobic incubation, some growth was observed (see the undiluted sample 0 with HU in *P. aeruginosa* wild-type and Δ*nrdD*) (**Figure 1**). However, any *P. aeruginosa* with either a class II RNR or a vitamin B_{12} biosynthesis gene mutation (ETS102Δ*nrdJ*, ETS125Δ*nrdJ*Δ*nrdD*, and ETS126Δ*cobN*) treated with HU showed no growth after 48 h (**Figure 1**) or even after 72 h (data not shown). This result indicates that after 48 h of HU treatment, class II RNR remains active and allows *Pseudomonas* growth. Adding vitamin B_{12} into the minimal medium containing 30 mM HU, re-establishes the optimal aerobic growth in the strains encoding an active class II RNR (NrdJ) enzyme (*P. aeruginosa* PAO1 wild-type; ETS103, Δ*nrdD* and ETS126, Δ*cobN* strains). Therefore, vitamin B_{12} availability (from biosynthesis or the environment) supports class II RNR activity and rescues class Ia RNR deficiency by HU inhibition under aerobic conditions. Thus, in this work, we demonstrated that a *cobN* gene mutation disrupted vitamin B_{12} biosynthesis and completely abolished class II RNR activity, inhibiting aerobic bacterial growth (ETS126, Δ*cobN*).

However, under anaerobic conditions, class II and III RNR mutants (Δ*nrdJ*, Δ*nrdD*, and Δ*nrdJ*Δ*nrdD*) grew slightly less than the *P. aeruginosa* PAO1 wild-type and Δ*cobN* deficient strains (**Figure 1**). Δ*cobN* mutant strain growth was unaffected anaerobically (undiluted sample, 0). This result suggests that the *cobN* gene was uninvolved in *P. aeruginosa* vitamin B_{12} biosynthesis under anaerobic conditions. Another *Pseudomonas* strain, *P. denitrificans*, was shown to only synthesize vitamin B_{12} aerobically (Roth et al., 1996). Thus, *P. aeruginosa* PAO1 cannot sustain proper growth anaerobically unless RNR activity is increased by externally adding vitamin B_{12} to the medium (1 µg/ml) (this work) or by increasing class III RNR gene copy numbers by complementing extra external NrdDG copies [ETS103 (Δ*nrdD*)+pETS60 (+NrdDG)] as previously described (Crespo et al., 2017). Nevertheless, the vitamin B_{12} anaerobic internalization pathway remains unknown, and more experiments are required.

Therefore, we demonstrated that class II RNR (NrdJ) is active in both aerobic and anaerobic conditions if vitamin B_{12} is available in the medium. However, class Ia and III RNR enzymes preferentially supply the dNTPs required for aerobic (Sjöberg and Torrents, 2011) and anaerobic (Crespo et al., 2017) bacterial DNA replication, respectively. Lack of class Ia and III RNR activity in planktonic culture, due to class Ia RNR activity inhibition by HU or by low *nrdD* expression levels, causes cell filamentation growth in *P. aeruginosa* PAO1 (Sjöberg and Torrents, 2011; Crespo et al., 2017), thus increasing its *nrd* expression (**Figure 2**). Adding vitamin B_{12} returns its cellular morphology to rod-shaped by restoring the DNA replication impairment by activating class II RNR (Crespo et al., 2017) and slightly decreasing expression of the three *nrd* genes (**Figure 2**), independently of B_{12}-riboswitch regulation (Vitreschak et al., 2003). Other vitamin B_{12}-dependent enzymes (methionine, cobalamin biosynthesis and some ribonucleotide reductases from other microorganisms) are usually regulated by a B_{12}-riboswitch on their promoter regions (Vitreschak et al., 2003; Borovok et al., 2006).

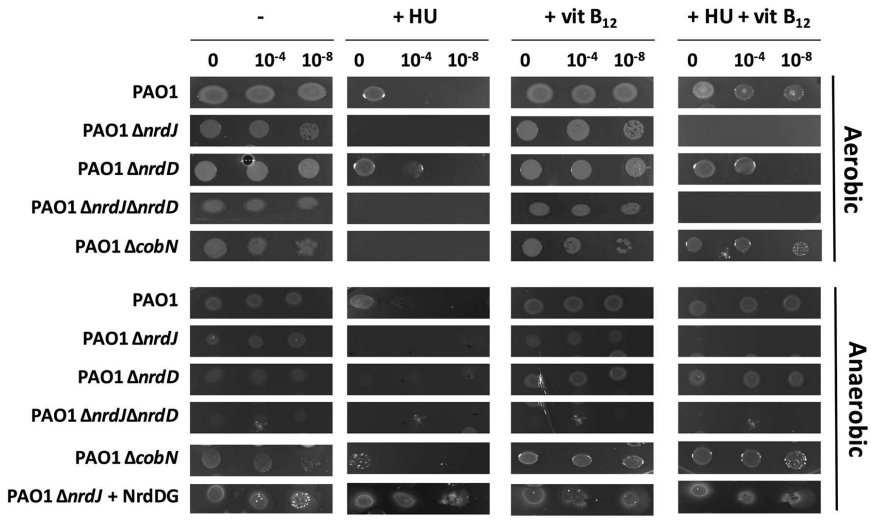

FIGURE 1 | Effect of hydroxyurea and vitamin B_{12} on *P. aeruginosa* PAO1 wild-type, Δ*nrdJ*, Δ*nrdD*, Δ*nrdJ*Δ*nrdD*, and Δ*cobN* strain growth. Five-microliter drops were plated from a 0, 10^{-4}, and 10^{-8} dilution into a solid medium containing 30 mM hydroxyurea (HU) and 1 μg/ml vitamin B_{12} (vit B_{12}) for 48 h. Pictures represent three independent experiments.

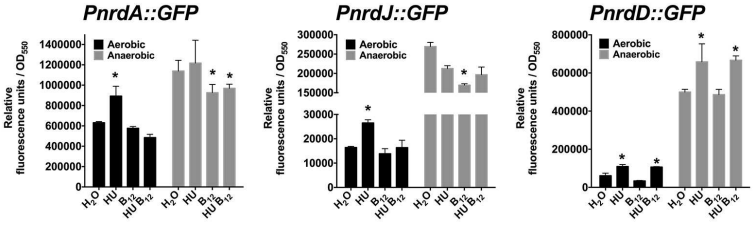

FIGURE 2 | Expression analysis of the different *P. aeruginosa* PAO1 RNR classes under HU and vitamin B_{12} treatment under aerobic and anaerobic conditions. Cultures were treated in the presence of HU (30 mM) and vitamin B_{12} (1 μg/ml) for 20 min prior to measure the relative fluorescence units of *PnrdA* (pETS134), *PnrdJ* (pETS180) and *PnrdD* (pETS136). The results are the mean of three independent experiments ± standard deviation. Asterisks over bars (*) indicate statistical differences compared to those without treatment (H_2O) ($p < 0.05$ in pairwise *t*-test calculated with GraphPad 6.0).

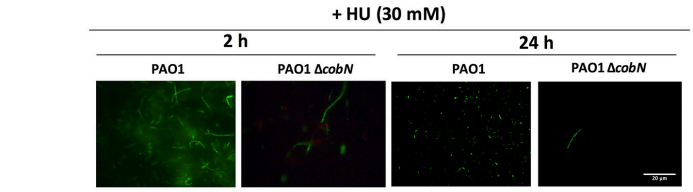

	PAO1	PAO1 Δ*cobN*	PAO1	PAO1 Δ*cobN*
OD_{550}	0.54 ± 0.06	0.42 ± 0.1	1.10 ± 0.07	0.10 ± 0.12
length (μm)	20.1 ± 2.00	22.0 ± 0.5	2.11 ± 0.20	14.7 ± 3.10

FIGURE 3 | Cell morphology after hydroxyurea treatment. Fluorescence microscopy images from aerobic *P. aeruginosa* PAO1 wild-type and Δ*cobN* growth visualized after 2 and 24 h of HU treatment. Cells were stained with the LIVE/DEAD BacLight Bacterial Viability Kit, and the bacterial length was measured using ImageJ software. The images represent at least three different experiments. Scale bars, 20 μm.

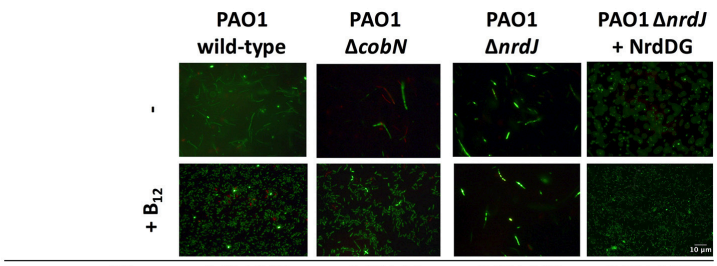

		PAO1 wild-type	PAO1 Δ*cobN*	PAO1 Δ*nrdJ*	PAO1 Δ*nrdJ* + NrdDG
-	OD_{550}	1.65 ± 0.30	1.57 ± 0.1	0.20 ± 0.20	1.87 ± 0.30
	length (µm)	23.1 ± 0.18	18.9 ± 4.0	39.0 ± 0.70	2.17 ± 0.30
+B_{12}	OD_{550}	1.95 ± 0.30	2.17 ± 0.2	0.30 ± 0.05	1.07 ± 0.02
	length (µm)	1.10 ± 0.18	1.90 ± 0.3	50.0 ± 3.00	1.70 ± 0.50

FIGURE 4 | CobN is not involved in *P. aeruginosa* PAO1 anaerobic growth. Fluorescence microscopy pictures of *P. aeruginosa* PAO1 wild-type, Δ*cobN*, Δ*nrdJ*, *and* Δ*nrdJ* + NrdDG cells stained with the LIVE/DEAD BacLight Bacterial Viability Kit at 16 h of anaerobic growth in MM ± vitamin B_{12}. The length was measured using ImageJ software. Scale bars, 10 µm.

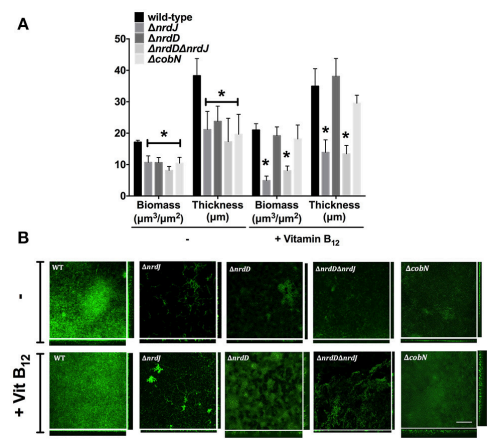

FIGURE 5 | Vitamin B_{12} enables *P. aeruginosa* biofilm formation though class II RNR activity. **(A)** The continuous-flow cell biofilm of *P. aeruginosa* PAO1 wild-type, Δ*nrdJ,* Δ*nrdD*, Δ*nrdJ*Δ*nrdD,* and Δ*cobN* strains was grown for 5 days in MM ± vitamin B_{12} (1 µg/ml). Biomass and thickness were calculated using COMSTAT software. Data are the average of three independent experiments. Asterisks over bars (*) indicate statistical differences ($p < 0.005$ in pairwise *t*-test calculated with GraphPad 6.0). **(B)** Pictures of the sum and the orthogonal views of biofilms stained with the LIVE/DEAD BacLight Bacterial Viability Kit before visualization by a confocal microscope. Images represent three independent experiments. Bars represent 200 µm.

TABLE 3 | Quantification of vitamin B_{12} levels by HPLC-MS.

	ng Vitamin B_{12}/mg protein			
	Aerobic exponential	Aerobic stationary	Anaerobic	Biofilm
PAO1	0^{nd}	0.32 ± 0.05	0^{nd}	3.72 ± 0.01
PAET1	0^{nd}	0.67 ± 0.06	0^{nd}	1.72 ± 0.05
PA14	0^{nd}	0.51 ± 0.02	0^{nd}	0.84 ± 0.01

Growth of P. aeruginosa PAO1, PAET1 and PA14 strains under aerobic (exponential OD550~0.5 and stationary OD550>2) and anaerobic conditions for 20 h (OD550~2) and under continuous-flow biofilm formation conditions (5 days). Values were normalized by protein concentration. Two independent experiments were performed, and the mean ± standard deviation is shown. nd, denotes Not-detected, below the technique detection limit.

In addition, *P. aeruginosa* PAO1 planktonic cells treated with HU for 2 h in minimal medium under aerobic conditions cause filamentous morphology (**Figure 3**); however, at 24 h post-HU treatment (late stationary phase), *P. aeruginosa* PAO1 cells return to their rod-shaped morphology without adding external vitamin B_{12} (**Figure 3**), indicating that DNA synthesis was restored only by class II RNR activity. Nevertheless, disrupting vitamin B_{12} biosynthesis using the *P. aeruginosa* PAO1 Δ*cobN* mutant strain causes filamentous cells even after 24 h of HU treatment. These results highlight an active vitamin B_{12} biosynthesis in *P. aeruginosa* PAO1 that specifically requires the *cobN* gene under aerobic stationary growing conditions for class II RNR activity and thus for DNA biosynthesis. However, vitamin B_{12} levels are insufficient during the initial hours of *P. aeruginosa* PAO1 growth (2 h) and likely reach optimal physiological levels of vitamin B_{12} after 24 h. Vitamin B_{12} biosynthesis pathway regulation requires further investigation.

Pseudomonas aeruginosa cell morphology under anaerobic conditions was filamentous due to the low class III RNR activity (Crespo et al., 2017). We also observed that the *P. aeruginosa* PAO1 Δ*cobN* mutant strain cell morphology was similar to the *P. aeruginosa* PAO1 strain, suggesting no vitamin B_{12} biosynthesis during anaerobic growth, even after

16 h (**Figure 4**). Hence, in anaerobic conditions, the *P. aeruginosa* PAO1 and Δ*cobN* strains growth needed external vitamin B_{12} supplementation for optimal class II RNR activity. This was demonstrated previously in the anaerobic *P. aeruginosa* PAO1 growth that was restored with an extra copy of *nrdDG* genes or by adding vitamin B_{12}, enhancing RNR activity (Crespo et al., 2017).

Biofilm Formation Depends on Vitamin B_{12} Synthesis

Class II and III RNR enzymes are necessary for biofilm formation when class II RNR is highly expressed (Crespo et al., 2016). Currently, it is unknown whether vitamin B_{12} is synthesized and influences class II RNR activity under biofilm conditions. Thus, we analyzed different *P. aeruginosa* strains (wild-type and isogenic mutant strains for *nrdJ, nrdD* and *cobN* genes) grown in a continuous-flow cell biofilm system. **Figure 5A** shows that aerobic biofilm formation in minimal media, measured as total biofilm biomass and average thickness, decreased when class II and III RNR were mutated. We previously reported a similar result for biofilm cells grown in LB-rich media (Crespo et al., 2016). The *P. aeruginosa* Δ*cobN* mutant strain (vitamin B_{12} deficient) decreased in biofilm formation compared to the *P. aeruginosa* PAO1 strain, similar to the produced levels in any *P. aeruginosa* deficient for class II RNR (Δ*nrdJ* and Δ*nrdJ*Δ*nrdD*) (**Figure 5A**). Furthermore, the

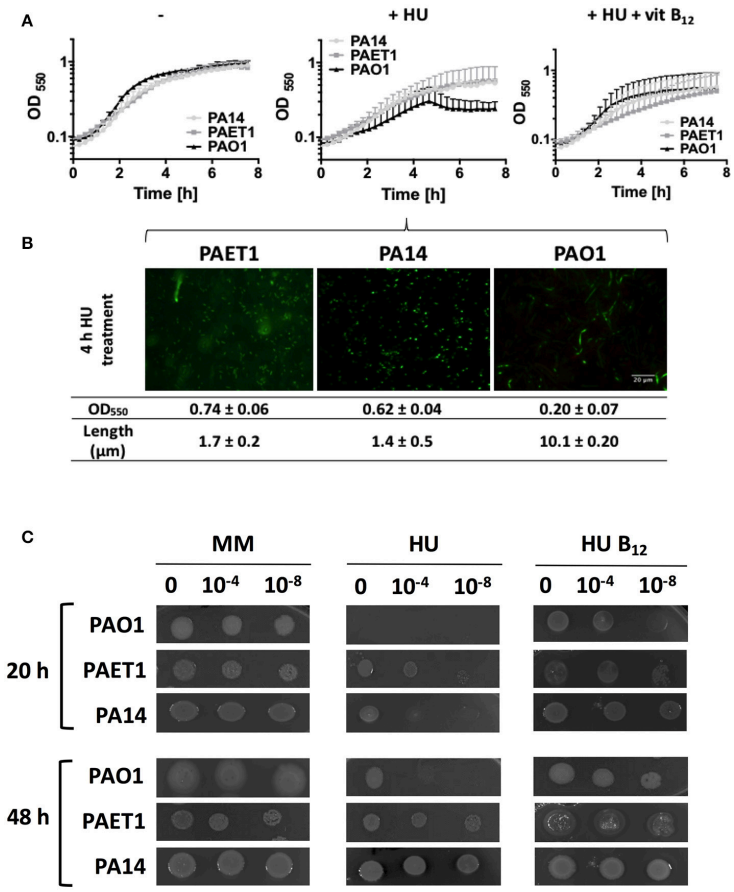

FIGURE 6 | *P. aeruginosa* PAET1 and PA14 strains are resistant to HU. **(A)** Growth curve of *P. aeruginosa* PAO1, PAET1 and PA14 strains in MM containing 30 mM hydroxyurea (HU) and 1 μg/ml vitamin B_{12}. **(B)** Cells were visualized 4 h after HU treatment. Images and values are representative of three independent experiments ± standard deviation. Bars represent 20 μm. **(C)** Aerobic *P. aeruginosa* PAO1, PAET1 and PA14 strain cell viability with HU and vitamin B_{12} at 20 or 48 h of incubation. Pictures represent three independent experiments. Cultures were diluted to 0, −4, and −8 for the growth.

biomass and thickness levels in the *P. aeruginosa* PAO1 Δ*nrdJ* and Δ*nrdJ*Δ*nrdD* mutant strains did not reach the wild-type strain levels even when vitamin B_{12} was added. However, the *P. aeruginosa* PAO1 Δ*nrdD* and Δ*cobN* mutant strain biofilm thickness increased considerably when vitamin B_{12} was added, indicating active class II RNR activity.

These results suggest an active vitamin B_{12} biosynthesis in the *P. aeruginosa* biofilm growth via the *cobN* gene. Moreover, supplying vitamin B_{12} enabled optimum *P. aeruginosa* PAO1 biofilm growth in the biofilm layers without active vitamin B_{12} biosynthesis due to oxygen concentration strengths, activating class II RNR. As expected, cell filamentation morphology, in the Δ*nrdJ* mutants, was restored by adding vitamin B_{12} to the continuous-flow biofilm (**Figure 5B**).

Vitamin B_{12} Availability During *P. aeruginosa* Aerobic and Biofilm Growth

We described that *P. aeruginosa* needs vitamin B_{12} availability during planktonic and biofilm growth, essential for class II RNR enzymatic activity. Thus, we elucidated for the first time the amount of vitamin B_{12} available for *P. aeruginosa* growth under different conditions (planktonic aerobic or anaerobic and biofilm) in different *P. aeruginosa* strains.

Quantifying vitamin B_{12} by HPLC-MS showed this molecule only in cells that were grown aerobically and in the stationary phase (**Table 3**). However, at exponential growth and in anaerobic conditions, vitamin B_{12} was detected below the technique detection limit, corroborating previous results under these conditions. Surprisingly, under 5-day-old continuous-flow biofilm *P. aeruginosa* PAO1 growth, cells produced a 10-fold increase in vitamin B_{12} compared to aerobic growth, indicating this biosynthetic pathway is activated under this circumstance. We suggested that vitamin B_{12} biosynthesis in biofilm is only produced in the upper-aerobic biofilm layer because we detected no vitamin B_{12} levels in cells grown anaerobically (**Table 3**). Some studies suggested that vitamin B_{12} (*cob*) aerobic synthesis genes are expressed more during biofilm growth (Anderson et al., 2008) in the mucoid phenotype (Rao et al., 2008) and the stationary phase (Fung et al., 2010), with downregulated anoxic conditions (Alvarez-Ortega and Harwood, 2007).

Previous studies showed different RNR activity in other *P. aeruginosa* strains under aerobic and anaerobic conditions (Crespo et al., 2017). Therefore, we analyzed vitamin B_{12} levels in strains more recently isolated, such as the *P. aeruginosa* PA14 and PAET1 strains, and we observed different vitamin B_{12} levels between strains. In *P. aeruginosa* PA14 and PAET1 strains, we identified increased vitamin B_{12} levels under aerobic conditions (1.6 and 2.1 times, respectively) (**Table 3**) and lower vitamin B_{12} levels under biofilm growth conditions compared to the *P. aeruginosa* PAO1 strain. These different vitamin B_{12} levels may affect RNR activity and expression (**Figure 2**), but further experiments are required to validate this hypothesis. It may be due to an active class III RNR detected in the most recently isolated strains compared to the *P. aeruginosa* PAO1 strain (Crespo et al., 2017).

P. aeruginosa Clinical Isolates Grow With Hydroxyurea Treatment

Increased vitamin B_{12} availability in the aerobic growth of *P. aeruginosa* PA14 and the clinical isolate PAET1 strains suggests higher class II RNR activity under this growing condition. We evaluated strain growth in cells with class Ia RNR inhibited by adding 30 mM HU, which were only growing with an active class II RNR. The results showed that any *P. aeruginosa* strain

TABLE 4 | Expression of *nrdA*, *nrdJ*, and *nrdD* genes of *P. aeruginosa* PAO1 and clinical isolates (PAET1 and PA14) strains with HU.

	Log-fold change (HU vs. H_2O)		
	Class Ia *nrdA*	**Class Ia *nrdJ***	**Class III *nrdD***
PAO1	9.19 ± 2.1	31.65 ± 3	50.46 ± 7.2
PAET1	27.74 ± 2.1	7.63 ± 1.1	16.38 ± 0.5
PA14	4.91 ± 0.8	1.18 ± 0.2	32.7 ± 0.9

Fold-change of nrd genes using qRT-PCR after 20 min of treatment with 30 mM HU compared with H_2O. The gap gene was used as an internal standard. Two independent experiments were analyzed, and the standard deviation was annotated.

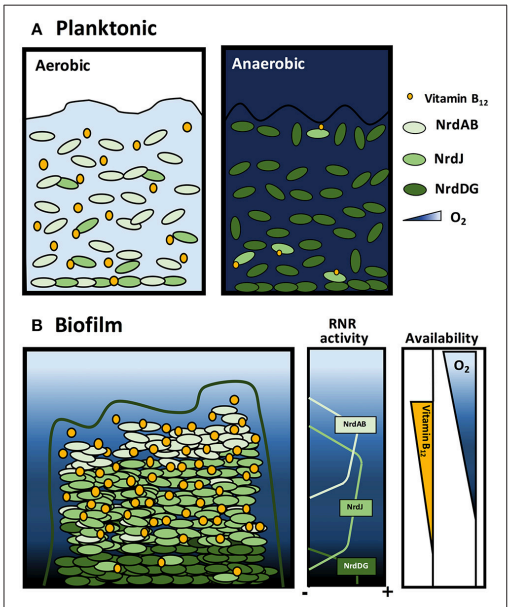

FIGURE 7 | Model of ribonucleotide reductase activity and vitamin B_{12} availability during *P. aeruginosa* planktonic and biofilm growth. Scheme of *P. aeruginosa* growing in **(A)** aerobic and anaerobic planktonic cultures and **(B)** biofilm. Orange circles represent the vitamin B_{12} gradient, blue indicates oxygen concentration gradients and green indicates class Ia, II and III RNR activity.

could grow when vitamin B_{12} was added (**Figure 6A**). In contrast to *P. aeruginosa* PAO1, the absence of external vitamin B_{12} in *P. aeruginosa* PA14 and the clinical isolate PAET1 strain did not affect their growth aerobically. Therefore, vitamin B_{12} is more available in these strains than in the *P. aeruginosa* PAO1 strain for class II RNR activity.

Additionally, the cell morphology shown in the *P. aeruginosa* PAO1 strain after 4 h of HU treatment was filamentous (∼10 μm). However, HU treatment of *P. aeruginosa* PA14 and PAET1 yielded rod-shaped cell morphology (1.4 and 1.7 μm), suggesting that their DNA replication was unimpaired (**Figure 6B**) after 4 h of treatment. However, *nrd* gene expression in *P. aeruginosa* clinical isolates strains was increased, suggesting that HU inhibited class I RNR as in the *P. aeruginosa* PAO1 strain (**Table 4**). This result was corroborated by analyzing their cell viability in a solid medium under HU treatment with and without vitamin B_{12}. *P. aeruginosa* PA14 and PAET1 strains grew in as little as 20 h in the presence of HU (**Figure 6C**) compared with 48 h for *P. aeruginosa* PAO1.

CONCLUSIONS

We demonstrated that vitamin B_{12} synthesis occurs under *P. aeruginosa* aerobic planktonic growth conditions with an active class Ia RNR that supplies dNTPs required for DNA replication (**Figure 7A**). Vitamin B_{12} cannot be synthesized anaerobically when *P. aeruginosa* cells are grown with class III RNR (**Figure 7A**; Crespo et al., 2017). Class II RNR is enzymatically active when vitamin B_{12} is available through internal biosynthesis or from the environment.

Pseudomonas aeruginosa growing in biofilm differs and requires a more in-depth analysis. Oxygen diffusion through the complex biofilm structure generates an oxygen concentration gradient with apparent cell distribution with different RNR class activity (**Figure 7B**; Crespo et al., 2016). We suggest that in the superficial biofilm layers, aerobic cells express class Ia RNR, whereas in the internal layers, anaerobic conditions require cells to express class II or III RNR (Crespo et al., 2016). However, class II RNR is highly expressed during biofilm formation and in aerobic environments (Sjöberg and Torrents, 2011; Crespo et al., 2016) but is oxygen-independent and vitamin B_{12}-dependent (aerobically synthetized). This leads us to ask under which conditions this RNR class enzymatically is active.

We suggest that external cells in a biofilm, which are in contact with aerobic environments, can synthesize vitamin B_{12}, and it can diffuse through the biofilm structure creating a vitamin B_{12} concentration gradient along this structure. In this sense, class II RNR can be active in areas with microaerophilic conditions where class Ia or class III RNR are inactive (**Figure 7B**). Consequently, these results bring us closer to understanding the *P. aeruginosa* cell division mechanism through dNTP synthesis in planktonic and biofilm conditions.

AUTHOR CONTRIBUTIONS

AC, NB-C, and ET: designed the study; AC and NB-C: performed the experiments. All authors analyzed the data, wrote the paper, and read and approved the final version.

ACKNOWLEDGMENTS

This work was supported in part by grants to ET from the Spanish Ministerio de Economia y Competitividad (MINECO/FEDER) (BIO2015-63557-R), Generalitat de Catalunya (2014 SGR01260 and CERCA programme), the EIT Health Program, the Catalan Fibrosis Association and La Caixa Foundation.

REFERENCES

Alvarez-Ortega, C., and Harwood, C. S. (2007). Responses of *Pseudomonas aeruginosa* to low oxygen indicate that growth in the cystic fibrosis lung is by aerobic respiration. *Mol. Microbiol.* 65, 153–165. doi: 10.1111/j.1365-2958.2007.05772.x

Anderson, G. G., Moreau-Marquis, S., Stanton, B. A., and O'toole, G. A. (2008). *In vitro* analysis of tobramycin-treated *Pseudomonas aeruginosa* biofilms on cystic fibrosis-derived airway epithelial cells. *Infect. Immun.* 76, 1423–1433. doi: 10.1128/IAI.01373-07

Arat, S., Bullerjahn, G. S., and Laubenbacher, R. (2015). A network biology approach to denitrification in *Pseudomonas aeruginosa*. *PLoS ONE* 10:e0118235. doi: 10.1371/journal.pone.0118235

Baelo, A., Levato, R., Julian, E., Crespo, A., Astola, J., Gavalda, J., et al. (2015). Disassembling bacterial extracellular matrix with DNase-coated nanoparticles to enhance antibiotic delivery in biofilm infections. *J. Control. Release* 209, 150–158. doi: 10.1016/j.jconrel.2015.04.028

Borovok, I., Gorovitz, B., Schreiber, R., Aharonowitz, Y., and Cohen, G. (2006). Coenzyme B12 controls transcription of the *Streptomyces* class Ia ribonucleotide reductase *nrd*ABS operon via a riboswitch mechanism. *J. Bacteriol.* 188, 2512–2520. doi: 10.1128/JB.188.7.2512-2520.2006

Broderick, K. E., Singh, V., Zhuang, S., Kambo, A., Chen, J. C., Sharma, V. S., et al. (2005). Nitric oxide scavenging by the cobalamin precursor cobinamide. *J. Biol. Chem.* 280, 8678–8685. doi: 10.1074/jbc.M410498200

Cotruvo Jr, J. A., and Stubbe, J. (2011). Class I ribonucleotide reductases: metallocofactor assembly and repair *in vitro* and *in vivo*. *Annu. Rev. Biochem.* 80, 733–767. doi: 10.1146/annurev-biochem-061408-095817

Crespo, A., Gavalda, J., Julian, E., and Torrents, E. (2017). A single point mutation in class III ribonucleotide reductase promoter renders *Pseudomonas aeruginosa* PAO1 inefficient for anaerobic growth and infection. *Sci. Rep.* 7:13350. doi: 10.1038/s41598-017-14051-2

Crespo, A., Pedraz, L., Astola, J., and Torrents, E. (2016). *Pseudomonas aeruginosa* exhibits deficient biofilm formation in the absence of Class, I. i., and iii ribonucleotide reductases due to hindered anaerobic growth. *Front. Microbiol.* 7:688. doi: 10.3389/fmicb.2016.00688

Crespo, A., Pedraz, L., and Torrents, E. (2015). Function of the *Pseudomonas aeruginosa* NrdR transcription factor: global transcriptomic analysis and its role on ribonucleotide reductase gene expression. *PLoS ONE* 10:e0123571. doi: 10.1371/journal.pone.0123571

de Lorenzo, V., Cases, I., Herrero, M., and Timmis, K. N. (1993). Early and late responses of TOL promoters to pathway inducers: identification of postexponential promoters in *Pseudomonas putida* with *lacZ-tet* bicistronic reporters. *J. Bacteriol.* 175, 6902–6907. doi: 10.1128/jb.175.21.6902-6907.1993

Fung, C., Naughton, S., Turnbull, L., Tingpej, P., Rose, B., Arthur, J., et al. (2010). Gene expression of *Pseudomonas aeruginosa* in a mucin-containing synthetic growth medium mimicking cystic fibrosis lung sputum. *J. Med. Microbiol.* 59, 1089–1100. doi: 10.1099/jmm.0.019984-0

Gale, G. R., Kendall, S. M., Mclain, H. H., and Dubois, S. (1964). Effect of Hydroxyurea on *Pseudomonas aeruginosa*. *Cancer Res.* 24, 1012–1020.

Garriga, X., Eliasson, R., Torrents, E., Jordan, A., Barbe, J., Gibert, I., et al. (1996). *nrdD* and *nrdG* genes are essential for strict anaerobic growth of *Escherichia coli*. *Biochem. Biophys. Res. Commun.* 229, 189–192. doi: 10.1006/bbrc.1996.1778

Hassett, D. J., Sutton, M. D., Schurr, M. J., Herr, A. B., Caldwell, C. C., and Matu, J. O. (2009). *Pseudomonas aeruginosa* hypoxic or anaerobic biofilm infections within cystic fibrosis airways. *Trends Microbiol.* 17, 130–138. doi: 10.1016/j.tim.2008.12.003

Heydorn, A., Nielsen, A. T., Hentzer, M., Sternberg, C., Givskov, M., Ersboll, B. K., et al. (2000). Quantification of biofilm structures by the novel computer program COMSTAT. *Microbiology* 146 (Pt 10), 2395–2407. doi: 10.1099/00221287-146-10-2395

Hoang, T. T., Karkhoff-Schweizer, R. R., Kutchma, A. J., and Schweizer, H. P. (1998). A broad-host-range Flp-FRT recombination system for site-specific excision of chromosomally-located DNA sequences: application for isolation of unmarked *Pseudomonas aeruginosa* mutants. *Gene* 212, 77–86. doi: 10.1016/S0378-1119(98)00130-9

Hofer, A., Crona, M., Logan, D. T., and Sjöberg, B. M. (2012). DNA building blocks: keeping control of manufacture. *Crit. Rev. Biochem. Mol. Biol.* 47, 50–63. doi: 10.3109/10409238.2011.630372

Jordan, A., and Reichard, P. (1998). Ribonucleotide reductases. *Annu. Rev. Biochem.* 67, 71–98. doi: 10.1146/annurev.biochem.67.1.71

Jordan, A., Torrents, E., Sala, I., Hellman, U., Gibert, I., and Reichard, P. (1999). Ribonucleotide reduction in *Pseudomonas* species: simultaneous presence of active enzymes from different classes. *J. Bacteriol.* 181, 3974–3980.

Julian, E., Baelo, A., Gavalda, J., and Torrents, E. (2015). Methyl-hydroxylamine as an efficacious antibacterial agent that targets the ribonucleotide reductase enzyme. *PLoS ONE* 10:e0122049. doi: 10.1371/journal.pone.0122049

Kjaergaard, K., Schembri, M. A., Ramos, C., Molin, S., and Klemm, P. (2000). Antigen 43 facilitates formation of multispecies biofilms. *Environ. Microbiol.* 2, 695–702. doi: 10.1046/j.1462-2920.2000.00152.x

Lee, K. M., Go, J., Yoon, M. Y., Park, Y., Kim, S. C., Yong, D. E., et al. (2012). Vitamin B12-mediated restoration of defective anaerobic growth leads to reduced biofilm formation in *Pseudomonas aeruginosa*. *Infect. Immun.* 80, 1639–1649. doi: 10.1128/IAI.06161-11

Quenee, L., Lamotte, D., and Polack, B. (2005). Combined *sacB*-based negative selection and cre-lox antibiotic marker recycling for efficient gene deletion in *Pseudomonas aeruginosa*. *BioTechniques* 38, 63–67. doi: 10.2144/05381ST01

Rao, J., Digiandomenico, A., Unger, J., Bao, Y., Polanowska-Grabowska, R. K., and Goldberg, J. B. (2008). A novel oxidized low-density lipoprotein-binding protein from *Pseudomonas aeruginosa*. *Microbiology* 154, 654–665. doi: 10.1099/mic.0.2007/011429-0

Roth, J. R., Lawrence, J. G., and Bobik, T. A. (1996). Cobalamin (coenzyme B12): synthesis and biological significance. *Annu. Rev. Microbiol.* 50, 137–181. doi: 10.1146/annurev.micro.50.1.137

Roth, J. R., Lawrence, J. G., Rubenfield, M., Kieffer-Higgins, S., and Church, G. M. (1993). Characterization of the cobalamin (vitamin B12) biosynthetic genes of *Salmonella typhimurium*. *J. Bacteriol.* 175, 3303–3316. doi: 10.1128/jb.175.11.3303-3316.1993

Schobert, M., and Jahn, D. (2010). Anaerobic physiology of *Pseudomonas aeruginosa* in the cystic fibrosis lung. *Int. J. Med. Microbiol.* 300, 549–556. doi: 10.1016/j.ijmm.2010.08.007

Sjöberg, B. M., and Torrents, E. (2011). Shift in ribonucleotide reductase gene expression in *Pseudomonas aeruginosa* during infection. *Infect. Immun.* 79, 2663–2669. doi: 10.1128/IAI.01212-10

Stewart, P. S., and Franklin, M. J. (2008). Physiological heterogeneity in biofilms. *Nat. Rev. Microbiol.* 6, 199–210. doi: 10.1038/nrmicro1838

Sullivan, M. J., Gates, A. J., Appia-Ayme, C., Rowley, G., and Richardson, D. J. (2013). Copper control of bacterial nitrous oxide emission and its impact on vitamin B12-dependent metabolism. *Proc. Natl. Acad. Sci. U.S.A.* 110, 19926–19931. doi: 10.1073/pnas.1314529110

Torrents, E. (2014). Ribonucleotide reductases: essential enzymes for bacterial life. *Front. Cell. Infect. Microbiol.* 4:52. doi: 10.3389/fcimb.2014.00052

Torrents, E., Poplawski, A., and Sjöberg, B. M. (2005). Two proteins mediate class II ribonucleotide reductase activity in *Pseudomonas aeruginosa*: expression and transcriptional analysis of the aerobic enzymes. *J. Biol. Chem.* 280, 16571–16578. doi: 10.1074/jbc.M501322200

Vitreschak, A. G., Rodionov, D. A., Mironov, A. A., and Gelfand, M. S. (2003). Regulation of the vitamin B12 metabolism and transport in bacteria by a conserved RNA structural element. *RNA* 9, 1084–1097. doi: 10.1261/rna.5710303

Warren, M. J., Raux, E., Schubert, H. L., and Escalante-Semerena, J. C. (2002). The biosynthesis of adenosylcobalamin (vitamin B12). *Nat. Prod. Rep.* 19, 390–412. doi: 10.1039/b108967f

Yoon, M. Y., Lee, K. M., Park, Y., and Yoon, S. S. (2011). Contribution of cell elongation to the biofilm formation of *Pseudomonas aeruginosa* during anaerobic respiration. *PLoS ONE* 6:e16105. doi: 10.1371/journal.pone.0016105

Yoon, S. S., Coakley, R., Lau, G. W., Lymar, S. V., Gaston, B., Karabulut, A. C., et al. (2006). Anaerobic killing of mucoid *Pseudomonas aeruginosa* by acidified nitrite derivatives under cystic fibrosis airway conditions. *J. Clin. Invest.* 116, 436–446. doi: 10.1172/JCI24684

Conflict of Interest Statement: The authors declare that the research was conducted in the absence of any commercial or financial relationships that could be construed as a potential conflict of interest.

ANNEX 2: ARTICLE 7

Optimal environmental and culture conditions allow the *in vitro* coexistence of *Pseudomonas aeruginosa* and *Staphylococcus aureus* in stable biofilms

Publicat a la revista *Scientific Reports* (Q1, IF_{2019} = 3.998)

DOI: 10.1038/s41598-019-52726-0

Novembre 2019

Autors: Maria del Mar Cendra[1]*, **Núria Blanco-Cabra**[1], Lucas Pedraz[1], Eduard Torrents[1]*

1 Bacterial Infections and Antimicrobial Therapies, Institute for Bioengineering of Catalonia (IBEC) The Barcelona Institute of Science and Technology (BIST), Barcelona, Spain.

* Correspondència: Dr. Eduard Torrents (etorrents@ibecbarcelona.eu);
Dr. Maria del Mar Cendra (mcendra@ibecbarcelona.eu)

Informació suplementaria disponible a https://doi.org/10.1038/s41598-019-52726-0.

www.nature.com/scientificreports

SCIENTIFIC REPORTS
nature research

OPEN

Optimal environmental and culture conditions allow the *in vitro* coexistence of *Pseudomonas aeruginosa* and *Staphylococcus aureus* in stable biofilms

Maria del Mar Cendra*, Núria Blanco-Cabra, Lucas Pedraz & Eduard Torrents*

The coexistence between species that occurs in some infections remains hard to achieve *in vitro* since bacterial fitness differences eventually lead to a single organism dominating the mixed culture. *Pseudomonas aeruginosa* and *Staphylococcus aureus* are major pathogens found growing together in biofilms in disease-affected lungs or wounds. Herein, we tested and analyzed different culture media, additives and environmental conditions to support *P. aeruginosa* and *S. aureus* coexistence *in vitro*. We have unraveled the potential of DMEM to support the growth of these two organisms in mature cocultured biofilms (three days old) in an environment that dampens the pH rise. Our conditions use equal initial inoculation ratios of both strains and allow the stable formation of separate *S. aureus* microcolonies that grow embedded in a *P. aeruginosa* biofilm, as well as *S. aureus* biofilm overgrowth when bovine serum albumin is added to the system. Remarkably, we also found that *S. aureus* survival is strictly dependent on a well-characterized phenomenon of oxygen stratification present in the coculture biofilm. An analysis of differential tolerance to gentamicin and ciprofloxacin treatment, depending on whether *P. aeruginosa* and *S. aureus* were growing in mono- or coculture biofilms, was used to validate our *in vitro* coculture conditions.

Most chronic infections occur due to the inherent capacity of some bacterial pathogens to grow in biofilms[1]. Although they have been historically investigated as monoculture events, some infection-associated biofilms are currently recognized to be mainly polymicrobial and involve synergistic interactions that often worsen the disease outcome[2,3].

Polymicrobial biofilms can develop greater antimicrobial resistance than single-species biofilms[4]. The way bacteria are distributed and interact with each other or with the host fluctuates depending on the environment[5,6]. For instance, *Pseudomonas aeruginosa*, in addition to forming large mushroom-shaped biofilm structures *in vitro*, can behave differently and form different bacterial arrangements *in vivo*. Clusters or aggregates perfectly arranged and determined by the different bacteria that are able to grow concurrently are more likely to occur during the establishment and persistence of the infection. Therefore, there is an intrinsic effect of the surrounding environment on the way microbes behave and establish their connections[3].

Regarding human pathogenesis, cystic fibrosis (CF) is a model example of how bacterial interactions within biofilms can modulate the outcome of the disease, thus playing a critical role in the patient's wellbeing[7]. CF is a lethal genetic disease characterized by the production of abnormal secretions in different organs[8]. Lungs especially are affected by CF. In the lung, a thick and dense mucus builds up over the pulmonary epithelium, converting it into the perfect niche for bacterial colonization and growth[9,10]. CF-affected lungs contain changing gradients of oxygen, nutrients and pH, which together provide a heterogeneous environment that favors the coexistence and proliferation of a wide range of microbial species and, consequently, exacerbating the progression of the disease[9]. *P. aeruginosa* and *Staphylococcus aureus* are two major pathogens commonly isolated from

Bacterial Infections and Antimicrobial Therapies Group, Institute for Bioengineering of Catalonia (IBEC), The Barcelona Institute of Science and Technology, Baldiri Reixac 15-21, 08028, Barcelona, Spain. *email: mcendra@ibecbarcelona.eu; etorrents@ibecbarcelona.eu

CF-affected airways and sputum. Although *S. aureus* usually colonizes the lung epithelium during childhood and *P. aeruginosa* is more likely to be acquired in the transition to adult life, both microorganisms have been detected coexisting and synergistically contributing to the disease severity[11,12]. A similar scenario is found in infected wounds, where both bacterial species can often be found infecting simultaneously[13]. Despite the knowledge that both organisms can grow in unison *in vivo*, it remains difficult to mimic the conditions that sustain this close relationship *in vitro*.

The discovery of the culture conditions able to maintain mixed *P. aeruginosa* and *S. aureus* simultaneous growth *in vitro* has become a scientific hotspot, and several studies can be found in the bibliography addressing the interactions of these microorganisms. In their attempt to elucidate the principles of the coexistence of these species, some studies have used a higher inoculation ratio of *S. aureus vs P. aeruginosa* to establish the mixed biofilm or introduced the latter once the *S. aureus* biofilm has been established[14]. Equal inoculation ratios of both microorganisms have also been tested; however, coexistence under these conditions did not last longer than 24 h or only information related to the mixed biofilm biomass (not from each organism independently within the cocultured biofilm) can be found in the literature[15–17]. Some researchers used *P. aeruginosa* supernatant to evaluate its impact on the coculture system[18–20], while other studies were based on wound models[21,22].

Our study focused on deciphering the optimal coculture conditions and environmental requisites that would allow the simultaneous and stable growth of *P. aeruginosa* and *S. aureus* in mixed biofilms over time. We reasoned that the achievement of a stable *in vitro* coculture biofilm, able to grow with balanced populations of both organisms and to remain for an extended period of time, would be useful to understand the pathophysiology associated with the interaction of these two-species and for generating optimized chemotherapies to treat such biofilm-related diseases. Therefore, we developed a combination of coculture conditions that enable the stable formation of *P. aeruginosa* and *S. aureus* mixed biofilms on different abiotic surfaces. The coculture biofilms were formed using equal initial bacterial inoculation ratios and grew stably for up to three days of testing in an environmental background that dampens the pH rise. Furthermore, we provide evidence that *S. aureus* survival during coculture biofilm growth with *P. aeruginosa* is strictly dependent on oxygen diffusion. To validate the combination of the coculture conditions and environmental prerequisites identified, we treated the mixed biofilms with known antibiotics to confirm differences in antibiotic tolerance depending on whether the strains were growing in mono- or coculture biofilms.

Results

Testing and analyzing *P. aeruginosa* and *S. aureus* balanced population co-growth in different culture media. The culturing conditions able to block the antagonistic relationship between *P. aeruginosa* and *S. aureus* *in vitro* have yet to be discovered. As shown in Fig. 1a-LB, when both bacterial strains are grown together in Luria-Bertani (LB) medium, *P. aeruginosa* tends to dominate the culture and compromise *S. aureus* survival in the system (at 28 h). As our goal was to achieve balanced and stable *P. aeruginosa* and *S. aureus* mixed growth, selection of the bacterial strains to use was thought to be crucial to accomplish our objective. In this study, we used the *P. aeruginosa* PA14 strain together with the *S. aureus* Newman strain. This pair of microorganisms has been used in other polymicrobial studies[15,18,23,24]; hence, we considered them suitable for use in our study.

LB, tryptic soy broth (TSB), Dulbecco's modified Eagle's medium (DMEM) and synthetic cystic fibrosis sputum medium 2 (SCFM2) were tested as a base to develop a medium that maintains the coexistence and growth of both organisms over time. Thus, mixed cultures of PA14 and Newman strains and the respective CFUs were analyzed after 0, 12, 24, 36 and 48 h of incubation. For PA14-Newman planktonic cultures grown in LB and SCFM2, a significant decrease in *S. aureus* Newman CFUs/mL ($p < 0.05$) was detected during the initial 24 h of incubation with no CFUs counted after 24–36 h post-initial inoculation (Fig. 1a,b - LB and SCFM2). In contrast, TSB and DMEM maintained *S. aureus* Newman survival at ~10^5 CFUs/mL over the 48 h with no significant changes detected after 12 h ($p > 0.05$; Fig. 1c,d - TSB and DMEM). PA14 growth was stable and maintained at ~10^{10}–10^{11} CFUs/mL in the different media tested except for SCFM2, in which the strain reached maximal growth at ~10^9 CFUs/mL (Fig. 1 - planktonic).

Since *P. aeruginosa* and *S. aureus* are commonly found in chronic infections promoted by biofilm formation[11], this type of growth was examined next. Coculture biofilm growth was assessed in independent 96-well polystyrene microtiter plates after 12, 24, 36, 48, 60 and 72 h (Fig. 1 - biofilm). Mixed biofilms grown in LB and SCFM2 showed similar patterns for PA14 and Newman strains in planktonic growth. However, while *Pseudomonas* maintained a constant number of biofilm-forming CFUs during the 72 h checked, the presence of Newman in the mixed biofilm progressively decreased, and by 48 h no *S. aureus* CFUs were detected in the cocultured biofilm (Fig. 1e,f - LB and SCFM2). Similar to the results obtained in the planktonic experiments, coculture growth in TSB or DMEM enhanced *S. aureus* survival in the mixed biofilm. However, while TSB supported Newman growth at ~10^6 CFUs/well for 36 h of incubation, *S. aureus* survival dropped by 48 h, with no countable CFUs detected from that time onward (Fig. 1g - TSB). In contrast, DMEM promoted constant Newman growth (~10^5–10^4 CFUs/well) in the mixed biofilm during the initial 48 h analyzed, with a slight decrease to ~10^2 CFUs/well after 60 h of incubation; no countable CFUs were detected only after 72 h (Fig. 1h - DMEM). Although significantly increased viability of *S. aureus* was detected when coculture biofilm was growing in DMEM, percentage numbers of the organism within the mixed biofilm did not vary among the media used (Supplementary Table S1). PA14 levels within the mixed biofilm were similar among the four media tested, with ~10^7–10^8 CFUs counted per well during the 72 h of the course of the experiment (Fig. 1 - biofilm).

The physiochemical environment where microbes grow can influence the bacterial distribution in the community[3]. Furthermore, pH homeostasis is critical to maintaining the integrity of all living cells[25,26]. Therefore, we next thought it important to examine the pH change during the coculture biofilm growth in the different media tested. The pH was evaluated at the initial establishment of the biofilms in microtiter plates at 37 °C and after 24, 48 and 72 h. Differences in pH changes were found depending on if biofilms were grown in monoculture

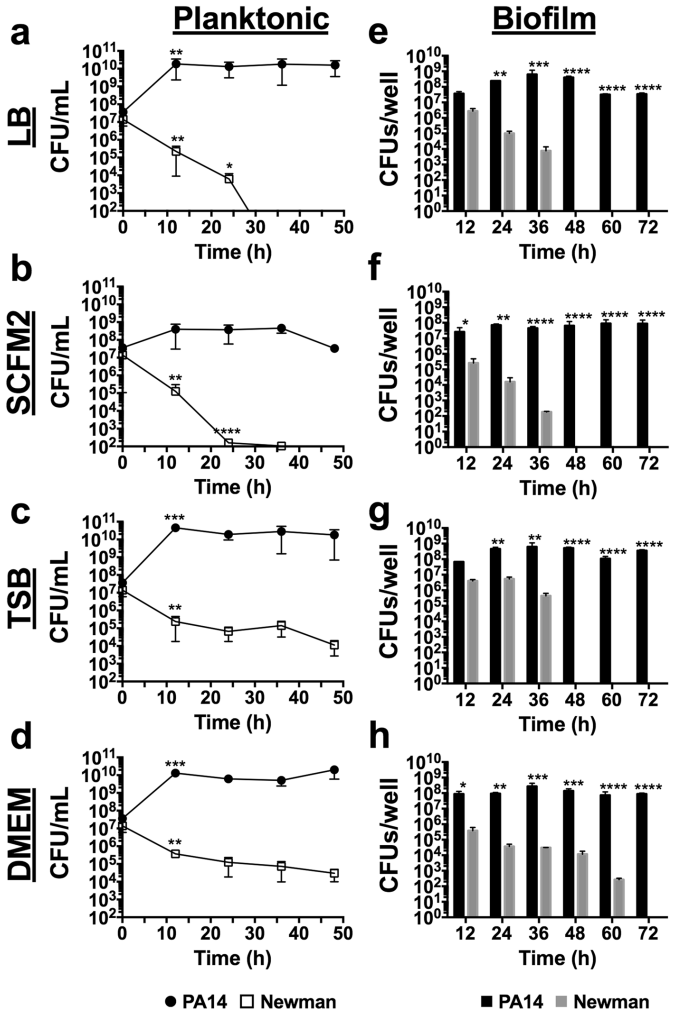

Figure 1. Time-course planktonic and biofilm growth of *P. aeruginosa* PA14 and *S. aureus* Newman in LB, SCFM2, TSB and DMEM. (**a**-**d**) $\log_{10}$ CFUs/mL of each bacterial strain during planktonic growth in coculture at the time of initial inoculation and after 12, 24, 36 and 48 h of incubation at 37 °C with shaking. (**e**-**h**) $\log_{10}$ CFUs/well of PA14 and Newman strains during coculture biofilm growth on 96-well polystyrene plates over 72 h of static incubation at 37 °C. Three independent experiments were performed for both experiments, and error bars indicate the standard error of the mean from the representative triplicate. Statistical significance between $\log_{10}$ CFUs/mL and between $\log_{10}$ CFUs/well at the different time points is indicated with an asterisk (*$p < 0.05$; **$p < 0.01$; ***$p < 0.001$; and ****$p < 0.0001$).

(Supplementary Fig. S1) or coculture (Fig. 2). As shown in Fig. 2, the pH rapidly increased when biofilms were grown in LB, SCFM2 or TSB, reaching pH ~8.7–8.8 by 48 h of incubation when growing in coculture. However, in DMEM, the pH was reduced and measured ~0.5–1 lower, ($p < 0.001$) compared to that of the other media during the 72 h tested. This rapid increase of pH was not observed when both organisms were grown in monoculture biofilms (Supplementary Fig. S1). In that case, pH tended to be maintained or acidified (especially for *S. aureus* monoculture biofilms), during the 72 h examined.

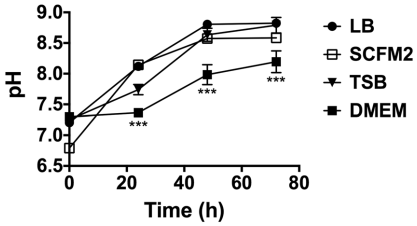

Figure 2. pH evolution during coculture biofilm growth in different culture media. The plot shows the pH measurements of the different supernatant phases of *P. aeruginosa* PA14 and *S. aureus* Newman coculture biofilms grown in LB, TSB, SCFM2 and DMEM. Measurements were performed at the time of initial inoculation (0 h) and after 24, 48 and 72 h of incubation at 37 °C. Statistical significance of the pH measured in DMEM at different time points compared to the pH measured in the other media at the same time points is denoted with asterisks (***$p < 0.001$).

Taken together, these results indicate that DMEM has the highest potential to maintain *S. aureus* survival over time when grown together with *P. aeruginosa*.

Optimizing *P. aeruginosa* and *S. aureus* coculture conditions. Several conditions have been described to influence *P. aeruginosa* and *S. aureus* fitness. Accordingly, we next looked for molecules or additives to supplement the DMEM with the aim of increasing Newman survival in the mixed biofilm. Therefore, nicotinamide adenine dinucleotide phosphate (NADPH; 0.2 mM), adenosine monophosphate (AMP; 10 mM), bovine serum albumin (BSA; 5% w/v) and L-arginine (L-arg; 0.4% w/v) were chosen to be tested for the ability to compromise *P. aeruginosa* pathogenesis (AMP, BSA and L-arg), influence *S. aureus* fitness (BSA) and combat oxidative stress (NADPH)[16,21,27–29].

To evaluate the effect of the different additives, mixed biofilms were grown in independent microtiter plates in DMEM supplemented with NADPH, BSA, AMP or L-arg (Fig. 3 and Supplementary Table S2) for 72 h at 37 °C, and the respective biofilm-forming CFUs were counted on selective agar plates. Generally, no major differences were detected in PA14 growth (CFU/well) within the coculture biofilm with any of the additives used compared to nonsupplemented DMEM (Fig. 1h - DMEM). Furthermore, *P. aeruginosa* CFUs/well were ~10^7–10^8 at all time-points and conditions checked (Fig. 3). A different scenario was observed with the *S. aureus* strain. Although all additives tended to maintain stable *S. aureus* Newman levels of ~10^6–10^7 CFUs/well during the initial 24 h (Fig. 3), the NADPH- or AMP-supplemented medium (Fig. 3a,c) did not enhance *S. aureus* growth after 36–48 h of incubation compared to nonsupplemented medium and by 60 h, no Newman CFUs were counted within the mixed biofilm in these two incubatory conditions. In contrast, coculture incubation in DMEM + BSA or DMEM + L-arg promoted sustained *S.* aureus CFU numbers of ~10^5–10^6 during the initial 48 h of the experiment, and these numbers decreased only after 60 h of incubation. Significantly, while in the presence of BSA, *S. aureus* CFUs were ~10^4 CFUs/well after 72 h of incubation; the L-arg condition showed a gradual decrease in the viability of the cocci, with ~10^2 CFUs/well counted at the end of the experiment (Fig. 3b,d). Remarkably, all additives increased the *S. aureus* cell percentage within the mixed biofilm if compared to that calculated in coculture biofilms grown in unsupplemented DMEM (Supplementary Table S1), with percentages calculated ~11–25% of the total mixed biofilm (Supplementary Table S2).

Oxygen diffusion within PA14-Newman mixed biofilms plays a key role in maintaining balanced bacterial populations. The next step was to evaluate other environmental parameters that could influence the coculture biofilm during *in vitro* growth. Since oxygen competition between *P. aeruginosa* and *S. aureus* has been described to compromise the viability of the latter in a CF model[15], this parameter was next assessed in our system.

We next aimed to identify the position inside the well where PA14-Newman biofilm growth occurred and to detect possible differences when compared to monoculture biofilm growth. Crystal violet staining of 48 h-old biofilms confirmed that the bacterial biofilm growth was limited to the air-liquid interphase (ALI) area of the microplate well (Fig. 4a). These results indicate that the CFU values determined in Fig. 3 come from cocultured biofilms formed in the ALI area of the microtiter plate. OD_{570} measurements revealed that PA14 forms a larger monoculture than the *S. aureus* strain. Interestingly, no additive effect was observed in the PA14 biofilm during coculture biofilm growth with *S. aureus* (Supplementary Fig. S2).

To further investigate the role of oxygen during coculture biofilm formation, we changed the *in vitro* microplate model to use coverslips. Thus, to analyze the immersed biofilm growth, the coverslip was placed in the bottom of the well of a 6-well plate and completely submerged in the medium. To assess the biofilm growing in the ALI area, the coverslip was positioned to line the well wall (see schematic representation in Fig. 4b). Crystal violet staining of 48 h-old biofilms revealed no significant differences between immersed biofilms, with similar intense violet staining detected between the mono- and cocultured biofilms (Fig. 4c). However, clear differences were observed between biofilms grown in the ALI area. While the PA14 monoculture biofilm showed more intense violet staining than the Newman monoculture biofilm, greater biofilm coverage of the coverslip was observed

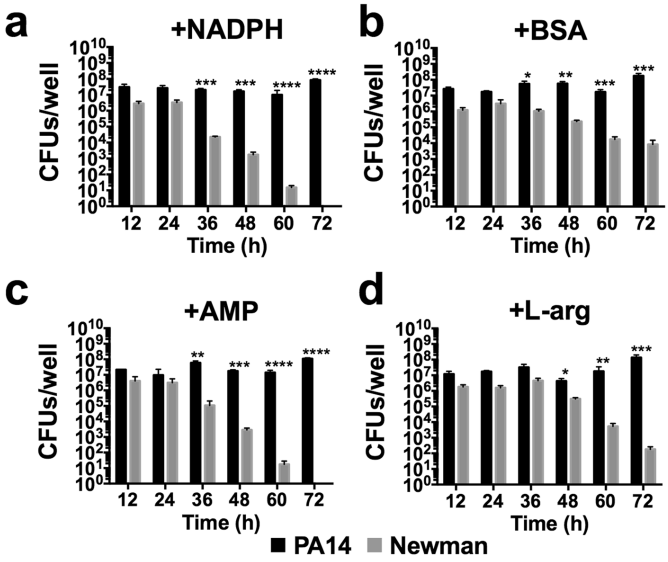

Figure 3. Effect of NADPH, BSA, AMP and L-arg on extending *S. aureus* survival during coculture biofilm growth with *P. aeruginosa*. Coculture biofilms were grown *in vitro* on 96-well polystyrene plates for 72 h in static conditions at 37 °C. The different graphs show biofilm cells of *P. aeruginosa* and *S. aureus* $\log_{10}$ CFUs/well during biofilm growth in DMEM supplemented with NADPH at 0.2 mM (**a**), BSA at 5% w/v (**b**), AMP at 10 mM (**c**) and L-arg at 0.4% w/v (**d**) after 12, 24, 36, 48, 60 and 72 h. Conditions were tested in triplicate, and bars represent the mean of three independent experiments. The standard error of the mean is included in the plots. Significant differences between PA14 and Newman CFUs/well at the different incubation times are indicated by asterisks (*$p < 0.05$; **$p < 0.01$; ***$p < 0.001$; and ****$p < 0.0001$).

with the *S. aureus* strain (Fig. 4c). Measurement of the stained biofilms revealed that the Newman monoculture biofilm covered ~7.5 mm of the coverslip, in contrast to the ~6 mm covered by the PA14 monoculture biofilm. An intensive violet-stained band of ~3 mm was detected in the middle of a greater coverage area of ~7.5 mm when both organisms were grown in unison (Fig. 4c).

Coculture viability was next analyzed to assess the coexistence of both organisms within the mixed biofilm depending on the proximity to the medium surface during growth. Since increased coculture biofilm was obtained in the presence of NADPH, BSA, AMP and L-arg in 96-well plates (Fig. 3), these additives were also included in the experiment. After three days of incubation, a greater presence of *S. aureus* was observed by confocal microscopy when biofilms were grown in the ALI area compared to when they were grown completely immersed in the medium (Fig. 4d). Increased growth of *S. aureus* in the ALI area was also confirmed by CFU counting (Fig. 4e). In the nonsupplemented DMEM (control) and DMEM + NADPH conditions, the *S. aureus* strain appeared to be dispersed over the glass, whereas in DMEM + BSA, DMEM + AMP and DMEM + L-arg, the strain emerged embedded in aggregates within the PA14 biofilm (Fig. 4d - ALI area). In the validation of the results obtained in Fig. 3, significantly increased numbers of the Newman strain were counted in the mixed biofilms incubated in DMEM including the different additives (Fig. 4d). A different scenario was observed when biofilms were grown immersed in the medium, wherein PA14 completely covered the different coverslips, and the Newman strain was barely detected (Fig. 4d - Immersed). Only Newman CFUs counted in the mixed biofilm grown in DMEM + BSA showed a significant increase relative to the control condition ($p < 0.05$), although the levels were drastically reduced compared to those counted in the ALI area (Fig. 4e). Interestingly, the addition of L-arg to the system resulted in a more dispersed PA14 biofilm formation compared to that visualized with the other additives (Fig. 4d - L-arg).

Overall, these results confirm that although different additives increase *S. aureus* survival during mixed biofilm growth with *P. aeruginosa*, biofilm formation in the ALI area is fundamental to achieving this enhanced survival of *S. aureus*.

A gradient of dissolved oxygen in the coculture biofilm system explains the differential bacterial growth. Different oxygen concentrations across the culture system may explain differential bacterial growth within the coculture biofilm. To validate this hypothesis, the dissolved oxygen concentration during biofilm incubation was measured in different areas of interest using an oxygen microsensor system (Fig. 5, Supplementary

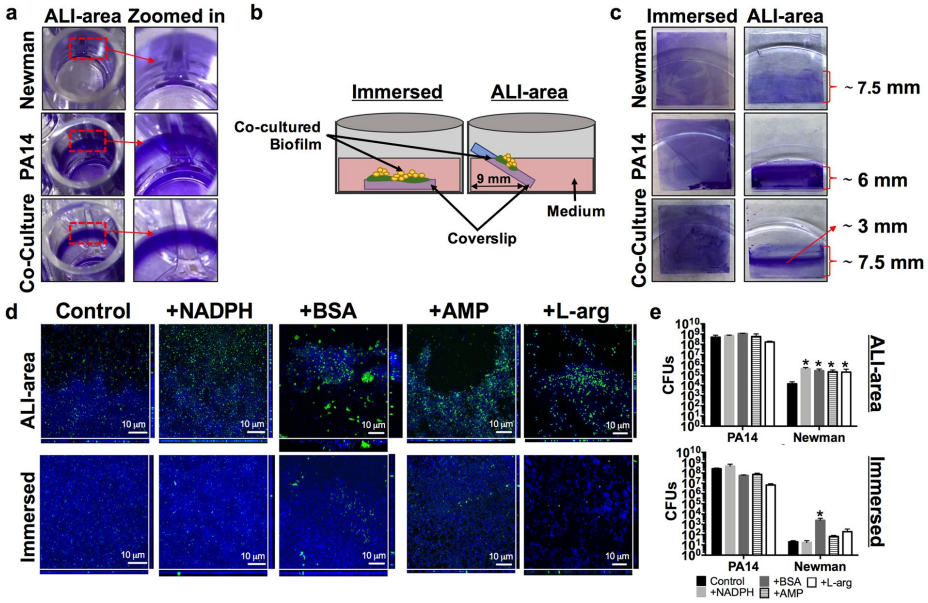

Figure 4. Balanced *P. aeruginosa* PA14 and *S. aureus* Newman populations growing in a coculture biofilm is dependent on the air availability. Total PA14 and Newman biomass grown in monoculture or coculture biofilms and stained with crystal violet. (**a**) Pictures show the biofilm growth of monoculture and coculture biofilms in the air-liquid interphase area (ALI area) of a 96-well plate. A zoomed image highlighting a region of interest of each biofilm is included in the figure. (**b**) Schematic representation of the coverslip position within the well during incubation of the PA14-Newman coculture biofilm immersed in the medium or in the ALI area. (**c**) Biofilm biomass staining of PA14 and Newman mono- and coculture biofilm growth over a coverslip immersed or in the ALI area. The length of the stained area in the coverslip is included on the plot. (**d**,**e**) PA14-Newman coculture biofilms grown in the ALI area or immersed in DMEM (control) and DMEM + NADPH, BSA, AMP and L-arg. (**d**) Confocal images of the mixed biofilms at the different time points were taken at 63X magnification, PA14 is shown in blue (DAPI) and Newman in green (CF^{TM}-488A). A representative image of each biofilm from three independent experiments. (**e**) Plots show the different $\log_{10}$ value of PA14 and Newman CFUs covering each coverslip after 3 days of incubation. The results show the mean of three independent experiments with the corresponding standard error of the mean. Statistical significance ($p < 0.05$) compared to the relative bacterial control condition is indicated by an asterisk (*) over each bar.

Fig. S3). Thus, the oxygen consumption rates in the area immediately above the immersed biofilm (ALI area) and in the medium surface (top position) were measured and analyzed over time (Fig. 5a). Additionally, a spatial oxygen profile was also measured in the medium immediately after the bottom area became depleted of oxygen (Fig. 5b). The microsensor measurements reflected a gradual decrease in the oxygen content from ~5.5 (~80% of the dissolved oxygen) to ~0 mg/L in the initial ~80 min when the PA14-Newman combined biofilm was growing completely immersed in the medium (Fig. 5a, green line). However, sensor placement in the ALI area (Fig. 5a, red line) confirmed a maintained oxygen concentration of ~5.5 mg/L during these initial 80 min. Progressive oxygen consumption was detected after that time point, reaching ~1 mg/L (~20% of the dissolved oxygen) by ~110 min from the initial incubation. Interestingly, the oxygen concentration was sustained at ~1 mg/L for approximately ~50 additional minutes before decreasing to ~0.5 mg/L (~6% of the dissolved oxygen). The oxygen levels were then maintained at ~0.5 mg/L without reaching complete depletion. A different result was obtained when the sensor was placed close to the medium surface (top position; Fig. 5a-blue line). In this position, and comparable to the ALI area, a sustained concentration of ~5.5 mg/L was measured during the initial 80 min of incubation. However, in this case, a linear oxygen decrease occurred immediately after that time point, reaching 0 mg/L after ~125 min (Fig. 5a). Analysis of the oxygen stratification at different depths revealed that most of the medium in which the coculture biofilm was growing was oxygen-free. This area showed 0 mg/mL oxygen and accounted for the initial ~3 mm of the medium depth. Only the area closest to the surface, the first ~1 mm, revealed oxygen content and showed a progressive increase that reached ~6.5 mg/L (~95% of the dissolved oxygen) at the medium surface (Fig. 5b).

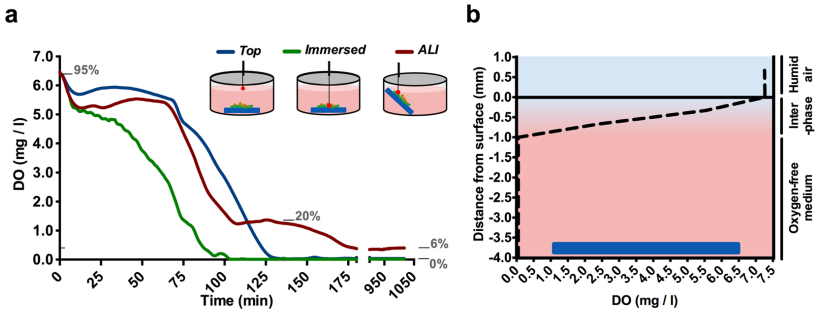

Figure 5. Differences in oxygen concentration depending on the position in the well where PA14 and Newman are cocultured and growing. Dissolved oxygen concentration (DO) was determined in the different areas of interest in the PA14 and Newman *in vitro* coculture biofilm model. (**a**) Plot shows the DO (mg/L; ppm) given by the optical fiber microsensor, depending on the position placed in the coculture system: top, immersed and in the ALI area. A schematic showing the approximate position of each measurement is included in the plot. The equivalence of significant DO values to the percentage of dissolved oxygen saturation (gray numbers) is provided as a reference. (**b**) DO at different depths of the culture well after the immersed area reached a DO of 0 mg/L (approximately 85 min of incubation). An interpretation of the oxygenation states across the different layers is provided on the right: **1**, humid air (the oxygen value is a result of the saturation of the sensor); **2**, oxygenated interphase; and **3**, anaerobic culture.

These results may suggest that, given the proximity to the surface, the ALI area would not reach oxygen depletion and would be able to maintain some oxygen content even though it would be a low percentage of the dissolved oxygen.

DMEM supports *P. aeruginosa* and *S. aureus* balanced coculture biofilm growth and stabilization over time. To reinforce the potential of our developed DMEM culture conditions in forming and preserving *P. aeruginosa-S. aureus* mixed biofilms, we established a continuous-flow biofilm. Continuous-flow biofilms are the closest approximation known for the growth of biofilms with similar physical, chemical and biological heterogeneity as those naturally formed *in vivo*[30].

After three days of continuous flow, we confirmed that only DMEM was able to sustain stable growth of both populations in the biofilm. Mixed biofilms grown in TSB (Fig. 6a) or TSB supplemented with BSA (Fig. 6b) did not show any growth or increase in *S. aureus* survival within the coculture system compared to those in DMEM (Fig. 6c,d,f). Biomass evaluation using the COMSTAT 2 software determined that when the experiment was performed in TSB, *P. aeruginosa* accounted for ~90% of the coculture biofilm, while *S. aureus* accounted for only ~10% of the system. The addition of BSA to TSB barely increased *S. aureus* growth, and its presence in the coculture biofilm was calculated to be ~15% in this incubatory condition (Fig. 6f). However, coculture biofilms grown in DMEM or DMEM + BSA revealed an increased presence of *S. aureus* when they were visualized with a confocal microscope (Fig. 6c,d). In general, we observed that both strains did not grow mixed together but independently and well distributed in the flow-cell channel. Interestingly, while microcolonies of *S. aureus* were detected growing embedded in the PA14 biofilm in unsupplemented DMEM (Fig. 6c), a thick and compact layer of *S. aureus* was visualized covering the *P. aeruginosa* biofilm when BSA was added to the flow system (Fig. 6d). COMSTAT 2 software revealed that this dense layer of Newman biofilm had an average thickness of ~12.50 μm, whereas the *P. aeruginosa* biofilm growing the beneath *S. aureus* was ~6.73 μm thick.

The orthogonal views, 3D representations and evaluation of the different regions of interest (ROIs) of the coculture biofilms were next analyzed to assess how bacterial populations were distributed within the mixed biofilm system. Our experimental approach confirmed the presence of *S. aureus* microcolonies growing in clusters within PA14 biofilms during growth with DMEM (Fig. 6c). Two schematic drawings are presented in Fig. 6e to clearly show how bacterial populations are distributed within the coculture biofilm during growth in DMEM and DMEM + BSA. Enumeration of these microcolonies revealed an average growth of approximately 65–90 of cells per bacterial aggregate, with a maximum count of approximately ~150 of Newman cells (Supplementary Fig. S4). These image analyses also verified that *S. aureus* biofilm growth occurred on top of the *P. aeruginosa* biofilm, which was particularly evident during incubation with DMEM + BSA (Fig. 6d,e). These results are in agreement with those presented in Fig. 4. Therefore, both bacterial species maintain separate growth and distribution in coculture biofilms. Biomass evaluation revealed balanced growth of both bacterial populations of ~35% and ~65% for Newman and PA14, respectively, during incubation in DMEM (Fig. 6f). However, and confirming the confocal microscopy observations, a greater percentage of the *S. aureus* Newman population was measured in DMEM + BSA, accounting for ~70% of the total coculture system (Fig. 6f).

The continuous-flow biofilm confirmed that DMEM favors the coexistence of *P. aeruginosa* and *S. aureus* in mixed biofilms. Furthermore, we also detected how the addition of BSA changed the architecture of the biofilm by increasing *S. aureus* proliferation and identified different spatial distributions of the strains in the biofilm.

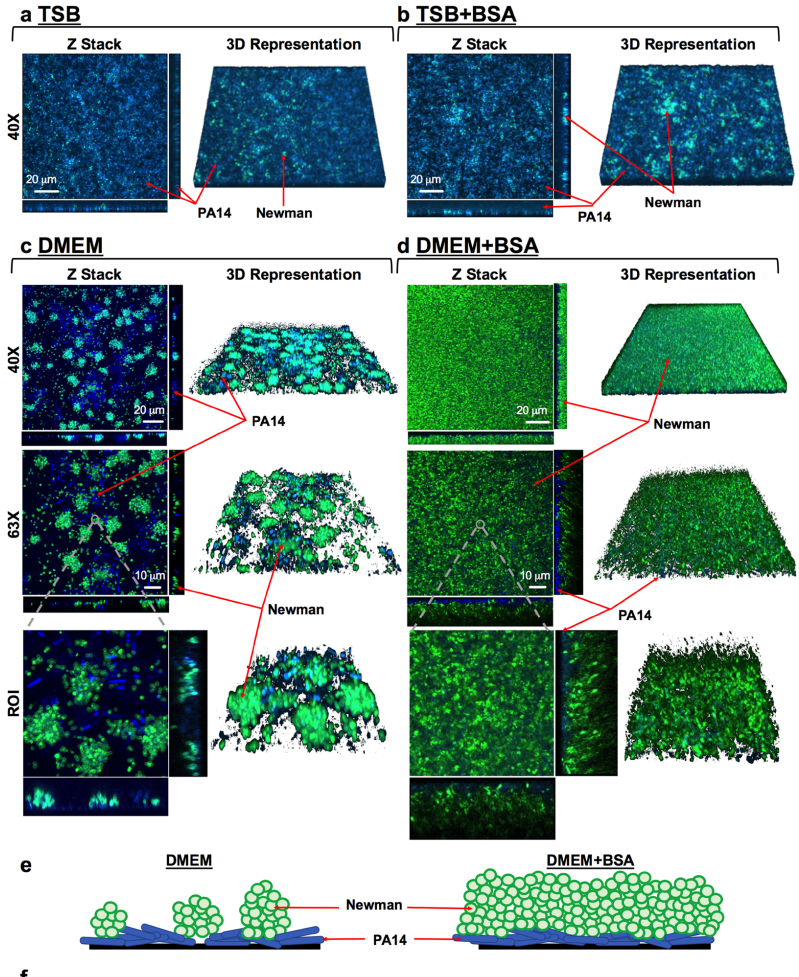

f

Coexistence %

TSB		TSB+BSA		DMEM		DMEM+BSA	
PA14	Newman	PA14	Newman	PA14	Newman	PA14	Newman
90%	10%	85%	15%	65%	35%	30%	70%

Figure 6. Balanced and stable *P. aeruginosa* PA14 and *S. aureus* Newman strain populations within a three-day-old mixed biofilm grown in continuous flow. PA14 and Newman were grown simultaneously in a continuous-flow biofilm in TSB (**a**), TSB + BSA (**b**), DMEM (**c**) and DMEM + BSA (**d**) for three days. At the indicated time point, the biomass growing over the different channels was stained with DAPI (blue, PA14) and CF^{TM}-488A (green, Newman) and visualized using confocal microscopy. The figure shows the composite of the sum of the slices (Z Stack), with the respective orthogonal views, and the 3D representation of each mixed biofilm formed using both ImageJ and ZEN software. Mixed biofilms were tested in triplicate, and a representative image from those taken at magnifications of 40X and 63X is shown. A region of interest (ROI), including the different microscope projections and representations, is also presented in the figure. Red arrows indicate PA14 and Newman strains within the mixed biofilm. (**e**) Schematic representations of the cocultured biofilm depending on growth in DMEM or DMEM + BSA from the previous confocal microscope Z-stacks and orthogonal views. *P. aeruginosa* is represented in blue, and *S. aureus* is represented in green. (**f**) Table shows the percentage of blue *Pseudomonas* and green *Staphylococcus* present in the different cocultured biofilms calculated from an average of 5–15 different microscope stacks using the COMSTAT 2 and ImageJ software.

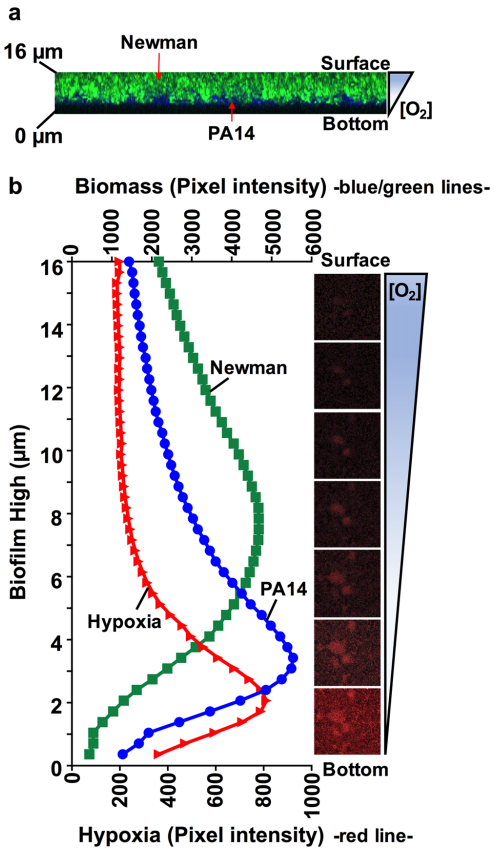

Figure 7. Oxygen stratification within the cocultured biofilm determines the spatial distribution of *P. aeruginosa* and *S. aureus* and their coexistence. (**a**) XZ-orthogonal view of a *P. aeruginosa* and *S. aureus* coculture biofilm grown in DMEM + BSA (see Fig. 6d). The image shows the separate position of Newman and PA14 within the ~16 µm-biofilm and the possible oxygen gradient present in the system. (**b**) Graph shows the average pixel intensities of PA14 (blue) and Newman (Green) biomasses (plotted on the upper Y-axis) compared to the oxygen-related red intensity (plotted on the lower Y-axis) along the different thicknesses (µm) of a 3-day-old cocultured biofilm in flow. Pixel intensity averages were calculated from ten different images using ImageJ software. Included in the figure, is a sequential set of micrographs showing the red fluorescence emission given by the hypoxia probe through the different biofilm layers, indicating the oxygen stratification present along the thickness of the continuous-flow cocultured biofilm. Intense red emission relates to the hypoxic environment through the different biofilm depths (µm), from the bottom to the surface, additionally indicated with a schematic of the oxygen gradient present in the system.

Oxygen stratification within the coculture biofilm is a key modulator of PA14 and Newman coexistence. We next wanted to verify the existence of an oxygen-stratified environment in the continuous-flow biofilm that may influence *S. aureus* survival and stable growth alongside *P. aeruginosa*. Oxygen diffusion within the biofilm was evaluated with the assumption that fresh and oxygenated medium was added continuously in the system (~6.5 mg/mL oxygen measured with the oxygen microsensor).

Orthogonal views of the coculture biofilm grown in the flow-cell channel confirmed the clear distribution of the *S. aureus* biofilm on top of *P. aeruginosa* in the area closest to the medium surface (Fig. 7a). Consequently, we next wanted to validate the presence of an oxygen gradient that could be crucial for Newman survival in the mixed biofilm, and a key modulator of the bacterial distribution detected. To probe different oxygen concentrations within the coculture system, the continuous-flow biofilm was analyzed using the Hypoxia Probe dye. The key attribute of this dye is that its fluorescence is quenched by oxygen, so the lower the oxygen concentration is, the greater the red fluorescence signal emitted by the stained cells, thus allowing the detection of an anaerobic

environment. Red-light emission (hypoxia) through the different layers of the coculture biofilm confirmed the bright fluorescence during the initial ~4 μm of biofilm thickness that gradually decreased across the bacterial community. Red fluorescence was barely detected in the more superficial biofilm layers, thus confirming aerobic conditions in that area (Fig. 7b). Additionally, pixel intensity analysis of the hypoxic region (red) corroborated that red emission peaked around the initial ~2 μm of the biofilm depth. Furthermore, the PA14-Newman biomass was also quantified in this continuous-flow biofilm. *P. aeruginosa* PA14 (blue) displayed a maximum peak intensity at ~3 μm of the biofilm depth, corresponding to the more anaerobic region of the biofilm, with fluorescence extending to a thickness of ~10 μm. *S. aureus* Newman (green) clearly showed a pixel intensity curve shifted to higher and more oxygenic biofilm layers (Fig. 7b). Green intensity measurements confirmed that *S. aureus* was barely detectable in the initial ~3 μm of the mixed biofilm (coinciding with the anoxic part of the biofilm); the intensity increased, achieving a maximum and extended peak at ~6–9 μm of depth, with fluorescence emission extending to ~14–10 μm of the biofilm thickness.

Taken together, these results demonstrate that the coculture biofilm formed in continuous flow also displays oxygen stratification across the different biofilm layers. *P. aeruginosa* growth occurred across the deepest layers of the biofilm, where less oxygen content was detected, while *S. aureus* biofilm growth was quantified closer to the biofilm surface, corresponding to the most oxygenated area.

Antibiotic resistance of *P. aeruginosa* and *S. aureus* is critically increased during coculture biofilm growth. Biofilm-associated infections have historically been treated as single-species events. Nevertheless, some of these infections are now known to be composed of multiple combinations of bacteria, involving complex interactions that can influence their fitness and antibiotic tolerance[2,4]. The demonstration of altered antibiotic susceptibilities of PA14 and Newman when grown in coculture biofilms was thought to be necessary to validate the combination of coculture conditions and environmental prerequisites identified in this study. Even though in DMEM + BSA condition presence of *S. aureus* within the mixed biofilm grown in microtiter plates was detected also after 72 h of coculture growth, we chose to evaluate the antimicrobial tolerance after 48 h since according to Fig. 3b, at that time-point Newman's CFUs in the coculture biofilm were counted ~100−fold higher than at 72 h. Hence, 48 h-old PA14 and Newman mono- and coculture biofilms were treated with ciprofloxacin (Cpx) and gentamicin (Gm). The respective biofilm-forming CFUs were subsequently counted on selective agar. The antibiotics and the range of concentrations used were chosen according to their reported minimal inhibitory concentrations (MICs) and their usage in treating both bacterial infections[4,31]. The experiment was performed in a 96-well microtiter plate and included BSA since it was the additive that showed the greatest potential for maintaining the stable growth of both bacterial populations *in vitro*.

Bacterial CFUs that remained viable within the mono- and the coculture biofilms after the antibiotic treatment were enumerated (Supplementary Table S3), and the percentages of viable CFUs that persisted in each biofilm after the different treatments, compared to each untreated biofilm, were subsequently calculated (Fig. 8). The Minimum Biofilm Eradication Concentration (MBEC) of each antibiotic against *P. aeruginosa* and *S. aureus* mono and coculture biofilms was also calculated (Table 1). Crystal violet staining of control wells confirmed that the mature biofilm grew in the ALI area of the well (data not shown). A similar behavioral pattern was observed in both organisms after the respective antibiotic treatments; however, *S. aureus* revealed a much greater benefit of growing in coculture than *P. aeruginosa*, since its viability during both treatments increased exponentially when grown in coculture with *P. aeruginosa*. As for *P. aeruginosa*, the bacterium exhibited ~38-, ~68- and ~390-fold higher tolerance to Gm treatment in coculture than in monoculture biofilm growth for concentrations of 0.5, 1 and 2 μg/mL, respectively, (Fig. 8a - graph PA14%) and ~7- and ~27.5-fold increased to Cpx treatment used at concentrations of 0.5 and 1 μg/mL (Fig. 8b - graph PA14%). The MBEC determinations (Table 1) confirmed that Gm treatment at ≥0.5 and ≥4 μg/mL and Cpx treatment at ≥0.5 and ≥2 μg/mL cleared PA14 from the mono- and coculture biofilms, respectively (Fig. 8a,b -graph PA14%). The percentage calculations revealed that growing *S. aureus* in coculture enhanced its capacity to persist in the presence of Gm >1000-fold, at a concentration of 0.5 μg/mL, and >470-fold at 1 μg/mL (Fig. 8a - graph Newman%). A similar pattern was detected for Cpx treatment; within a coculture biofilm with *P. aeruginosa*, the viability of *Staphylococcus* increased ~400-fold when the antibiotic was used at 0.5 μg/mL and >468-fold when it was used at 1 μg/mL (Fig. 8b - graph Newman%). Only doses ≥2 μg/mL of Gm or Cpx cleared *S. aureus* from the mixed biofilm. In contrast, treatments with 0.5 μg/mL with any of the antibiotics used was sufficient to clear *S. aureus* from a 48 h-old monoculture biofilm (Fig. 8a,b - graph Newman% and Table 1). When these high concentrations were used, the viability of the *S. aureus* strain was drastically reduced.

Comparisons between the percentages of the viable *P. aeruginosa* and *S. aureus* CFUs in the coculture biofilm after the antibiotic treatments to those calculated in the monoculture biofilms revealed significance in all cases ($p < 0.001$). These results confirm the increased antibiotic tolerance of *P. aeruginosa* PA14 and *S. aureus* Newman strains when grown in a mixed biofilm rather than in a monoculture biofilm, thus validating the coculture conditions established in this study.

Discussion

Biofilm-associated infections are currently a critical worldwide threat[32–34]. The increasing emergence of antimicrobial-resistant bacteria and the knowledge that some of these infections are polymicrobial challenge the antimicrobial chemotherapy to administrate and aggravates the disease outcome[2,35,36]. *P. aeruginosa* and *S. aureus* are two major pathogens commonly found growing together in intricate biofilms in disease-affected lungs[11] or wounds[13]. Herein, we have unraveled the potential of DMEM to sustain a *P. aeruginosa* PA14 and *S. aureus* Newman combined biofilm for up to three days *in vitro* and identified BSA as a valuable and critical additive that significantly increases *S. aureus* survival and growth in the coculture system. Remarkably, we also demonstrated the importance of continuous oxygen diffusion in limiting *S. aureus* survival and keeping the growth of both

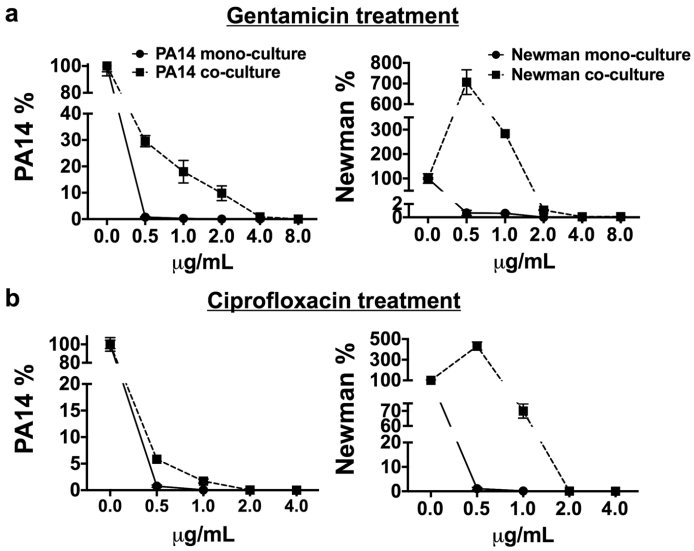

Figure 8. *P. aeruginosa* PA14 and *S. aureus* Newman coculture biofilms induce enhanced tolerance to antibiotic treatment compared to monoculture biofilms. After 48 h, matured mono- and cocultured PA14 and Newman biofilms grown in microtiter plates were treated with 0.5, 1.0, 2.0, 4.0 and 8.0 μg/mL gentamicin (**a**) and 0.5, 1.0, 2.0, and 4.0 μg/mL ciprofloxacin (**b**) for 15 h. Symbols in the plots represent the remaining percentage of CFUs of each strain in the biofilm after different antibiotic treatments compared to the relative untreated biofilm. Each graph shows the percentages of PA14 and Newman CFUs compared according to whether the biofilms were grown in mono- or coculture. Percentages were calculated according to the bacterial CFUs counted on selective agar plates after different antimicrobial treatments (Supplementary Table S3). Analysis of the statistical significance between the calculated percentages of bacterial CFUs that remained in the cocultured biofilm (after each antibiotic treatment) and those calculated in the monocultured biofilms revealed significance with $p < 0.0001$ in all cases.

	MBEC (μg/mL)	Biofilm reduction
Gentamicin		
PA14 monoculture	0.5	≥99%
PA14 coculture	4	≥99%
Newman monoculture	0.5	≥99%
Newman coculture	2	≥99%
Ciprofloxacin		
PA14 monoculture	0.5	≥99%
PA14 coculture	2	≥99%
Newman monoculture	0.5	≥99%
Newman coculture	2	≥99%

Table 1. MBEC values of gentamicin and ciprofloxacin antibiotics against *P. aeruginosa* PA14 and *S. aureus* Newman in monoculture or coculture biofilms.

bacterial populations balanced, highly influencing their distribution in the coculture biofilm. Furthermore, using our developed coculture conditions, we confirmed that the antimicrobial susceptibilities of *P. aeruginosa* and *S. aureus* differ depending on whether they are growing in monoculture or coculture in biofilms.

Among the different media evaluated (LB, TSB and SCFM2), DMEM was the greatest at controlling *S. aureus* survival during simultaneous growth (planktonic and biofilm) with *P. aeruginosa*. DMEM is a rich culture medium used in routine cell culture experiments, which contains numerous amino acids, vitamins, and inorganic salts, among other components[37]. Remarkably, the D-glucose concentration in this medium is ~17.5 mM, which is greater than the usual 0.2% (~11.1 mM) added to LB or TSB medium in routinely used biofilm formation protocols[38–40], or the 3 mM present in the SCFM2 medium[41]. In healthy people, glucose concentration in the airway surface

liquid (ASL) is ∼0.4 mM, 12 times lower than blood glucose[42,43]. However, lung inflammation, caused by diseases such as CF or chronic airway inflammation, increases glucose flux through the epithelial cell membrane, raising ∼10–12 times the glucose concentration in the ASL. Different studies have described how increased glucose levels in ASL promote bacterial lung infection[42,44,45]. Furthermore, diabetes affected-people have wound healing issues and increased risk of infection due to an impaired host defence[46]. Glucose is not the preferred carbon source of *P. aeruginosa*[47] but is the preferred carbon source of *S. aureus*, which exhibits preferential uptake of this sugar, especially during infection[48]. Therefore, it is plausible to hypothesize that *S. aureus* could benefit from the high glucose concentration in DMEM and grow without competition for the substrate. Additionally, a differential planktonic growth pattern was detected in *S. aureus* Newman depending on whether the bacterium was grown in DMEM or TSB (Supplementary Fig. S5). In DMEM, *S. aureus* grew rapidly and achieved late-exponential/stationary phase, with growth maintained during the course of the experiment. However, in TSB, the strain exhibited the usual bacterial growth curve with lag, exponential and stationary phases. This result indicates increased efficiency of *S. aureus* growth in DMEM, especially during the initial stage of growth, which we hypothesize could be beneficial during simultaneous biofilm growth with *P. aeruginosa* to rapidly form a microcolony after initial attachment, thus providing defense against *Pseudomonas*[49]. *S. aureus* growth in firmly packed microcolonies during coculture biofilm growth with *P. aeruginosa* PAO1 has been previously seen by Yang and coworkers[50]. In our study, this microcolony formation may also be facilitated by the increased concentration of NaCl present in the DMEM formulation (∼120 mM), which is >3-fold higher than in LB, TSB or SCFM2 and has been seen to stimulate biofilm aggregation and growth[51,52]. The concentration of glutamine present in DMEM (∼2.5 mM) may also affect the coexistence of both microorganisms by diminishing the specific competition for this amino acid, as a nitrogen and energy source, which has been recently reported to occur early during coculture[53].

Significantly, DMEM contains HEPES (4-(2-hydroxyethyl)-1-piperazineethanesulfonic acid; ∼15 mM), which is considered a "good buffer" for its limited effect on biochemical reactions and for being chemically and enzymatically stable, among other properties[54]. The buffering properties of HEPES were evident in the growing coculture biofilms, and the pH rise was dampened compared to that measured in the other media (Fig. 2). pH homeostasis is critical to maintaining the integrity of cytoplasmic proteins in all living cells, and their optimal pH fluctuates in a narrow range of 7.4–7.8[25,26]. Although SCFM2 contains 3-morpholinopropanesulfonic acid, it failed to maintain the pH levels in the coculture. This synthetic CF medium was developed based on CF sputum that contained high concentrations of *P. aeruginosa*[41], which may explain why SCFM2 did not support *S. aureus* viability in the system. Additionally, a factor increasing the perturbation of *P. aeruginosa* and *S. aureus* coexistence in this fluctuating pH environment is the production of different proteases by *P. aeruginosa* in an alkaline environment of pH ∼8. In particular, the *P. aeruginosa* staphylolytic protease LasA possesses optimal activity at approximately pH 8.5[55–57].

DMEM supplementation with BSA and L-arginine increased *S. aureus* viability throughout the 72 h of coculture biofilm growth with *P. aeruginosa*. Although coculturing the biofilm in DMEM + L-arg increased the Newman biofilm-forming CFUs, confocal microscopy revealed an altered coculture biofilm architecture, with disaggregated clumps covering the coverslip (Fig. 4d), which is consistent with the phenotype promoted by L-arginine that has been seen in other biofilm communities[58–60]. Thus, we conclude that among the additives tested, BSA possesses the greatest potential to increase *S. aureus* viability and maintain the population balance in a well-engineered coculture biofilm with *P. aeruginosa*. Subsequent experiments in flow-cell biofilms corroborated the effect of BSA in increasing *S. aureus* survival and growth during mixed biofilm formation with *P. aeruginosa* (Fig. 6d). Although albumin has been described to diminish *P. aeruginosa* killing of *S. aureus* in wounds by binding and sequestering *Pseudomonas* quorum sensing molecules[21], which is also likely what occurred in our model, we also believe albumin has a direct effect on *S. aureus* viability, although further experiments are needed to confirm this hypothesis. Albumin is the main plasma protein and a carrier of numerous molecules, such as metals and other ions, bilirubin, amino acids, fatty acids, enzymes, and hormones[61]. With an unknown mechanism, it is known that the presence of this protein in the culture medium enhances *S. aureus* growth exponentially, possibly by scavenging traces of protein-bound nutrients[62–64]. Therefore, we suggest that albumin could play a direct role in inducing prompt microcolony formation by increasing the proliferation rate of *S. aureus* in a hostile environment with *P. aeruginosa*. Furthermore, although expression of different virulence factors of *Pseudomonas* has detected increased during coculture growth with *S. aureus* (e.g. LasA protease or pyocyanin production)[53], some staphylococcal factors (e.g. the Panton-Valentin leukocidin protein) have been also observed during these coculture conditions, which may be playing a role also in competing with the *Pseudomonas*[65].

Remarkably, in this study, we demonstrate an important role for oxygen in achieving continuous and stable coculture biofilms of *P. aeruginosa* and *S. aureus*. We also observed a differential distribution of the bacterial populations depending on the oxygen content in the surrounding environment. Lungs are not entirely aerobic, especially those affected by CF, in which the thick mucus present in the airways generates diverse oxygen content between pulmonary regions, thus enhancing the heterogeneity of microbes able to proliferate and persist at the same site[66–68]. Oxygen diffusion also mediates the different spatial distribution of bacteria in wounds; hence, *P. aeruginosa* has been found deeper in the tissue than *S. aureus*, which grows predominantly at the wound surface[13]. *Pseudomonas* is able to grow in anaerobic conditions in the presence of nitrates, which are included in the DMEM formulation. *S. aureus* encodes a set of genes required for growth either aerobically or anaerobically[69,70]; however, aerobic respiration is preferred by *S. aureus* during monoculture growth. Despite these metabolic preferences, during simultaneous growth with *P. aeruginosa*, oxygen competition between organisms drives *S. aureus* to shift to fermentative metabolism. This metabolic shift is also triggered by the expression of siderophores, phenazines and other exoproducts (i.e., 2-heptyl-4-hydroxyquinoline N-oxide (HQNO) production) by *Pseudomonas* that compromise *S. aureus* viability[15,71]. In our model, increased *S. aureus* Newman survival was detected when the coculture biofilms were grown in the ALI area, either in a 96-well plate or over coverslips, rather than during complete medium immersion. Furthermore, we confirmed the existence of an oxygen gradient across the medium

depth during biofilm growth, with a continuous micro-oxygenated phase at the medium surface (corresponding to the ALI area). Therefore, we hypothesize that persistent oxygen diffusion at the ALI area of the coculture system increases *S. aureus* survival within the mixed biofilm by diminishing the oxygen competition between the organisms and the subsequent production of *P. aeruginosa* molecules that eventually kill *S. aureus*.

The public health concern about biofilm-associated diseases is linked to the altered antimicrobial susceptibilities that these communities present[36]. Unoptimized therapies and variations in the antibiotic concentration across the biofilm layers promote the development of resistance since bacteria are usually exposed to subinhibitory concentrations of the antimicrobial[4]. Exacerbating the problem is the fact that these biofilms tend to be composed of multiple species, with different fitness values and high levels of cooperative and synergistic interactions that are often detrimental to the host[2,4]. For instance, the simple addition of *P. aeruginosa* supernatant to *S. aureus* Newman biofilms has been seen to be sufficient to increase the tolerance of *S. aureus* to a wide range of antibiotics, such as vancomycin, tobramycin and oxacillin[18]. Furthermore, it has been seen that continuous exposure of *S. aureus* to *P. aeruginosa* HQNO promotes the formation of antibiotic-resistant small colony variants of the bacterium, enhancing its resistance to aminoglycosides[23]. *P. aeruginosa* and *S. aureus* showed enhanced tolerance to gentamicin and ciprofloxacin antibiotics when they were grown in coculture biofilms (Fig. 8). Hence, we believe that the use of the conditions revealed in this study allows the stable formation of *P. aeruginosa* PA14 and *S. aureus* Newman coculture biofilms involving the intricate and interspecific relations responsible for influencing the antimicrobial tolerance of each strain.

In summary, in this study, we elucidated the potential of DMEM for *P. aeruginosa* and *S. aureus in vitro* coculture. Additionally, we have discovered that supplementing DMEM with BSA and providing continuous oxygen diffusion allows the formation of a mature mixed biofilm with stable populations of *P. aeruginosa* and *S. aureus*. This study provides useful insights about the establishment of a *P. aeruginosa* and *S. aureus* combined biofilm *in vitro*, which we believe would be of help for the study of phenotypes derived from this clinically challenging bacterial cooperation as well as for optimizing the antimicrobial therapy used to treat these infections.

Methods

Bacterial strains and growth conditions. *Pseudomonas aeruginosa* PA14 wild type[72] and *Staphylococcus aureus* Newman (ATCC 13420) were used throughout this study, although *S. aureus* ATCC 12600 and ATCC 29213 were also initially tested. Overnight cultures (O/N) were performed aerobically at 37 °C in Luria-Bertani medium (LB; Scharlab, S.L., Barcelona, Spain) and in tryptic soy broth (TSB; Scharlab, S.L.) for the PA14 and Newman strains, respectively.

***P. aeruginosa* PA14 and *S. aureus* Newman coculture medium conditions.** LB, TSB, synthetic cystic fibrosis sputum medium 2 (SCFM2), prepared as previously described[41], and Dulbecco's modified Eagle's medium/nutrient mixture F-12 (DMEM; Thermo Fisher Scientific, Waltham, Massachussetts) were tested. When required, reduced nicotinamide adenine dinucleotide phosphate (NADPH; 0.2 mM), adenosine monophosphate (AMP; 10 mM), bovine serum albumin (BSA; 5% w/v) and L-arginine (0.4% w/v) were added to the medium. O/N cultures of PA14 and Newman strains were washed twice with 1X phosphate-buffered saline (PBS, pH = 7.4). To prepare the initial mixed bacterial suspension, each strain was inoculated at a final optical density $\lambda = 550$ nm (OD_{550}) of 0.05 for planktonic experiments, and an OD_{550} of 0.10 for biofilm experiments.

Planktonic coculture growth. Mixed bacterial suspensions in a final volume of 20 mL were incubated aerobically at 37 °C with vigorous shaking (200 rpm). At given time points, each planktonic culture was serially diluted in 1X PBS and plated on LB agar (Scharlab, S.L.) to count *P. aeruginosa* CFUs, and tryptic soy agar (TSA; Scharlab, S.L.) supplemented with 7.5% (w/v) NaCl to selectively count *S. aureus* CFUs[73].

Coculture biofilm growth under static conditions. Static *P. aeruginosa* PA14-*S. aureus* Newman mixed biofilm growth was tested on (i) plastic and (ii) glass surfaces:

(i) **Plastic surface:** 200 µl of each mixed bacterial suspension was inoculated in triplicate in 96-well polystyrene plates with a flat bottom (Corning; Sigma-Aldrich, San Luis, Missouri) and incubated at 37 °C without shaking. At different time points, the planktonic phase was removed, and each well was washed three times with 1X PBS. The biofilm phase formed over the wall of each well was removed using a pipette tip, and the triplicates were mixed together. For CFU quantification, each biofilm cell suspension was placed in an ultrasonic bath (USC100T, VWR) for 5 min and subsequently vortexed for 30 seconds, to help dispersing the biofilm. Bacterial suspensions were then serially diluted in 1X PBS and plated on selective agar as described for planktonic growth. Separately, the biofilm mass formed inside the well was stained with 0.1% (w/v) crystal violet, and the biomass (OD_{570}) was determined as previously described[74].

(ii) **Glass surface:** 18 × 18 mm coverslips (Menzel-Gläser, Thermo Fisher Scientific) were placed in a 6-well polystyrene plate with lid (Dd biolab, Barcelona, Spain), and each well was filled with 3 mL of the PA14-Newman bacterial suspension. The coverslip was positioned completely immersed in the bacterial suspension or only half immersed. The half immersion, with the air-liquid interphase (ALI) area, was achieved by placing the coverslip at a ~45° angle against the wall of the well (see Fig. 4b). Unattached cells were removed after three hours of incubation, and 3 mL of fresh medium was subsequently added again. This procedure was repeated every 12 h during the course of the experiment. At the given time points, the coverslip, covered with the established mixed biofilm, was gently washed with PBS. To determine bacterial CFUs, biofilm-forming cells were scraped off the coverslip, and serial dilutions were plated on selective agar plates as described above. In addition, the biomass of the PBS-washed coverslip was stained with crystal violet or with different dyes for confocal microscopy as described below.

pH measurements. The pH of the supernatant phase of each PA14 and Newman monoculture and coculture biofilm was measured using a GLP 21 pH meter (Crison®, Hospitalet de Llobregat, Barcelona). For this experiment, biofilms were grown in a volume of 3 mL in 6-well polystyrene plates. pH measurements were taken in triplicate for each culture medium and time point, directly in the microplate well where the biofilm was growing.

Confocal laser scanning microscopy and image analysis. To differentially stain *P. aeruginosa* PA14 and *S. aureus* Newman, a Bacterial Viability and Gram Stain kit (Biotium, Fremont, California) was used following the manufacturer's instructions. This kit uses the cell membrane differences between gram-negative and gram-positive bacteria to differentially stain each species. Briefly, the kit combines DAPI to stain the bacterial DNA blue with CF™-488A-wheat germ agglutinin (WGA) to bind, specifically, the N-acetylglucosamine present in the peptidoglycan of the cell wall in gram-positive bacteria. Consequently, *P. aeruginosa* PA14 will be stained blue, and *S. aureus* Newman will be stained green. To detect bacterial cells growing in different oxygen concentrations, we used the phosphorescent light-emitting iridium complex Hypoxia Probe (Organogenix; Bionova científica, Barcelona, Spain) according to the manufacturer's instructions.

Stained bacteria were imaged using a Zeiss LSM 800 confocal laser scanning microscope (CSLM, Zeiss, Oberkochen, Germany), and images were analyzed with ImageJ and ZEN (Zeiss software).

Assessment of the oxygen concentration in the coculture system. The coculture biofilm was established as described above but using lids for the 6-well plates with small holes drilled in the desired locations. After the addition of fresh medium, the plate was transferred to equipment for oxygen measurement described in Supplementary Fig. S3. The dissolved oxygen was measured using an Oxymicro Fiber-Optic Sensor System (World Precision Instruments) connected to a micro-optode oxygen sensor in a syringe-type housing (PreSens, Regensburg, Germany); the needle of the housing crossed the lid of the plate, and the optical fiber was placed using the plunger at the desired location. All measurements were compensated with temperature using a temperature probe placed directly above the culture plate.

Micro-optodes were calibrated using temperature-compensated measurements of water saturated with air (100% air saturation, 8.25 mg/L at 25 °C and 1 atm) and a 10 g/L solution of sodium dithionite (0% O_2).

Coculture biofilm incubated in a continuous-flow system. The *P. aeruginosa* and *S. aureus* mixed bacterial suspension (each strain at $OD_{550} = 0.10$) was inoculated in a three-channel flow-cell (DTU Systems biology, Technical University of Denmark). Media was pumped at a constant flow rate of 42 µl per minute and channel using an Ismatec ISM 943 pump (Ismatec, Wertheim, Germany), as previously described[75]. After 3 days of growth, biofilms were stained with the Bacterial Viability and Gram Stain kit or with the Hypoxia Probe and observed by confocal microscopy. Images were generated, and biomass was calculated using ImageJ and COMSTAT 2 software[75]. Percentage of *S. aureus* in the coculture biofilm was calculated taking the pixels given by *S. aureus*-CF™-488A (channel 0) from the pixels given by the total DAPI staining (channel 1). *P. aeruginosa* percentage in the coculture biofilm was subsequently obtained by subtracting the percentage of *S. aureus* coverage from the total biofilm (100%).

Antimicrobial treatments and minimum biofilm eradication concentration (MBEC) calculations. *P. aeruginosa* PA14 and *S. aureus* Newman 48 h coculture biofilms in 96-well polystyrene plates were treated with gentamicin sulfate (Panreac AppliChem, Castellar del Vallès, Spain) at concentrations of 0.5, 1, 2, 4 and 8 µg/mL and with ciprofloxacin hydrochloride (Cayman Chemical, Ann Arbor, Michigan) at 0.5, 1, 2 and 4 µg/mL to investigate possible alterations on antibiotic tolerance depending if they were cultured in mono or in coculture biofilms. Furthermore, different MBEC were also calculated according to the treatment concentration that eradicated ≥99% of the biofilms[76]. After 15 h of incubation with antibiotics, biofilms were washed with 1X PBS and scraped off each well and subsequently sonicated and vortexed as previously detailed. Serial dilutions were then plated on selective agar plates.

Statistics. Differences in bacterial CFUs/mL and CFUs/well between time points or strains were analyzed using one-way ANOVA with Dunnett's multiple comparison test using GraphPad Prism 6.0 software. To compare the significance between the percentages of bacterial CFUs that remained in the coculture biofilm after gentamicin and ciprofloxacin treatment compared to those calculated in the monoculture biofilms, we used the χ^2 test[77].

Received: 17 June 2019; Accepted: 22 October 2019;
Published online: 08 November 2019

References

1. Bjarnsholt, T., Ciofu, O., Molin, S., Givskov, M. & Hoiby, N. Applying insights from biofilm biology to drug development - can a new approach be developed? *Nat Rev Drug Discov* **12**, 791–808, https://doi.org/10.1038/nrd4000 (2013).
2. Murray, J. L., Connell, J. L., Stacy, A., Turner, K. H. & Whiteley, M. Mechanisms of synergy in polymicrobial infections. *J Microbiol* **52**, 188–199, https://doi.org/10.1007/s12275-014-4067-3 (2014).
3. Stacy, A., McNally, L., Darch, S. E., Brown, S. P. & Whiteley, M. The biogeography of polymicrobial infection. *Nat Rev Microbiol* **14**, 93–105, https://doi.org/10.1038/nrmicro.2015.8 (2016).
4. Algburi, A., Comito, N., Kashtanov, D., Dicks, L. M. & Chikindas, M. L. Control of Biofilm Formation: Antibiotics and Beyond. *Appl Environ Microbiol* **83**, https://doi.org/10.1128/AEM.02508-16 (2017).
5. Baas Becking, L. G. M., Canfield, D. E., Sherwood, D. & Stuip, M. *Baas Becking's: geobiology, or, introduction to environmental science* (Wiley Blackwell, 2016).
6. Fuhrman, J. A. Microbial community structure and its functional implications. *Nature* **459**, 193–199, https://doi.org/10.1038/nature08058 (2009).

7. Goss, C. H. & Burns, J. L. Exacerbations in cystic fibrosis. 1: Epidemiology and pathogenesis. *Thorax* **62**, 360–367, https://doi.org/10.1136/thx.2006.060889 (2007).
8. Kreda, S. M., Davis, C. W. & Rose, M. C. CFTR, mucins, and mucus obstruction in cystic fibrosis. *Cold Spring Harb Perspect Med* **2**, a009589, https://doi.org/10.1101/cshperspect.a009589 (2012).
9. Yang, L., Jelsbak, L. & Molin, S. Microbial ecology and adaptation in cystic fibrosis airways. *Environ Microbiol* **13**, 1682–1689, https://doi.org/10.1111/j.1462-2920.2011.02459.x (2011).
10. Puchelle, E., Bajolet, O. & Abely, M. Airway mucus in cystic fibrosis. *Paediatr Respir Rev* **3**, 115–119 (2002).
11. Hauser, A. R., Jain, M., Bar-Meir, M. & McColley, S. A. Clinical significance of microbial infection and adaptation in cystic fibrosis. *Clin Microbiol Rev* **24**, 29–70, https://doi.org/10.1128/CMR.00036-10 (2011).
12. Hotterbeekx, A., Kumar-Singh, S., Goossens, H. & Malhotra-Kumar, S. *In vivo* and *In vitro* Interactions between *Pseudomonas aeruginosa* and *Staphylococcus* spp. *Front Cell Infect Microbiol* **7**, 106, https://doi.org/10.3389/fcimb.2017.00106 (2017).
13. Fazli, M. *et al*. Nonrandom distribution of *Pseudomonas aeruginosa* and *Staphylococcus aureus* in chronic wounds. *J Clin Microbiol* **47**, 4084–4089, https://doi.org/10.1128/JCM.01395-09 (2009).
14. Woods, P. W., Haynes, Z. M., Mina, E. G. & Marques, C. N. H. Maintenance of *S. aureus* in Co-culture With *P. aeruginosa* While Growing as Biofilms. *Front Microbiol* **9**, 3291, https://doi.org/10.3389/fmicb.2018.03291 (2018).
15. Filkins, L. M. *et al*. Coculture of *Staphylococcus aureus* with *Pseudomonas aeruginosa* Drives *S. aureus* towards Fermentative Metabolism and Reduced Viability in a Cystic Fibrosis Model. *J Bacteriol* **197**, 2252–2264, https://doi.org/10.1128/JB.00059-15 (2015).
16. Limoli, D. H. *et al*. *Pseudomonas aeruginosa* Alginate Overproduction Promotes Coexistence with *Staphylococcus aureus* in a Model of Cystic Fibrosis Respiratory Infection. *MBio* **8**, https://doi.org/10.1128/mBio.00186-17 (2017).
17. Wijesinghe, G. *et al*. Influence of Laboratory Culture Media on *in vitro* Growth, Adhesion, and Biofilm Formation of *Pseudomonas aeruginosa* and *Staphylococcus aureus*. *Med Princ Pract* **28**, 28–35, https://doi.org/10.1159/000494757 (2019).
18. Orazi, G. & O'Toole, G. A. *Pseudomonas aeruginosa* Alters *Staphylococcus aureus* Sensitivity to Vancomycin in a Biofilm Model of Cystic Fibrosis Infection. *MBio* **8**, https://doi.org/10.1128/mBio.00873-17 (2017).
19. Alves, P. M. *et al*. Interaction between *Staphylococcus aureus* and *Pseudomonas aeruginosa* is beneficial for colonisation and pathogenicity in a mixed biofilm. *Pathog Dis* **76**, https://doi.org/10.1093/femspd/fty003 (2018).
20. Orazi, G., Ruoff, K. L. & O'Toole, G. A. *Pseudomonas aeruginosa* Increases the Sensitivity of Biofilm-Grown *Staphylococcus aureus* to Membrane-Targeting Antiseptics and Antibiotics. *MBio* **10**, https://doi.org/10.1128/mBio.01501-19 (2019).
21. Smith, A. C. *et al*. Albumin Inhibits *Pseudomonas aeruginosa* Quorum Sensing and Alters Polymicrobial Interactions. *Infect Immun* **85**, https://doi.org/10.1128/IAI.00116-17 (2017).
22. DeLeon, S. *et al*. Synergistic interactions of *Pseudomonas aeruginosa* and *Staphylococcus aureus* in an *in vitro* wound model. *Infect Immun* **82**, 4718–4728, https://doi.org/10.1128/IAI.02198-14 (2014).
23. Hoffman, L. R. *et al*. Selection for *Staphylococcus aureus* small-colony variants due to growth in the presence of *Pseudomonas aeruginosa*. *Proc Natl Acad Sci USA* **103**, 19890–19895, https://doi.org/10.1073/pnas.0606756104 (2006).
24. Baldan, R. *et al*. Adaptation of *Pseudomonas aeruginosa* in Cystic Fibrosis airways influences virulence of *Staphylococcus aureus in vitro* and murine models of co-infection. *PLoS One* **9**, e89614, https://doi.org/10.1371/journal.pone.0089614 (2014).
25. Padan, E., Bibi, E., Ito, M. & Krulwich, T. A. Alkaline pH homeostasis in bacteria: new insights. *Biochim Biophys Acta* **1717**, 67–88, https://doi.org/10.1016/j.bbamem.2005.09.010 (2005).
26. Krulwich, T. A., Sachs, G. & Padan, E. Molecular aspects of bacterial pH sensing and homeostasis. *Nat Rev Microbiol* **9**, 330–343, https://doi.org/10.1038/nrmicro2549 (2011).
27. Zhu, Y. *et al*. *Staphylococcus aureus* biofilm metabolism and the influence of arginine on polysaccharide intercellular adhesin synthesis, biofilm formation, and pathogenesis. *Infect Immun* **75**, 4219–4226, https://doi.org/10.1128/IAI.00509-07 (2007).
28. Sheng, L. *et al*. Interkingdom adenosine signal reduces *Pseudomonas aeruginosa* pathogenicity. *Microb Biotechnol* **5**, 560–572, https://doi.org/10.1111/j.1751-7915.2012.00338.x (2012).
29. Deng, X. *et al*. Steady-state hydrogen peroxide induces glycolysis in *Staphylococcus aureus* and *Pseudomonas aeruginosa*. *J Bacteriol* **196**, 2499–2513, https://doi.org/10.1128/JB.01538-14 (2014).
30. Stewart, P. S. & Franklin, M. J. Physiological heterogeneity in biofilms. *Nat Rev Microbiol* **6**, 199–210, https://doi.org/10.1038/nrmicro1838 (2008).
31. Amirkia, V. D. & Qiubao, P. The Antimicrobial Index: a comprehensive literature-based antimicrobial database and reference work. *Bioinformation* **5**, 365–366 (2011).
32. Parsek, M. R. & Singh, P. K. Bacterial biofilms: an emerging link to disease pathogenesis. *Annu Rev Microbiol* **57**, 677–701, https://doi.org/10.1146/annurev.micro.57.030502.090720 (2003).
33. Malyshkin, A. P. Chronic infections: causes and possible approach to treatment. *Research Journal of Infectious Diseases* **2**, https://doi.org/10.7243/2052-5958-2-3 (2014).
34. Sadekuzzaman, M., Yang, S., Mizan, M. F. R. & Ha, S. D. Current and Recent Advanced Strategies for Combating Biofilms. *Comprehensive Reviews in Food Science and Food Safety* **14**, 491–509, https://doi.org/10.1111/1541-4337.12144 (2015).
35. Wolcott, R., Costerton, J. W., Raoult, D. & Cutler, S. J. The polymicrobial nature of biofilm infection. *Clin Microbiol Infect* **19**, 107–112, https://doi.org/10.1111/j.1469-0691.2012.04001.x (2013).
36. Del Pozo, J. L. Biofilm-related disease. *Expert Rev Anti Infect Ther* **16**, 51–65, https://doi.org/10.1080/14787210.2018.1417036 (2018).
37. Dulbecco, R. & Freeman, G. Plaque production by the polyoma virus. *Virology* **8**, 396–397 (1959).
38. Sambrook, J. *Molecular cloning: a laboratory manual* (Third edition. Cold Spring Harbor, N.Y.: Cold Spring Harbor Laboratory Press, [2001] ©2001, 2001).
39. Mc, C. N. Laboratory tests in the diagnosis of brucellosis. *Am J Public Health Nations Health* **39**, 866–869 (1949).
40. O'Toole, G. A. Microtiter dish biofilm formation assay. *J Vis Exp*, https://doi.org/10.3791/2437 (2011).
41. Turner, K. H., Wessel, A. K., Palmer, G. C., Murray, J. L. & Whiteley, M. Essential genome of *Pseudomonas aeruginosa* in cystic fibrosis sputum. *Proc Natl Acad Sci USA* **112**, 4110–4115, https://doi.org/10.1073/pnas.1419677112 (2015).
42. Mallia, P. *et al*. Role of airway glucose in bacterial infections in patients with chronic obstructive pulmonary disease. *J Allergy Clin Immunol* **142**, 815–823 e816, https://doi.org/10.1016/j.jaci.2017.10.017 (2018).
43. Baker, E. H. & Baines, D. L. Airway Glucose Homeostasis: A New Target in the Prevention and Treatment of Pulmonary Infection. *Chest* **153**, 507–514, https://doi.org/10.1016/j.chest.2017.05.031 (2018).
44. Brennan, A. L. *et al*. Airway glucose concentrations and effect on growth of respiratory pathogens in cystic fibrosis. *J Cyst Fibros* **6**, 101–109, https://doi.org/10.1016/j.jcf.2006.03.009 (2007).
45. Pezzulo, A. A. *et al*. Glucose depletion in the airway surface liquid is essential for sterility of the airways. *PLoS One* **6**, e16166, https://doi.org/10.1371/journal.pone.0016166 (2011).
46. Abu-Ashour, W., Twells, L. K., Valcour, J. E. & Gamble, J. M. Diabetes and the occurrence of infection in primary care: a matched cohort study. *BMC Infect Dis* **18**, 67, https://doi.org/10.1186/s12879-018-2975-2 (2018).
47. Rojo, F. Carbon catabolite repression in *Pseudomonas*: optimizing metabolic versatility and interactions with the environment. *FEMS Microbiol Rev* **34**, 658–684, https://doi.org/10.1111/j.1574-6976.2010.00218.x (2010).
48. Vitko, N. P., Grosser, M. R., Khatri, D., Lance, T. R. & Richardson, A. R. Expanded Glucose Import Capability Affords *Staphylococcus aureus* Optimized Glycolytic Flux during Infection. *MBio* **7**, https://doi.org/10.1128/mBio.00296-16 (2016).

49. Lister, J. L. & Horswill, A. R. *Staphylococcus aureus* biofilms: recent developments in biofilm dispersal. *Front Cell Infect Microbiol* **4**, 178, https://doi.org/10.3389/fcimb.2014.00178 (2014).
50. Yang, L. *et al*. Pattern differentiation in co-culture biofilms formed by *Staphylococcus aureus* and *Pseudomonas aeruginosa*. *FEMS Immunol Med Microbiol* **62**, 339–347, https://doi.org/10.1111/j.1574-695X.2011.00820.x (2011).
51. Lim, Y., Jana, M., Luong, T. T. & Lee, C. Y. Control of glucose- and NaCl-induced biofilm formation by *rbf* in *Staphylococcus aureus*. *J Bacteriol* **186**, 722–729 (2004).
52. Rode, T. M., Langsrud, S., Holck, A. & Moretro, T. Different patterns of biofilm formation in *Staphylococcus aureus* under food-related stress conditions. *Int J Food Microbiol* **116**, 372–383, https://doi.org/10.1016/j.ijfoodmicro.2007.02.017 (2007).
53. Tognon, M., Kohler, T., Luscher, A. & van Delden, C. Transcriptional profiling of *Pseudomonas aeruginosa* and *Staphylococcus aureus* during *in vitro* co-culture. *BMC Genomics* **20**, 30, https://doi.org/10.1186/s12864-018-5398-y (2019).
54. Good, N. E. *et al*. Hydrogen ion buffers for biological research. *Biochemistry* **5**, 467–477 (1966).
55. Harjai, K. *et al*. Effect of pH on production of virulence factors by biofilm cells of *Pseudomonas aeruginosa*. *Folia Microbiol (Praha)* **50**, 99–102 (2005).
56. Kessler, E., Safrin, M., Olson, J. C. & Ohman, D. E. Secreted LasA of *Pseudomonas aeruginosa* is a staphylolytic protease. *J Biol Chem* **268**, 7503–7508 (1993).
57. Duan, K. & Surette, M. G. Environmental regulation of *Pseudomonas aeruginosa* PAO1 Las and Rhl quorum-sensing systems. *J Bacteriol* **189**, 4827–4836, https://doi.org/10.1128/JB.00043-07 (2007).
58. Kolderman, E. *et al*. L-arginine destabilizes oral multi-species biofilm communities developed in human saliva. *PLoS One* **10**, e0121835, https://doi.org/10.1371/journal.pone.0121835 (2015).
59. Borriello, G., Richards, L., Ehrlich, G. D. & Stewart, P. S. Arginine or nitrate enhances antibiotic susceptibility of *Pseudomonas aeruginosa* in biofilms. *Antimicrob Agents Chemother* **50**, 382–384, https://doi.org/10.1128/AAC.50.1.382-384.2006 (2006).
60. Jakubovics, N. S. *et al*. Critical roles of arginine in growth and biofilm development by *Streptococcus gordonii*. *Mol Microbiol* **97**, 281–300, https://doi.org/10.1111/mmi.13023 (2015).
61. Peters, T. Jr. Serum albumin. *Adv Protein Chem* **37**, 161–245 (1985).
62. Cheng, A. G., Missiakas, D. & Schneewind, O. The giant protein Ebh is a determinant of *Staphylococcus aureus* cell size and complement resistance. *J Bacteriol* **196**, 971–981, https://doi.org/10.1128/JB.01366-13 (2014).
63. de Chateau, M., Holst, E. & Bjorck, L. Protein PAB, an albumin-binding bacterial surface protein promoting growth and virulence. *J Biol Chem* **271**, 26609–26615 (1996).
64. Dekio, S. & Jidoi, J. Effect of serum albumin on growth of *Staphylococcus aureus* in synthetic tissue culture medium. *J Dermatol* **10**, 505–508 (1983).
65. Miller, C. L. *et al*. Global transcriptome responses including small RNAs during mixed-species interactions with methicillin-resistant *Staphylococcus aureus* and *Pseudomonas aeruginosa*. *Microbiologyopen* **6**, https://doi.org/10.1002/mbo3.427 (2017).
66. Lambiase, A., Catania, M. R. & Rossano, F. Anaerobic bacteria infection in cystic fibrosis airway disease. *New Microbiol* **33**, 185–194 (2010).
67. Worlitzsch, D. *et al*. Effects of reduced mucus oxygen concentration in airway *Pseudomonas* infections of cystic fibrosis patients. *J Clin Invest* **109**, 317–325, https://doi.org/10.1172/JCI13870 (2002).
68. Filkins, L. M. & O'Toole, G. A. Cystic Fibrosis Lung Infections: Polymicrobial, Complex, and Hard to Treat. *PLoS Pathog* **11**, e1005258, https://doi.org/10.1371/journal.ppat.1005258 (2015).
69. Fuchs, S., Pane-Farre, J., Kohler, C., Hecker, M. & Engelmann, S. Anaerobic gene expression in *Staphylococcus aureus*. *J Bacteriol* **189**, 4275–4289, https://doi.org/10.1128/JB.00081-07 (2007).
70. Crespo, A., Gavalda, J., Julian, E. & Torrents, E. A single point mutation in class III ribonucleotide reductase promoter renders *Pseudomonas aeruginosa* PAO1 inefficient for anaerobic growth and infection. *Sci Rep* **7**, 13350, https://doi.org/10.1038/s41598-017-14051-2 (2017).
71. Voggu, L. *et al*. Microevolution of cytochrome bd oxidase in Staphylococci and its implication in resistance to respiratory toxins released by *Pseudomonas*. *J Bacteriol* **188**, 8079–8086, https://doi.org/10.1128/JB.00858-06 (2006).
72. He, J. *et al*. The broad host range pathogen *Pseudomonas aeruginosa* strain PA14 carries two pathogenicity islands harboring plant and animal virulence genes. *Proc Natl Acad Sci USA* **101**, 2530–2535 (2004).
73. Chapman, G. H. The significance of sodium chloride in studies of staphylococci. *J Bacteriol* **50**, 201–203 (1945).
74. Cendra Mdel, M., Juarez, A. & Torrents, E. Biofilm modifies expression of ribonucleotide reductase genes in *Escherichia coli*. *PLoS One* **7**, e46350, https://doi.org/10.1371/journal.pone.0046350 (2012).
75. Crespo, A., Blanco-Cabra, N. & Torrents, E. Aerobic Vitamin B12 Biosynthesis Is Essential for *Pseudomonas aeruginosa* Class II Ribonucleotide Reductase Activity During Planktonic and Biofilm Growth. *Front Microbiol* **9**, 986, https://doi.org/10.3389/fmicb.2018.00986 (2018).
76. Macia, M. D., Rojo-Molinero, E. & Oliver, A. Antimicrobial susceptibility testing in biofilm-growing bacteria. *Clin Microbiol Infect* **20**, 981–990, https://doi.org/10.1111/1469-0691.12651 (2014).
77. Pearson, K. On the criterion that a given system of deviations from the probable in the case of a correlated system of variables is such that it can be reasonably supposed tohave arisen from random sampling. *Philosophical Magazine* **302**, 157–175 (1900).

Acknowledgements
This work was supported in part by grants to E.T. from the La Caixa Foundation, Spanish Ministerio de Ciencia, Innovación y Universidades (MINECO/FEDER) (BIO2015-63557-R and RT12018-098573-B-100), the CERCA programme/Generalitat de Catalunya (2017 SGR01079) and the Catalan Cystic Fibrosis association. L.P. is thankful to the Generalitat de Catalunya for its financial support through the FI program (2015-FI-B-00817).

Author contributions
M.C. and E.T. designed the study. M.C., N.B.-C. and L.P. performed the experiments. All authors analyzed the data. M.C. and E.T. wrote the paper. All authors revised and approved the final version of the paper.

Competing interests
The authors declare no competing interests.

Additional information
Supplementary information is available for this paper at https://doi.org/10.1038/s41598-019-52726-0.

Correspondence and requests for materials should be addressed to M.d.M.C. or E.T.

Reprints and permissions information is available at www.nature.com/reprints.